Università degli Studi di Cagliari

DOTTORATO DI RICERCA

INGEGNERIA DEL TERRITORIO

Ciclo XXV

Risk Analysis and Mitigation of Seawater Intrusion for the Gaza Strip Coastal Aquifer under Climate Induced Changes

Settore scientifico disciplinare di afferenza

ICAR/02 Costruzioni idrauliche e marittime e idrologia

Presentata da:	Dott.ssa Marta Dentoni
Coordinatore Dottorato:	Prof. Roberto Deidda
Tutors/Relatori:	Prof. Roberto Deidda Ing. Giuditta Lecca Prof. Claudio Paniconi

Esame finale anno accademico 2011 – 2012

Abstract

Coastal aquifers are in hydraulic contact with the sea; prolonged overpumping of groundwater can lead to inland encroachment and/or vertical up-coning of the interface (transition or mixing zone) between these regimes, causing salt contamination of freshwater aquifers. In the Mediterranean area, seawater intrusion (SWI) has sometimes become a major threat to coastal area freshwater resources, mainly due to lack of appropriate groundwater resources management. Current projections of future potential climatic scenarios further complicate the overview, because the worst considered possibilities provide critical predictions about the decline of the average amount of water available (in terms of both inflows and outflows); furthermore, the projected sea-level rise (SLR) could significantly alter the position and morphology of coastline. A proper analysis and risk assessment of areas subject to SWI, and the evaluation of the coastal basins hydrological response to climate variability, appear to be essential for the design of water management measures that are necessary to mitigate environmental and socio-economic impacts.

The key objectives of the study are: 1) development of a methodology of SWI risk analysis in coastal aquifers; 2) application of the methodology to a real case-study (Gaza Strip coastal aquifer, Palestinian Territories) to assess the risk of saltwater ingression and 3) analysis of the effectiveness of mitigation strategies on SWI Risk to support the planning of future spatial and territorial organization. The aquifer system is studied with a simulation code to assess the feasibility of risk mitigation measures under climate induced changes, by the means of simulation/optimization methods, which can provide the quantitative information needed for the management of groundwater resources, with respect to assigned objectives and constraints. Results show that (i) SWI risk assessment can be addressed by means of groundwater simulation models, calibrated against field measures, as a tool to evaluate future contamination in response to projected climate scenarios and exploitation plans, and that (ii) mitigation measures can be developed, according to some predefined criteria, and expected benefits can be quantified.

The research is carried out within the CLIMB project, funded by the 7th Framework Programme of the European Commission.

Acknowledgements

I would like to express my sincere gratitude to my supervisors Prof. Roberto Deidda, for giving me the opportunity of this doctoral research and his support toward more critical approach in science, Eng. Giuditta Lecca, for her strong contribution on founding the basis for this work and her continuously encouraging support throughout these intensive years, and Prof. Claudio Paniconi, for his precious reviews and his thorough approach to hydrogeological science.

My gratitude goes to CRS4 supervisors, responsibles and colleagues, who kindly supported my doctoral research; my special thanks go to the Environmental Science group, Marino Marrocu and Gabriella Pusceddu, for their help and support on troubleshooting climate models data issues.

This thesis was developed in the framework of the European project CLIMB, "Climate Induced Changes on the Hydrology of Mediterranean Basins: Reducing Uncertainty and Quantifying Risk through an Integrated Monitoring and Modeling System (CLIMB)", 7th Framework Programme, call FP7ENV-2009-1, topic ENV.2009.1.1.5.2; my sincere thanks to our Palestinian colleagues Prof. Samir Afifi, for his effort on coordinating the work on the Gaza Strip site, Dr. Khalid Qahman, for his support in facing the Gaza Strip aquifer issues, and Eng. Samir Alnahhal.

Last, but not least, I thank my family for the patience and support.

All these people deserve to be credited for the results achieved within this work.

Table of Contents

List of Figures

List of Tables

Introduction

General

According to current climate projections (IPCC, 2007), Mediterranean countries are at high risk for an even pronounced susceptibility to changes in the hydrological budget. These changes are expected to have severe direct impacts on the management of water resources, agricultural productivity and drinking water supply. The different regions of the Mediterranean landscape are already experiencing and expecting a broad range of natural and man-made threats to water security, such as severe droughts, extreme flooding, salinization of coastal aquifers, degradation of fertile soils and desertification due to poor and unsustainable management practices.

Coastal aquifers in the Mediterranean are often affected by seawater intrusion, which has sometimes become a major threat to coastal area freshwater resources, mainly due to lack of appropriate groundwater resources management; current projections of future potential climatic scenarios are providing critical predictions about the decline of the average amount of available water, together with a progressive reduction of natural groundwater recharge; yet, the sea-level rise (SLR) could alter the position of coastline, probably affecting Salt Water Intrusion (SWI) in coastal areas. Unless appropriate adaptation measures are undertaken, these changes will give rise to an increasing potential for tensions and conflict among the socio-political and economic actors in this vulnerable regions.

Problem definition

There is scientific consensus that climate induced changes on the hydrology of Mediterranean regions are presently occurring and are projected to amplify in the future, but little knowledge is available about the quantification of these changes, which is hampered by a lack of suitable and cost effective hydrological monitoring and modeling systems. In particular, current projections of future hydrological change, based on regional climate model results and subsequent hydrological modeling schemes, are very uncertain and poorly validated. Although these problems could affect a great number of coastal areas, the Fourth Report of the Intergovernmental Panel on Climate Change

(IPCC) still reports that there "has been very little research on the impact of climate change on groundwater" and that "the few studies of climate impacts on groundwater for various aquifers show very site-specific results" (Kundzewicz et al., 2007).

SWI problems and their management are intrinsically complex due to the number of interacting phenomena. In order to assess the behaviour of the saline water body under various conditions of recharge and discharge, and also under climate induced changes, it is necessary to achieve a good knowledge of the hydraulic conditions of the aquifer system, eventually identifying the extent of the problem. A proper analysis and risk assessment of areas subject to SWI, and the evaluation of hydrological response of the coastal basins to climate variability, appear to be essential for the design of water management measures that are necessary to mitigate environmental and socio-economic impacts.

Motivation and research objectives

The specific objective of this thesis is to establish a management strategy for sustainable development and management of the Gaza Strip coastal aquifer (GCA) system, starting from the development of a general methodology for the analysis and risk assessment of seawater intrusion in coastal aquifers, integrating the state-of-the-art methodologies in the international context.

Risk can be defined as the probability of harmful consequences or expected losses, such as disruption of economic activity or environmental damage, in a certain area and in a certain period of time, resulting from interactions between natural or human-induced hazards and vulnerable conditions. For SWI in coastal aquifers, different phenomena are taken in account for risk assessment, including projected climate induced changes and sea level rise.

The research objectives can be summarized as following:

1) development of a risk assessment methodology of seawater intrusion in coastal aquifers by the means of process-based framework, including hydrogeological modeling;
2) application of the methodology to a real case-study (Gaza Strip aquifer, Palestinian Territories) to assess the risk of saltwater ingression under climate induced changes;

3) assessing impact of mitigation strategies (for aquifer restoration) on Salt Water Intrusion (SWI) Risk

To achieve these objectives, the peculiar elements of the methodology of risk analysis for coastal aquifers are identified, by understanding and quantifying the decisive causes and predisposing factors for risk, evaluating also the impact of possible future climate scenarios.

The methodology is applied to the Gaza Strip hydrogeological basin, in which the problem of SWI is so exacerbated that corrective measures are needed to properly manage the groundwater and to restore it. This aquifer system is studied with a simulation code, verifying the applicability of risk mitigation measures under climate induced changes. Therefore, a 3D hydrogeological model of the Gaza Strip coastal aquifer based on CODESA-3D (Gambolati et al,. 1999; Lecca, 2000) is used, allowing to simulate complex coupled problems of flow and contaminant transport in groundwater, in the presence of a fluid phase of variable density.

The research is undertaken as part of the CLIMB project funded by the European Commission within the 7th Framework Programme, in the framework of which the hydrogeological model is calibrated with data made available by the Palestinian partner (University of Gaza, IUG) in WP5 development objective, and it is used to simulate the response of the hydrological basin to selected potential future scenarios of climate change, processed and made available by experts who collaborated in carrying out the WP4 of same project. The integration of hydrological model results and socio-economic factor analysis will enable the development of a risk analysis and assessment, eventually evaluating economic and social-environmental losses, in terms of the probability that consequences occur in strategic areas (i.e. pumping wells areas). In order to formulate mitigation strategies for the SWI risk in the study area, groundwater management schemes are assessed by the means of methods of simulation/optimization (Qahman et al., 2009), that can provide quantitative information needed for the management of groundwater resources with respect to assigned objectives and constraints.

Valid findings will be made available for improved site-specific monitoring and modeling systems for water resources and use assessments under changing climate conditions; important output of the research in the study site will be the development of a set of

recommendations for an improved monitoring and modeling strategy for climate change impact assessment.

Thesis Outline

This thesis consists of eight chapters after the introductory part.

Chapter 1 proposes the state-of-the-art of available studies on the related works that the thesis is based on, illustrating relative progress and open issues.

Chapter 2 proposes the basic elements of salt water intrusion (SWI) risk methodology, whose final goal is providing an indication of a community's probability to consume saltwater contaminated groundwater. The approach of the proposed SWI Risk Analysis methodology is based on the origin-pathway-target model, in which the 3 elements are: 1) the origin of seawater intrusion, which is the seaside boundary of the aquifer; 2) the pathway, which is the horizontal and vertical groundwater flow in the aquifer; 3) the target, which is the water pumped from wells. The final value of SWI risk is evaluated by applying the overlay principle to three thematic maps coming from the 3 elements above described, namely Hazard map (H), Vulnerability map (V) and Elements map (E). In this study, the Hazard (H) to SWI is set identifying areas where salt concentration is higher than a fixed level in relative medium time periods; thus, hazard is calculated by the means of a 3D hydrogeological model, allowing to simulate coupled problems of variably saturated flow and contaminant transport in groundwater, in the presence of a fluid phase of variable density, and to assess possible future scenarios of how groundwater system can evolve under climate induced changes conditions and sea level rise (SLR). The Vulnerability (V) to SWI is calculated using the GALDIT method (Chachadi and Lobo-Ferreira, 2003, 2007), a large-scale indexing method which considers six parameters that control the potential saltwater intrusion in groundwater. The possible consequences of a contamination are evaluated on the wells (elements, E) by considering their use (agriculture, industrial, drinking purposes) and their operational pumping values.

Chapter 3 presents a suite of computational tools to cope with SWI, including all the essential steps to develop and test management measures to restore groundwater quality in coastal aquifers. The used framework is based on the integration of existing tools, consisting in: 3D modeling (coupled density-dependent groundwater flow and miscible

salt transport in coastal aquifer) using CODESA-3D (Gambolati et al., 1999; Lecca 2000); automatic calibration of the hydrogeological model using PEST (Doherty, 2002); simulation/optimization model, to assess management and mitigation strategies for SWI, using a genetic algorithm (Carrol, 1996).

Chapter 4 illustrates an overview of the Gaza coastal aquifer (GCA) study site, presenting and analyzing geographical, climatological and hydrogeological data.

Chapter 5 illustrates the projections of future climate scenarios on the Gaza Strip area, processed as a part of an extensive work carried out by a group of people in the framework of the CLIMB project, funded by the European Commission within the 7th Framework Programme. Thanks to the research undertaken as part of the project, future climate scenarios have been processed and made available by experts who collaborated in carrying out the "Climate Models Auditing and Downscaling" Work Package of same work; during the project, a simple but precise and rigorous auditing assessment of mean states, monthly fluctuations, and extremes, of precipitation and temperature has been obtained by comparing the outputs of 14 Regional Climate Models (RCMs) part of the ENSEMBLES project, with a gridded data set of observations (E-OBS). A selection of these multimodel climate outputs is further analyzed for the specific site of the Gaza Strip area.

Chapter 6 focuses on the development of hydrogeological model of the study site, aiming, on one hand, at reproducing the past evolution of the system and, on the other hand, the future possible evolution of the same aquifer system. The 3D hydrogeological model of the Gaza Strip is 3D is implemented with CODESA-3D (Gambolati et al,. 1999; Lecca, 2000), allowing to simulate complex coupled problems of flow and contaminant transport in groundwater, in the presence of a fluid phase of variable density; the model is setup, calibrated and validated with all measured and estimated data made available by the Islamic University of Gaza (IUG). The non-linear response of the hydrological model is investigated at the catchment scale driving the same model by multimodel climate outputs. The results are further analyzed, and the use of one optimization methodology to assess management strategies in the coastal aquifer under induced climate changes is proposed. A simple management scenario is assessed using the simulation/optimization method illustrated in Chapter 3, in order to identify optimal schemes to prevent/mitigate

saltwater intrusion in the Gaza Strip coastal aquifer under climate change conditions, by minimizing the variation of current pumping rates while constraining salt concentrations.

Chapter 7 presents the SWI risk assessment methodology applied to the study site; the final goal is to verify, under climate induced changes, the appropriateness of proposed risk mitigation measures formulated in Chapter 6 to cope with marine ingression in the study area.

Chapter 8 summarizes the main contributions of this thesis. The main outcome responds to the key objective of this work, that is to develop, by using together different existing tools, a SWI risk assessment methodology; then, to apply the methodology to a real case-study of the Gaza Strip aquifer, and assessing impact of mitigation strategies for aquifer restoration on Salt Water Intrusion (SWI) Risk. Furthermore, a set of recommendations for an improved monitoring, modeling and management strategy for groundwater resources under changing climate conditions is developed for the Gaza Strip coastal aquifer.

Chapter 1 - Literature review

Coastal aquifers in the Mediterranean are often affected by seawater intrusion, which has sometimes become a major threat to coastal area freshwater resources, mainly due to lack of appropriate groundwater resources management. Current projections of future potential climatic scenarios (IPCC, 2007) further complicate the overview, because the worst considered possibilities provide critical predictions about the decline of the average amount of available water, together with a progressive reduction of natural groundwater recharge; yet, the projected sea-level rise (SLR) could alter the position of coastline, making it possible consistent increasing of Salt Water Intrusion (SWI).

A proper analysis and risk assessment of areas subject to seawater intrusion, and the evaluation of hydrological response of the coastal basins to climate variability, appear to be essential for the design of water management measures that are necessary to mitigate environmental and socio-economic impacts. The Gaza Strip aquifer represents a clear example of such SWI correlate problems, and it is assumed as study site in this work.

In this Chapter is briefly illustrated the state-of-the-art of the main topics above cited.

1.1 Seawater intrusion

Sea water intrusion (or salt water intrusion, SWI) is the encroachment of saline water into fresh ground water regions in coastal aquifer settings. SWI has been studied extensively for well over a century, starting from the last part of 1900 (Badon-Ghyben, 1888; Herzberg, 1901); due to its socioeconomic impact, this issue has received an ample attention from the international scientific community during the last 50 years (Cooper, 1964; Henry, 1964; Pinder and Cooper, 1970; Custodio and Bruggeman, 1987; Voss and Souza, 1987; Werner and Gallagher, 2006; Werner et al., 2012).

Under normal conditions, without any anthropogenic activity, the freshwater flows into the sea, due to the natural hydraulic gradient existing toward the sea. Under the sea bottom there is a zone of contact between the lighter freshwater flowing to the sea and the heavier, underlying, seawater; in this transition zone, freshwater and saltwater are mixed together (Figure 1.1). Density varies across the transition zone between the highest values

of sea waters to lower values of freshwater. The width of this zone is, under certain conditions, relatively smaller than the thickness of the aquifer, so that the boundary can be considered as a sharp interface separating the two regions occupied by the two fluids, the freshwater and saltwater one, assumed immiscible. Therefore, in case the transition zone is wide, this assumption is invalid (Bear et al., 1999) and the interface is assumed diffusive.

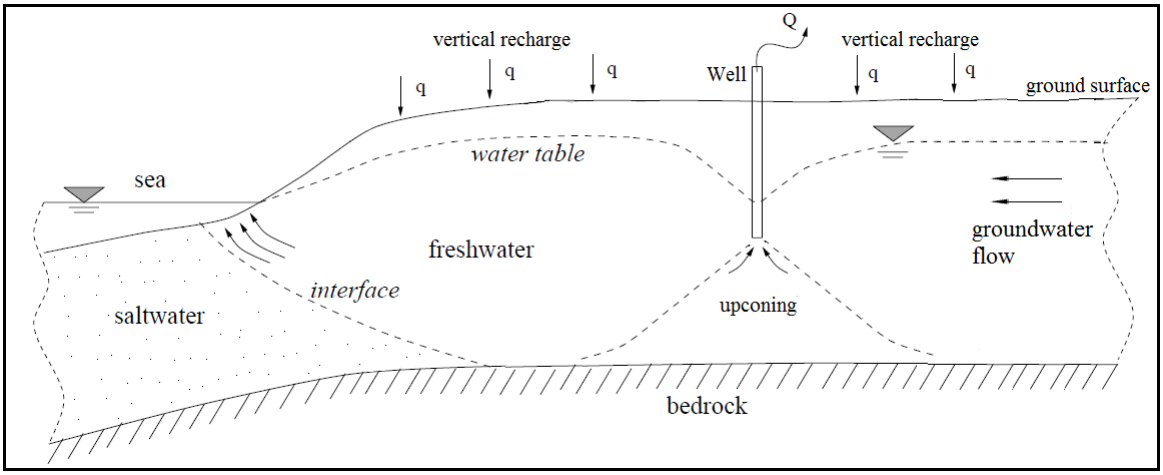

Figure 1.1 - Simplified diagram of a coastal unconfined aquifer setting.

The classic relationship between seawater and freshwater in coastal aquifers is that assumed by Ghyben and Herzberg in the late nineteenth Century, roughly assuming simple hydrostatic conditions in a homogeneous, unconfined aquifer (Freeze and Cherry, 1979), considering that the flow in the aquifer is essentially horizontal (a statement that is equivalent to the Dupuit assumption) and perpendicular to the coast, and using difference in density between the two types of water to predict the depth to the interface, is given by:

$$\xi = \frac{\rho_f}{\rho_s - \rho_f} h_f - \frac{\rho_s}{\rho_s - \rho_f} h_s \approx 40 h_f \quad (1.1)$$

Where ξ is the depth of interface below the datum, ρ_s and ρ_f are the saltwater and freshwater density, h_s and h_f are the piezometric heads in saltwater and freshwater zones (Figure 1.2), with the first one considered in this scheme equal to zero; the equation consider the actual densities of freshwater equal to 1.000 g/cm^3 and of sea water equal to 1.025 g/cm^3, so that the theoretical depth to the saline interface is 40 times the elevation

of the water table above sea level. Therefore, if the water table in an unconfined coastal aquifer is lowered by 1 m, the interface will rise by 40 m. However, being it a dynamic interface, the calculation is very approximate.

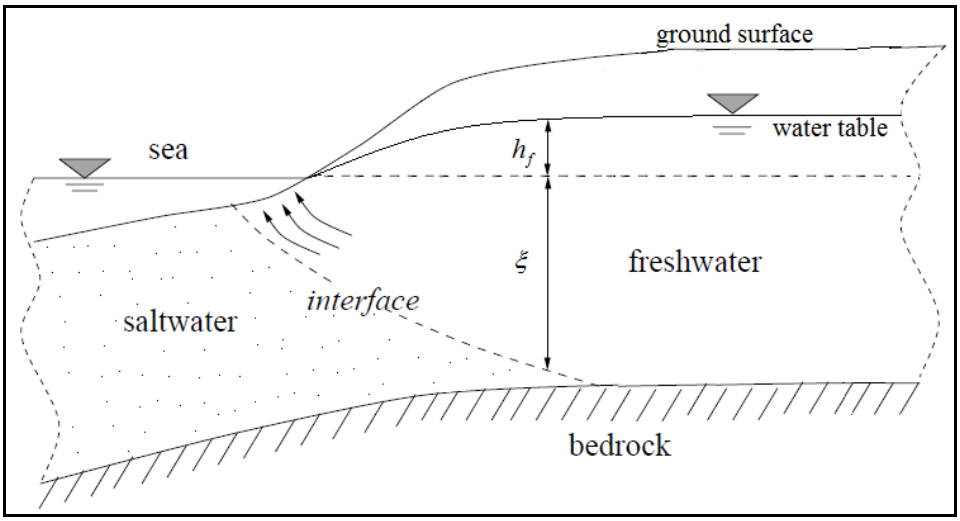

Figure 1.2 – Saltwater-freshwater depth interface.

Associated with SWI there are several interacting factors and processes, such as (Werner et al., 2012) dispersive mixing, tidal effects, density effects including unstable convection, surface hydrology (e.g., recharge variability and surface–subsurface interactions), paleo-hydrogeological conditions (i.e., leading to trapped ancient seawater), anthropogenic influences, and geological characteristics. All these factors, coupled with other processes such as geochemical reactions, influence the aquifer hydraulic and transport properties, providing a great number of possible settings in which SWI can occur and posing in this way a significant challenge in identifying the primary SWI controlling factors.

As indicated before, the thickness of mixing zone between freshwater and intruding saltwater can vary considerably, depending the site-specific system. This phenomenon is actually the result of transport processes driven by density gradients, diffusion, dispersion, and kinetic mass transfer; all of them are influenced by the aquifer characteristics, such as spatial heterogeneity in the geologic structure, temporal and spatial variability in groundwater recharge, long-term variations in sea level position, and pumping activities.

The heterogeneity of the aquifer system could create spatial variation in hydraulic proprieties that control dissolved transport by perturbing fluid flow (Diersch and Kolditz, 2002)); both particular geological structures (Calvache and Pulido-Bolsch, 1997) and variations in the aquifer bottom (Abarca et al., 2007) can lead to preferential flow paths in which transport and SWI can occur more rapidly. The impact of the simplification of heterogeneity, also by considering 2D instead of 3D conceptual models (Kerrou and Renard, 2010), is significantly different both in magnitude and in general trends.

The influence of sea-level fluctuation on SWI can vary in complexity, depending on the events (i.e. episodic, long-term process) which has driven it. In general, recovery time in case of episodic events (tsunamis, storms) is estimated to be in the range of few years (Illangasekare et al., 2006; Violette et al., 2009), while long term events such as tidal dynamics impose time-averaged head conditions at the coast that exceed mean sea level (Nielsen, 1990; Ataie-Ashtiani et al., 2001; Song et al., 2006).

Pumping from coastal aquifers can cause the so-called upconing process, that is the vertical rise of saltwater from the bottomed part of the aquifer and the progressive reduction of freshwater zone in the well area; this phenomenon depends on a large number of factors, such as hydraulic proprieties of the aquifer, pumping rates, initial position of the interface, density difference between fresh and salt water, groundwater recharge, regional flow rate, wells and aquifer geometries (Reilly and Goodman, 1987; Saeed et al., 2002). The increase in abstraction from aquifers may result in inversion of the flow from the sea towards the inland causing increasing of saltwater intrusion

1.1.1 SWI monitoring and control methods

A large number of coastal aquifers are threatened by SWI, which is a global issue, considering that (Freeze and Cherry, 1979) a substantial proportion of the earth's population (70%) lives along or near coastlines and 95% of the earth's water lies in the oceans and seas at high levels of salinity. In coastal areas groundwater is considered the main source of water supply and that mixing a small quantity (2–3%) of saltwater with groundwater makes it unfit for different uses.

In densely populated coastal regions like the Mediterranean basin, fresh groundwater resources are used for domestic, agricultural, and industrial purposes; prolonged

overpumping of groundwater is increasing, leading to inland encroachment and/or vertical up-coning of seawater, mainly due to population and economic growth, intensified agricultural development, and the loss of surface freshwater resources due to pollution and contamination. As results, water-resource managers face a long-term struggle in safeguarding existing coastal fresh groundwater supplies from the hazards of seawater intrusion from natural and anthropogenic causes.

SWI affects, mainly, arid and semi-arid zones, where dense population and touristic development are coupled to scarce water resources and require intense exploitation of groundwater (particularly in the dry season); the Mediterranean coast is a clear example of this phenomenon (Yakirevich et al., 1998; Pulido-Bosch et al., 1999; Paniconi et al., 2001; Giambastiani et al., 2007; Antonellini et al., 2008). The measurement of current SWI situation in coastal areas requires a rather long temporal observation of aquifer changes, including both hydraulic heads and water salinity trends. It is really difficult to clearly delineate the real spatial and temporal extent of SWI, as the process is typically slow and historical data are commonly scarce. Yet, although different measurement methods are used (head and water quality measurements, geophysical field campaigns, environmental tracers), the general outcomes is that the monitoring of SWI is difficult and it is needed to properly design the measurement infrastructures (Werner et al., 2012).

However, in some areas the problem is so exacerbated that the contaminated groundwater is intruding as its entire volume may cease to be available for use (‘aquifer failure’). To face SWI problem, a number of methods have been used to control SWI to protect, restore or, at least, to reverse current negative trends of quality of groundwater resources in coastal aquifers. A comprehensive introduction to this topic was presented by Custodio (1987); Oude Essink (2001) provides a summary of SWI control measures. The available methods can be grouped (Abarca et al., 2006) into actions over the water demand (i.e., reduce pumping), actions over the recharge (i.e., artificial recharge and territorial planning), relocation of abstraction wells and additional engineering solutions (i.e., seawater intrusion barriers, artificial recharge, abstraction of saline water). Many limitations of the previous methods have been reported in the literature such as the source and the cost of fresh water and applicability of such methods (Abd-Elhamid and Javadi, 2010). Nevertheless, whatever decision of management policy is chosen, it is necessary to

deeply analyze the current and actual local situation. The good knowledge of the aquifer system and the ability to forecast its future behaviour under different natural stresses and human impacts are necessary conditions to properly manage this kind of problems.
Numerical simulation (Bear et al., 1999), based on field measurements evidences, is the usual tool to investigate SWI in coastal aquifers and to support, by also the means of combining and coupling optimization models with it, the assessment of future groundwater resources management scenarios.

1.1.2 Modeling SWI: state-of-the-art, challenges

Seawater and freshwater are, in typical aquifers, separated by an interface across which a mixing zone develops due to the dispersive effects. As above mentioned, this interface is generally dispersed, but, in order to simplify the problem, it should be considered as a sharp interface separating the two regions occupied by the two fluids, the freshwater and saltwater one, assumed immiscible; yet, the problem can be furthermore simplified if assuming the Dupuit assumption (predominantly horizontal flow). This approach, however, is invalid if the transition zone is relatively wide.
The characteristics of transition zones between freshwater and saltwater in coastal aquifers and the dynamics of their movements have been understood for several decades (Todd, 1959; Cooper et al., 1964). As soon as there was the advent of digital computers, numerical algorithms and solution methods were developed to solve the equations for variable-density groundwater flow and transport that represent saltwater intrusion (Pinder and Cooper, 1970; Segol and Pinder, 1976). Computer codes then became available to simulate SWI for user-specified aquifer geometries and characteristics in the two dimensions of a cross-sectional profile (Voss, 1984; Sanford and Konikow, 1985). The availability of mathematical tools promoted a growing interest in the study, and the three-dimensional modeling of SWI became possible. An exhaustive review of this topic is provided by Bear et al. (1999) and, recently, by Werner et al. (2012), and it is not repeated here. Majority of the existing models consider a limited number of mechanisms controlling solute transport in seawater intrusion. Available numerical models consider sharp interface or diffusive interface, only steady-state flow conditions or transient analysis, and others consider variably saturated porous media or neglect the unsaturated

zone. For sure, the more realistic model of the actual aquifer system requires always a greater computational effort (Ataie-Ashtiani et al., 1999), and sometimes it is necessary to accurately simulate and reproduce important natural and/or artificial recharge components of the aquifer's water balance (Paniconi et al., 2001).

SWI is essentially a three-dimensional (3D) problem, conveying important problematic aspects such as heterogeneity in aquifer properties and geometry, dispersion and diffusion, degree of aquifer confinement, hydrogeochemical processes, which usually are extremely difficult to adequately consider together and, also, to adequately reproducing in all existing models. It must be considered that usually a 3D-SWI model is not simple to develop, mainly due to the complexity of the involved physical processes (Carrera et al., 2010); several difficulties must be faced in the modeling procedure, e.g.: aquifer characterization, caused usually by scarcity of adequate hydrogeological field data which drives to many unknown parameters (recharge, boundary conditions,...); spatial and temporal variability of natural processes; the need for solving two coupled non-linear equations; and often low sensitivity of state variables (e.g. heads and concentrations) to aquifer properties.

3D-SWI modeling is a representation of actual aquifer systems, which is very sensitive to geological features and the heterogeneity of hydraulic conductivity; the numerical simulation itself cannot guarantee a successful modeling if the calibration procedure is not properly carried out (Carrera et al, 2005). So that, a fundamental and complex step in the process of understanding aquifer behaviour is the calibration procedure, which aims to estimate some aquifer parameters, such as hydraulic conductivities (which are usually basic elements in order to determine underground flows), against field observed values. Calibration can be considered an integral part of the process of modeling and developing understanding of a hydrogeological system (Poeter and Hill, 1997); thus, it is becoming a standard part of model application.

For a long period, the calibration of hydrological model has been performed manually, by trial-and-error parameter adjustment, which requires a strong knowledge of the system and entails a high subjectivity about the goodness-of-fit of the parameter values. Eventually, it can be a very long-time-consuming task. In the last decades manual calibration has been slowly substituted by automatic calibration, which facilitates

enormously the task of modeling, reducing both the subjectivity and the computing time involved in the calibration procedure. A large set of softwares, classified as based either on local (e.g. gradient methods) or global (e.g. Genetic Algorithm (GA), Shuffled Complex Evolution (SCE) algorithm (Duan et al., 1992), and Simulated Annealing (SA) (Sumner et al., 1997)) search strategies, can be found in the scientific literature, and they can be relatively easily linked to the physical model. Due to all these features and to the large increase of computing power, in the last years automatic calibration has become a typical procedure in the field of hydrogeological modeling.

It is evident that, being 3D-SWI modeling a representation of the aquifer system, it must ensure also a valid correspondence with the aquifer actual evolution. It means that, after the calibration procedure, the model should be validated against fields observed values, namely groundwater heads and salt concentration groundwater. Although not always remarked in common groundwater fields studies, this step is also fundamental in order to establish the appropriateness of the model implementation, and surely gives the most improved understanding of groundwater system behaviour and is the basis for the development of management hypothesis.

For coastal aquifers whose SWI is quite critical, a management scheme to control the phenomenon needs to be assessed (Zhou et al., 2003), and in the evaluation of it, the support of a simulation/optimization tool could be helpful (Das and Datta, 1999).

The final goal of a simulation model is to help the understanding of the behaviour of the modeled system and then to enhance the possibility to find out a good management scheme of the system. Groundwater simulation models can simulate the response of the hydrogeological system to a specified set of input. So that, in order to identify the optimal management strategy for the system, it is necessary to set up several different management schemes, to test their feasibility through the simulation model and then choose the best one analysing the set of results coming from all different scenarios. Like the manual calibration procedure, this method requires a long computing and post-processing time due to a large amount of data.

A possible solution to ensure both a strong reduction in the time needed and a robust solution of the problem is the use of an optimization model, which is used to identify the best possible choice from a set of feasible alternatives. It usually uses mathematical

expressions of the problem to minimize or maximize some objective functions, which are frequently restricted by constraints on the values of the variables. Several authors (Shamir et al., 1984; Willis and Finney, 1988; Cheng et al., 2000) showed the use of optimization approach in the solution of SWI problems; when simulation and optimization models are combined, they demonstrate all their power (Das and Datta, 1999). Groundwater simulation models can be linked with optimization techniques in a single framework to overcome the weakness of using simulation or optimization alone; by the means of this coupled system, the modeler can specify the desired values of the water-resource system (such as minimum groundwater head levels or maximum allowed groundwater salt concentration) and the S/O model determines, from a set of possible strategies, a single management scenario (i.e. pumping strategy) that best fits the modeler's desired values. The linkage techniques used to combine these models can be based on binding constraints in the optimization model (embedding technique), or by using a response matrix (Gorelick, 1983; Ndambuki et al., 2000; Yang et al., 2001) or by an external linkage of simulation and optimization model (Das and Datta, 2001).

Due to the complexity and non-linearity of the process of SWI in coastal aquifer, the embedding technique (which become dimensionally too large also for interconnected PCs, considering the usual possibility of higher resolution along the spatial and temporal scales) and the response matrix approach seem to be inadequate to be linked with the relative model simulation.

As an alternative, it is possible to link SWI simulation model with a general purpose optimization-based management tool using the simulation/optimization approach (Barlow, 2005; Bhattacharya and Datta, 2005); the range of possible mathematical techniques includes linear programming (LP, Mantoglou, 2003), non-linear programming (NLP, Mantoglou and Papantoniou, 2008) and evolutionary algorithms (EA, Kourakos and Mantoglou, 2009; Dhar and Datta, 2009; Ataie-Ashtiania and Ketebchi, 2011), whose the most popular approach is genetic algorithms (GA, Nicklow et al., 2010). Recent SWI simulation/optimization studies are based on non-traditional algorithms, such as EA, because of their effectiveness in converging on the global optimum for highly non-linear or irregular problems (Bhattacharya and Datta, 2005; Qahman et al., 2005; Mantoglou and Papantoniou, 2008).

1.2 Groundwater risk assessment methodologies

Groundwater is a natural drinking water resource often subjected to severe human impact; strategies are required to preserve optimum groundwater quality, and so management of this vital natural resource has become a worldwide priority. In Europe, the European Water Framework Directive (2000), which is intended to provide a common framework for water resource policy and management, has given additional impetus to this issue.

Groundwater protection and management issues are often addressed by either vulnerability or risk assessments. While vulnerability assessments identify sensitive zones of a system based on hydrogeological criteria, groundwater risk assessments additionally consider the presence of potential contamination sources or polluting activities (Gogu and Dassargues, 2000). The most commonly used vulnerability mapping procedures are based on empirical point rating systems that bring together key factors believed to influence the solute transport processes (e.g. Aller et al., 1987). However, Gogu and Dassargues (2000) emphasize the need for process-based risk and vulnerability assessments, since groundwater dynamics are rarely explicitly evaluated in such mapping approaches.

In the last years, the international scientific community has shown great interest on this topic and, thus, many works focused on environmental management for groundwater protection (Adams and Foster, 1992; Morris, 2001; Eliasson et al., 2003; Gerth and Forstner, 2004).

Different methods have been developed and applied for assessing the risk of groundwater contamination (Zwahlen et al., 2004; Andreo et al., 2006; Mimi and Assi, 2009) but only minor attention has been given to definitely finalize SWI risk assessment methodology, although salinization of groundwater can be considered a special category of pollution that threatens groundwater resources and coastal regions. Nisi et al. (2000) gave the scheme of a methodology which aims at assessing saline ingression risk in coastal areas; Ball and Campbell (2006) provided a screening tool for the assessment of saline intrusion risk to coastal aquifers in Scotland. Wriedt and Bouraoui (2009) developed a simple screening methodology for large scale assessment of SWI risk along the Mediterranean coast of the European Union (EU) based on a two different assessment procedures, the

first one based on the balance of groundwater recharge and water abstractions and the second one based on a quantitative characterization of SWI for standardized aquifers.

Milnes (2005, 2011) proposed a framework for a process-based salinization risk assessment methodology in which SWI and solute recycling salinization are evaluated separately, finalizing a composite salinization risk index and identifying the relative map.

However, these methodologies do not consider either impacts of potential climate changes in hydrological processes (changes in groundwater recharge, SLR) nor human induced impacts that could affect SWI.

1.3 Coastal aquifers and climate induced changes

A large number of coastal aquifers are threatened by saltwater intrusion, due to human activities and natural events such as climate change. In densely populated coastal regions like the Mediterranean basin, fresh groundwater resources are used for domestic, agricultural, and industrial purposes (Custodio, 2010); prolonged overpumping of groundwater is increasing, leading to inland encroachment and/or vertical up-coning of seawater, mainly due to population and economic growth, intensified agricultural development, and the loss of surface freshwater resources due to pollution and contamination.

Current projections of future potential climatic scenarios (IPCC, 2007) further complicate the overview, providing critical predictions about the average amount of water availability (in terms of both inflows and outflows), within a progressive reduction of natural groundwater recharge. Furthermore, one expected effect due to global warming is the sea-level rise (SLR), which could alter the position and morphology of coastline.

The sea level rise and changes in freshwater recharge and evapotranspiration patterns will exacerbate the pressures on the coastal groundwater systems and, as indirect consequence, the progressive groundwater encroachment of saltwater.

The resulting loss of fresh groundwater resources will impact on population growth, availability of fresh groundwater resources and all the related socio-economic activities.

Although these problems could affect a great number of coastal areas, the Fourth Report of the Intergovernmental Panel on Climate Change (IPCC) still reports that there “has been very little research on the impact of climate change on groundwater” and that “the

few studies of climate impacts on groundwater for various aquifers show very site-specific results" (Kundzewicz et al., 2007).

1.3.1 Climate change projections issues

Climate is a dynamic system and is subject to natural variations at various time-scales, from years to millennia. If a significant change in climate variables from one period to another occurs, it is referred to as climate change (Refsgaard et al., 1989); climate variability is defined as the variation from year to year and generally occurs as a result of natural and/or man-made activities.

Measurements all over the world show that the average temperature of the earth has risen by 0.5±0.7 °C since the beginning of the 20th century; the cause of this phenomenon has been identified in the increasing of concentration of active greenhouse gases, which have warmed up the atmosphere, leading to the so call "global warming".

Although there is a general consensus that climate change is an ongoing phenomenon, many uncertainties are involved in the calculation of this process and it is not univocally clear the rate of these changes. Some crucial issues (IPCC, 2007) which can affect water resources can be summarized as follows:

1- Projected warming is expected to be greatest at the highest northern latitudes, and least over the Southern Oceans and parts of the North Atlantic Ocean;

2- Snow cover is projected to contract, and they are projected widespread increases in thaw depth over most permafrost regions;

3- The more optimistic globally averaged rises in sea level at the end of the twenty-first century are between 0.11–0.38 m, but an extreme scenario gives a rise up to 0.88 m;

4- It is very likely that hot extremes, heat waves and heavy precipitation events will continue to become more frequent;

5- Decreases in the amount of precipitation are likely in most subtropical land regions, whereas increases are very likely at high latitudes.

Several Global Circulation Models (GCMs) and Regional Climate Models (RCMs), based on nowadays conditions, have been set to forecast the weather for the next decades; those projections are the tool for generating future climate projections for input to recharge and hydrogeological models.

1.3.2 Impacts of climate changes on groundwater

The water cycle can be altered by climatic variations, such as increasing/decreasing of precipitations, temperatures and evaporation patterns. The knowledge of climate variations both in space and time is very important in order to adapt human habits to climate change; the key issues in the study of this problem are (Dragoni and Sukhija, 2008): 1) the amplitude and rate of global climate change over the next decades and century; 2) evaluate extreme droughts and floods, sea level changes, groundwater recharge, soil degradation, deforestation, loss of biodiversity, and changes in ecosystem functioning, based on the global mean climate; 3) assessing vulnerability and sustainability of water resources for the human population in general and groundwater in particular.

Impact of assumed future conditions on groundwater is currently a challenging study field (Arnell, 1999; Brouyére et al., 2004; Döll and Flörke, 2005; Holman, 2006; Candela et al., 2009; Döll, 2009; Crosbie et al., 2010; Sulis et al., 2011). Changes in climatic characteristic (i.e. rainfall and evapotranspiration) will primarily affect the hydrological cycle and secondary groundwater (Loàiciga et al., 1996; Kundzewicz, 2008; Kundzewicz et al., 2008) by modifying recharge patterns, contributing to affect SWI in coastal groundwater. Also sea level rise will contribute in exacerbating this phenomenon (Gornitz, 1991; Bobba, 2002). Changes in several other factors relate to human activities, such as land use settings (Ranjan et al., 2006), demographics, and adaptation feedbacks too (Nicholls and Lowe, 2004), will surely change coastal aquifers equilibrium. All these secondary effects contribute significantly to the threat of SWI (Austin et al., 2009), but they seem to be extremely difficult to be taken into account in one holistic coastal groundwater model.

Although not simple, it is needed to take in account some kind of coupling between the main part of physical forcing and the hydrogeology. In the last decade, it has been done within empirical models which relate climatic factors to groundwater conditions (Bloomfield et al., 2003) or through the use of physically based recharge models (Jyrkama and Sykes, 2007; Scibek and Allen, 2006; Toews and Allen, 2009a) and groundwater flow models (Scibek et al., 2007; Toews and Allen, 2009b; Nyenje and Batelaan, 2009; Rozell and Wong, 2010).

SWI studies usually consider sea-level rise (SLR) that, associated with climate change (i.e. due to changes in atmospheric pressure, expansion of oceans and seas as they warm, and melting of ice and glaciers), can be a significant process in salt water intrusion (Loàiciga et al., 2009). The Intergovernmental Panel on Climate Change (IPCC, 2007) predicts that by 2100, global warming will lead to a sea-level rise of between 110 and 880 mm, causing a progressive inland migration of the mixing zone between fresh and saline water. In fact, the rise in sea water levels increases water heads in the seaside boundary of a coastal aquifer exacerbating the phenomenon of sea water intrusion. From a theoretical point of view, the above illustrated Ghyben-Herzberg relationship (equation 1.1), based on the sharp interface assumption, gives an useful strong approximation of the expected interface depth, considering the hydrostatic equilibrium between two immiscible fluids of different density. On the basis of these assumptions, and stating that the linearity of Ghyben-Herzberg relationship is not warranted and it represents an oversimplification, a one meter height of free water table above mean sea level ensures 40 m of freshwater below sea level; it follows that every 10 cm of sea level rise causes 4 m of reduction in the freshwater thickness.

A simple conceptual framework for coastal unconfined aquifers affected by sea level rise is provided Werner and Simmons (2009), who identified conditions under which major changes in the salt water toe are incurred for very small changes in key hydrogeological variables, highlighting the importance of inland boundary conditions on the sea-level rise impact; the conceptualization assumes steady-state conditions, a sharp interface sea water-fresh water transition zone, homogeneous and isotropic aquifer properties, and constant recharge. Numerical experiments of transient sea level rise were analysed by Watson et al. (2010) and Webb and Howard (2011), considering hypothetical coastal unconfined aquifers within different parameter combinations and ranging the time scales from decades to centuries, coming to different results and stating that, in general, the process of sea water intrusion depends on many hydraulic, geometric and transport parameters, so that usually quantitative prediction of the expected effects of sea level rise on sea water intrusion can be evaluated through numerical models (Sherif and Singh, 1999) which are focused on site specific transient studies. Results coming from these studies are not giving a general conclusion on potential long-term effects of SLR on SWI,

ranging from no impacts to several kilometres of interface movement (Oude Essink et al., 2010). The general outcome of these studies is, however, that each coastal site is affected by SLR in a specific way.

Recently in the scientific community it is growing the expectation to improve the methodological issues related to handling GCMs and RCMs outputs as driving forcing for groundwater system. The general methodological recommendation for hydrogeologists to consider in groundwater-related climate change impact and adaptation studies can be summarized as follows (Holman et al, 2011):

1) Use climate scenarios from multiple GCM or RCMs, in order to better recognize the importance of climate model uncertainty in hydrological studies;
2) Use multiple emissions scenarios, which should be considered equally probable;
3) Consider the implications of the choice of downscaling methods, as GCM or RCM outputs of future climate are generally downscaled (Fowler et al. 2007) because scales of climate and hydrological models are different and biases exist between simulated and observed climatic variables;
4) Properly consider hydrogeological model structural error and model uncertainty, as all groundwater studies are influenced by the validity of their system representation and conceptualisation;
5) Evaluate across a range of groundwater levels and/or climate conditions;
6) Consider socio-economic change, in particular its effect on land-use change and water demand;
7) Consider the efficacy of adaptation responses;
8) Consider adaptation within robust decision-making paradigms.

This set of recommendations seems to be appropriate also for SWI modeling under climate induced changes; their appropriate implementation surely can give an improved holistic understanding of groundwater system behaviour in uncertain futures. It must be recognized, however, that all these recommendation have time and computational costs which sometimes are over the possibility of a single specific site study.

1.4 The Gaza Strip coastal aquifer

The Gaza Strip is a semi-arid region located in the Mediterranean basin; it covers a long and narrow rectangular coastal area of about 365 km^2 between Egypt and Israel.

The Gaza coastal aquifer is the main source of water for agriculture, domestic, and industrial purposes in Gaza Strip. An estimated 1.5 million people live in Gaza by the end of 2010, with a density of about 4,500 people/km^2, making it one of the most overcrowded areas in the world. Due to the continuous population growth, the total water demand in the Gaza Strip is strongly increasing. Nowadays, the need of water is not satisfied by the available resources, and this is causing a huge deficit between water demand and supply (Qahman and Larabi, 2006); the overexploitation of the coastal aquifer is leading to a constant drop in the water level, which can be estimated to be about 20-30 cm each year.

Groundwater quality in the Gaza aquifer is considered generally poor. About 5,000 wells are located in the area, but most of them are not anymore suitable for drinkable purpose because the quality of the extracted water is very low, exceeding World Health Organization (WHO) standards both for chlorides (250 mg/l), due both to pollution and Salt Water Intrusion, and for nitrate (50 mg/l), this latter caused quite exclusively by pollution. So that, two main problems currently challenge the groundwater resources in Gaza Strip area: a) progressive salinity of water extracted from wells which exceeds WHO standards, and b) raising of nitrate levels in the drinking water.

During the last decades several studies have been carried out to analyze SWI in the Gaza Strip (Yakirevich et al., 1998; Melloul and Collin, 2000; Moe et al., 2001; Qahman and Larabi, 2006), but the aquifer quality situation is so critical (Shomar et al., 2010) that this problem is still a long way from being solved and corrective measures are needed to restore groundwater quality and properly manage the aquifer.

1.5 Conclusions and open issues

On the basis of the state-of-the art review proposed in the above paragraph, there are still some open issues on the three main topic interrelate to this work.

1) Calibrating complex models in general and in particular in case of scarcity quality or quantity of data (e.g. lateral inflow, hydrogeological setting, unsaturated soil properties…);
2) Definition of mitigation strategies under climate change (setting optimal pumpings scheme);
3) Lack of SWI risk assessment methodology which includes a process-based framework, properly considering both impacts of potential climate changes in hydrological processes (changes in groundwater recharge, SLR) and human induced impacts that could affect SWI.
4) Coupling climate change conditions and models to forecast SWI, and definition of impacts of climate change on coastal aquifers groundwater.

Chapter 2 - Risk analysis methodology

The approach of the proposed Saltwater Risk Analysis methodology is based on the assumption that risk can be defined as the probability of harmful consequences or expected losses (e.g. disruption of economic activity or environmental damage), in a certain area and in a certain period of time, resulting from interactions between natural or human-induced hazards and vulnerable conditions. The proposed methodology for the assessment of SWI risk is based on the origin-pathway-target model, in which the 3 elements are described as follows:

1) The origin of seawater intrusion is the seaside boundary of the aquifer, which is a linear source of salinity;
2) The pathway is the horizontal and vertical groundwater flow in the aquifer;
3) The target is the water which is extracted from wells.

The final value of SWI risk is evaluated by applying the overlay principle to three thematic maps coming from the 3 elements above described, namely Hazard map (H), representing the origin of SWI, Vulnerability map (V), representing the pathway of the groundwater flow, and Elements map (E), representing the target of SWI.

The Hazard (H) to SWI is calculated by the means of a 3D hydrogeological model, allowing to simulate coupled problems of variably saturated flow and contaminant transport in groundwater, in the presence of a fluid phase of variable density, and to assess possible future scenarios of how groundwater system can evolve. The Vulnerability (V) to SWI is calculated using the GALDIT method, using six parameters that control the potential saltwater intrusion in groundwater. The possible consequences of a contamination are evaluated on the wells (elements, E) by considering their use (agriculture, industrial, drinkable purposes) and their operational pumping values.

Evaluation of the SWI Risk provides an indication of a community's probability to consume saltwater contaminated groundwater. The risk area maps resulting from this methodology are a promising tool for the design of groundwater management schemes.

2.1 Approach to risk analysis methodology

The main objective of this work is to elaborate a framework for a risk assessment methodology by proper considering both impacts of potential climate changes in hydrological processes (changes in groundwater recharge, SLR) and human induced impacts that could affect SWI.

The approach is based on the assumption that risk can be defined as the probability of harmful consequences or expected losses (e.g. disruption of economic activity or environmental damage), in a certain area and in a certain period of time, resulting from interactions between natural or human-induced hazards and vulnerable conditions.

The basis for a process-based methodology is provided by Milnes (2011), who proposed a framework for a salinization risk assessment methodology in which SWI and solute recycling salinization are evaluated separately and then finalized in a composite salinization risk index, eventually identifying the relative map. However, considering that SWI is a particular contamination risk, Milnes' methodology doesn't properly consider a 'European approach' on seawater intrusion risk assessment that should be based on the (1)origin - (2)pathway - (3)target model.

Being the application field similar as the one proposed in Zwahlen (2004), which focuses on groundwater contamination, the following assumptions are taken as furthermore basis for the proposed risk analysis methodology:

1) Origin is the term used to describe the location of a potential contaminant release.
2) The pathway includes everything between the origin and the target. For resource protection, the pathway consists of the mostly vertical passage within the protective cover, for source protection it also includes horizontal flow in the aquifer.
3) The target is the water, which has to be protected. For resource protection the target is the groundwater surface, for source protection it is the water in the well or spring.

In the particular case of Salt Water Intrusion, the above assumptions are then assessed as following (Figure 2.1):

1) The origin is the location of potential seawater intrusion, which is a linear source of salinity that is detected in the seaside boundary of the coastal aquifer;

2) The pathway is the horizontal saltwater flow through the aquifer.
3) The target is the water extracted from in the wells operating in the coastal aquifer.

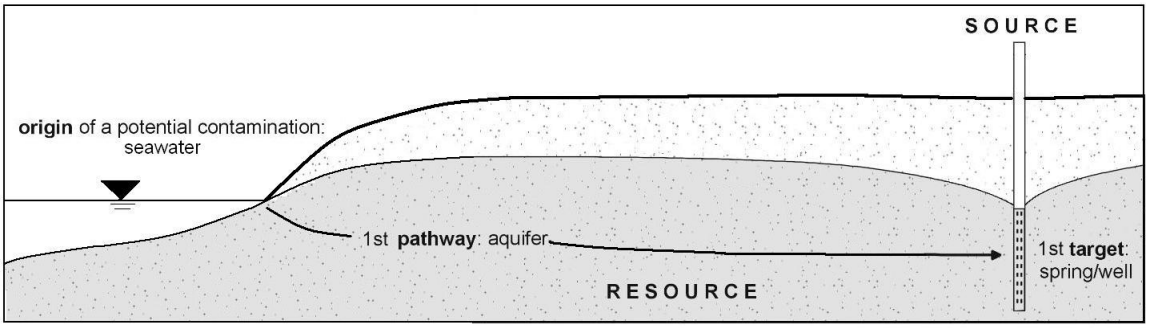

Figure 2.1 - Origin-pathway-target model for saltwater intrusion risk methodology

The risk of groundwater contamination due to saltwater intrusion thus depends on the hazard (origin), the vulnerability of the system (pathway) and the potential consequences of a saltwater contamination event, i.e. its impact on the groundwater extracted from wells (target). As SWI is a complex dynamic process, it is necessary to provide a process-based identification of the spatial variability of this process. This fundamental aspect is analysed in the hazard (H) assessment by identifying SWI through field investigations and a numerical model, which can allow simulating three-dimensional coupled problems of variably saturated flow and contaminant transport in groundwater, in the presence of a fluid phase of variable density.

As the scope of the methodology is to map out zones that are prone to further SWI, the spatial overlay principle is applied, by the means of risk matrixes, to the hazard map (H), the vulnerability map (V) and elements map (E).

2.2 Hazard

Stated that "…environmental hazard (is) an event, or continuing process, which if realized, will lead to circumstances having the potential to degrade, directly or indirectly, the quality of the environment…" (Royal Society (London) Study Group, 1992); in the context of groundwater contamination, a hazard is defined as a potential source of contamination resulting from human activities taking place mainly at the land surface (Zwahlen, 2004). In the field of saltwater contamination, the potential source of contamination is saltwater which intrudes from the sea; this phenomenon can be exacerbated, from one side, by natural and climate change possible impacts, and on the

other hand from human activities such as overpumping. So that, the hazard assessment should consider the potential degree of harmfulness of such events, and the likelihood of a saltwater contamination event.

The hazard estimation concept as proposed in this study considers two factors which control the degree of harmfulness of hazard: 1) possible climate change impacts on the SWI; 2) possible impacts of overpumping. In the proposed methodology, however, hazard is identified as the most likely effects of these two factors on saltwater intrusion (in terms of saltwater concentration) in a certain period of time. While the second factor can be usually estimated on the basis of aquifer management choices, the first factor needs to be assessed from deeper analysis on future climate projection nowadays. Yet, a clear separation between human and climate induced changes impacts is commonly hardly to be identified, so that these two effects are proposed to be analysed together.

2.2.1 Hazard assessment

As coastal aquifers are dynamical systems, and climate induced changes and human inducted impacts are dynamical too, obviously the only analysis of field measurements of salt water intrusion can provide a partial projection on how the system could evolve. So that, it seems to be fundamental the analysis of the aquifer system by the means of modeling and, in particular, within a numerical model which can allow to simulate three-dimensional coupled problems of variably saturated flow and contaminant transport in groundwater, in the presence of a fluid phase of variable density. In few words, hazard depends on SWI modeling results (coming from numerical models) based on projected scenarios both for aquifer management and climate change impacts. Hence, hazard is representing a forecast of the coastal aquifer SWI situation in a certain period of time. In this methodology, it is proposed to set hazard by identifying areas where salt concentration is higher than a fixed level in relative medium time periods.

For the salt concentration level, it is proposed to set it as 10% of total dissolved salts (TDS) in saltwater, which represents a possible simple reference for unsuitable waters for agricultural purposes (it corresponds to around 2,500 mg/l of chlorides concentrations, considered in this study linear within TDS).

For the forecasting time periods, it is proposed to set them as 5, 10, 20 and 30 years, representing a possible compromise solution between climate induced changes effects (which are usually long term effects, particularly in groundwater field) and the needing of adopting or projecting groundwater management schemes in the short / medium-term.
The adopted Hazard Classes are proposed in Table 2.1.

Hazard Class index	TDS (normalized)	Time Period	Hazard Class	Hazard map color
1	0.10	≤ 5 years	Very high	red
2	0.10	≤ 10 years	High	orange
3	0.10	≤ 20 years	Moderate	yellow
4	0.10	≤ 30 years	Low	green
5	0.10	> 30 years	Very Low	white

Table 2.1 – Hazard classes

Although the proposed hazard mapping procedure is based on SWI dynamic non-linear process, the results obtained by numerical modeling are strongly affected dependent on the modeling assumptions and on field data quality. Yet, in order to oversimplificate the application of the methodology, it is only considered the class equal to 0.1 normalized concentration of TDS, which can bring to strong approximate the hazard assessment. Furthermore, the syntheses of the results are static images, which clearly represent a limitation of the provided information.

2.3 Vulnerability

Hydrogeologists have failed to reach a consensus concerning the definitions of and reference terms for groundwater vulnerability assessment (Gogu and Dassargues, 2000), however in this study "vulnerability" refers to the relative propensity for SWI to occur.
There is little published guidance for rapidly assessing of the vulnerability of large regions to SWI. For groundwater contamination, the commonly applied methods consist on indexing methods, such as the DRASTIC (Aller et al., 1987), EPIK (Doerfliger and Zwahlen, 1997), GOD (Foster, 1987) or SINTACS (Civita and de Rigibus, 1995), which consider key factors that can influence the solute transport process.
The only example of a large-scale indexing approach for assessing coastal aquifer vulnerability to SWI is the GALDIT method (Chachadi and Lobo-Ferreira, 2001; Lobo-Ferreira et al., 2007), which adopts simple indicators of the propensity for SWI to occur.

The GALDIT acronym reflects the factors presumed to control SWI, namely Groundwater occurrence/aquifer type, Aquifer hydraulic conductivity, groundwater Level, Distance from the sea water source, Impact of existing status of SWI in the area. The parameter values associated with the six GALDIT controlling factors are converted to "importance" scales of 2.5 to 10, and then aggregated to produce vulnerability scores using subjective weightings.

Other coastal aquifer vulnerability assessment techniques are based on analysis on different coastal impacts, tending to focus on specific stresses, such as the CVI (Coastal Vulnerability Index) approach of Thieler and Hammar-Klose (1999) and the CVI(SLR) (Coastal Vulnerability Index–Sea-Level Rise) indexing method of Ozyurt (2007).

Werner et al. (2011) proposes an approach based on conventional SWI mathematics for steady-state conditions, resulting as an improvement over existing methods for characterizing SWI vulnerability; therefore, the coastal aquifer conceptualization is highly idealized, within a strong simplification of the conceptual system and the assumptions inherent in the analytical model.

2.3.1 Vulnerability with GALDIT

In this study the GALDIT method (Chachadi et al., 2003, 2007) is used to compute vulnerability to SWI, because this method considers the specific seawater intrusion vulnerability by evaluating six particular factors all directly influencing sea encroachment events or depending on them; those factors represent measurable parameters for which data are generally available from a variety of sources. Each factor is evaluated with respect to the other to determine the relative importance of each factor. A relative weight ranging from 1 (least significant) to 4 (most significant) is assigned to each GALDIT factor; a rating value between 1 and 10 is attributed to each parameter depending on local conditions, stating that high values correspond to high vulnerability.

The factors that influence sea water intrusion are identified as follows:

1) Groundwater occurrence, or aquifer type (ranking and weight in Table 2.2);

2) Aquifer hydraulic conductivity (ranking and weight in Table 2.3);

3) Level of ground water above sea (ranking and weight in Table 2.4);

4) Distance from the shore, as distance inland perpendicular from the shoreline (ranking and weight in Table 2.5);

5) Impact of existing status of sea water intrusion in the area (ranking and weight in Table 2.5);

6) Thickness of the aquifer being mapped (ranking and weight in Table 2.7).

Indicator (G)	Weight (w_1)	Indicator Variables	Importance Rating
Groundwater occurrence / Aquifer Type	1	Confined aquifer	10
		Unconfined aquifer	7.5
		Leaky confined aquifer	5
		Bounded aquifer (recharge and/or impervious boundary aligned parallel to the coast)	2.5

Table 2.2 – Ratings for different hydrogeological conditions

Indicator (A)	Weight (w_2)	Indicator Variables		Importance Rating
		Class	Range	
Aquifer hydraulic conductivity (m/day)	3	High	> 40	10
		Medium	10-40	7.5
		Low	5-10	5
		Very Low	< 5	2.5

Table 2.3 – Ratings adopted for the GALDIT parameter A

Indicator (L)	Weight (w_2)	Indicator Variables		Importance Rating
		Class	Range	
Height of ground water level above m.s.l. (m)	4	High	< 1.0	10
		Medium	1.0-1.5	7.5
		Low	1.5-2.0	5
		Very Low	< 2.0	2.5

Table 2.4 - Ratings adopted for the GALDIT parameter L

Indicator (D)	Weight (w_4)	Indicator Variables		Importance Rating
		Class	Range	
Distance of the point from shore (m)	4	Very small	< 500	10
		Small	500-750	7.5
		Medium	750-1000	5
		Far	> 1000	2.5

Table 2.5 - Ratings adopted for the GALDIT parameter D

Indicator (I)	Weight (w_5)	Indicator Variables		Importance Rating
		Class	Range of Cl/(HCO_3+CO_3) in e.p.m. in groundwater	
Impact status of existing seawater intrusion	1	High	> 2	10
		Medium	1.5-2.0	7.5
		Low	1-1.5	5
		Very low	< 1	2.5

Table 2.6 - Ratings adopted for the GALDIT parameter I

Indicator (T)	Weight (w_6)	Indicator Variables		Importance Rating
		Class	Range	
Aquifer thickness (saturated) (m)	2	Large	> 10	10
		Medium	7.5-10	7.5
		Small	5-7.5	5
		Very small	< 5	2.5

Table 2.7 - Ratings adopted for the GALDIT parameter T

Computing the individual indicator scores, summing them and dividing them by the total weight give the GALDIT index:

$$GALDIT - Index = (w_1 * G + w_2 * A + w_3 * L + w_4 * D + w_5 * I + w_6 * T) / \sum_{1=1}^{6} w_i =$$

$$= (1 * G + 3 * A + 4 * L + 4 * D + 5 * I + 6 * T) / 15$$

The minimum and maximum GALDIT Index varies between 2.5 to 10. The vulnerability of the area to saltwater intrusion is assessed based on the magnitude of the GALDIT Index, as described in Table 2.8; the vulnerability map color is added for the proposed methodology.

Classification	GALDIT Index Range	Vulnerability Classes	Vulnerability map color
1	≥ 7.5	High vulnerability	Red
2	5-7.5	Moderate vulnerability	Orange
3	< 5	Low vulnerability	Yellow

Table 2.8 - Vulnerability Classes

The GALDIT method has got the same limitation of index methods, which mainly consists on subjectiveness and lack of theoretical underpinnings in converting hydrogeological characteristics into vulnerability to SWI. Nonetheless, the method is easy to apply and interpret to achieve a first-order assessment of vulnerability.

2.4 Elements and adverse consequences

The possible consequences of a contamination are evaluated on the wells (elements, E) by considering their use (agriculture, industrial, drinkable purposes) and their operational pumping values. As each wells has got a relative 'well capture zone' (Nobre et al., 2007), it is evaluated the relative 'influence' circular area centred in each pumping well; the radius of this area is a non-linear function of pumping rates (Bear, 1979).

In few words, the Elements which can be at SWI risk are detected on wells location and their purposes and production rates. The Elements rating considers the radius of influence areas, which can be depicted from typical cone of depressions in unconfined aquifers (Javandel and Tsang,1986; Fetter, 2001). However, in this study it is proposed a strong simplified scheme to rapidly assess the radius of the influence areas as function of pumping volumes; in Table 2.9 is illustrated the proposed configuration of Elements rating.

Pumping Wells		Radius	Pumping rate (m^3/y)	Elements map color
Purpose	Level			
Drinking	Very High	700 m	> 1,000,000	Red
		600 m	500,000 – 1,000,000	
		500 m	100,000 – 500,000	
		300 m	< 100,000	
Agricultural/ Drinking	High	300 m	< 100,000	Orange
Agricultural	Moderate	100 m	< 100,000	Green
Different uses (only sporadic)	Low	100 m	< 50,000	Blue

Table 2.9 – Elements rating

2.5 SWI Risk assessment

As the scope of the methodology is to map out zones that are prone to further SWI, the spatial overlay principle is applied to the hazard map (H, based on information deduced from numerical flow and transport simulations), the vulnerability map (V, based on the index method GALDIT and elements map (E, based on wells location and their purposes and production rates).

In order to evaluate the total SWI risk, the procedure is finalized by the means of simple risk matrix technique (Foster, 1987; Daly and Misstear, 2002; Zwahlen, 2004). In a first step, the hazard and vulnerability indices are aggregates in a "Risk intensity map", and in

the second step “Risk intensity map” is aggregates within Elements map in a “Total Risk map”. Table 2.10 and Table 2.11 illustrate the matrixes.

Hazard / Vulnerability	Very High	High	Medium	Low
High	Very High	Very High	High	Medium
Moderate	Very High	High	Medium	Low
Low	High	Medium	Low	Low

Table 2.10 – Risk intensity map matrix

Elements / Risk Intensity	Very High	High	Medium	Low
Very High	Very High	Very High	High	Medium
High	Very High	Very High	High	Medium
Medium	High	High	Medium	Low
Low	High	Medium	Low	Low

Table 2.11 – Total risk map matrix

Another possibility should be to combine the effects of the vulnerability and the hazard by using a mathematical approach, which results in smooth values (not classes) of infinitely variable risk values. This approach needs to achieve a very high precision through the overall procedure, but it is unlikely that the information available for the study site would permit such a precision; so that, in this study the simple above described approach is preferred.

2.6 Summary and conclusions

Although the proposed risk mapping procedure is theoretically useful, it is based on the underlying assumption of properly-weighted superposition of different single maps with different meanings; the synthesis of the results are static images, which clearly represents a limitation of the provided information.

SWI is a dynamic density-driven flow and transport non-linear process, and the results obtained by numerical modeling are strongly dependent on the modeling approach and assumptions, on field data quality and on the model calibration. It should be taken into

account that results may be biased by the chosen modeling approach, representing it a severe restriction in some cases.

However, the risk area maps resulting from this methodology can be adopted as a tool for the design of groundwater management schemes, as they are condensing relevant information from complex dynamic processes obtained from numerical simulations and visualize the results in simple and static maps. This can make it possible to decision makers, who are not familiar with groundwater dynamics, to access to such synthetic simple information.

Chapter 3 - A suite of computational tools to cope with SWI

In this study, an integration of computational tools including all the essential steps to develop and test management measures to restore groundwater quality in coastal aquifers, is presented. The proposed and used framework consists in:

- 3D modeling (coupled density-dependent groundwater flow and miscible salt transport in coastal aquifer) using CODESA-3D (Gambolati et al., 1999; Lecca 2000);
- automatic calibration of the hydrogeological model using PEST (Doherty, 2002);
- simulation/optimization model, to assess management and mitigation strategies for SWI, using a genetic algorithm (Carrol, 1996).

Simulation is based on a density-dependent advective-dispersive solute transport 3D-model, which allows to properly describing SWI problem in coastal aquifers. The calibration procedure is based on the coupling of the physical model with a nonlinear parameter estimation technique, allowing identifying an optimal set of parameters against field observed values by means of minimization of an objective function. In order to find out a set of plausible management solutions, what is usually done is to run a large set of simulations (each based on a previously calibrated hydrological model) with different management options as input. Genetic algorithm (**GA**) is used as the optimization technique in the proposed Simulation/Optimization model, which allows to identify optimal management schemes under user-prescribed conditions, namely management goals and constraints.

The integration of tools consists in a in-house model (CODESA-3D) and two open-source codes: PEST (available at http://www.pesthomepage.org/) and GA (available at http://cuaerospace.com/carroll/ga.html).

3.1 3D modeling with CODESA-3D

The COupled DEnsity-dependent variably SAturated groundwater flow and miscible salt transport 3D model (CODESA-3D) is a distributed, fully three dimensional, variably

saturated flow and miscible transport finite element model, accounting for spatial and temporal variability of model parameters and boundary conditions (Putti and Paniconi, 1995; Gambolati et al., 1999; Lecca, 2000). The flow and solute transport processes are coupled through the variable density of the filtrating mixture made of water and dissolved matter (salt, pollutants). The flow module considers the case of variably saturated porous medium, applicable both to the unsaturated (soil) and the saturated (groundwater) zone, while the transport module assumes the complete mixing between freshwater and saltwater bodies giving rise to a variably dense filtrating fluid with a non-reacting solute (salt). CODESA-3D solves the system in terms of pressure heads and concentration; derived from these fields, it is possible to examine water table levels, groundwater velocities and saltwater-freshwater mixing zone.

The CODESA-3D mathematical model is expressed in terms of two unknowns. The first one is the equivalent freshwater pressure head $\psi(x,y,z,t)=\frac{p}{\rho_0 g}$, where p is the pressure, ρ_0 is the freshwater density and g is the gravitational constant; a derived variable is the equivalent freshwater hydraulic head $h=\psi+z$, where z is the vertical coordinate directed upward. The second unknown is the normalized concentration of salt $c(x,y,z,t)=\frac{\tilde{c}}{\tilde{c}_{\max}}$, defined as the ratio between actual ($\tilde{c}$) and maximum ($\tilde{c}_{\max}$) absolute concentration of salt in the water solution. The value of $\tilde{c}_{\max}$ is the maximum concentration of salts in the system, and for saltwater intrusion problems it corresponds to the average salt concentration of seawater. In this model the variable density ρ of the solution is expressed by the linear function $\rho=\rho_0(1+\varepsilon c)$ where $\varepsilon=(\rho_S-\rho_0)/\rho_0$ is the density difference ratio and ρ_S the solution density at the maximum concentration $c=1$. The coupled system of variably saturated groundwater flow and miscible salt transport equations are:

$$\begin{cases} \sigma\dfrac{\partial\psi}{\partial t}=-\nabla\cdot\vec{v}-\phi S_w\varepsilon\dfrac{\partial c}{\partial t}+\dfrac{\rho}{\rho_0}q \\ \phi\dfrac{\partial(S_w c)}{\partial t}=-\nabla\cdot(c\vec{v})+\nabla\cdot(D\nabla c)+qc^*+f \end{cases} \qquad (3.1)$$

Where $\sigma(\psi, c)$ is the general storage term; t is time; ∇ is the gradient operator; $\vec{v}$ is the Darcy velocity vector; ϕ is porosity; $S_w(\psi)$ is the water saturation; q is the injected (positive)/extracted (negative) volumetric flow rate; D is the dispersion tensor, c^* is the normalized concentration of salt in the injected/extracted fluid, and f is the volumetric rate of injected/extracted solute that does not affect the velocity field.

To complete the mathematical formulation of the flow and transport problem, initial and Dirichlet, Neumann, or Cauchy boundary conditions are added.

For a comprehensive description of the mathematical and numerical model of the CODESA-3D the reader is referred to Gambolati et al. (1999). The model has been applied to several coastal aquifers in the Mediterranean basin affected by seawater intrusion problems (Lecca et al., 2001; Paniconi et al., 2001; Cau et al., 2002; Kerrou et al., 2007; Qahman et al., 2009). CODESA-3D is the computational engine of the grid-enabled Web demonstrative hydrology application AQUAGRID (http://grida3.crs4.it).

3.2 Automatic calibration coupling CODESA-3D with PEST

The Usually a 3D-SWI model is not simple to develop, mainly due to the complexity of the involved physical processes, the basin geometry and heterogeneity of hydrogeological characteristics (Carrera et al., 2009). Several difficulties must be faced in the modeling procedure, e.g.: aquifer characterization, caused usually by scarcity of adequate hydrogeological field data which drives to many unknown parameters (recharge, boundary conditions,...); spatial and temporal variability of natural processes; the need for solving two coupled non-linear equations (1); and often low sensitivity of state variables (e.g. heads and concentrations) to aquifer properties. A fundamental and complex step in the process of understanding aquifer behaviour is the calibration procedure, which aims to estimate some aquifer parameters, such as hydraulic conductivities, which are usually basic elements in order to determine underground flows. Calibration can be considered an integral part of the process of modeling and developing understanding of a hydrogeological system (Poeter and Hill, 1997; Hill, 1998); thus, it is becoming a standard part of model application.

For a long period, the calibration of hydrological model has been performed manually, by trial-and-error parameter adjustment, which requires a strong knowledge of the system

and entails a high subjectivity about the goodness-of-fit of the parameter values. Eventually, it can be a very long-time-consuming task. In the last decades manual calibration has been slowly substitute by automatic calibration, which facilitates enormously the task of modeling, reducing both the subjectivity and the computing time involved in the calibration procedure. A large set of softwares, classified as based either on local (e.g. gradient methods) or global (e.g. Genetic Algorithm (GA), Shuffled Complex Evolution (SCE) algorithm (Duan et al., 1992), and Simulated Annealing (Sumner et al. 1997) search strategies, can be found in the scientific literature, and they can be relatively easily linked to the physical model. Due to all these features and to the large increase of computing power, in the last years automatic calibration has become a typical procedure in the field of hydrogeological modeling.

Among these models, in this study it is adopted PEST (Doherty, 2002), which can be used to estimate parameters for about any existing computer model, even if a user has not access to the model source code. It is currently being used in many science and engineering fields and, in particular, it has become a groundwater industry standard and used to implement automatic calibration modules in some of the most popular computer codes, such as MODFLOW (McDonald and Harbaugh, 1988) and SWAT (Arnold et al., 1993).

All these peculiar features are the motivation of the coupling of PEST with the CODESA-3D model (Lecca, 2004; Lecca and Cau, 2006), to create an overall optimization model (Figure 3.1). In this integrated procedure PEST iteratively reads state variables (e.g. h) from the output files produced by the CODESA-3D model and finds optimal model parameters (e.g. K) minimizing the objective function Φ:

$$\Phi = \sum_{i=1}^{NC} w_i (h - \bar{h})_i^2 \qquad (3.2)$$

i.e. the sum of square weighted residuals between simulated (h) and field measured ($\bar{h}$) state variables at NC control points; the variable h is time dependent, and, although not remarked, it is not a linear variable. The weight associated to w_i (which usually has a default equal to 1) depends on the relative importance of the observations, making it possible to assume some measurements more important than others in determining the optimization outcome. Minimization is based on the gradient-based Gauss–Marquard–

Levenberg (GML) algorithm (Levenberg, 1944; Marquardt, 1963). While for linear models the GML algorithm can give the optimal parameter set just in one iteration, for non-linear models like CODESA-3D the procedure is iterative (Figure 3.1); at each iteration, the relationship between selected model parameters (inputs) and model-generated observation (outputs) is linearized by the means of the Taylor expansion about the actual best parameter set, hence the derivatives of all outputs with respect to all parameters are calculated. Then the linearized problem is solved for a better parameter set and this set is tested by a new model run. The iterative procedure is stopped when the objective function reduces to a minimum corresponding to a user-defined threshold; however, as this value usually can be not prior assessed, the optimization process can be also terminated after a certain number of iterations, if since over the last n (default used value is 3) successive iterations the objective values are within a relative distance prescribed by a termination criteria control variable.

The correlation coefficient (R) is another measure of goodness of fitness; it is independent from the number of observations involved in the parameter estimation process, and also from the levels of uncertainty associated with observations. Generally an acceptable value of R should be above 0.9 for the fit between model outputs and observations (Hill, 1998). This coefficient is calculated as:

$$R = \frac{\sum_i (w_i c_i - m)(w_i c_{oi} - m_o)}{\left[\sum_i (w_i c_i - m)(w_i c_i - m) \sum_i (w_i c_{oi} - m_o)(w_i c_{oi} - m_0) \right]^{1/2}} \quad (3.3)$$

where c_i is the *i-th* observation value, c_{oi} is the model-generated counterpart to the *i-th* observation value, m is the mean value of weighted observations, m_o is the mean of weighted model-generated counterparts to observations and w_i is the weight associated with the *i-th* observation.

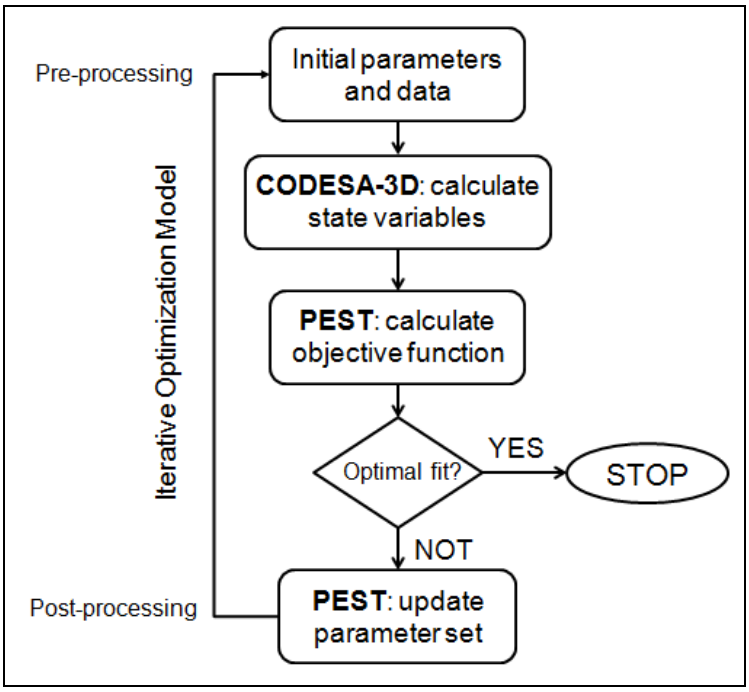

Figure 3.1 – CODESA-PEST module

The final output of PEST reported the detailed record of the process, in which the optimized parameter values (e.g. K) are printed within the 95% confidence limits; also, there is the possibility to analyse the parameter covariance and the correlation coefficient matrices calculated during the overall process. Other important outputs are represented by *parameter sensitivity*, which measures composite changes in outputs generated by variations in the value of the parameter, and *observation sensitivity*, which measures all adjustable parameters change that followed by changes in the value of real observation. Parameter sensitivity is useful in order to identify the parameters that could degrade the performance of the optimization process through lack of sensitivity to outputs, while observation sensitivity is useful to identify observations that are more important to the inversion process due to their information content. The analysis of this information could help the modeler to refine the conceptual model of the studied system, to better exploit available data, and also to eventually plan field campaigns of data acquisition.

3.3 Simulation/optimization method

For coastal aquifers whose SWI is quite critical, a management scheme to control the phenomenon needs to be assessed (Zhou et al, 2003), and in the evaluation of it, the support of a simulation/optimization tool could be helpful (Das and Datta, 1999).

The final goal of a simulation model is to help the understanding of the behaviour of the modeled system and then to enhance the possibility to find out a good management scheme of the system. Groundwater simulation models can simulate the response of the hydrogeological system to a specified set of input. So that, in order to identify the optimal management strategy for the system, it is necessary to set up several different management schemes, to test their feasibility through the simulation model and then choose the best one analysing the set of results coming from all different scenarios. Like the manual calibration procedure, this method requires a long computing and post-processing time due to a large amount of data.

A possible solution to ensure both a strong reduction in the time needed and a robust solution of the problem is the use of an optimization model, which is used to identify the best possible choice from a set of feasible alternatives. It usually uses mathematical expressions of the problem to minimize or maximize some objective functions, which are frequently restricted by constraints on the values of the variables. Several authors (Shamir et al., 1984; Willis and Finney, 1988; Cheng et al., 2000) showed the use of optimization approach in the solution of SWI problems; when simulation and optimization models are combined, they demonstrate all their power (Das and Datta, 1999). Groundwater simulation models can be linked with optimization techniques in a single framework to overcome the weakness of using simulation or optimization alone; by the means of this coupled system, the modeler can specify the desired values of the water-resource system (such as minimum groundwater head levels or maximum allowed groundwater salt concentration) and the S/O model determines, from a set of possible strategies, a single management scenario (i.e. pumping strategy) that best fits the modeler's desired values. The linkage techniques used to combine these models can be based on binding constraints in the optimization model (embedding technique), or by using a response matrix (Gorelick, 1983; Ndambuki et al., 2000; Yang et al., 2001) or by an external linkage of simulation and optimization model (Das and Datta, 2001). Due to the complexity and

non-linearity of the process of SWI in coastal aquifer, the embedding technique (which become dimensionally too large also for interconnected PCs, considering the usual possibility of higher resolution along the spatial and temporal scales) and the response matrix approach seem to be inadequate to be linked with the relative model simulation. Therefore, as an alternative, it is possible to link SWI simulation model with a general purpose optimization-based management tool using the simulation/optimization approach (Barlow, 2005; Bhattacharjya and Datta, 2005).

3.3.1 Genetic algorithm (GA)

In many science and engineering fields, such as chemical engineering and mechanics (Carroll, 1996), have been tested successfully the so-called Global Optimization (GO) techniques, such as the Genetic Algorithms (GA), the structure of which is proved to be relatively simple (Goldberg, 1989). GAs are a family of combinatorial methods that search for solutions of complex problems using an analogy between optimization and natural selection. GAs are inspired by Darwin's theory about evolution, where the strongest offspring in a generation are more likely to survive and reproduce. At the beginning of the algorithm, a large population (initial population) of random chromosomes is created. The initial population is formed by individuals, which represent possible solutions that are selected within the predetermined lower and upper bounds of each model parameter to be optimized. Solutions from one population are taken and used to form a new population. This is motivated by the hope that the new population will be better than the old one. New generation of individuals are reproduced from the old generation through random selection, crossover and mutation based on certain probabilistic rules. The selection is made according to solutions fitness (objective function): the more suitable they are the more chances they have to reproduce. Gradually, the population will evolve toward the optimal solution.

Qahman et al. (2005) linked the density-dependent variably saturated groundwater flow and salt transport CODESA-3D model and the D.L. Carroll's FORTRAN Genetic Algorithm (GA) Driver (1999, http://cuaerospace.com/carroll/ga.html); in this S/O procedure the decision variables, tested for optimality, were pumping rates and the objective function and constraints were based on potential head and salt concentrations at

the wells, respectively; only steady state conditions were examined. Alnahhal et al. (2010) adopted a different S/O model considering transient-state conditions, to find out optimal management schemes for a small square area of the Gaza Strip aquifer system subjected to SWI.

3.3.2 Simulation/Optimization model coupling CODESA-3D with GA

The S/O model is the last module of the proposed framework, in which the main idea of the procedure is to test the feasibility of management options by the means of the framework of Pareto optimality, considering two conflicting objectives: maximizing pumping rates from the aquifer wells while limiting the salinity of the water withdrawn.

The operational scheme of the Simulation/Optimization model is described in Figure 3.2. In this S/O model, the decision variables, tested for optimality, are pumping rates, while constraints and objectives functions are setup by the means of a weighted sum, as proposed by Qahman (2004), which incorporates two objectives into a single scalar objective function, subjected to constraints. The resulting optimization model generally reads:

$$Max\ Z = w_1 \sum_{i=1}^{n} Q_i - w_2 \sum_{i=1}^{n} Q_i C_i \qquad (3.4)$$

where $i = 1,..,n$ is the well index, w_1 and w_2 are the sum weights, and the design variables Q_i (decision variables) and C_i (modeled variables) represent the discharge rate and the salt concentration at the *i-th* well, respectively.

Constraints to equation (4) are: $0 \le Q_i \le Q_{\max}$, with the maximum discharge given by the aquifer safe yield divided by the number of pumping wells, and $0 \le C_i \le C_{\max}$.

GA parameters has been setup following the recommendation by Carroll (1999) as follows: population size (i.e. how many set of possible solutions (chromosomes) are in population in one generation) set as 5; maximum generations number set as 200, according to results from Qahman K. (2004) and Alnahhal et al. (2010), and based on a parametric analysis showing that the fitness value is not changed by further increasing the number of generations; crossover and mutation probabilities, set as 0.5 and 0.02, respectively. GA parameters are summarized in Table 3.1.

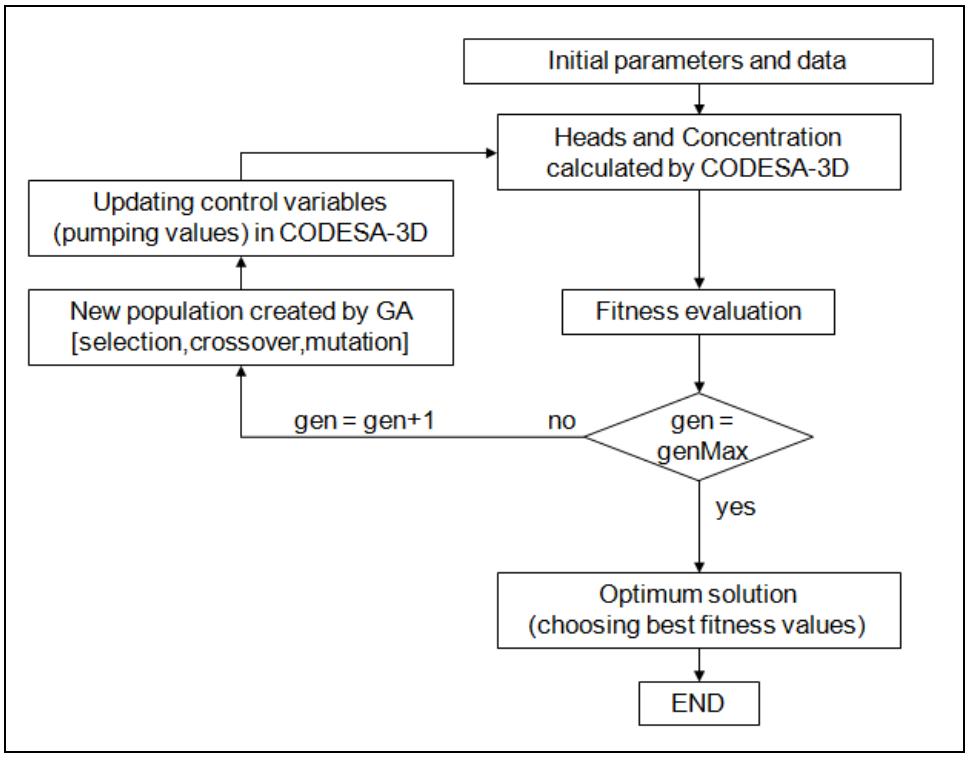

Figure 3.2 – CODESA-3D–GA module

Pumping weight w_1	Salinity weight w_2	Individual length	Population size	Max generations number	Crossover probability	Mutation probability
1	1-200	96	5	200	0.5	0.02

Table 3.1 – GA parameters (from Alnahhal et al. (2010))

In this configuration, CODESA-3D is run 1,000 times (i.e. 5 possible solutions multiplied to 200 generations).

The relative weights in equation (4) are determined by means of a parametric trade-off calculation. Set w_1 equal to 1, the model has to be run in transient-state several times with changing w_2 values in the range 1-200. The optimal value of salinity weighting parameter w_2, as shown in Figure 3.3, ensures maximum total pumping (which corresponds to high percentages of the possible total pumping amount) while a total salt mass extracted (which depends on feasible values of salt concentrations) within the reasonable limits of the feasibility region.

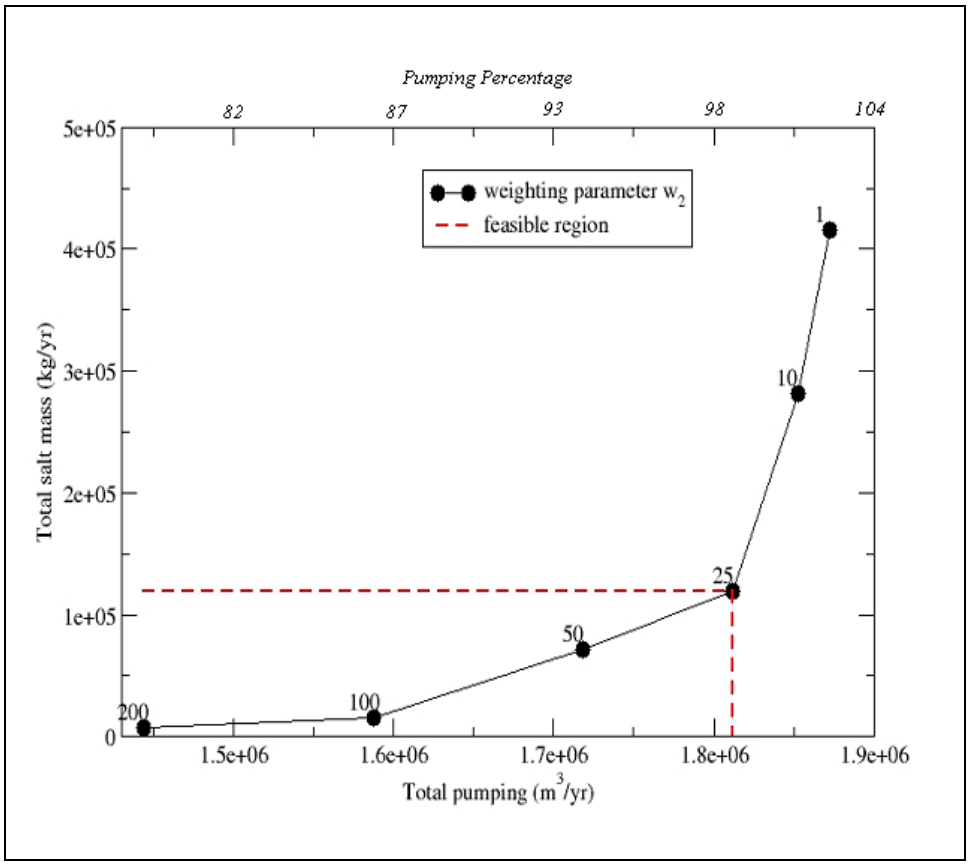

Figure 3.3 – Trade-off curve (from Alnahhal et al. (2010))

Assessing the optimal relative weighting is needed to ensure the goodness of the fitness function, so that this procedure has to be properly evaluated before starting the S/O model.

3.4 Summary and conclusions

A common contamination occurrence in coastal aquifers is Salt Water Intrusion (SWI), which can be exacerbated is the aquifer is overexploited. This phenomenon, which can bring to very low quality of groundwater, can be modeled by developing a groundwater flow and transport model, and eventually use it for assessing the management strategies to minimize the occurrence of saltwater intrusion.

In this study, an integration of computational tools including all the essential steps to develop and test management measures to restore groundwater quality in coastal aquifers, is presented. The integration of computational tools designed to assess saltwater intrusion in coastal areas and to manage groundwater resources under natural and human induced

stresses. The proposed and used framework consists in 3 interconnected modules: 1) 3D hydrogeological modeling, 2) automatic calibration procedure and 3) simulation/optimization technique.

The first module is simulation, performed with the CODESA-3D model (Gambolati et al., 1999; Lecca, 2000), a distributed, fully three dimensional, density-dependent variably saturated groundwater flow and miscible salt transport finite element code. The automatic calibration procedure (2nd module) is based on the external coupling of the simulation and optimization (PEST; Doherty, 2002) modules. PEST code is configured to read state variables from the model outputs and to provide new estimates for selected model parameters, by means of a minimization process of the square differences between simulated and measured values at selected control points. The third module is the simulation/optimization model, based on the coupling of a genetic algorithm (GA, Carroll 1999) with the simulation model.

The integration of tools consists in one in-house model (CODESA-3D) and two open-source codes: PEST (available at http://www.pesthomepage.org/) and GA (available at http://cuaerospace.com/carroll/ga.html).

Chapter 4 - The Gaza Strip Study Area

The Gaza Strip is a semi-arid region located in the Mediterranean basin; it covers a long and narrow rectangular coastal area of about 365 km^2 between Egypt and Israel.

The Gaza coastal aquifer is the main source of water for agriculture, domestic, and industrial purposes in Gaza Strip. An estimated 1.5 million people live in Gaza by the end of 2010, with a density of about 4,500 people/km^2, making it one of the most overcrowded areas in the world. Due to the continuous population growth, the total water demand in the Gaza Strip is strongly increasing. Nowadays, the need of water is not satisfied by the available resources, and this is causing a huge deficit between water demand and supply (Qahman and Larabi, 2006).

Also, making the aquifer overexploited, the problem of SWI is so exacerbated that corrective measures are needed to restore groundwater quality and properly manage the aquifer. During the last decades several studies have been carried out to analyze Salt Water Intrusion in the Gaza Strip (Yakirevich et al., 1998; Melloul and Collin, 2000; Moe et al., 2001; Qahman and Larabi, 2006), but the aquifer quality situation is so critical (Shomar et al., 2010) that this problem is still a long way from being solved.

4.1 Background and problem statement

The Gaza Strip lies on the Eastern coast of the Mediterranean Sea, within the Middle East; it is a part of the Palestinian coastal plain, where it forms a long and narrow rectangle; its length along the cost is approximately 40 km and its width ranges from 6 to 12 km. It is located between longitudes 34° 2" and 34° 25" east, and latitudes 31° 16" and 31° 45" north, on the most south-eastern coast of Palestine on the Mediterranean Sea. The total area is estimated to be about 365 Km^2.

It has a 51 km border with Israel in the east and north, and an 11 km border in the southwest with Egypt, near the city of Rafah. Khan Younis is located 7 km northeast of Rafah, and several towns around Deir el-Balah are located along the coast between it and Gaza City. Beit Lahia and Beit Hanoun are located to the north and northeast of Gaza City, respectively.

The territory takes its name from Gaza-city, its main city and administrative centre; the Gaza Strip is subdivided in 5 governorates under the jurisdiction of the Palestinian National Authority (PNA).

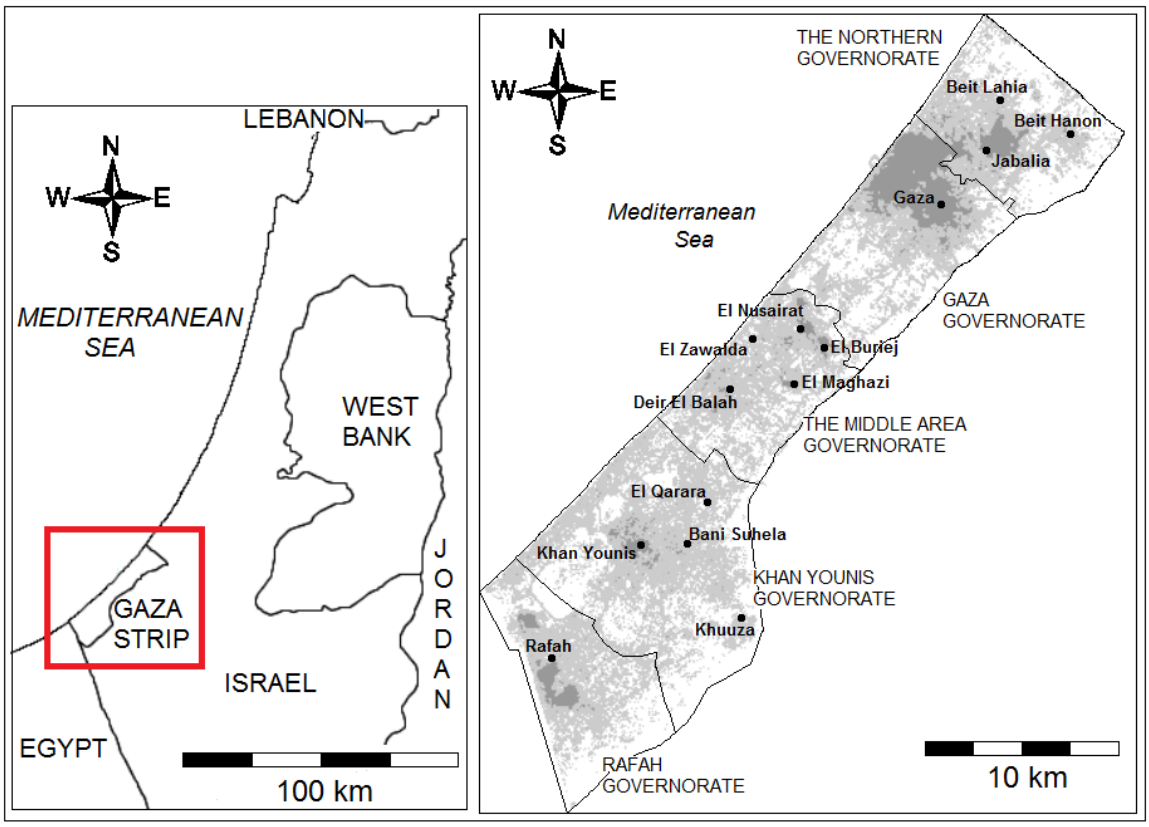

Figure 4.1 –The Gaza Strip

The growth and population distribution of the Gaza Strip have been strongly influenced by historical and political developments. Estimates for the population changes in the Gaza Strip were done by the Palestinian Ministry of Planning and the Palestinian Bureau of Statistics. Until 1947, the Gaza Strip's population did not exceed 80,000 people, but since 1960's there has been no official population count conducted in the Gaza Strip. The total Palestinian population in Gaza strip by the end of 1997 was approximately 1 million; by the year 2007 the population had increased by 39%, reaching 1.42 million people. An estimated 1.5 million people live in Gaza by the end of 2010, with a density of about 4,500 people/km^2, making it one of the most overcrowded areas in the world (Palestinian Central Bureau of Statistics -PCBS, 2006). Considering the nowadays population growth rate of about 3.5%, by year 2035 the population will reach a total

number of about 3,7 million. This rate plays a big role in the planning and management of water resources, being water consumption in strong relationship within demography (Alnahhal, 2009). The abstraction rates have increased over the last three decades, due to inadequate available water imports to Gaza, expanding population and the drilling and use of unlicensed wells; this over-abstraction has caused saline intrusion and this problem is becoming rapidly worse over time. A second problem is due to contamination of the shallow groundwater from activities at the surface or near-surface of the land in Gaza, arising mainly from wastewater (Shomar et al., 2010), characterized by high levels of nitrates in the groundwater. The result of these problems in combination is that the water quantity available to the population in Gaza is inadequate, and the water quality falls well short of accepted international guidelines for potable resources (i.e. for use as drinking water, or more broadly for domestic use).

On the basis of modeling future water quality, it has been stated that the Gaza groundwater will soon become so contaminated that its entire volume will cease to be available for use ('aquifer failure').

4.2 Meteorological data

The Gaza Strip is located in the transitional zone between a temperate Mediterranean climate in the west and north, and an arid desert climate of the Sinai Peninsula in the east and south. The Gaza Strip has got a semi-arid Mediterranean climate with a long hot and dry summer subject to drought, and short cool and rainy winter.

4.2.1 Temperature, humidity and solar radiation

The average mean daily temperature ranges from 26°C in summer and 12°C in winter. The annual mean of air temperature, annual mean of maximum air temperature, and the annual mean of minimum air temperature is 21.0 ºC, 23.6 ºC, and 17.7 ºC respectively as observed in the meteorological station of Gaza city in 2005 (PCBS, 2006). Temperature gradually changes throughout the year, and reaches its maximum in August (summer) and its minimum in January (winter); average of the monthly maximum temperature ranges from about 17.6 ºC for January to 29.4 C° for August. The average of the monthly minimum temperature for January is about 9.6 ºC and 22.7 ºC for August.

The daily relative humidity fluctuates between 65% in daytime and 85% at night in summer, and between 60% and 80% respectively in winter. The mean annual solar radiation amounts to 2,200 J/cm^2/day.

4.2.2 Rainfall

Regarding the rainfall data and measurements of Gaza Strip, there are two well defined seasons: the wet season, starting in October and extending into April; and the dry season, extending from May to September. Actually, the rainy season extends from about mid-October to the end of March, with essentially no rain falling in the remaining months.

Precipitation data of 12 raingauging stations for the period from 1973 to 2010 show a Mean Areal Rainfall (MAR) over the last period equal to around 300 mm/y, according to isohyetal method; the average annual volume of rainfall over the Gaza Strip is calculated to be around 120 Mm^3/y, where nearly 50% of this amount is harvested in both December and January from each year. Annual average rainfall varies considerably across the Gaza Governorates, from about 440 mm/y at the north-eastern border (Beit-Lahia station) to around 220 mm/y in Rafah at the south-western border with Egypt. On the other hand, for the same station there are very significant variations from year to year; the annual rainfall shows a significant spatial variation over the Gaza Strip climatic station for the period 1973 to 2010.

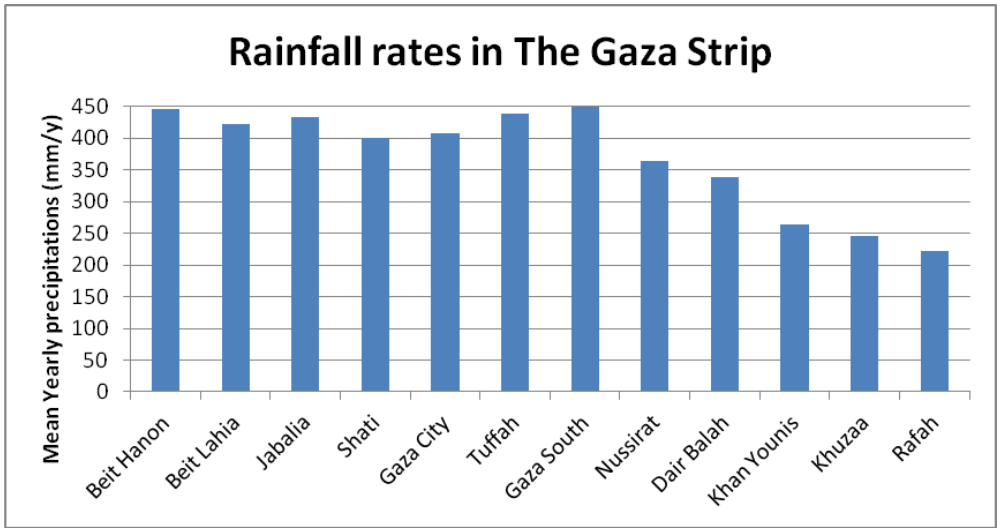

Figure 4.2 – Mean yearly rainfall rates measured in the rainfall gauging station in the Gaza Strip.

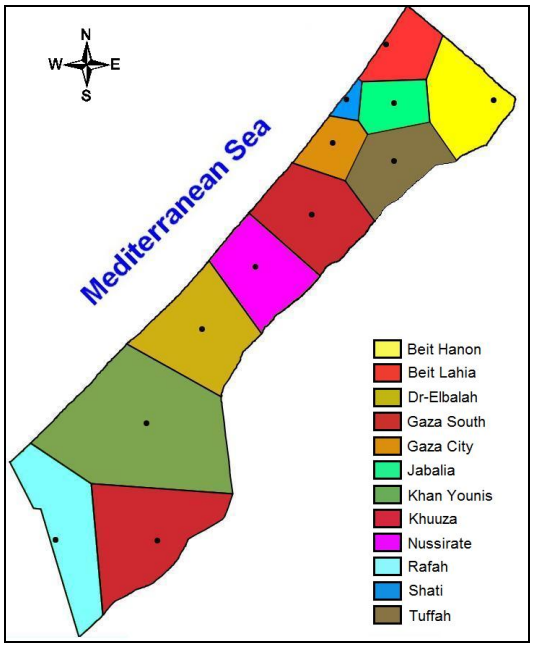

Figure 4.3 – Rainfall stations with relative Thiessen polygons in the Gaza Strip.

In the past, the porous soils of much of the Gaza region easily absorbed most of this rainfall and provided the primary source for recharging the groundwater aquifer of the region, especially along the coastal where sand dunes are the main soil structure. There are no natural depressions in the area except in Wadi Gaza, which crosses the middle of the strip from east to west and is connected to the sea. There are some wadis, like Wadi Salqa in the south, which have no connection to the sea. Most of the urban areas of the Gaza Governorates do not have a natural drainage outlet because of their low lying topography. Heavy rainfall causes storm water to collect in low areas and flood streets and walkways. Rapid growth has decreased the open areas available for percolation of rainwater and has greatly increased the runoff to low lying areas.

4.2.3 Evaporation and evapotranspiration

The mean monthly evaporation in Gaza Governorates varies significantly throughout the year. The monthly average potential evaporation over 25 years in Gaza varies between maximum of 174 mm in July and minimum of 63 mm in January, with an annual average potential evaporation of 1,300 mm. Evaporation rates for the Gaza Strip are assessed within Penman-Monteith method, detailed described in Appendix B, which also illustrate an application to the Gaza Strip site.

4.3 Topography and soil

Land surface elevations gradually slopes downwards from east to west, ranging from the eastern highest point Abu 'Awdah (Joz Abu 'Auda), at 105 meters above the mean sea level, to the mean sea level in the west. The terrain is flat or rolling, with dunes pushing in from the coast towards east, particularly in the southern part of the Gaza Strip. The Gaza topography (Figure 4.4) is characterized by elongated ridges and depression parallel to the coastline, dry streambeds and sand dunes. The ridges and depressions generally extend in a NNE-SSW direction, parallel to the coastline; they are narrow and consist of "Kurkar" sandstone. The sand dunes are 30-60 m above mean sea level and cover a total area of 70 km^2; the surface elevations of individual ridges range between 20 m and 90 m above mean sea level.

The major depressions are filled with alluvial sediments from storm water. The parallel Kurkar ridges have been dissected by Wadi Gaza, the largest surface water feature in Gaza which rarely flows due to water diversion at the east of Gaza borders by Israelis.

The soil in the Gaza Strip is mainly composed by sands, clay and loess (Figure 4.5, Table 4.1); different values of recharging coefficients represent the fraction of net recharging rain which actually infiltrates into the aquifer, taking into account also land use features.

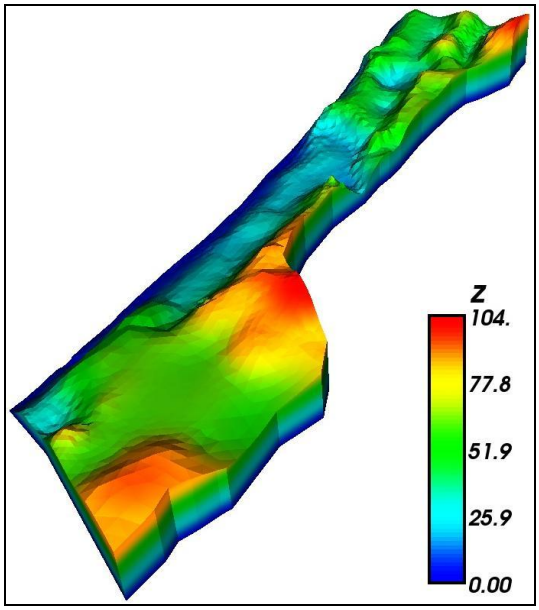

Figure 4.4 – The Gaza Strip topography

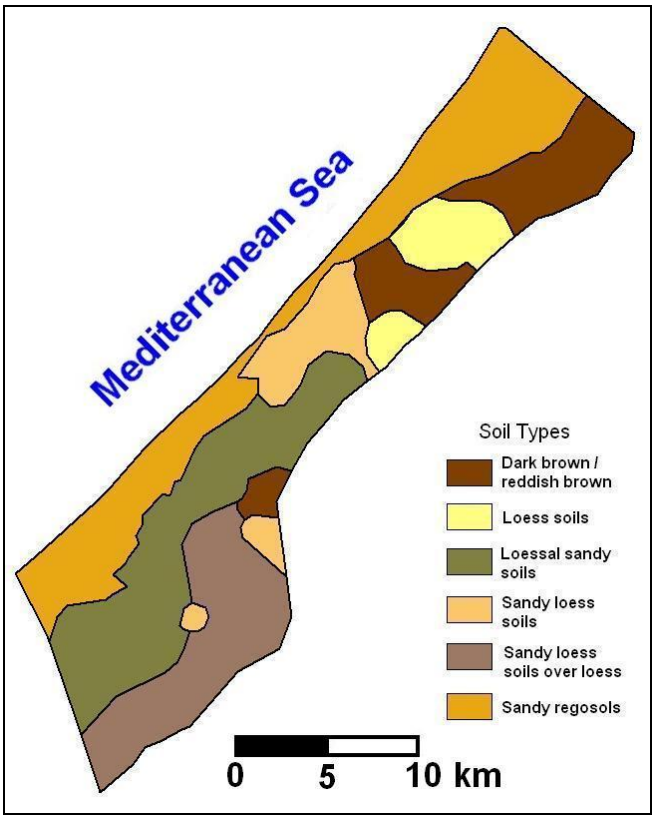

Figure 4.5 – The Gaza Strip soil map (1996)

Soil types	Area (km^2)	Area (% of total)	Recharge coefficient (C_{rech})
Dark brown / reddish brown	50.61	13.9	0.025
Sandy regosols	107.29	29.4	0.70
Loess soils	23.9	6.6	0.15
Sandy loess soil	34.09	9.3	0.30
Loessal sandy soil	82.46	22.6	0.25
Sandy loess soil over loess	64.68	17.8	0.35
Total	364.26	100	

Table 4.1 –Soil types in the Gaza Strip

Along the coast there is a zone of varying thickness with rather uniform dune sands while more inland there are zones consisting of loess loamy soils. The sand dunes extend up to 4-5 km inland, and are wider in the north and in the south than in the centre. Further inland to the east, the soil becomes less sandy with more silt, clay and loess.

The sand soil forms the majority of the area (around 80% of total area) and it is located along the coastline from south to the northern border of the Strip, with a thickness ranging from 2 meters to about 50 meters; usually it is in the form of sand dunes

overlying alluvial soils in a shallow layer creating ideal conditions for fruit plantations. The sand in study area is further of regosols and sandy loess types.

Clay soil is mainly located in the north-eastern part of the Gaza Strip, and it is of dark brown or reddish brown types. Loess soil is found around Wadis, where the approximate thickness reaches about 25 to 30 meters.

4.4 Land Use

The land use and land cover (LULC) map of Gaza strip in 2004 and 2010, obtained using remote sensing data and ground observations are shown in Figure 4.6. In Table 4.2 is illustrated a comparison of calculated LULC total surface and percentages for the two years; in 2004, 'olive orchards' class is included in 'mixed agriculture' class (from CLIMB project deliverables).

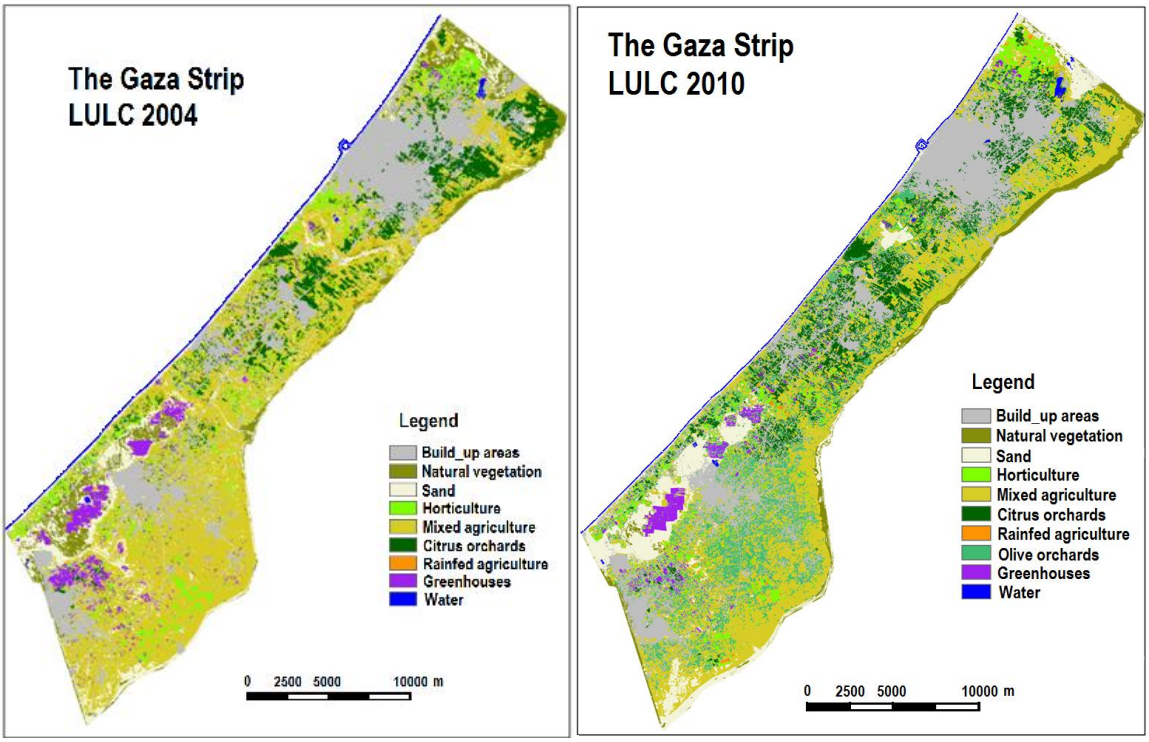

Figure 4.6 – LULC for The Gaza Strip: 2004 (left) and 2010 (right).

The land is scarce and the pressure on it is increasing rapidly for all kinds of uses; urban, industrial, and agricultural uses. Nowadays, agricultural land occupies about 225 km^2 and the urbanized area about 90 km^2, representing respectively around 62% and 25% of the total area of the Gaza Strip. Future expansion is expected for the domestic use only,

producing an increase of total amount of rainwater losses due to urbanization as surface run-off and resulting in an increasing pressure on underground water resources

Class name	Area (ha) 2010	% 2010	Area (ha) 2004	% 2004
Water	-	-	-	-
Built-up areas	9151	25.0%	8370	22.8%
Natural vegetation	1265	3.5%	2424	6.6%
Horticulture	1775	4.8%	2363	6.5%
Greenhouses	814	2.2%	1365	3.7%
Sand	3539	9.7%	4263	11.6%
Citrus orchards	3646	9.9%	3182	8.7%
Rainfed agriculture	335	0.9%	152	0.4%
Mixed agriculture	11323	30.9%	14543	39.7%
Olive orchards	4814	13.1%		
Total	36662	100.00%	36662	100.00%

Table 4.2 - Comparison of calculated LULC total surface and percentages of Gaza Strip in 2004 and 2010; in 2004, 'olive orchards' class is included in 'mixed agriculture' class.

4.5 Hydrogeology

Three valleys (Wadis) are crossing Beit Hanoun, Gaza and Salga areas forming the hydrological feature of the area. The Wadi Gaza is the biggest one, running in the central part of the Gaza Strip and discharging into the Mediterranean Sea. Nowadays, as Israel has retained and changed the course of the three Wadis, they have become dry.

4.5.1 The coastal aquifer geology

The coastal aquifer of the Gaza strip is a part of a regional groundwater system covering Israel and Egypt areas (Figure 4.7); it extends alongside the Mediterranean Sea for 120 km from Mountain in the north Israel to Gaza Strip and Sinai in the south, and its width varies between 7 to 20 km. The aquifer extends only 40 km long in the Gaza Strip.

The regional area consists of a littoral zone, a strip of younger dunes situated on top of a system of older Pleistocene beach ridge, and to the east alluvial and loessial plains. The main aquifer is composed of calcareous sandstone with a thickness varying from about 120 m at the shoreline to few meters in the east (US Geological Survey, 1998).

The geology of the Gaza Strip area consists of a series of Mesozoic to the Quaternary geological formations sloping gradually from east towards the west. It is a Pleistocene-age granular aquifer (Kurkar Group), formed by marine and eolian calcareous sandstone ("kurkar"), reddish silty sandstone ("hamra"), silts, unconsolidated sands and conglomerates with intercalation of clay of marine origin and loam. Some of them are lenses which are randomly distributed in the area, causing local perched water conditions

(Shomar et al., 2010); others begin at the coast, extending 2-5 km inland, and separate the aquifer into various subaquifers, indicated as A, B and C (Figure 4.8).

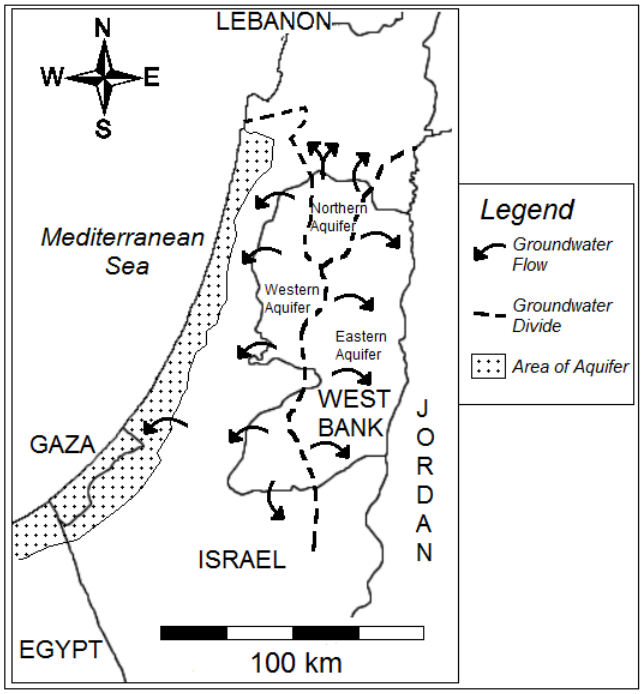

Figure 4.7 – Regional aquifer system

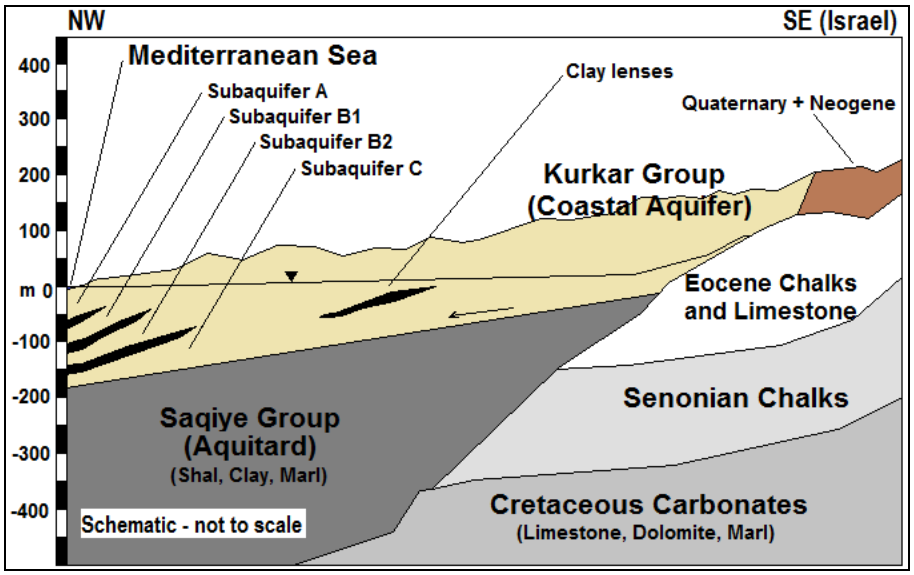

Figure 4.8 – Schematic geological cross-section through the study area; this cross-section could be located anywhere in the GCA, although the existence and position of the subaquifers, clay lenses and aquitards vary from north to south; arrow within the section indicates the direction of undisturbed groundwater flow driven by slope of the water table

Subaquifer A is phreatic, whereas B and C become confined toward the sea. The aquifer overlies marine clay of Neocene age, known as Saqiya Clay aquiclude, which is the bottom of the aquifer. The average thickness of the aquifer body is about 150 m, reaching its maximum of about 200 m near Gaza city and its minimum of about 20 m in the eastern part (landward boundaries) and in the south, near the city of Rafah.

4.5.2 Hydraulic proprieties of the Gaza Aquifer

Several pumping test campaigns have been carried out to determine hydraulic parameters. There are more than 5,000 wells within the borders of Gaza strip, but only few municipal wells screened across more than one subaquifer have been tested to determine hydraulic parameters. From results of pump tests carried out, aquifer transmissivity values range between 700 and 5,000 m^2/d. Corresponding values of hydraulic conductivity (K) are mostly within a relatively narrow range of 20-80 m/d. Little is known about any differences in hydraulic properties with depth or between the different sub-aquifers. Specific yield values are estimated to be about 15-30 percent while the storativity is about 10^{-4} from tests conducted in Gaza. A study by University of Gaza in year 2002 in north of Gaza to estimate these parameters indicated a transmissivity value of 2,400 m^2/d, an average hydraulic conductivity of 32 m/d, and a specific yield of 0.24 which are in the range of values measured from the Coastal Aquifer Management Plan (CAMP) project.

4.5.3 Groundwater Flow and Water Levels

The undisturbed regional groundwater flow is mainly perpendicular to coastline (Moe et al., 2001), with a general direction east towards west, where fresh groundwater discharges to the Mediterranean Sea. Locally flow patterns are strongly disturbed by overpumpings; large cones of depression are located in different areas within the Gaza Strip, i.e. near Gaza city in the north and Khuzaa and Rafah in the south, causing water levels below mean sea level and producing hydraulic gradient from the Mediterranean Sea towards the major pumping wells (usually municipal).

Representations of the 1935 and 2010 flow field are presented in Figure 4.9 from which it is possible to highlight the general decrease of groundwater levels in time. The actual situation shows, in the northern part of Gaza, water levels ranging from about 10 meters above mean sea level at the eastern border to mean sea level along the shore; in the

southern part, the water level gradient is steeper, from about 20 meters above sea level near the eastern border to mean sea level along the shore.

The overexploitation of the coastal aquifer is leading to a constant drop in the water level, which can be estimated to be about 20-30 cm each year.

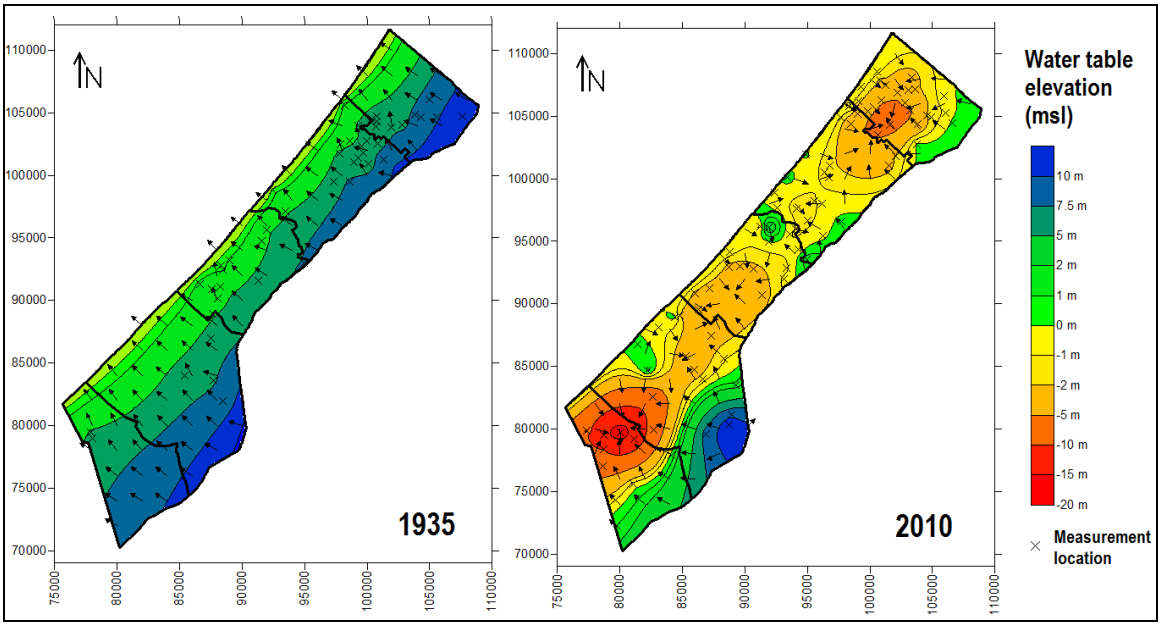

Figure 4.9 - Representation of 1935 (left) and 2010 (right) water flow

4.5.4 Groundwater Quality

Groundwater quality in the Gaza aquifer is considered generally poor. About 5,000 wells are located in the area, but most of them are not anymore suitable for drinkable purpose because the quality of the extracted water is very low, exceeding WHO standards both for chlorides (250 mg/l), due both to pollution and Salt Water Intrusion, and for nitrate (50 mg/l), this latter caused quite exclusively by pollution. So that, two main problems currently challenge the groundwater resources in Gaza Strip area: a) progressive salinity of water extracted from wells which exceeds WHO standards and b) raising of nitrate levels in the drinking water.

4.5.4.1 Groundwater salinity and Salt Water Intrusion

Groundwater salinity is considered to be one of the most pressing problems of the water supply system.

The analysis of salinization patterns in most areas of the coastal aquifer, in terms of chlorides concentrations, indicates a pronounced acceleration of salinization rates.

Contour maps representation of 1935 and 2010 groundwater chlorides concentration (taken at the depth of control wells, whose depth ranges from20 to 100-120 m below the land surface) are illustrated in Figure 4.10; it is interesting to note current large areas of lower chlorides concentrations close to the southern coastline, where there are located several greenhouses.

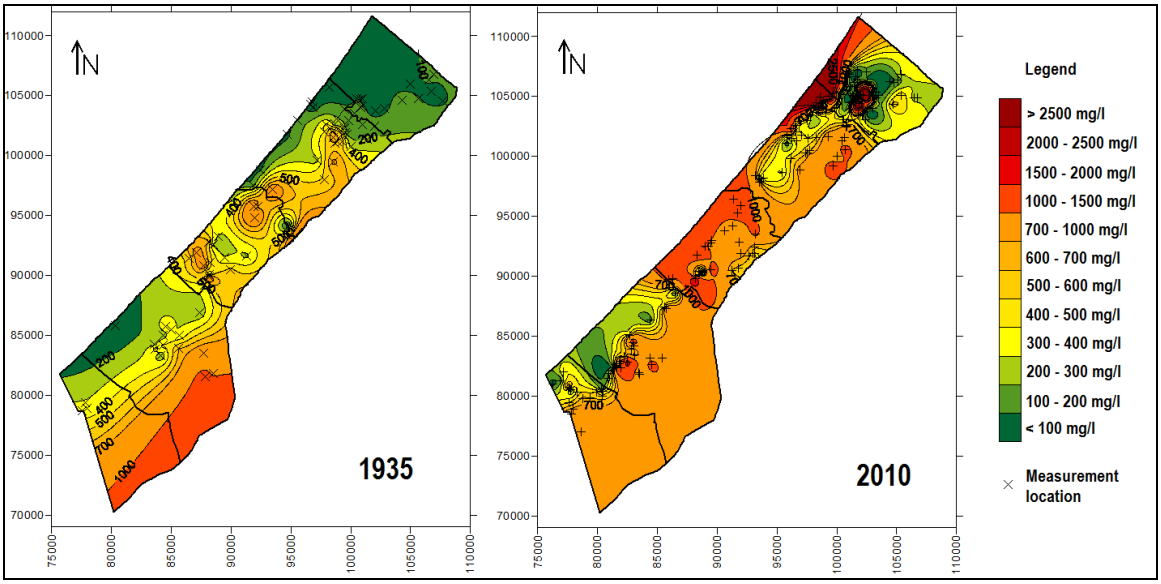

Figure 4.10 - Representation of 1935 (left) and 2010 (right) chlorides concentration in groundwater

In general, salinization in coastal aquifers may be caused by a single process or a combination of different processes, such as seawater intrusion, upconing of brines from the deeper parts of the aquifer, flow of saline water from the adjacent Eocene aquifer, return flow from irrigation water, and leakage of wastewater. Ghabayen et al. (2006) identified areas within different salinity sources using ionic and isotopic ratios in the shallow part of the Gaza aquifer, showing that there are three major sources of groundwater salinity: leakage of brackish saline water flowing from adjacent areas along the eastern boundary of the coastal aquifer, sea water intrusion along the coast from the west, and flow of deeper very saline water from the bottom part of the aquifer.

The existence of seawater intrusion in the Gaza aquifer has been well documented by many modern studies, within salinization patterns available in terms of chlorides concentrations (mg/l of Cl^-), indicating that seawater intrusion extends from 1 to 2.5 km along the coastal boundary of the Gaza Strip, especially in Gaza city and Jabalia (in the north) and Khan Younis and Rafah (in the south). These areas correspond to the largest

pumping quantities, where the groundwater levels lie several meters below the mean sea level.

4.6 Groundwater balance and water demands

The Gaza Strip has a severe crisis on water resources due to the increase of demand on water for both domestic and agriculture purposes, those causing a net imbalance of about 50 Mm^3/y between inflows and outflows, which are better described in following and then summarize in Table 4.3. All the values are referred to average climatic conditions, total abstractions and return flows, because the Gaza coastal aquifer is a dynamic system with continuously changing amount of inflows and outflows.

The main source of freshwater for the aquifer is rainfall (P), which is extremely reduced by the evapotranspiration (ET). Rainfall occurs in the period from October to March, while the rest of the year is usually completely dry; average annual rainfall varies from 400 mm/y in the north to 200 mm/y in the south; the evapotranspiration measurements and calculations indicate that the average annual value for the Gaza Strip is around 1,500 mm/year. It is estimated that the total rainfall recharge ranges approximately from 40 to 45 Mm^3/y.

In the water balance are considered some other source of freshwater:

a) Lateral Inflow (LI), coming from the eastern part of the aquifer which is contact with the bigger regional aquifer; its value cannot be evaluated univocally, depending on outer conditions relatively to the bigger regional aquifer, so it is derived from the hydrologic balance and it is estimated to be in range between 10 and 40 Mm^3/y (Moe et al., 2001; Qahman and Larabi, 2006);

b) Leakage from water distribution system (L), which is usually estimated as percentage of distributed water, accounting an amount of about 10-15 Mm^3/y;

c) Agricultural return, or Return Flow (RF), which is a portion of the water used for irrigation that infiltrates in the aquifer; this value is estimated as percentage of pumping water for irrigation purposes and, for the Gaza Strip, it is usually set as 25% of the pumping at individual wells (Qahman and Larabi, 2006);

d) Wastewater return flow (WR), both from pipes and from septic systems (Waste Water Treatment plant (WWTP));

e) Loss of aquifer storage (S), calculated as a fraction of stored water in the aquifer.

Others inflows are due to seawater intrusion. This phenomenon is being monitored by a multipurpose groundwater monitoring network settled throughout the region, to observe groundwater levels and nitrate and chloride content. The saltwater inflow is estimated to be in a range of 10-45 Mm^3/y (Moe, 2001; Qahman and Larabi, 2006).

Inflow	**Mm^3/yr**	**Outflow**	**Mm^3/yr**
Rainfall (P)	40-45	Agricultural Wells	88
Lateral Inflow (LI)	10-40	Municipal Wells	84
Leakage from Water Distribution System	10-15	Mekorot	4
Agricultural Return Flow (AR)	20	Discharge (D)	10-50
Wastewater Return Flow (WR)	10		
Loss of aquifer storage (S)	2-3		
Salt Water Intrusion (SWI)	10-45		
total	102-183	total	186-226

Table 4.3 - Water inflows and outflows

Water abstraction (Q) is the main cause of outflow in the aquifer. In fact, groundwater has been the main source of freshwater in the Gaza Strip for agricultural, industrial and drinkable purposes. As cited before, there are thousands of pumping wells in the area.

On the basis of the available data on population, population growth, number of wells and their reported abstraction values on the last decades, it has been estimated, starting from 1935, the abstraction rate of the pumping wells which are reported in Figure 4.12 (adapted from Qahman and Larabi, 2006); it was estimated that, in the year 2006, approximately 170 Mm^3/y of water was pumped from about 4,600 wells (126 municipals) for domestic and agricultural purpose (Palestinian Water Authority- PWA, 2007). Some Mm^3/y are supplied from Israeli Water Mekorot.

Another outflow is the freshwater discharge (D) into the sea; this phenomenon is due to the natural gradient from uphill (east) to downhill (west). The value of this amount of water is usually estimated as difference between the other terms of the balance.

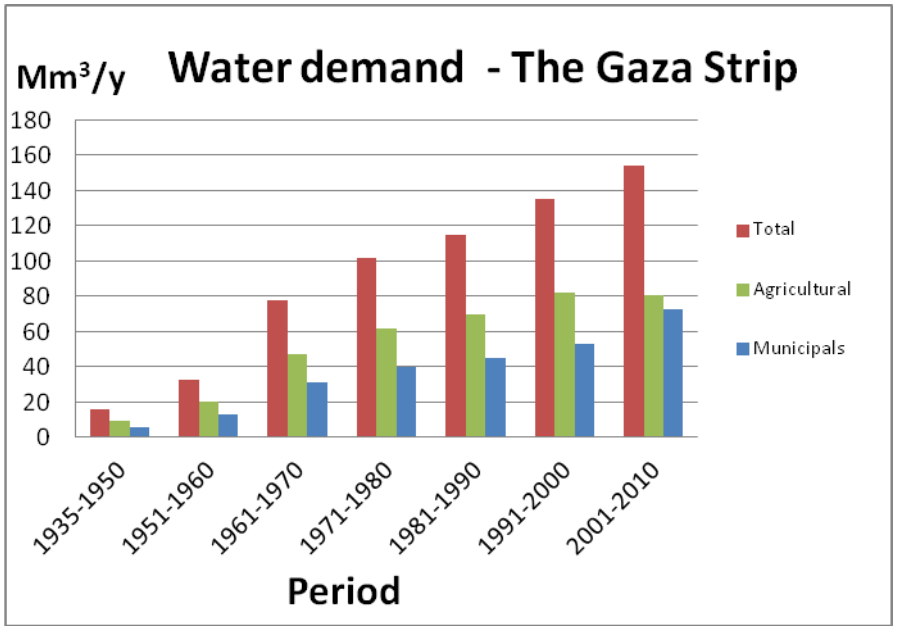

Figure 4.11 – Municipal and agricultural demand: estimation (from 1935 to late 90s, after Qahman and Larabi, 2006) and actual values until 2010.

4.7 Water Management hypothesis

The supply of fresh water to the population in Gaza at the present time relies almost totally on the underlying groundwater (Coastal Municipalities Water Utility-CMWU, 2010). The annual sustainable yield of the aquifer within the boundary of the Gaza Strip is quoted as around 50-55 Mm^3/y. Recent rates of pumping from the aquifer are estimated at 170 Mm^3/y in 2010, within municipal and industrial demand accounting for about 90 Mm^3/y. While municipal need is expected to become the major demand in the water sector, the agricultural water demand is expected to slowly decreasing in the area, oscillating (up and down) within the normal range from 75-85 Mm^3/y, due to the economic growth and political instability conditions in the Gaza Strip.

So that, water demand management has become a must to sustain Gaza Strip development and satisfy population needs; in order to reach both the goal of increasing water quality and quantity of groundwater, a mix of currently available options and sub-options has been characterized for the Gaza Strip at the strategic level (Weinthal et al., 2005) Mason et al., 2009), summarized in the following:

1) The domestic water distribution system should be upgraded;

2) Desalination plants (short term and long term) should be introduced, creating new fresh water from sea water and blending it back into limited volumes of groundwater (Assaf, 2001).
3) The reuse of treated wastewater should be strongly introduced and accelerated;
4) The use of water use in the agricultural sector in Gaza should be reviewed.

About municipal and industrial demands, it is expected an increase in total demand which will be supply by reuse of wastewaters and desalinization waters; the net pumping scenario for domestic demand is illustrated in Figure 4.12 and Table 4.4 (data provided by University of Gaza-IUG). It is also expected a total decrease in the agriculture water needs from around 80 Mm^3/y in 2010 to about 60 Mm^3/y in 2035.

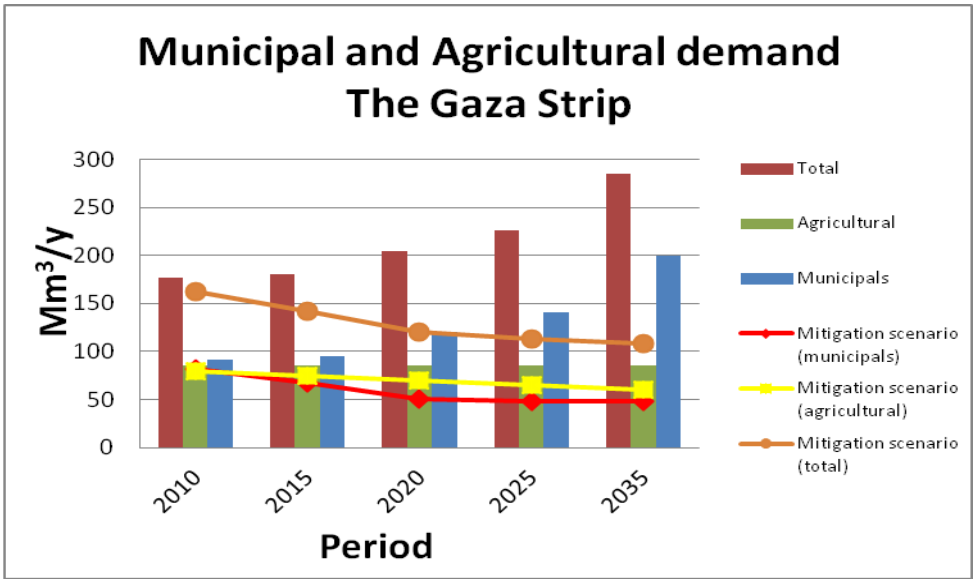

Figure 4.12 – Municipal and agricultural demand: estimation of pumpings and mitigation (management) options until 2035

Governorate	Year	Population	Managed Pumping for Municipal well (m^3/y)	Not Managed Pumping for Municipal well (m^3/y)
North	2010	299,627	22,030,009	21,982,134
Gaza		536,474	32,113,958	32,113,333
Middle		222,758	10,224,944	12,521,227
Khan Younis		214,190	8,598,468	8,599,728
Eastern villages		72,431	2,162,673	3,965,597
Rafah		173,328	6,840,752	6,832,589
Total		**1,518,808**	**81,970,804**	**81,970,804**
North	2012	320,968	22,030,009	22,024,824
Gaza		586,113	24,440,400	33,159,343
Middle		238,624	8,580,420	12,803,371
Khan Younis		214,190	5,781,600	9,381,522
Eastern villages		77,591	2,162,673	3,964,900
Rafah		205,911	6,840,752	9,018,902
Total		**1,643,397**	**69,835,854**	**86,976,786**
North	2015	355,862	23,140,252	23,120,354
Gaza		637,163	22,181,963	34,884,674
Middle		270,650	7,264,778	11,854,470
Khan Younis		237,476	5,781,600	10,401,449
Eastern villages		86,026	2,162,673	3,767,939
Rafah		228,298	6,272,102	9,999,452
Total		**1,815,475**	**66,803,366**	**89,457,531**
North	2020	422,653	19,693,296	23,140,252
Gaza		771,799	15,406,650	42,255,995
Middle		314,222	3,317,850	17,203,655
Khan Younis		282,047	5,781,600	15,442,073
Eastern villages		102,172	2,162,673	5,593,917
Rafah		271,145	4,566,150	14,845,189
Total		**2,164,038**	**50,928,219**	**118,481,081**
North	2025	501,979	19,003,905	27,483,350
Gaza		916,655	14,051,588	50,186,861
Middle		373,197	2,528,465	20,432,536
Khan Younis		334,983	5,781,600	18,340,319
Eastern villages		121,348	2,162,673	6,643,803
Rafah		322,035	4,224,960	17,631,416
Total		**2,570,198**	**47,753,190**	**140,718,341**
North	2035	708,091	19,003,905	38,767,982
Gaza		1,293,033	14,051,588	70,793,557
Middle		526,431	2,528,465	28,822,097
Khan Younis		472,527	5,781,600	25,870,853
Eastern villages		171,174	2,162,673	9,371,777
Rafah		454,262	4,224,960	24,870,845
Total		**3,625,519**	**47,753,190**	**198,497,165**

Table 4.4 - Net pumping scenarios for domestic demand until 2035

4.8 Summary and conclusions

The Gaza Strip is a semi-arid region located in the Mediterranean basin; it covers a long and narrow rectangular coastal area of about 365 km^2 between Egypt and Israel.

The Gaza coastal aquifer is the main source of water for agriculture, domestic, and industrial purposes in Gaza Strip. An estimated 1.5 million people live in Gaza by the end of 2010, with a density of about 4,500 people/km^2, making it one of the most overcrowded areas in the world. Due to the continuous population growth, the total water demand in the Gaza Strip is strongly increasing. Nowadays, the need of water is not satisfied by the available resources, and this is causing a huge deficit between water demand and supply (Qahman and Larabi, 2006).

Also, making the aquifer overexploited, the problem of SWI is so exacerbated that corrective measures are needed to restore groundwater quality and properly manage the aquifer. During the last decades several studies have been carried out to analyze Salt Water Intrusion in the Gaza Strip (Yakirevich et al., 1998; Melloul and Collin, 2000; Moe et al., 2001; Qahman and Larabi, 2006), but the aquifer quality situation is so critical (Shomar et al., 2010) that this problem is still a long way from being solved.

Chapter 5 - Future Climate Scenarios

In the future, the Earth system will be affected by the consequences of increasing temperatures, changing patterns of precipitation, and sea level rise; current projections of future potential climatic scenarios (IPCC, 2007) for the Mediterranean area provide critical predictions about the decline of the average amount of water availability (in terms of both inflows than outflows).

Different scenarios have been generated by the International Panel on Climate Change (IPCC); however, only the data for the most probable and accepted scenario, the A1B, are proposed in this study. This research has been undertaken as part of the CLIMB project, funded by the European Commission within the 7th Framework Programme, in the framework of which future climate scenarios have been processed and made available by experts who collaborate in carrying out the "Climate Models Auditing and Downscaling" Work Package of same project. A simple but precise and rigorous auditing assessment of mean states, monthly fluctuations, and extreme, of precipitation and temperature has been obtained by comparing the outputs of 14 Regional Climate Models (RCMs) part of the ENSEMBLES project, with a gridded data set of observations (E-OBS). Using this data set for verification in the 1951-2010 period, it has been possible to rank the models' performance, for the chosen parameters. Further analysis on predictions of climate change have been done about the Gaza Strip, comparing historical measured daily rainfall rates within modeled daily rainfall rates.

The scope of this analysis is to identify actual and future scenarios of climate change that are considered to finally hypothesize the possible impacts on the Gaza Strip hydrological basin; the climate variables which affect more the hydrological cycle of a basin are precipitation (P) and evaporation (ET) rates. While the variable P can be evaluated from outputs of climate models, ET should be assessed within a standard method (i.e. Penman-Monteith simplified method, Appendix B) starting from other modeled variables, namely temperatures (T), wind (W), relative humidity (RH) and solar radiation (Rs). Hence, further analysis is focused on the variable P and T.

5.1 Climate models

The Climate Models (CMs) are numerical tools which aim at simulating the present or the future climate of the Earth, furnishing values of weather (in a statistical sense) for periods lasting from 10 years to thousands of years. In order to make hypothesis on the future climate, it must be clear that the climate of a region is the averaged weather (measured within a reference period of 30 years or more) over a region; so that, the output of the CM must be averaged to have projections of climate variability.

The method to produce several different time series of physical quantities like temperature, precipitation, wind speed and direction, and many others, is based on using different CMs in parallel varying the initial conditions (scenario) of CM, for instance the variation of CO_2 level in atmosphere. The time series obtained from the CM have only a limited precision to forecast real future events; however, they are able to reproduce the season cycles for climate variables like the wet/dry seasons and the mean temperature of a region. In other words, CMs produce statistics of weather.

5.2 Future climate scenarios

Climate scenarios are released by the International Panel for Climate Change (IPCC) and are grouped as families containing individual scenarios with common themes. The six families of scenarios discussed in the IPCC's Third Assessment Report (TAR) and Fourth Assessment Report (AR4) are A1FI, A1B, A1T, A2, B1, and B2.

Scenario descriptions (http://www.ipcc.ch/ipccreports/sres/emission/index.php?idp=21) are based on those in AR4, which are identical to those in TAR, and they can be described in the following.

The A1 scenarios are about a more integrated world and they are characterized by:

• Rapid economic growth;

• A global population that reaches 9 billion in 2050 and then gradually declines;

• The quick spread of new and efficient technologies;

• A convergent world, in the sense of income and way of life converge between regions, with extensive social and cultural interactions worldwide.

There are subsets to the A1 family based on their technological emphasis:

• A1FI - An emphasis on fossil-fuels (Fossil Intensive);

• A1B - A balanced emphasis on all energy sources;

• A1T - Emphasis on non-fossil energy sources.

The A2 scenarios are of a more divided world and they are characterized by:

• A world of independently operating, self-reliant nations;

• Continuously increasing population;

• Regionally oriented economic development;

• Slower and more fragmented technological changes and improvements to per capita income;

The B1 scenarios are of a world more integrated, and more ecologically friendly; they are characterized by:

• Rapid economic growth as in A1, but with rapid changes towards a service and information economy;

• Population rising to 9 billion in 2050 and then declining as in A1;

• Reductions in material intensity and the introduction of clean and resource efficient technologies;

• An emphasis on global solutions to economic, social and environmental stability.

The B2 scenarios are of a world more divided, but more ecologically friendly; they are characterized by:

• Continuously increasing population, but at a slower rate than in A2;

• Emphasis on local rather than global solutions to economic, social and environmental stability;

• Intermediate levels of economic development;

• Less rapid and more fragmented technological change than in A1 and B1.

The scenario A1B is the most commonly used in the climate models scenario, as it represents the "average" scenario with a world well connected, a moderate use of fossil fuels (more integrated with other renewable energies); also, the regional climate models at high resolution have an almost complete dataset only for the A1B scenario.

Justified by the above mentioned reasons, in this study only the A1B scenario ENSEMBLES project outputs are used.

5.3 Climate models involved in the study

The CMs selected for the analysis are derived from the work of the Fourth Assessment Report of the IPCC (Intergovernmental Panel on Climate Change); they produce results of simulations based on different scenarios, for different climate variables which cover long periods of time (40 years). Two categories of models are involved in this study:

• General Circulation Models (GCMs), which have a large grid covering all the Earth. They are described and collected by the official database of the IPCC project.

• Regional Climate Models (RCMs) from the ENSEMBLES project, which dataset are provided from 1951 to 2100, at a daily scale, on a 0.22° grid which results, at mid-latitudes, in a resolution of about 22-25 km. These simulations are newer and still incomplete in many variables, but the ENSEMBLES high resolution RCMs have the more complete dataset for the A1B scenario, which is considered the more realistic one.

The ENSEMBLES RCM minimum covered area is illustrated in Figure 5.1, with the location of the Gaza Strip study site.

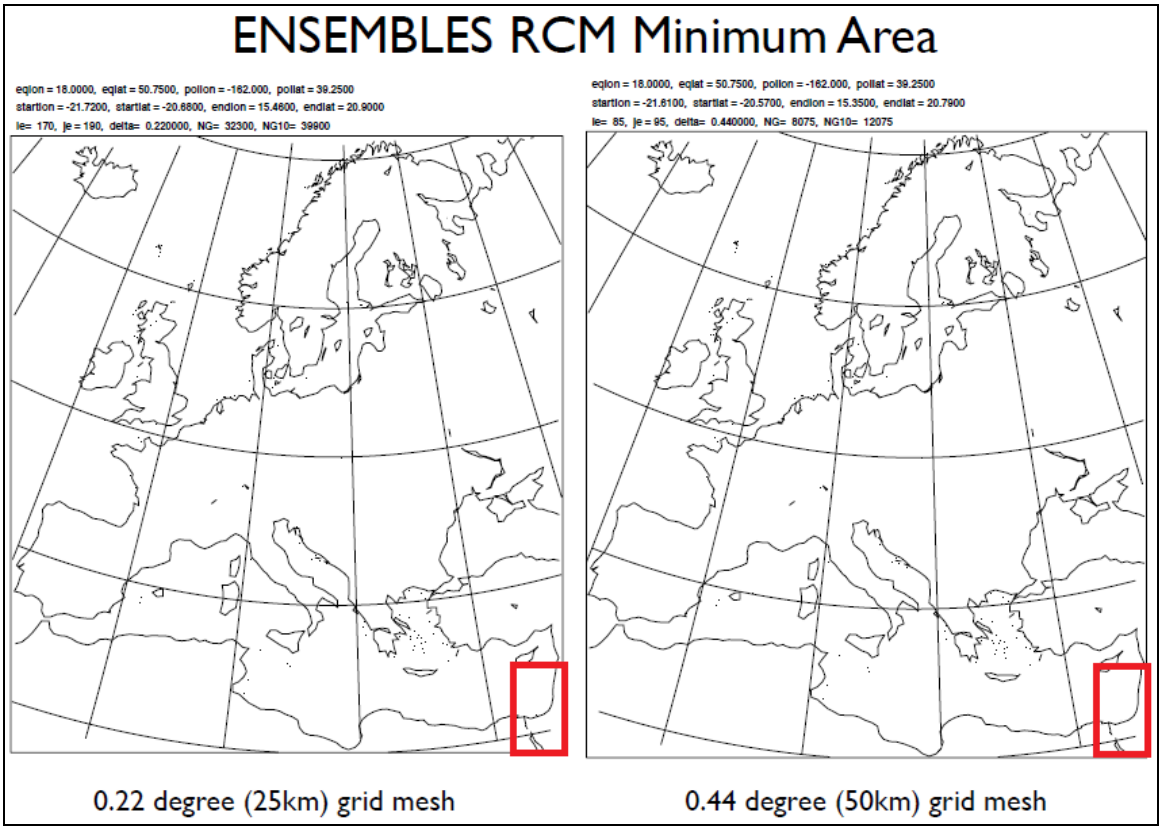

Figure 5.1 - ENSEMBLES RCM minimum area (the limits of the areas are reported in the upper part, in terms of latitude and longitude) with the localization (in red) of the Gaza Strip area

The GCMs and RCMs involved in the ENSEMBLES project are illustrated in Table 5.1 and Table 5.2; Table 5.3 shows the GCM-RCM matrix combinations of models involved in the A1B scenario for the ENSEMBLES project, and related acronyms.

GCM	Description
HCH	Hadley Centre for Climate Prediction, Met Office, UK, HadCM3 Model (high sensitivity)
HCS	Hadley Centre for Climate Prediction, Met Office, UK, HadCM3 Model (standard sensitivity)
HCL	Hadley Centre for Climate Prediction, Met Office, UK, HadCM3 Model (low sensitivity)
ARP	Meteo-France, Centre National de Recherches Meteorologiques, CM3 Model Arpege
ECH	Max Planck Institute for Meteorology, Germany, ECHAM5 / MPI OM
BCM	Bjerknes Centre for Climate Research, Norway, BCM2.0 Model

Table 5.1 - GCMs involved in the ENSEMBLES project

RCM	Description
RCA	RCA Sweden
HIR	HIRAM5 Denmark
CLM	CLM Switzerland
HRM	HadRM3Q3 UK
RMO	RACMO2 Netherlands
REM	REMO Germany

Table 5.2 - RCMs involved in the ENSEMBLES project

GCM / RCM	HadleyC, Std.	HadleyC, Low	HadleyC, High	ECHam 5	ARPege	BCM
HadRM ●	HCS_HRM ●	HCL_HRM ●	HCH_HRM ●			
REMo ◆				ECH_REM ◆		
HIRham ■	HCS_HIR ■			ECH_HIR ■	ARP_HIR ■	BCM_HIR ■
CLM ▲	HCS_CLM ▲					
RacMO ▼				ECH_RMO ▼		
RCA 3 ▶		HCL_RCA ▶	HCH_RCA ▶	ECH_RCA ▶		BCM_RCA ▶

Table 5.3 - GCM-RCM matrix combinations of models involved in the A1B scenario for the ENSEMBLES project, and related acronyms

5.4 The Gaza Strip study site – methods and results

In the framework of the CLIMB project, starting from outputs of ENSEMBLES project, a simple but precise and rigorous auditing assessment of mean states, monthly fluctuations, and extremes, of precipitation and temperature is obtained by comparing the outputs of 14 Regional Climate Models (RCMs) part of the ENSEMBLES project, with a data set of observations (E-OBS), hosted by the CRU (Centre of Research Unit) of the Hadley Centre, within the same grid used by the ENSEMBLES RCMs. A detailed description of this data set can be found in Haylock et al. (2008).

Since the Gaza Strip is located very close to the boundary of the gridded area (Figure 5.1), where the model output is expected to be very noisy, the Gaza study site data should not be considered as reliable as the other areas' ones; although further analysis should be done about this issue, not any deeper analysis is undertaken in this study.

The variables outputs are available (for most of RCMs) until year 2100; therefore, a deeper analysis on climate variables is undertaken for the Gaza Strip only until year 2070. All the analysis is undertaken for only gridded points which are not in the sea, due to different phenomenon involved in calculations on those points. After the auditing procedure, both modeled temperatures and precipitation variables are bias corrected with reference to CRU dataset for all the 4 chosen RCM models, as CMs are supposed to simulate the climate, reproducing as well the seasonally cycle of that region, within monthly and seasonally biases.

Assuming that at least 30 years of daily observations can define regional climate, and as for the Gaza Strip is available a long-time period historical dataset for 8 operating Rainfall Station (indicated, within acronyms, in Figure 5.2, which also shows the gridded points of CRU observed and RCM modeled data), another methodology is applied to bias correct modeled precipitation variables within measured daily precipitation by the means of the daily translation method (Mpelasoka and Chiew, 2009), indicated in the following as the QQplot methodology.

Both methodology are described in the following paragraphs; further analysis are made on the only gridded point internal in the study site area (Figure 5.2), indicated from now as p2362.

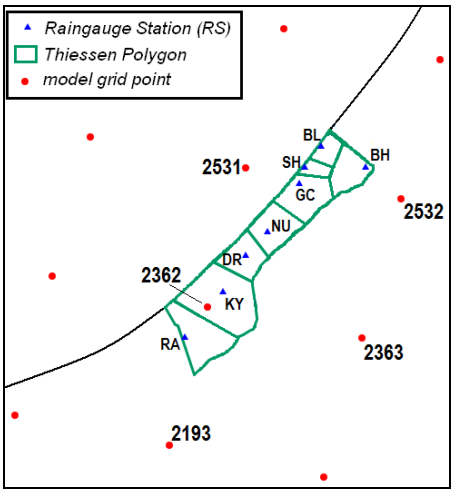

Figure 5.2 – The CRU and RCMs gridded points for the Gaza Strip, with Rainfall stations locations

Due to the peculiar features of the Gaza Strip site (small and flat area) and of the process investigated (long term process), in this study the downscaling procedure is not applied at all, except for a furthermore 'correlation' task described in the QQplot procedure.

5.4.1 CRU auditing and bias correction

Following the definition of climate given by the World Meteorological Organization (WMO), the climate datasets are divided in 5 time-slices, each 30 years long, for the period 1951-2100. A comparison is made for the daily precipitation (P) and daily mean temperature (T), between model data and the CRU E-OBS (CRU from now on) data for the 2 periods in which CRU reference data are available (1951-1980 and 1981-2010). For each grid point and for these variables (P and T), they are evaluated monthly averages of the variable for each year and each 30-years period, and then compared three statistical indicators of CRU dataset, namely the absolute error (AEA) of monthly averages, the absolute error of the monthly fluctuations (AEF) and the absolute error of the extremes (AEE). Since both precipitation and temperature play a major role in determining a basin's hydrologic response, it is necessary to identify for the basin a unique group of models to use for future analysis, satisfying a criteria of minimal error; this is obtained by introducing two a-dimensional skill score indicators for mean values and fluctuations and for extremes. An effective way to represent AEA and AEF skill indicators, and to evaluate model performance for the study area, is a Cartesian plot, in which AEA is x coordinate and AEF is y coordinate; as the errors (both of monthly averages and of

fluctuations) within the first climatic period are well correlated with the corresponding during the second period, the skill evaluation can be definitely set for the entire period 1951 to 2010. In order to get a final analysis, results of the two variables are combined, making it possible to get the AEA-AEF adimensional plots shown in Figure 5.3.

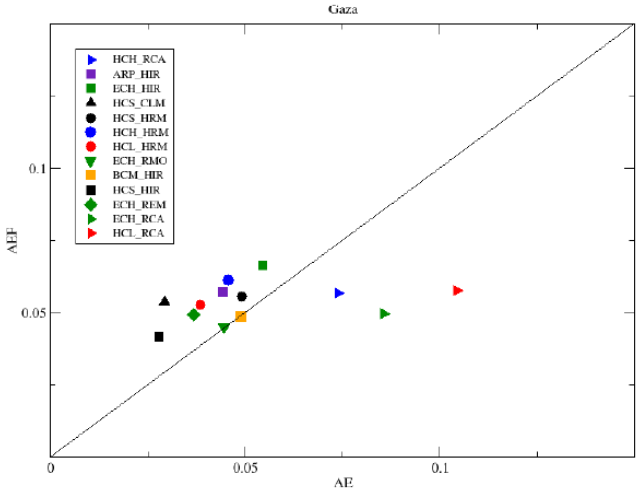

Figure 5.3 – Gaza: AEA-AEF skill scores plot for each of the 14 RCMs for the climatic period 1951-2010, obtained combining precipitation and 2-meters temperature errors.

In this case, the best four models are: ECH_REM, ECH_RMO, BCM_HIR and HCS_HIR. Unfortunately, data for BCM_HIR and HCS_HIR are available only until year 2050, so that these two RCMs are not considered for further analysis in this study. Therefore, in order to gain at least 4 models to be analyzed, in this part of the study are used other 2 RCMs (ECH_RCA, HCH_RCA) having them got quite good skill ratings.

Hence, within this study (and within CLIMB project too, from which this consideration are coming) they are used modeled results coming from ECH_REM, ECH_RMO, HCH_RCA and ECH_RCA, being them two different RCMs initialized with the same GCM initial condition and boundary conditions and two runs of the same RCM fed with two different GCMs.

Yet, as the best 'performance' is detected to be for the ECH_RMO climate model, results coming from these model are furthermore analysed in the following, focusing most attention to the only gridded point inside the Gaza Strip (p2362).

After the auditing procedure above illustrated, both modeled temperatures and precipitation variables have been bias corrected with reference to CRU dataset for all the

4 chosen RCM models, as CMs are supposed to simulate the climate, reproducing as well the seasonally cycle of that region, within monthly and seasonally biases.

A variety of methods can be used to account for the systematic mismatch between observed and simulated climate variables over a considered control period (Anandhi et al., 2011; Stoll et al., 2011). In order to reduce the climate scenario errors, the QQplot approach, known in literature as 'daily translation method' (Mpelasoka and Chiew, 2009) is applied with modeled and observed (CRU) daily precipitation and temperatures data in the Gaza Strip. The 'daily translation method' has been shown to perform as well as more sophisticated statistical downscaling methods (Themeßl et al., 2011) and to be skilful in other hydrologic impact studies (Wood et al., 2004; Maurer and Hidalgo, 2008). The basilar assumption of this methodology is that CMs are supposed to simulate the climate, which is essentially the statistics of precipitation, temperature, wind and other meteorological parameter in a given region over long periods (30 years for WMO), reproducing as well the seasonally cycle of that region. CMs are, at least, seasonally biased, and they can be bias corrected by correcting their statistics; a possible solution is to correct directly seasonal probability distribution function.

Establishing a correspondence between modeled and measured values linked by the same value of the cumulative distribution function (CDF), it is possible to eliminate the CDF variable and obtain directly a calibration plot; so that, a quantile scaling technique (Sulis et al., 2012) is used to establish a relationship for the control period (1981-2010) between CRU and RCM-simulated daily values at the different ranks/percentiles defined by interpolating directly from the empirical CDF for each time series. Assuming that the biases are stationary in time, this relationship is separately applied for each of the 12 months to translate the future climate model data.

The results of the bias correction for the 4 chosen models are not further analysed here, excepted for ECH_RMO model. In Figure 5.4 they are graphically compared precipitation values, in terms of mean monthly values, for the period 1981-2010, relative to ECH_RMO outputs (p2362) with and without CRU bias correction for p2362, and measured values in the Rainfall Station (KY) nearest to p2362. It is evident that modeled climate precipitations are underestimated in comparison with real values for all the year, with exception for the months from June to September (months from 6 to 9, dry season).

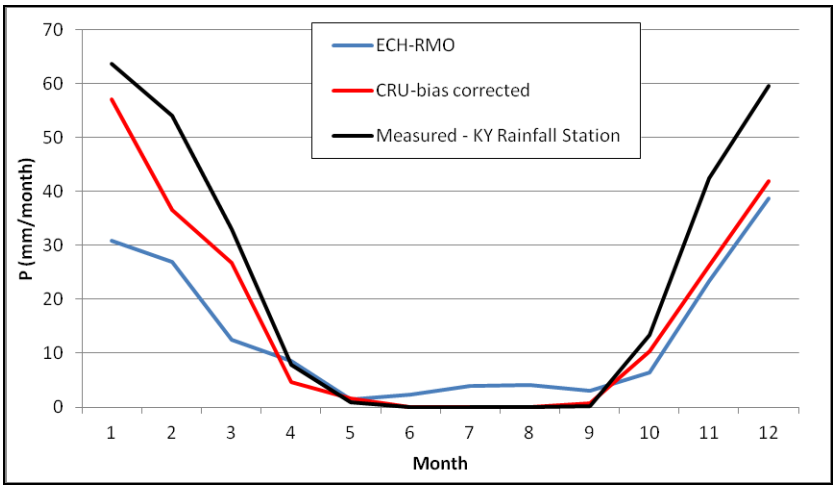

Figure 5.4 – Comparison of monthly mean values of precipitation for the period 1981-2010: ECH_RMO outputs (p2362) with and without CRU bias correction, and measured values in the nearest to p2362 Rainfall Station (KY).

The same bias correction is applied to modeled future precipitation values, supposing that the applied correction can be reasonably the same applied on the modeled past values. In Figure 5.5 they are graphically compared precipitation values, in terms of monthly mean values, for the period 2011-2040 (left part) and 2041-2070 (right part), relative to ECH_RMO outputs for p2362, with and without CRU bias correction.

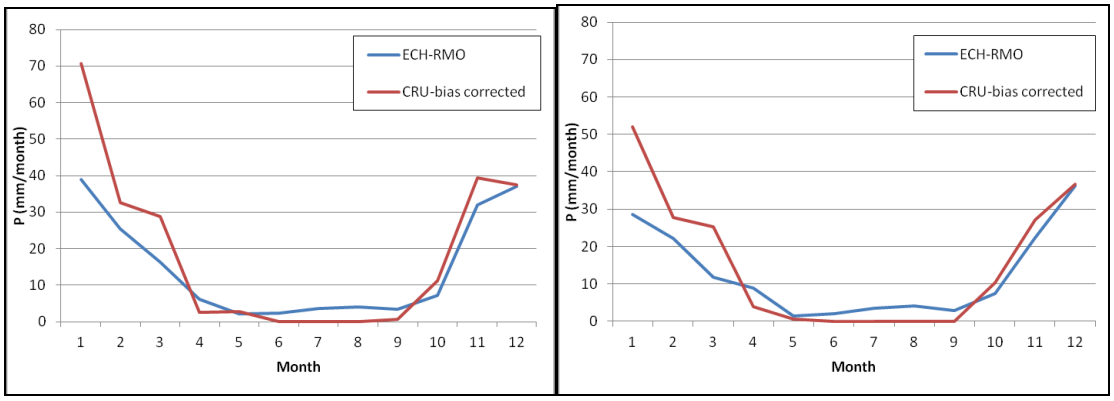

Figure 5.5 - Comparison of monthly mean values of precipitation for the period 2011-2040 (left) and 2041-2070 (right): ECH_RMO outputs (p2362) with and without CRU bias correction

In Figure 5.6 they are graphically compared temperatures values, in terms of mean monthly averaged (t_{avg}), minimum (t_{min}) and maximum (t_{max}) values, for the period 1981-2010, relative to ECH_RMO outputs for p2362 with and without CRU bias correction.

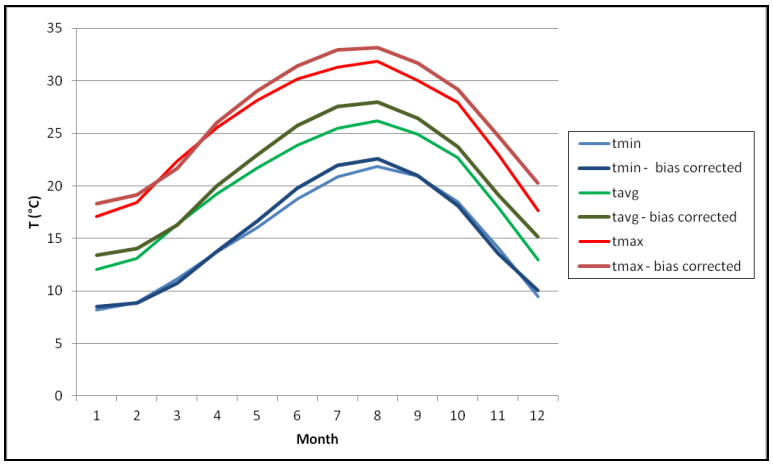

Figure 5.6 - Comparison of monthly mean values of temperatures for the period 1981-2010: ECH_RMO outputs (p2362) with and without CRU bias correction.

In Figure 5.7 they are graphically compared temperatures values, in terms of monthly mean values, for the period 2011-2040 and 2041-2070 relative to ECH_RMO outputs for p2362 with CRU bias correction.

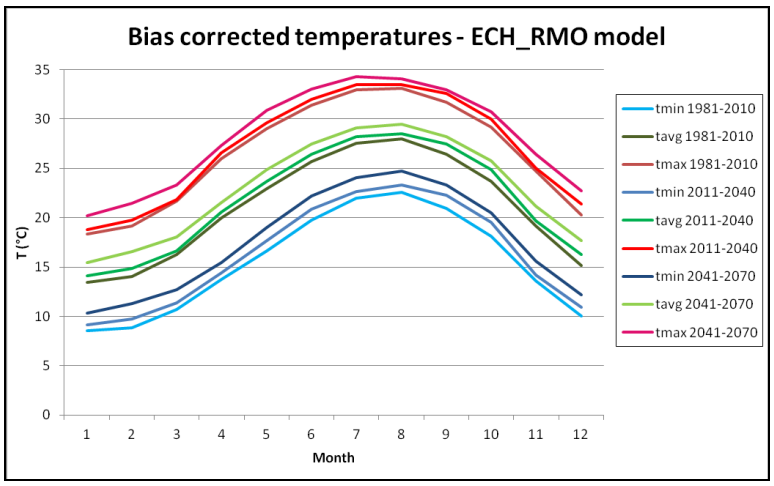

Figure 5.7 – Comparison of monthly mean values of temperatures for the periods 1981-2010, 2011-2040 and 2041-2070: ECH_RMO outputs (p2362) with CRU bias correction

5.4.2 QQplot methodology with historical precipitation data

The same quantile scaling technique above described (QQplot methodology) is used to establish a relationship for the control period (1981-2010) between observed (Gaza Strip rainfall station measured values) and RCM-simulated precipitation daily values at the different ranks/percentiles defined by interpolating directly from the empirical CDF for each time series; yet, it has been again assumed that the biases are stationary in time, so

that this relationship is separately applied for each of the 12 months to translate the future climate model data.

For the Gaza Strip site, in which there is a strong difference between northern and southern mean yearly rainfall (see Chapter 4) the QQplot methodology above described is applied to two model grid points, being the 2532.nd representative of "northern climate" and the 2362.nd representative of the "southern climate" (reference to Figure 5.2).

Thus, the QQplot methodology is used to assess precipitation values in the location of the operational Rainfall Stations. In few words, for each Rainfall Station are assessed precipitations values, by correlating precipitation outputs of one grid point between 2532.nd and 2362.nd of each chosen RCMs with measured precipitations values in the nearest Rainfall Station. The criteria to assign a rainfall station to a grid point is the vicinity, as illustrated in Figure 5.8.

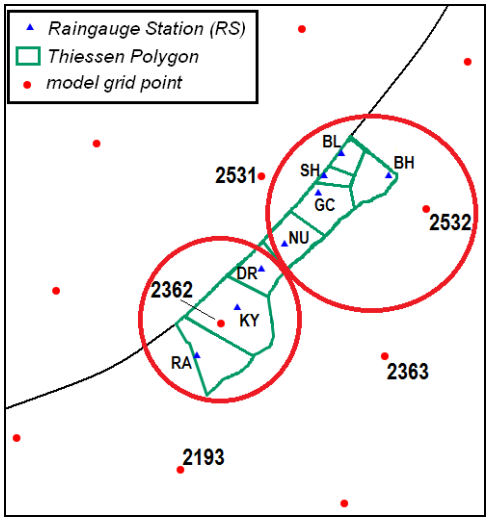

Figure 5.8 – Assigning Rainfall Station to a grid point by the vicinity criteria

The procedure is applied to the outputs of all the chosen 4 models, the results of which are not further analysed here excepting for ECH_RMO model.

In Figure 5.9 they are graphically compared precipitation values, in terms of mean monthly values, for the period 1981-2010, relative to ECH_RMO outputs for p2362 with and without QQplot calibration, and measured values in the Rainfall Station (KY) nearest to p2362. Comparing this graph with Figure 5.4, it is evident how the QQplot methodology is able to better bias correct modeled precipitations with real rainfall values.

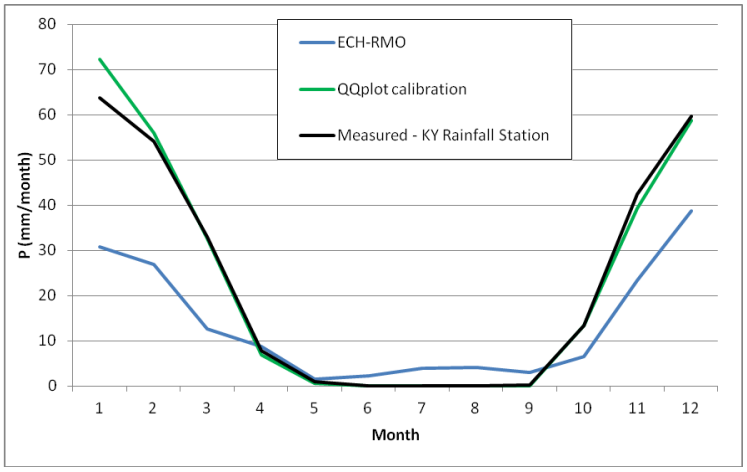

Figure 5.9 - Comparison of monthly mean values of precipitation for the period 1981-2010: ECH_RMO outputs (p2362) with and without QQplot calibration, and measured values in the nearest to p2362 Rainfall Station (KY)

The same methodology is applied to modeled future precipitation values, supposing that the applied correction can be reasonably the same applied on the modeled past values. In Figure 5.10 they are graphically compared precipitation values, in terms of monthly mean values, for the period 2011-2040 (left part) and 2041-2070 (right part), relative to ECH_RMO outputs for p2362, with and without QQplot calibration by the means of real precipitation values.

In Figure 5.11 they are graphically compared precipitation values, in terms of monthly mean values for the period 1981-2010, relative to measured values for each Rainfall Station (left part) and to ECH_RMO QQplot calibrated values (right part).

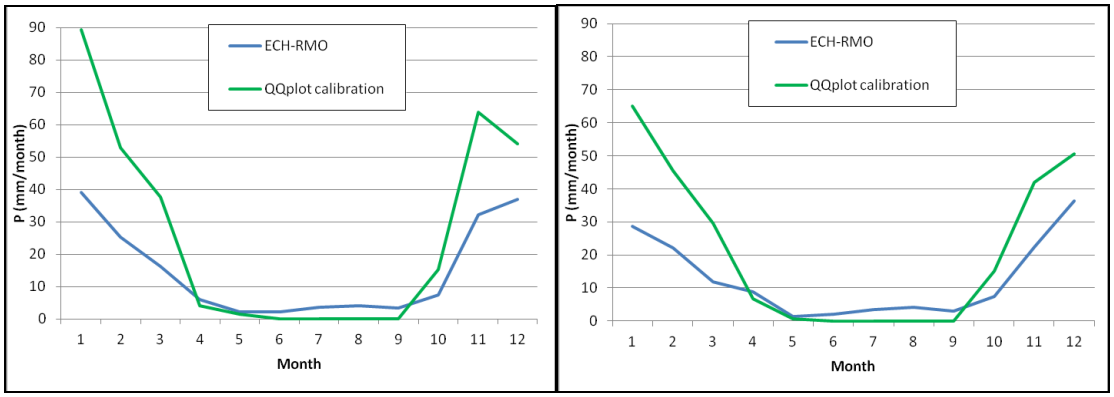

Figure 5.10 - Comparison of monthly mean values of precipitation for the period 2011-2040 (left) and 2041-2070 (right): ECH_RMO outputs (p2362) with and without QQplot calibration.

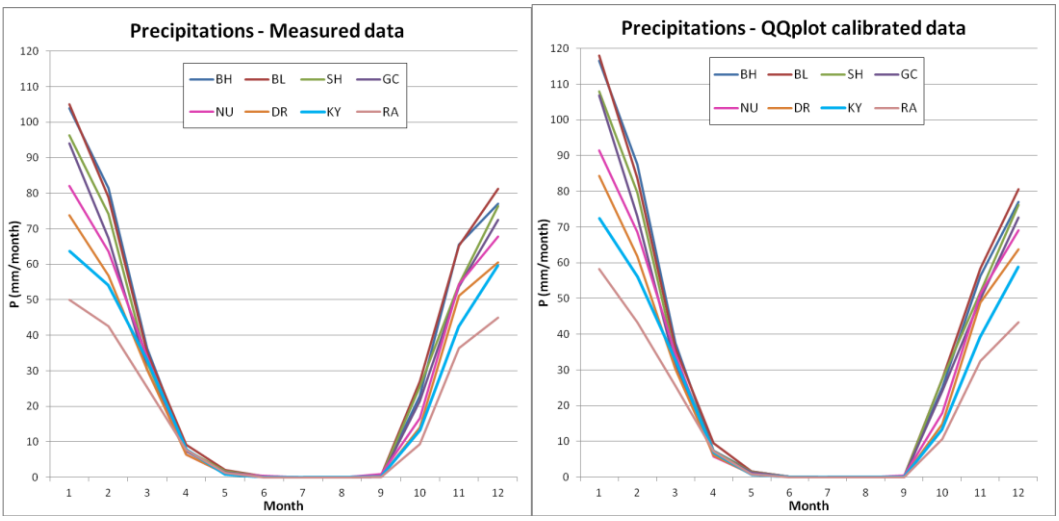

Figure 5.11 - Comparison of monthly mean values of precipitation for the period 1981-2010: measured values (left) and QQplot ECH_RMO calibrated values (right) for each Rainfall Station.

In Table 5.4 is proposed a comparison between mean monthly values of precipitations for overall the Rainfall Stations, while in Table 5.5 is proposed a comparison between mean annual values of precipitations for each Rainfall Station, in order to better quantify the differences between bias corrected and measured precipitations values in the period 1981-2010. The difference between measured and calibrated values is less than 4%, considering mean yearly values.

Month	Measured P (mm/month)	Calibrated P (mm/month)	Difference (mm)	Difference (%)
January	83.58	94.46	10.89	13.0
February	64.88	69.20	4.32	6.7
March	32.15	32.65	0.50	1.6
April	7.55	7.12	-0.42	-5.6
May	1.35	1.09	-0.27	-19.8
June	0.23	0.09	-0.14	-60.8
July	0.00	0.00	0.00	0.0
August	0.00	0.00	0.00	0.0
September	0.31	0.14	-0.17	-55.8
October	18.79	20.12	1.33	7.1
November	52.88	48.55	-4.33	-8.2
December	67.53	67.66	0.13	0.2
Total	329.24	341.07	11.83	3.6

Table 5.4 - Measured and QQplot calibrated precipitation values, in terms of mean monthly values for overall Rainfall Stations in the period 1981-2010.

Rainfall Station	Acronym	Measured P (mm/y)	Calibrated P (mm/y)	Difference (mm)	Difference (%)
Beit Hanon	BH	396.74	409.10	12.36	3.1
Beit Lahia	BL	404.59	415.73	11.13	2.7
Shati	SH	369.17	385.51	16.33	4.4
Gaza City	GC	348.85	365.93	17.07	4.9
Nussirate	NU	327.12	339.88	12.76	3.9
Dair Balah	DR	294.64	310.84	16.20	5.5
Khan Younis	KY	275.08	279.76	4.68	1.7
Rafah	RA	217.70	221.81	4.12	1.9
	Mean	329.24	341.07	11.83	3.6

Table 5.5 - Measured and QQplot calibrated precipitation values, in terms of mean yearly values for each Rainfall Station, in the period 1981-2010.

In Table 5.6 they are compared precipitation values in terms of extreme events (as defined by WMO standard, i.e. 'extreme events' if daily precipitation >10 mm/d and 'very extreme events' if daily precipitation >20 mm/d) per year for the period 1981-2010, relative to measured values for each Rainfall Station and to ECH_RMO QQplot calibrated values. The difference between measured and calibrated values are less than 4%, considering mean yearly values.

Rainfall Station	Acronym	Extreme events per year				Very Extreme event's per year			
		Real	Calibrated	Difference	Difference (%)	Real	Calibrated	Difference	Difference (%)
Beit Hanon	BH	13.2	13.6	0.4	3.3	6.4	6.6	0.2	3.6
Beit Lahia	BL	13.2	13.2	0.0	0.0	6.4	6.5	0.1	1.6
Shati	SH	12.9	13.0	0.1	0.5	5.7	6.0	0.3	5.3
Gaza City	GC	12.3	12.6	0.3	2.2	5.3	5.4	0.1	1.9
Nussirat	NU	11.0	11.5	0.5	4.6	4.9	5.4	0.5	9.5
Dair Balah	DR	10.5	10.9	0.4	4.1	4.8	5.0	0.2	4.1
Khan Younis	KY	9.2	9.5	0.4	4.0	4.1	4.1	-0.1	-1.6
Rafah	RA	7.0	7.4	0.3	4.7	2.7	2.8	0.1	3.8
	mean	11.2	11.5	0.3	2.9	5.0	5.2	0.2	3.5

Table 5.6 - Measured and EHC_RMO QQplot calibrated precipitation values, in terms of extreme events per year, for each Rainfall Station, in the period 1981-2010.

5.4.3 Analysis on climate variables for the Gaza Strip basin

The scope of the analysis on modeled climate variables is to identify actual and future scenarios of climate change that are considered to finally hypothesize the possible impacts on the Gaza Strip hydrological basin. The variables which affect more the hydrological cycle of the basin, modifying directly the recharging amount of coastal aquifers, are precipitation (P) and evaporation (ET); the difference of these two variables (P-ET) is the net recharging precipitation (NetP), which represent the main climate-dependent impacting.

While the variable P can be evaluated from outputs of climate models, ET is assessed with the evaluation of potential evapotranspiration (ET_0) within Penman-Monteith simplified method (Appendix B) starting from other modeled variables, namely temperatures (T), wind (W), relative humidity (RH) and solar radiation (Rs). ET values are considered equal to ET_0 during rainy days and equal to 0 in dry days.

Although affecting ET patterns, the W, RH and Rs variables are used in this study without any biased procedure, coming directly from RCMs outputs, so that no further analysis is proposed on them; however, further analysis is proposed on the ET patterns and their effects on precipitation rates in the period 1981-2070. An analysis of the only biased and calibrated variables (P and T) is proposed in the following, for the period between 1981 and 2070. Yet, being the ECH_RMO model the best 'performer' for the Gaza Strip site, only results coming from this model are analysed, focusing most attention to the only gridded point inside the study site (p2362); the others 3 models, not deeper analysed here, give similar results (in terms both of quantity and quality) for all the considered periods for the T variables, while for P values are briefly reported averaged values at the end of this paragraph.

As shown in the above paragraphs, it is evident that modeled precipitations are underestimated in comparison with measured rainfall values (1981-2010 period of reference); this problem can be due to a series of chained conceptual issues that pertains to RCM gridded points, which actually represents a 'averaged daily value' for the representative squared area of about 22-25 km of side.

However, by the means of bias correction and calibration procedures by using measured precipitation values at the Rainfall Stations, the QQplot method is able to better

reproduce precipitation values in Rainfall Stations location points, achieving small discrepancies with the real precipitation values. So that, the QQplot calibrated future precipitation values are considered in this study to properly represent the most likely rainfall evolution for the periods 2011-2040 and 2041-2070.

In Table 5.7 are compared the mean yearly values of precipitation, for all considered periods and for all the considered Rainfall Stations, only for the ECH_RMO model. The mean difference between the precipitations of modeled historical period and of modeled periods 2011-2040 and 2041-2070 is about +14% and -10% respectively. Hence, these results indicate that ECH_RMO model is projecting, after year 2010, 30 years of mean quite higher rains, and then 30 years of mean lower rains.

Station	Precipitation 1981-2010 (p0) [mm/y]	Precipitation 2011-2040 (p1) [mm/y]	Precipitation 2041-2070 (p2) [mm/y]	Difference (p1)-(p0) [mm]	Difference (p1)-(p0) [%]	Difference (p2)-(p0) [mm]	Difference (p2)-(p0) [%]
BH	409.10	464.61	370.76	55.51	13.57	-38.34	-10.34
BL	415.73	471.02	376.00	55.29	13.30	-39.73	-10.57
SH	385.51	437.40	350.43	51.89	13.46	-35.08	-10.01
GC	365.93	415.18	331.23	49.25	13.46	-34.69	-10.47
NU	339.88	385.56	309.88	45.68	13.44	-30.01	-9.68
DR	310.84	355.20	279.62	44.36	14.27	-31.22	-11.17
KY	279.76	318.62	255.01	38.86	13.89	-24.74	-9.70
RA	221.81	254.33	202.88	32.52	14.66	-18.94	-9.33
mean	341.07	387.74	309.48	46.67	13.76	-31.59	-10.16

Table 5.7 – Comparison of the mean yearly values of precipitation for the periods 1981-2010, 2011-2040 and 2041-2070 for all the considered Rainfall Stations, for the calibrated ECH_RMO modeled values.

In Table 5.7 are compared the mean yearly values of extreme events, for all considered periods and for all the considered Rainfall Stations, only for the ECH_RMO model. The mean difference between the precipitations of modeled historical period (1981-2010) and of the modeled periods 2011-2040 and 2041-2070 is, for extreme events, about +6% and -18% respectively and for very extreme events about +22% and -6%. Hence, these results indicate that ECH_RMO model is projecting, after year 2010, 30 years of increasing of extreme events and strong increasing of very extreme events, and then 30 years of strong decreasing of extreme events and moderate decreasing of very extreme events.

These results seem to be slightly in accordance with ENSEMBLES project results, which states, for 2011-2040 period, higher precipitations rates (in terms of extreme events) in

some areas of the Mediterranean basin and, for 2041-2070, a general decrease in precipitation rates for the same areas.

Rainfall Station Acronym	Extreme events per year							Very Extreme event's per year						
	1981-2010 (p0)	2011-2040 (p1)	2041-2070 (p2)	Difference (p1)-(p0)		Difference (p2)-(p0)		1981-2010 (p0)	2011-2040 (p1)	2041-2070 (p2)	Difference (p1)-(p0)		Difference (p2)-(p0)	
				No.	%	No.	%				No.	%	No.	%
BH	13.6	14.2	11.0	0.5	3.9	-2.6	-19.3	6.6	8.1	5.9	1.5	22.1	-0.7	-5.4
BL	13.2	13.8	10.9	0.6	4.5	-2.3	-17.4	6.5	8.0	5.9	1.5	23.7	-0.6	-4.5
SH	13.0	13.7	10.6	0.7	5.7	-2.4	-18.3	6.0	7.0	5.5	1.0	17.2	-0.5	-3.9
GC	12.6	13.4	10.3	0.8	6.3	-2.3	-18.3	5.4	6.7	5.2	1.3	23.5	-0.2	-1.6
NU	11.5	12.2	9.1	0.7	6.1	-2.4	-20.6	5.4	6.2	5.2	0.9	16.1	-0.2	-1.5
DR	10.9	11.7	8.9	0.8	7.3	-2.0	-18.3	5.0	6.0	4.7	1.0	19.9	-0.3	-2.7
KY	9.5	10.3	7.8	0.7	7.7	-1.7	-18.2	4.1	5.0	4.1	1.0	23.8	0.0	0.3
RA	7.4	8.3	6.6	0.9	12.2	-0.8	-10.4	2.8	3.9	2.9	1.1	39.8	0.2	2.3
mean	11.5	12.2	9.4	0.7	6.3	-2.1	-18.0	5.2	6.4	4.9	1.2	22.1	-0.3	-2.5

Table 5.8 - Comparison of the mean yearly values of extreme events for the periods 1981-2010, 2011-2040 and 2041-2070, in terms of number per year, for all the considered Rainfall Stations, for the calibrated ECH_RMO modeled values.

For the Temperatures values, historical data on the Gaza Strip are not sufficient to clarify the performance of the CRU bias corrected T values (averaged, minimum and maximum) in this study site. Nevertheless, they are considered to appropriately describe past and future patterns of temperatures for the area. In Table 5.9 are compared the mean yearly values of temperatures, in terms of average, maximum and minimum values, for all considered periods on p2362, for the ECH_RMO model.

The mean difference between the average temperatures of modeled historical period and of modeled periods 2011-2040 and 2041-2070 is about +0.7°C and +1.9°C respectively; for the minimum temperatures, the difference is about +0.9°C and +2.2°C; for the maximum temperatures, the difference is about +0.6°C and +1.7°C. Hence, these results indicate that ECH_RMO model is projecting, after year 2010, a general increasing of temperatures, with 30 years of increasing of temperatures values in the range between 0.5°C and 1.0°C, and then 30 years of further increasing of temperatures values in the range between 1°C and 1.3°C.

These results seem to be in accordance with ENSEMBLES project results, which states, both for 2011-2040 and 2041-2070 period a general increase in Temperatures values for the Mediterranean areas.

Temperatures	Period (p0) 1981-2010 [°C]	Period (p1) 2011-2040 [°C]	Period (p2) 2041-2070 [°C]	Difference (p1)-(p0) [°C]	Difference (p1)-(p0) [%]	Difference (p2)-(p0) [°C]	Difference (p2)-(p0) [%]
T_{avg}	+21.02	+21.77	+22.94	+0.75	+3.6	+1.92	+9.1
T_{min}	+15.45	+16.33	+17.62	+0.87	+5.7	+2.16	+14.0
T_{max}	+26.46	+27.04	+28.13	+0.58	+2.2	+1.67	+6.3

Table 5.9 - Comparison of the mean yearly values of temperatures for the periods 1981-2010, 2011-2040 and 2041-2070 for the point p2362, for the calibrated ECH_RMO modeled values.

ET patterns are assessed by evaluating potential evapotranspiration (ET_0) within Penman-Monteith simplified method (Appendix B), considering the CRU bias corrected temperatures values (average, minimum and maximum) assessed for the only inner grid point p2362, and 3 not bias corrected variables, namely wind (W), relative humidity (RH) and solar radiation (Rs); in Table 5.10 are reported ET_0 mean monthly values of modeled historical period and of modeled periods 2011-2040 and 2041-2070, considering variables coming from the only ECH_RMO model.

The mean difference between the ET of modeled historical period and of modeled periods 2011-2040 and 2041-2070 is about +2% and +6% respectively.

ET values are then assessed day by day, considered equal to ET_0 during rainy days and equal to 0 in dry days. In this study it is hence proposed an analysis of ET effects on precipitation rates (evaluated with the QQplot methodology) in the period 1981-2070, by considering mean yearly values for each considered Rainfall station, only for the model ECH_RMO (Table 5.11); ET rates are in the range of 16-25% of precipitation values (P). The mean difference between the ET of modeled historical period and of modeled periods 2011-2040 and 2041-2070 is about +6% and -7% respectively. The mean difference between the net recharging precipitation (NetP, set equal to P-ET) of modeled historical period and of modeled periods 2011-2040 and 2041-2070 is about +16% and -11% respectively.

These results indicate that ECH_RMO model is projecting, after year 2010, 30 years of slightly higher ET patterns and higher NetP values, and then 30 years of slightly lower ET and NetP patterns. However, it must be considered that, due to the increase of extreme events and very extreme events of precipitation, NetP patterns should be much less than these, as runoff component for sure will be hampered. Further analysis should be conducted on this issue.

	1981-2010 (p0)	2011-2040 (p1)	2041-2070 (p2)	Difference (p1)-(p0)	Difference (p1)-(p0)	Difference (p2)-(p0)	Difference (p2)-(p0)
Month	[mm]	[mm]	[mm]	[mm]	[%]	[mm]	[%]
1	62.62	57.14	67.52	-5.48	-8.75	+4.90	+7.83
2	64.73	64.40	64.35	-0.33	-0.51	-0.38	-0.59
3	92.89	95.51	99.04	+2.62	+2.82	+6.15	+6.62
4	126.20	130.94	127.09	+4.74	+3.76	+0.89	+0.71
5	161.15	164.11	173.65	+2.95	+1.83	+12.49	+7.75
6	150.03	165.57	171.98	+15.54	+10.36	+21.96	+14.63
7	168.36	170.28	177.01	+1.93	+1.15	+8.65	+5.14
8	164.76	166.39	175.48	+1.63	+0.99	+10.72	+6.50
9	143.96	138.97	150.43	-4.99	-3.47	+6.47	+4.50
10	114.67	111.66	122.16	-3.00	-2.62	+7.50	+6.54
11	79.23	83.04	91.57	+3.81	+4.81	+12.34	+15.58
12	61.31	68.76	59.35	+7.45	+12.15	-1.97	-3.21
TOTAL	1389.89	1416.75	1479.62	+26.86	+1.93	+89.73	+6.46

Table 5.10 - Comparison of the mean monthly values of ET_0 for the periods 1981-2010, 2011-2040 and 2041-2070 for the point p2362, for the calibrated ECH_RMO modeled values.

In order to better analysed such results, it also proposed a summary of the trends for the modeled precipitation (P), evaporation (ET), NetP and Temperatures values without any bias correction and with bias correction, in the only internal gridded point (p2362), indicated in Table 5.12 in terms of mean yearly values for the periods 1981-2010, 2011-2040 and 2041-2070, for the ECH_RMO model.

It is evident how such modeled and bias corrected variables are, in some cases, quite different in values; nevertheless, the trends in the future considered periods (indicated in the table as p1 and p2) with reference to historical period (p0) are extremely similar.

More in details, bias and not bias corrected P values show the trend of around +10 and +13.9% for the first period and of -6.9 and -9.7% for the second period respectively; bias and not bias corrected T_{avg} values show the trend of around +0.68°C and +0.75°C for the first period and of +1.97°C and +2.16°C for the second period respectively. In few words, it can be depicted that both bias corrected and non-bias corrected modeled values are showing quite the same trends for the future considered periods.

Rainfall Stations	Variables	1981-2010 (p0)	2011-2040 (p1)	2041-2070 (p2)	Difference (p1)-(p0)	Difference (p1)-(p0)	Difference (p2)-(p0)	Difference (p2)-(p0)
Acronym		[mm]	[mm]	[mm]	[mm]	[%]	[mm]	[%]
BH	P	409.10	464.61	370.76	+55.51	+13.57	-38.34	-10.34
	ET	71.75	77.12	67.98	+5.38	+7.49	-3.77	-5.55
	ET (% of P)	17.54	16.60	18.33	-	-	-	-
	Net P (P-ET)	337.35	387.49	302.78	+50.14	+14.86	-34.57	-11.42
BL	P	415.73	471.02	376.00	+55.29	+13.30	-39.73	-10.57
	ET	76.92	82.38	72.67	+5.47	+7.11	-4.25	-5.84
	ET (% of P)	18.50	17.49	19.33	-	-	-	-
	Net P (P-ET)	338.81	388.64	303.33	+49.83	+14.71	-35.48	-11.70
SH	P	385.51	437.40	350.43	+51.89	+13.46	-35.08	-10.01
	ET	70.99	76.29	67.21	+5.31	+7.47	-3.78	-5.62
	ET (% of P)	18.41	17.44	19.18	-	-	-	-
	Net P (P-ET)	314.52	361.11	283.22	+46.59	+14.81	-31.30	-11.05
GC	P	365.93	415.18	331.23	+49.25	+13.46	-34.69	-10.47
	ET	70.12	75.60	66.44	+5.48	+7.81	-3.68	-5.54
	ET (% of P)	19.16	18.21	20.06	-	-	-	-
	Net P (P-ET)	295.81	339.58	264.80	+43.77	+14.80	-31.01	-11.71
NU	P	339.88	385.56	309.88	+45.68	+13.44	-30.01	-9.68
	ET	64.82	70.17	61.34	+5.34	+8.24	-3.48	-5.68
	ET (% of P)	19.07	18.20	19.80	-	-	-	-
	Net P (P-ET)	275.06	315.39	248.54	+40.33	+14.66	-26.52	-10.67
DR	P	310.84	355.20	279.62	+44.36	+14.27	-31.22	-11.17
	ET	60.35	62.36	55.72	+2.01	+3.33	-4.63	-8.30
	ET (% of P)	19.41	17.56	19.93	-	-	-	-
	Net P (P-ET)	250.49	292.84	223.90	42.34	16.90	-26.59	-11.88
KY	P	279.76	318.62	255.01	38.86	13.89	-24.74	-9.70
	ET	59.67	61.44	55.18	1.77	2.97	-4.49	-8.15
	ET (% of P)	21.33	19.28	21.64	-	-	-	-
	Net P (P-ET)	220.09	257.17	199.84	+37.09	+16.85	-20.25	-10.13
RA	P	221.81	254.33	202.88	+32.52	+14.66	-18.94	-9.33
	ET	54.32	55.41	49.57	+1.09	+2.01	-4.76	-9.60
	ET (% of P)	24.49	21.79	24.43	-	-	-	-
	Net P (P-ET)	167.49	198.92	153.31	+31.43	+18.76	-14.18	-9.25
mean P		341.07	387.74	309.48	+46.67	+13.76	-31.59	-10.16
mean ET		66.12	70.10	62.01	+3.98	+5.81	-4.10	-6.78
mean ET (% of P)		19.74	18.32	20.34	-	-	-	-
mean Net P (P-ET)		274.95	317.64	247.46	+42.69	+15.80	-27.49	-10.98

Table 5.11 - Comparison of the mean yearly values of ET and net P (P-ET) for the periods 1981-2010, 2011-2040 and 2041-2070 for all the considered Rainfall Stations, with ECH_RMO bias corrected values.

Variables		Units	1981-2010 (p0)	2011-2040 (p1)	2041-2070 (p2)	Difference (p2)-(p0)	% Difference (p2)-(p0)	Difference (p3)-(p1)	% Difference (p3)-(p1)
Not bias corrected	P	mm/y	162.03	178.37	151.55	+16.34	+10.09	-10.48	-6.92
	ET	mm/y	86.00	86.39	78.95	+0.40	+0.46	-7.05	-8.93
	NetP	mm/y	76.03	91.98	72.60	+15.94	+20.97	-3.43	-4.73
	T_{max}	°C	25.30	25.98	27.27	+0.68	+2.67	+1.97	+7.21
	T_{avg}	°C	19.71	20.47	21.68	+0.75	+3.83	+1.97	+9.09
	T_{min}	°C	15.21	16.06	17.29	+0.85	+5.58	+2.08	+12.02
Bias corrected	P	mm/y	279.76	318.62	255.01	+38.86	+13.89	-24.74	-9.70
	ET	mm/y	59.67	61.44	55.18	+1.77	+2.97	-4.49	-8.15
	NetP	mm/y	220.09	257.17	199.84	+37.09	+16.85	-20.25	-10.13
	T_{max}	°C	21.02	21.77	22.94	+0.75	+3.6	+1.92	+9.1
	T_{avg}	°C	15.45	16.33	17.62	+0.87	+5.7	+2.16	+14.0
	T_{min}	°C	26.46	27.04	28.13	+0.58	+2.2	+1.67	+6.3

Table 5.12 – Comparison of the mean yearly values of P, ET and NetP (P-ET) and T for the periods 1981-2010, 2011-2040 and 2041-2070 for the ECH_RMO not bias and bias corrected modeled values in the inner gridded point (p2362).

Although not reported in this paragraph, NetP is also assessed for the other 3 climate models, ECH_RCA, ECH_REM and HCH_RCA; so that, in Table 5.13 are reported the yearly mean values of NetP for the periods 2011-2040 and 2041-2070 for the 4 climate models considered in this study, relatively to the only inner gridded point (p2362).

Period / Climate Model	1981-2010 (p0)	2011-2040 (p1)	2041-2070 (p2)	Difference (p1)-(p0)	% Difference (p1)-(p0)	Difference (p2)-(p0)	%Difference (p2)-(p0)
ECH_RCA (CC1)	220.09	253.63	238.01	+33.5	+15.2	+17.9	+8.1
ECH_REM (CC2)	220.09	239.90	212.67	+19.8	+9.0	-7.4	-3.4
ECH_RMO (CC3)	220.09	257.17	199.84	+37.1	+16.8	-20.3	-9.2
HCH_RCA (CC4)	220.09	196.93	210.72	-23.2	-10.5	-9.4	-4.3

Table 5.13 - Comparison of the mean yearly values NetP (P-ET) for the periods 2011-2040 and 2041-2070 for the 4 considered models with bias corrected variables, in the inner gridded point (p2362).

For the first future period considered (p1), 3 models are showing an increasing trend (with reference to historical scenario p0) in NetP of around 10% but the HCH_RCA is denoting a decreasing of about -10%; for the second period (p2) 3 models are showing a general decreasing in NetP but the ECH_RCA is showing an increasing of about +8%.

What is expected is that such 4 depicted trends will affect in different ways the groundwater system in the Gaza Strip area; the expected effects of changes in climate dynamics on the aquifer water balance can be roughly assessed, at least for the vertical inflow fluxes (groundwater vertical recharging amounts), strongly correlated to the NetP rates. Thus, groundwater recharging amounts due to NetP, will probably vary within the

magnitudes illustrated in the above reported Table 5.13; however, a briefly discussion about this issue is proposed in Chapter 6, paragraph 6.6.

5.5 Summary and conclusions

Precipitation (P) and evaporation (ET) patterns above described and calculated for the 4 models ECH_RMO, ECH_REM, ECH_RCA and HCH_RCA, are supposed to impact on the future hydrological cycle of the Gaza site, as they represent the two factors determining net rainfall recharge. In particular, it is supposed that different patterns in P and ET will affect in different way the aquifer system, as these two values are used as the basis of the setup of recharging patterns for the coastal aquifer, aiming in this way to represent the future evolution of the overall system.

In this Chapter has been proposed a deeper analysis on the Gaza strip area, for only the ECH_RMO modeled variables, which are bias corrected within CRU data (for T variables) and, for P variables, within historical data, both by the means of the QQplot methodology. This last correction highlights that modeled precipitation values (P) are strongly different from historical measured data; this may be due to the different spatial resolutions, and also to series of chained conceptual issues that pertains to RCM gridded points, which actually represents a 'averaged daily value' for the representative squared area of about 22-25 km of side. The trend of bias corrected and not bias corrected variables have been further compared, highlighting quite the same trends for both the considered future periods.

The main outcomes from the analysis on future projected variables coming from 4 different GCM-RCM models applied on the Gaza Strip area are summarized in the following, with reference to 1981-2010 historical period:

1) Precipitation rates will have an increase in the next 30 years, and then a decrease in the following 30 years;
2) Extremes precipitations events (daily precipitation >10 mm/d) will have an increase in the next 30 years, and then a decrease in the following 30 years;
3) Very extreme precipitation events (daily precipitation >20 mm/d) will have an increase in the next 30 years and then a decrease in the following 30 years;
4) Temperatures will rise up to 2°C in the next 60 years;

5) ET patterns will slightly increase in the next 30 years and then decrease in the following 30 years;
6) The net recharging precipitation (NetP, set equal to P-ET) will increase in the next 30 years and then decrease in the following 30 years.
7) NetP values will have a direct impact on groundwater recharge, and however it must be considered that, due to the increase of extreme events and very extreme events of precipitation, the patterns should be much less than these, as runoff component for sure will be hampered. Further analysis should be done on this issue.

The expected effects of changes in climate dynamics on the aquifer water balance can be roughly assessed, at least for the vertical inflow fluxes (groundwater vertical recharging amounts), strongly correlated to the NetP rates. Thus, groundwater recharging amounts due to NetP, will probably vary within the magnitudes illustrated in the above reported Table 5.13; however, a briefly discussion about this issue is proposed in Chapter 6, paragraph 6.6.

Chapter 6 - The Gaza Strip hydrogeological model

The 3D hydrogeological model of Gaza Strip coastal aquifer is developed and then implemented using the CODESA-3D code (Gambolati et al,. 1999, Lecca, 2000) allowing to simulate coupled problems of variably saturated flow and contaminant transport in groundwater, in the presence of a fluid phase of variable density.

The setup of the physical setting of the Gaza Strip aquifer has been depicted from a large amount of data provided by the Islamic University of Gaza (IUG). The analyzed data include geology and geomorphology, hydrology, hydrogeology, estimates of natural recharge and available water resources as a result of groundwater exploitation, historical data of hydraulic heads and salt concentrations. After initial model set-up, several tests, in steady-state and transient-state conditions, are performed to verify physical consistency and numerical robustness. Other simulations are performed to assess boundary conditions (lateral inflow) at the eastern part of the domain, namely fixed freshwater fluxes prescribed at the inland border as derived from the whole basin water balance. Some input data of the system are updated according to results of these simulations.

The adopted calibration procedure is based on the coupling of the simulation (CODESA-3D) and optimization (PEST) modules, minimizes the distance between simulated and field-measured heads in the least-squares sense; the adjustable parameters changed during the minimization procedure under steady-state conditions are assumed the hydraulic conductivity values of the horizontal and vertical aquifer zones, whose initial values are set according to some prior knowledge. The model is calibrated in steady-state conditions with 1935 water levels, considering average climate conditions and natural conditions (‘no-pumping’ scenario); calibration results are obtained assuming that the lateral inflow is not uniformly distributed along the eastern side of the aquifer, with higher mean values in the northern part and lower mean values in the southern areas, according to the distribution of the average yearly rainfall registered at the gauging stations.

The model is then validated for the period 1935-2000 and additionally validated until 2010; those latter simulated fields of water tables and groundwater salt concentration are used to simulate the response of the hydrological basin to future scenarios of climate

change and, by the means of a simulation/optimization model, to assess management and mitigation strategies for SWI, using a genetic algorithm (Carrol, 1996).

6.1 3D model with CODESA-3D

In this study the adopted approach consists on a full integration of a data collection, management, analysis and, as well as, the detailed numerical model itself.

Groundwater modeling, and CODESA-3D modeling too, can be also considered an iterative process, where the data collection and the review process, the conceptual model, the form of the numerical model and its parameters, are all subject to change as new information is inferred during the modeling process.

Based on all available data, the CODESA-3D model of the Gaza aquifer is built adopting a step-by-step procedure that can be summarized as following:

1) Setup the three-dimensional model of the aquifer domain;
2) Calibrate the model in steady-state flow conditions, within mean climatic variable conditions and without considering pumping rates, against measured groundwater heads (control variables) relative to 1935 field campaign, setting hydraulic conductivity (K) as adjustable model parameters (design variables);
3) Validate the model in transient-state conditions for the period 1935-2000, within mean climatic variable conditions and within considering estimated production rates for wells in the area;
4) Additional validate the model in transient-state conditions for the period 2001-2010, considering actual measured climatic variable conditions and actual pumping rates for all wells in the area.

Simulations are carried out in steady state (natural conditions, without pumping rates) and transient state (with actual pumping rates) conditions to analyze current and future aquifer trends in terms of water levels and solute concentrations.

All the modeling steps are described in more details in the next paragraphs.

6.1.1 The model geometry construction

As CODESA-3D is a Finite Element Model (FEM), it has been necessary to identify the triangular mesh of the aquifer domain. So that, the model domain is adequately discretized using Argus One pre and post processor computer software based on the finite

element method. The final 3D mesh of the aquifer system contains 39,408 nodes and 200,445 tetrahedra (Figure 6.1, right part); this mesh, denser in proximity of major wells, is built from the layer-by-layer replication of a 2D triangulation made of 9,545 triangles and 4,926 nodes (Figure 6.1, left part).

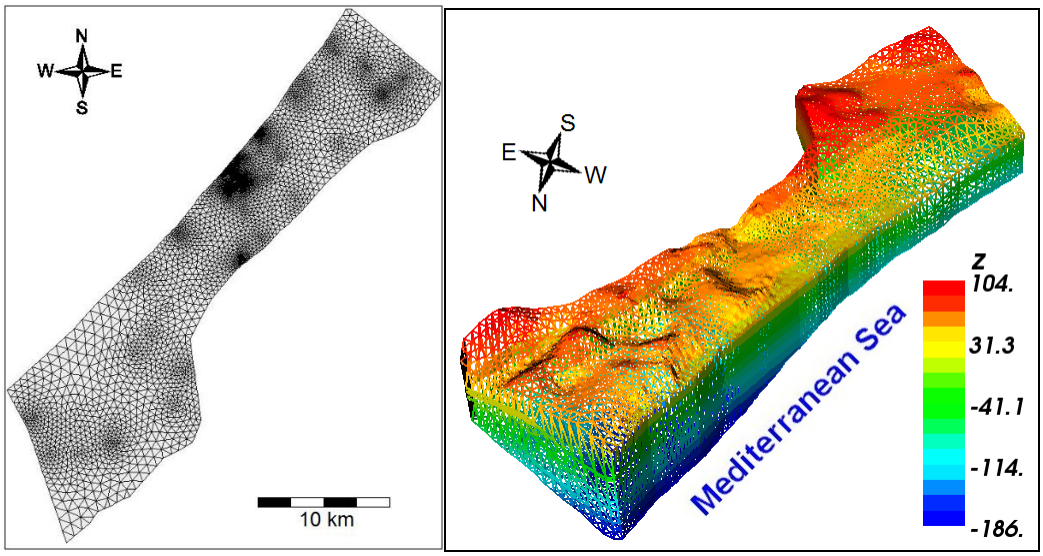

Figure 6.1 – Mesh 2D (left side) and mesh 3D (right side) – Gaza strip hydrogeological model

The model is then discretized vertically into 7 layers of different thickness, corresponding to the regional hydrogeological units: phreatic aquifer (unit 1), aquifers (units 3, 5 and 7) and aquitards (units 2, 4 and 6); in Figure 6.2 it represented the schematic vertical discretization within 2 km from the coastline.

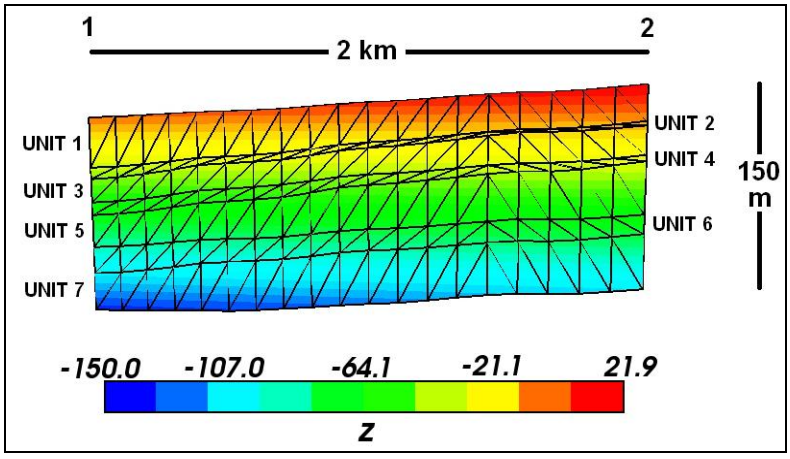

Figure 6.2 – Schematic vertical discretization

The top elevation of the first layer is spatially variable and corresponds with land surface elevation. The domain's bottom corresponds with upper surface of "Saqiya group"

geological unit (post-Eocene marine clay). The internal vertical zoning is based on the geological information provided by the Islamic University of Gaza (IUG), consisting of spatial distributed information (elevation) of the aquifer geological strata for the study domain. Having only a single layer for each different geologic formation is problematic for a FEM model as it will not be able to accurately handle the K variations from one formation to the next; so that, 7 layers is perhaps not sufficient from a numerical point of view, but, in order to have reasonable CPU times (also related to the Simulation/optimization model, as described in the following paragraph 6.7), it is not realistically discretized with many more layers.

6.1.2 Aquifer Input Parameters

The conceptual hydrogeological 3D model considers 24 hydraulic conductivity (K) potential parameters to be estimated, corresponding to the horizontal and vertical components of 11 different horizontal areas (derived from the soil map, represented within numbered areas in Figure 6.3), and assuming one horizontal and one vertical value for all the intermediate clayey layers, in order to highlight possible anisotropies of clay (Qahman and Larabi, 2006); the above described conceptualization is further illustrated in the following paragraph 6.2, showing how it impacts in the calibration procedure. An anisotropic value of 100 m and 20 m, dictated by the adopted grid spacing, is taken for solute dispersivity coefficients α_L and α_T respectively. Freshwater and saltwater densities are imposed equal to 1,000 and 1,025 kg/l, respectively. For water retention characteristics it is assumed Huyakorn et al. (1984) semi-empirical constitutive relationship, in which the effective saturation S_e is expressed as $\frac{1}{(1+\Lambda)^{\gamma}}$ if $\psi < \psi_a$ while set equal to 1 if $\psi \geq \psi_a$, with the parameter $\Lambda = \alpha^{\beta}(\psi_{\alpha} - \psi)^{\beta}$, being ψ_a the air entry pressure and the values α, β and γ are constants; the water saturation is expressed as $S_w = (1 - S_{wr})S_e(\psi) + S_{wr}$, being S_{wr} the residual water saturation; the relative conductivity is expressed as $K_r(\psi) = S_e^{\,n}$. The parameters are assumed to represent sandy soils, imposing α=0.015, β=2, γ=3, ψ_a=-10, S_{wr}=0.01 and n=2.

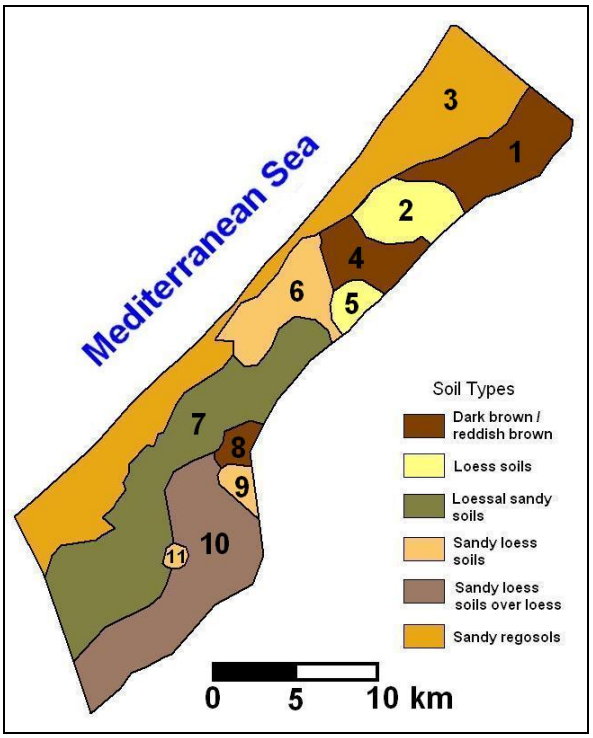

Figure 6.3 – Soil map and 3D-model horizontal zoning

Other parameters (specific storage, specific yield) that pertain to the Gaza aquifer hydraulic properties, as described in paragraph 3.1, are reported in Table 6.1. Model parameters that pertains to groundwater flow and solute transport (e.g. density ratio,…) are obtained from scientific literature data about similar types of sediments.

Parameter – from field campaigns	Unit	Value
Hydraulic Conductivity (K) - sand	m/d	20 - 80
Hydraulic Conductivity (K) - clay	m/d	0.01
Porosity - sand	%	35
Porosity - clay	%	50
Specific yield	%	15 - 30

Table 6.1 - Hydraulic parameters

6.1.3 Boundary conditions

After considering groundwater flow in the study area, as the flow lines are perpendicular to coastal shoreline in natural conditions (Chapter 4, paragraph 4.5.3), zero flux Neumann boundary condition are imposed to northern and southern boundaries. Another zero flux Neumann boundary condition is imposed at the bottom of the aquifer system, in order to consider it as an impermeable surface.

Dirichlet boundary conditions are imposed at the western boundary, along the coast, where the aquifer is in contact with the seawater body, imposing a constant head (h) derived from a hydrostatic pressure along the vertical boundary of the sea side and a constant concentration for seawater considered at the reference salt concentration (in terms of Chlorides) of 25 grams/litre.

An assigned recharge of freshwater flux is prescribed at the eastern border (inland lateral flow) as derived from the hydrologic balance, and its value has been adjusted during the model runs and calibration.

The surface nodes are subjected to atmospheric forcing, with the net recharge rate (Re) considered variable in space and uniform in time, according to soil characteristics and the recorded rainfall data from gauging stations located in the area (Chapter 4) during the period 1973-2010.

The net recharge rate (Re) is then calculated as:

$$\mathrm{Re} = (P - ET) \cdot C_{rech} = P_{net} \cdot C_{rech}$$

Where:

P: total rainfall;

ET: evapotranspiration, depicted from potential evapotranspiration (ET_0) assessed with Penman-Monteith equation (Appendix B);

P_{net}: net recharging rain;

C_{rech}: recharging coefficient (Chapter 4, Table 4.2), representing the fraction of net recharging rain which actually infiltrates into the aquifer.

6.1.4 Internal hydrologic stress

In the area there are more than 5,000 wells, a great part of them extremely denser in some areas, so that approximately 1,600 clustered wells are set up in the numerical model (Figure 6.4); this procedure is defined in order to avoid an excessive density of nodes.

The clustering procedure is applied separately for agricultural and municipal wells.

Agricultural wells are clustered by grouping them into an assigned model node, which is the closer to each agricultural well; pumpings are assigned to the clustered wells summing up pumpings of the relative assigned agricultural wells; depths of clustered wells are setup as the mean depth of the relative assigned agricultural wells, detecting the

closest node model in the vertical direction. This procedure makes it possible to identify around only 1,450 agricultural clustered wells.

The most operational municipal wells are located in the model nodes, so that the clustering procedure is adopted only for certain groups of wells; the procedure is the same as for agricultural ones.

Wells' depths range between 20 and 100-120 m below the land surface, and they are known for all the municipal wells and most part of the agricultural wells, which are in general less deeper; missing depth data are estimated on the basis of the information on the closest wells and the local geological strata. Nevertheless, depths of clustered wells is further update in the validation procedure, in order to guarantee always assigned vertical nodes under the simulated water level.

Yet, clustered wells are not setup in the model boundary nodes, in order to avoid any overlapping effect with boundary conditions.

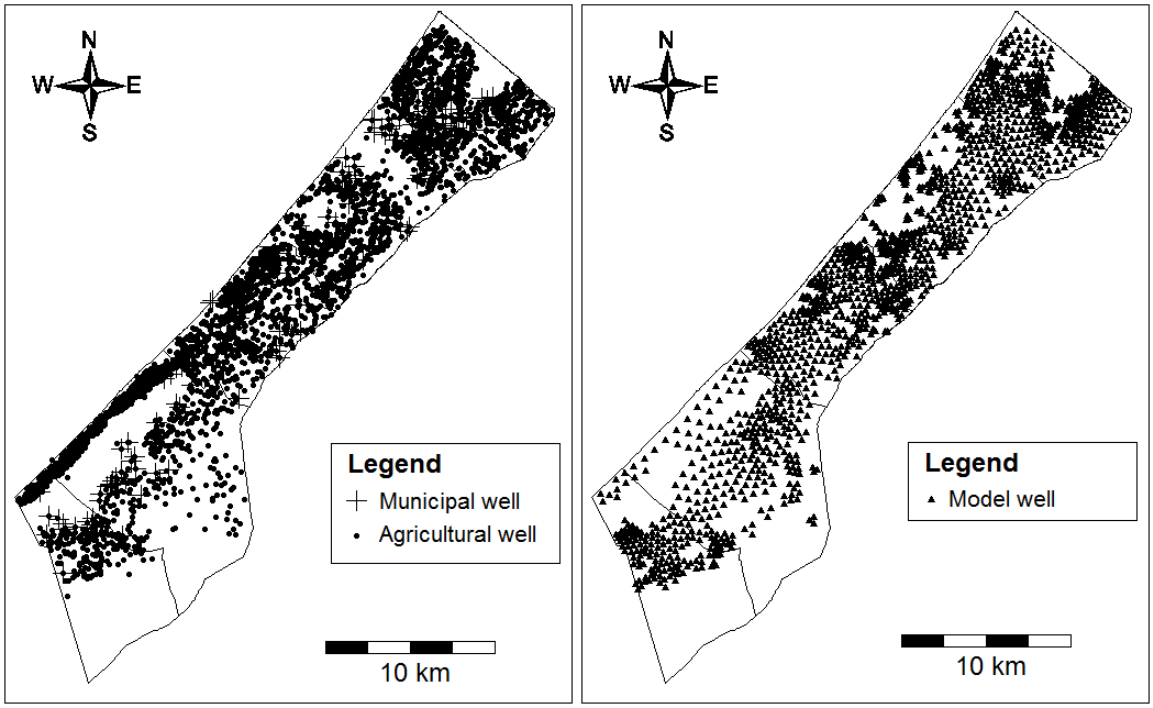

Figure 6.4 - Agricultural and municipal wells (left), and model clustered wells (right)

Wells' production rates are estimated on the basis of the overall groundwater abstraction from the Gaza aquifer starting from 1935 (Chapter 4, paragraph 4.6). For the period 2001-2010 they have been setup the actual pumping rates both for agricultural and municipal rates but, due to several uncertainties on illegal wells, the overall wells'

abstraction has been update, mainly in the southern part of the model, during the validation procedure.

6.1.5 Initial conditions

Initial conditions of the model are setup starting from results coming from steady-state calibration procedure, which aims to reproduce initial flow conditions in 1935. For the transport problem, the internal aquifer salinity is considered at the reference normalized concentration of 0 mg/l; the model is also setup considering initial condition based on the 1935 field measurements of chlorides concentrations in control wells.

6.2 Calibration with PEST - Steady state

The Gaza Strip model is calibrated in steady-state flow conditions against measured groundwater heads (control variables) relative to 1935 field campaign, considering a pre-development scenario (no-pumping). To calibrate the model the optimization module PEST-CODESA-3D (Lecca, 2004), which has been previously described in Chapter 3, is applied. Adjustable model parameters (design variables) of the calibration procedure are hydraulic conductivity (K). Many of the data items in the PEST control file are used to "tune" PEST's operation to the case in hand; such items include parameter change limits, parameter transformation types, and termination criteria. The initial setup of PEST control file is based on Lecca and Cau (2006) and it is reported in Figure 6.5; the values of which are properly described in Doherty (2002) and they are not illustrated in details here.

For the initial calibration setup no prior information has been added.

In order to properly finalize the calibration procedure they are setup some calibration datasets, identified in the following by the capital letter C and an increasing number.

```
pcf
* control data
restart  estimation
    24  43    1      0     1
    1     1 single point   1   0   0
  5.0   2.0   0.3  0.03    10
  3.0   3.0 0.001
  0.1
   30  0.01     3     3  0.001    3
    1     1     1
* parameter groups
k  relative 0.01  0.0  switch  2.0 parabolic  PARGPNME INCTYP DERINC DERINCBL FORCEN DERINCMUL NRELPAR
* parameter data
kh_aquif-01   log  factor   0.000231481    1.000000E-07   1.000000E-03 k  1.0000   0.00000E+00  1
kv_aquif-01   log  factor   2.31481E-05    1.000000E-08   1.000000E-04 k  1.0000   0.00000E+00  1
kh_aquif-02   log  factor   0.000347222    1.000000E-07   1.000000E-03 k  1.0000   0.00000E+00  1
kv_aquif-02   log  factor   3.47222E-05    1.000000E-08   1.000000E-04 k  1.0000   0.00000E+00  1
kh_aquif-03   log  factor   0.000925926    1.000000E-07   1.000000E-03 k  1.0000   0.00000E+00  1
kv_aquif-03   log  factor   9.25926E-05    1.000000E-08   1.000000E-04 k  1.0000   0.00000E+00  1
kh_aquif-04   log  factor   0.000231481    1.000000E-07   1.000000E-03 k  1.0000   0.00000E+00  1
kv_aquif-04   log  factor   2.31481E-05    1.000000E-08   1.000000E-04 k  1.0000   0.00000E+00  1
kh_aquif-05   log  factor   0.000347222    1.000000E-07   1.000000E-03 k  1.0000   0.00000E+00  1
kv_aquif-05   log  factor   3.47222E-05    1.000000E-08   1.000000E-04 k  1.0000   0.00000E+00  1
kh_aquif-06   log  factor   0.000462963    1.000000E-07   1.000000E-03 k  1.0000   0.00000E+00  1
kv_aquif-06   log  factor   4.62963E-05    1.000000E-08   1.000000E-04 k  1.0000   0.00000E+00  1
kh_aquif-07   log  factor   0.000405093    1.000000E-07   1.000000E-03 k  1.0000   0.00000E+00  1
kv_aquif-07   log  factor   4.05093E-05    1.000000E-08   1.000000E-04 k  1.0000   0.00000E+00  1
kh_aquif-08   log  factor   0.000231481    1.000000E-07   1.000000E-03 k  1.0000   0.00000E+00  1
kv_aquif-08   log  factor   2.31481E-05    1.000000E-08   1.000000E-04 k  1.0000   0.00000E+00  1
kh_aquif-09   log  factor   0.000462963    1.000000E-07   1.000000E-03 k  1.0000   0.00000E+00  1
kv_aquif-09   log  factor   4.62963E-05    1.000000E-08   1.000000E-04 k  1.0000   0.00000E+00  1
kh_aquif-10   log  factor   0.000578704    1.000000E-07   1.000000E-03 k  1.0000   0.00000E+00  1
kv_aquif-10   log  factor   5.78704E-05    1.000000E-08   1.000000E-04 k  1.0000   0.00000E+00  1
kh_aquif-11   log  factor   0.000462963    1.000000E-07   1.000000E-03 k  1.0000   0.00000E+00  1
kv_aquif-11   log  factor   4.62963E-05    1.000000E-08   1.000000E-04 k  1.0000   0.00000E+00  1
kh_aquitard   log  factor   2.315e-05      1.000000E-10   1.000000E-04 k  1.0000   0.00000E+00  1
kv_aquitard   log  factor   2.315e-06      1.000000E-10   1.000000E-05 k  1.0000   0.00000E+00  1
* observation groups
obsgroup
* observation data
h001 5.20000E+00  1.0 obsgroup
.....
h043 1.14200E+01  1.0 obsgroup
* model command line
./doit_PEST
* model input/output
Gaza-K.tpl  Gaza-K.inp
Gaza-K.ins  h-control.out
* prior information
```

Figure 6.5 - Control file and K values in PEST.

6.2.1 Calibration Dataset 1 (C1)

The dataset corresponds to the model setting described above in this Chapter. Lateral Inflow (LI) is a uniform distributed flux along the eastern side of the aquifer in the range between 5 and 50 Mm^3/y.

As reported before, the calibration model considers 24 hydraulic conductivities (K) to be determined. In Figure 6.5 are shown initial K-values and their allowed range (lower boundary e upper boundary). It is chosen a simple scheme and a wide range of K-values, in order to facilitate as much as possible the calibration procedure, trying at the same time to properly consider a medium degree of heterogeneity. The distribution of 1935 measured values, with the relative measure identification number (ID), is reported in Figure 6.6.

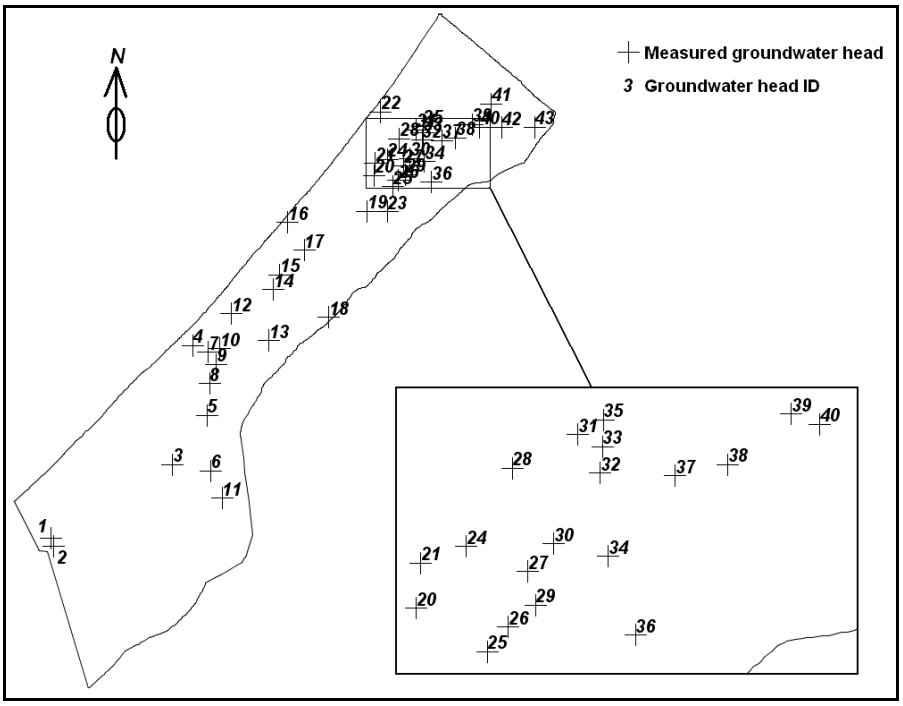

Figure 6.6 - 1935 measured points ID

The evaluation of the calibration effectiveness is based on the analysis of the residuals ($\Delta h = h - \bar{h}$), the objective function (Φ; equation 3.2, Chapter 3, paragraph 3.2), the correlation coefficient (R; equation 3.3, Chapter 3, paragraph 3.2) and the standard variance of residuals (σ). Other considerations are made on simulation outputs relatively to the h spatial distribution.

The first attempt on calibrating the GW model shows that (Table 6.2, Table 6.6):

1. the objective function (Φ) shows a value of 17.91 m, while residuals has a mean value of 0.06 m; the standard variance (σ) of residuals shows the values of 0.94 m, which means that the calibration procedure is not getting optimal results; the correlation coefficient (R) shows a good value (0.95), which demonstrate a certain linear dependency between real-h and calculated-h;

2. residuals have got some big positive values in the northern part of the aquifer while some big negative values in the southern part (Figure 6.8, with reference to Figure 6.6), which means that probably there is a mean flow distribution with different behaviour from north to south.

3. the LI (total) value, which has been updated manually during the calibration procedure, shows the best feasibility when set equal to 40 Mm^3/yr.

6.2.2 Calibration Dataset 2 (C2)

This calibration exercise uses results from the first calibration. In particular, LI is a not uniform distributed flux along the east side of the aquifer, with higher values in the northern part and lower values in the southern areas.

The LI-flux distribution has been established according to the distribution of average yearly rainfall registered at the 8 gauging stations located in the eastern part of the aquifer (Figure 6.7) taking into account that the northern station (Beit Hanon) has a yearly cumulative rainfall that is nearly the double of the southern one (Rafah).

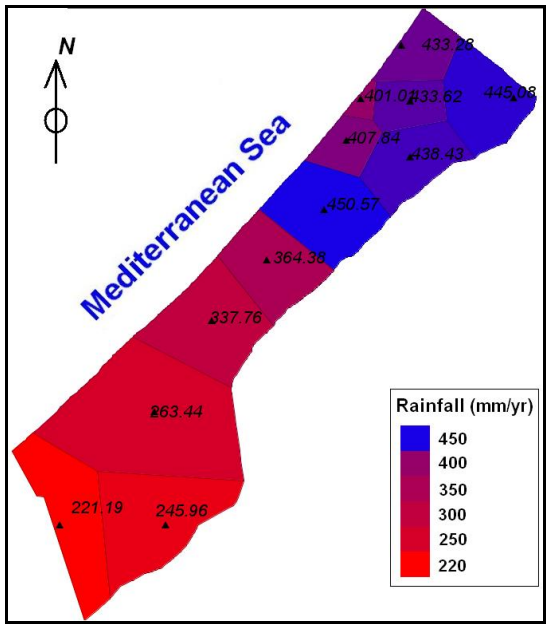

Figure 6.7 - Rainfall Gauging stations and respective Thiessen Polygons, with annual mean values (mm/yr)

As before, different total values of LI are tested to identify the best one, which results around 35 Mm^3/yr; Table 6.3 reports the mean LI flux values for the 8 areas. The calibration model parameters are the same of 'C1'.

The outputs of the calibration procedure (Table 6.2, Table 6.6) show that:

1. the mean value of residuals (-0.10 m) is higher of the 'C1' (in the absolute way), the Φ value (12.26 m) and the standard variance of residuals (0.68 m) have got both lower values than 'C1', which means that the calibration procedure is getting better results and the not-uniform distribution of LI could be reasonable; the correlation coefficient R is also slightly higher than before (0.97);

2. residuals have not the particular distribution of 'C1', but they have positive and negative values throughout the aquifer (Figure 6.8, with reference to Figure 6.6).

All these consideration make it possible to highlight the good calibration result, relatively to h-values.

At this point all outputs from the last simulation are being considered, to verify consistency of the model. In particular, it has been considered the overall hydrological balance of the aquifer, which values are shown in Table 6.6; the values relative to SWI and freshwater outflow (FWO), which are in the order of 2,000 Mm^3/yr, seem to be out of scale, referring to the relative usual values taken in account in the previous studies. It could be inferred that the total in/out (I/O) flux through the seawater/freshwater boundary is probably assuming an excessive magnitude.

6.2.3 Calibration Dataset 3 (C3)

On the evidence of the 'C2' calibration results that show a seawater intrusion inflow of excessive magnitude (2,000 Mm^3/yr), for the third automatic calibration model it is assumed that the seaside of the aquifer should be considered only partially in direct contact with seawater (upper part).

It means that the local Dirichlet boundary condition, based on the imposition of a constant head (h) derived from a hydrostatic pressure along the vertical boundary of the sea side, should be reviewed.

A possible solution consists in changing the value h, considering it from a certain depth level in the vertical (L_0, with depth z_0, in m a.m.s.l.) not variable with z anymore ($h = -\varepsilon z$) but fixed ($h = -\varepsilon z_0$). The level L_0 corresponds to the bottom of the third unit (sandy materials), which is the top of the fourth unit (lens of clay); the average depth of L_0 is about 65 m above zero; the value z_0, being the aquifer depth irregular, is different for each part of the aquifer and, in particular, for each node of the coastline. No other hypotheses have been made on this boundary condition.

The outputs of the 'C3' calibration procedure (Table 6.2, Table 6.6) show that, while the Φ value (16.11 m) and the standard variance of residuals (0.85 m) have got higher values then before, the correlation coefficient R have similar values to 'C2'; residuals have positive and negative values throughout the aquifer (Figure 6.8, with reference to Figure

6.6); SWI and FWO are both assuming much lower values than the previous calibration, in the range of 150 Mm^3/yr.

It should be considered that these two last values are more comparable with the previous studies' ones.

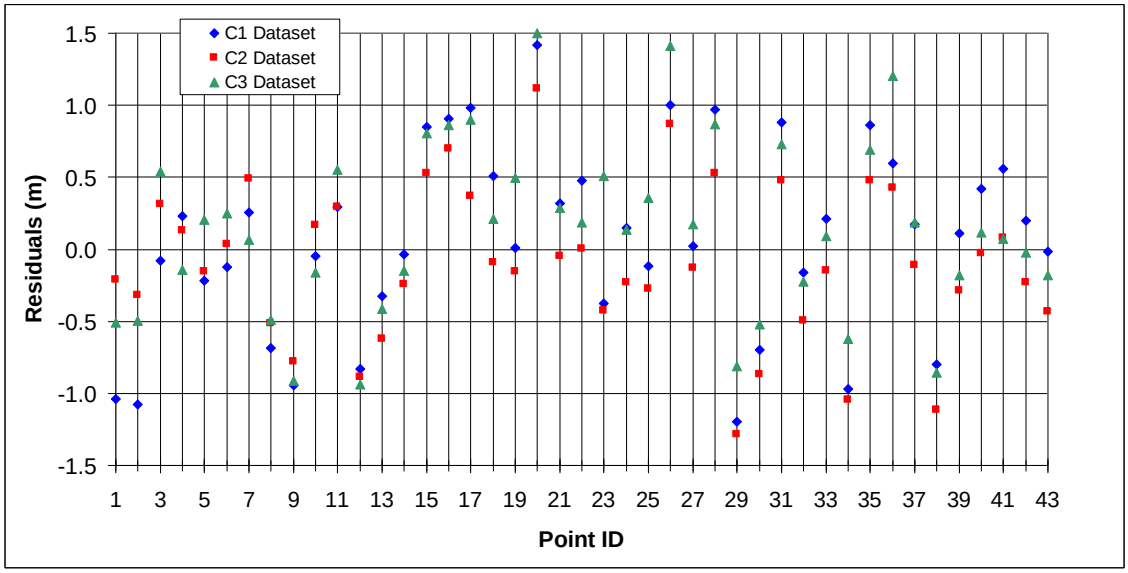

Figure 6.8 – Residuals in control wells (measured point ID)

Parameter ID	C1 dataset		C2 dataset		C3 dataset	
	Kh	Kv	Kh	Kv	Kh	Kv
1	2.17E-04	1.00E-04	2.32E-04	1.00E-04	1.40E-04	1.00E-04
2	1.34E-04	1.00E-05	1.00E-04	1.00E-05	1.00E-04	1.00E-05
3	3.41E-04	1.00E-04	3.15E-04	1.00E-04	2.00E-04	1.00E-05
4	5.94E-05	1.00E-05	1.77E-04	1.91E-05	1.00E-04	1.00E-05
5	4.53E-04	1.00E-05	1.00E-03	1.00E-05	1.00E-04	3.33E-05
6	3.76E-04	1.00E-06	2.76E-04	7.68E-05	1.50E-04	1.00E-05
7	1.00E-03	1.00E-04	4.28E-04	1.00E-04	5.11E-04	1.00E-04
8	2.92E-04	1.00E-04	2.79E-04	1.00E-05	1.00E-04	1.00E-05
9	1.00E-04	1.00E-06	1.00E-04	1.57E-05	1.08E-04	1.17E-05
10	9.14E-04	1.00E-06	4.48E-04	1.00E-05	2.72E-04	1.00E-05
11	3.00E-04	1.00E-06	1.00E-04	3.15E-05	1.00E-04	1.11E-05
Clays (A)	5.00E-07	1.00E-07	5.00E-07	1.00E-07	5.00E-07	1.00E-07

Table 6.2 - Calibrated values of K (m/s) – C1-C2-C3 dataset

Station Id (SID)	Station name	Rainfall (mm/yr)	Total lateral area (m^2)	LI mean Flux/m^2 (C1)	LI mean Flux/m^2 (C2)	LI mean Flux/m^2 (C3)
8	Beit Hanon	445.08	921203	2.29E-07	3.20e-07	7.08E-08
7	Tuffah	438.43	984465	2.29E-07	3.12e-07	6.98E-08
6	Gaza South	450.47	615245	2.29E-07	3.24e-07	7.17E-08
5	Nussirate	364.38	567595	2.29E-07	2.63e-07	5.80E-08
4	Dr-Elbalah	337.76	652564	2.29E-07	2.43e-07	5.37E-08
3	Khan Younis	263.44	740346	2.29E-07	1.88e-07	4.19E-08
2	Khuzaa	245.96	803329	2.29E-07	1.74e-07	3.91E-08
1	Rafah	221.19	259202	2.29E-07	1.59e-07	3.52E-08
Total Lateral Inflow (Mm^3/yr)				40	34.4	20

Table 6.3 - Lateral flux (LI) in terms of mean values per square meter (C1, C2 and C3)

6.2.4 Calibration Dataset 4 (C4)

At this point of the calibration procedure, more interest is focused on the K-optimized values. Although the last calibration model (C3) shows a good consistency with the real behaviour of the aquifer, other consideration should be done about the K values setup.

Generally speaking, all the previous calibration models have shown a same trend in the evaluation of all K-values (Table 6.2). In the proposed scheme of layers (compared within the previous one in Figure 6.9), the setup of which has been chosen simple enough while guaranteeing a certain degree of heterogeneity, upper and lower layers are assuming the same K-value, which means a range around $10^{-3}/10^{-5}$ m/s.

Although geological information about the Gaza Aquifer shows that it could be considered made up by high permeability materials except for clayey layers (Qahman and Larabi, 2006), the proposed configuration hardly represents the real hydrogeological situation, because the considerable mean depth of the aquifer (close to 150 meters) should lead up to lower K-values (in magnitude) in the lower part of the aquifer, due to the geological sedimentation process.

It is assessed another calibration setup, in which lower layers have got K-values in a range of $10^{-5}/10^{-7}$ m/s, while the superficial layer has been considered high-permeable with K-values in a range of $10^{-3}/10^{-5}$ m/s.

Also, although there have been assumed uniform distributed layers of clays throughout the aquifer, the typical geological sections of the Gaza Strip aquifer usually shows continuum stratum of clays only for the first 3-5 km from the coastline to the inner part of the aquifer (Chapter 4, paragraph 4.5.1).

So that, it is assumed that clays are only in the first part of the aquifer, with values of K in a range of 10^{-7}-10^{-8} m/s. The setup of 'C4' calibration has been chosen, again, in order to simplify as much as possible the parameter scheme and to facilitate the calibration procedure, trying at the same time to properly consider a certain degree of heterogeneity. In Table 6.4 it is provided a comparison with to the previous K-zonation.

This configuration leads to consider a different LI flux distribution on the eastern aquifer side, with higher values in the upper parts and lower values in the lower parts, because of the lower quantity of water flowing in the downer layers. The used LI partial flux are reported in Table 6.5, within the same Station ID of Table 6.3.

Although different tests have been assessed, it has not been possible to obtain good results with lower K-values for the bottomed layers; so that, the best configuration reveals high values of K also in the lower layers (Table 6.5).

The outputs of the 'C4' calibration procedure (Table 6.6) show that the Φ value (16.33 m), the standard variance of residuals (0.96 m) have got higher values then before; the correlation coefficient R have got high value (0.96); SWI and FWO are both assuming values in the range 600-700 Mm^3/yr.

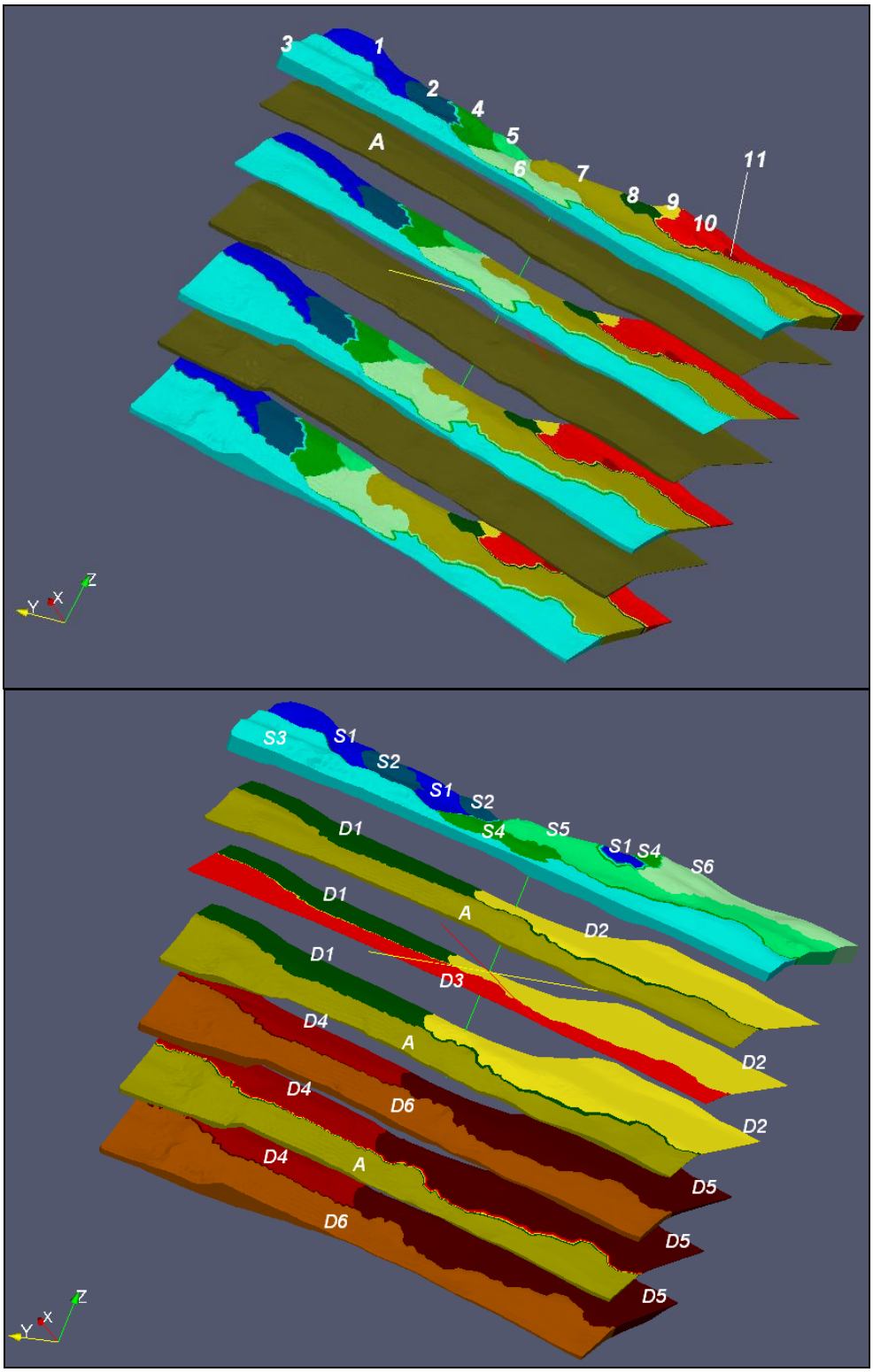

Figure 6.9 – 3D distribution of K-parameters for C1, C2 and C3 setup (top) and for C4 setup (bottom)

C4 material ID	Kh	Kv	C1,C2, C3 materials	layers
S1	1.19E-04	1.00E-04	1, 4, 8	1
S2	1.00E-04	7.00E-06	2, 5	1
S3	3.21E-04	1.00E-04	3	1
S4	1.45E-04	1.00E-04	6, 9	1
S5	1.00E-03	1.00E-04	7	1
S6	9.15E-05	1.00E-06	10, 11	1
Clays (A)	2.72E-08	5.00E-08	clays	2,4,6
D1	5.00E-05	5.00E-06	1, 2(part), 4(part), 5, 6(part)	2,3
D2	5.00E-05	5.00E-06	7,8,9,10,11	2,3
D3	5.00E-05	5.00E-06	3, 2(part), 4(part), 6(part)	3
D4	5.00E-05	5.00E-06	1, 2(part), 4(part), 5, 6(part)	4,5,6,7
D5	5.00E-05	5.00E-06	7,8,9,10,11	4,5,6,7
D6	5.00E-05	5.00E-06	3, 2(part), 4(part), 6(part)	5,7

Table 6.4 - Calibrated K of C4, with corresponding materials and layers adopted in C1, C2, C3

SID	LI mean flux (unit 1)	LI mean flux (unit 2)	LI mean flux (unit 3)	LI mean flux (unit 4)	LI mean flux (unit 5)	LI mean flux (unit 6)	LI mean flux (unit 7)
8	8.58E-08	7.15E-08	5.72E-08	4.29E-08	2.86E-08	1.43E-08	9.54E-10
7	8.46E-08	7.05E-08	5.64E-08	4.23E-08	2.82E-08	1.41E-08	9.40E-10
6	8.69E-08	7.24E-08	5.79E-08	4.34E-08	2.90E-08	1.45E-08	9.65E-10
5	7.03E-08	5.86E-08	4.69E-08	3.51E-08	2.34E-08	1.17E-08	7.81E-10
4	6.51E-08	5.43E-08	4.34E-08	3.26E-08	2.17E-08	1.09E-08	7.24E-10
3	5.08E-08	4.23E-08	3.39E-08	2.54E-08	1.69E-08	8.47E-09	5.65E-10
2	4.74E-08	3.95E-08	3.16E-08	2.37E-08	1.58E-08	7.91E-09	5.27E-10
1	4.27E-08	3.56E-08	2.84E-08	2.13E-08	1.42E-08	7.11E-09	4.74E-10

Table 6.5 - Lateral flux mean values (in $m^3/s/m^2$) for C4

Statistics of Residuals	Unit	C1 dataset	C2 dataset	C3 dataset	C4 dataset
Φ	m	17.91	12.26	16.11	16.33
R	/	0.95	0.97	0.96	0.96
Mean Δh	m	0.06	-0.10	0.13	0.07
Max Δh	m	1.42	1.11	1.49	1.36
Min Δh	m	-1.20	-1.28	-0.94	-1.13
σ	m	0.94	0.68	0.85	0.96
Number of observation points	/	43	43	43	43
Water Balance					
LI	Mm^3/yr	40.0	34.4	20.0	10.0
Vertical Recharge	Mm^3/yr	24.6	24.6	24.6	24.6
SWI	Mm^3/yr	2491.3	2491.3	123.0	630.7
FWO	Mm^3/yr	-2554.4	-2554.4	-167.1	-662.3

Table 6.6 - Statistics and balance for overall 4 calibration datasets

6.2.5 Overall discussion on calibration procedure

After the calibration procedure within the 4 calibration datasets above illustrated, the model is run in short and long term-transient state mode, in order to verify model robustness. Yet, the simulated heads for the year 1970 (adding estimated pumping rates for all wells in the area) are roughly compared within the respective field measured heads, highlighting possible strong difference between the modeled and real water table fields. Unfortunately, the C3 and C4 calibrated datasets show some critical problems for the water table field in several areas of the study site, within producing strong depressions affecting overall the domain; those problems are most likely due to the chosen K-configurations and they are not deeper discuss here; major effort will be done to address this issue in next studies relate to CODESA-3D model.

As the C2 model produces better results of C1 (in terms of residuals and other statistics), this setup is used to perform the validation procedure of the model, described in the following paragraphs. The calibrated water table field is proposed in Figure 6.10, compared with the measured water levels in 1935.

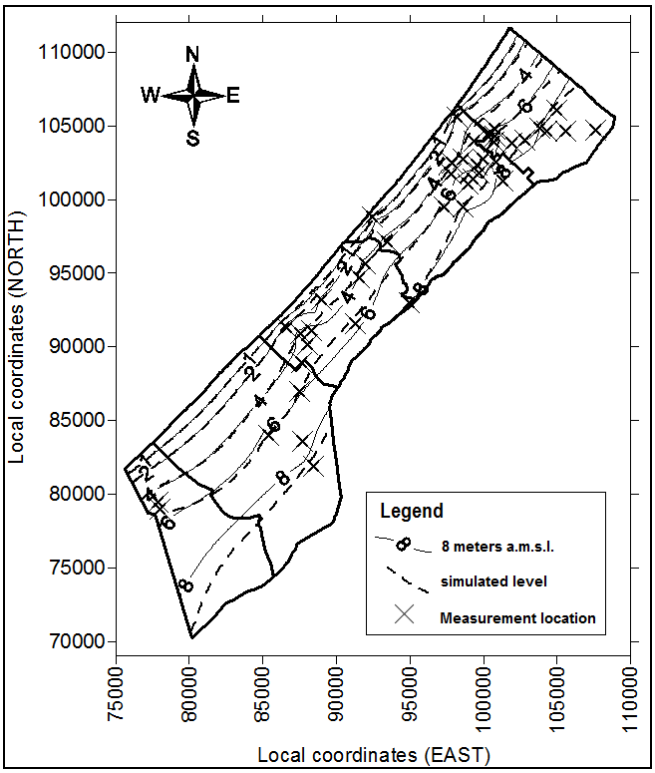

Figure 6.10 –Calibrated water table field (dot lines) and measured water levels in 1935

However, it must be considered that the calibration procedure is constrained by the assumption that all the parameters involved in the calibration procedure are independent.
Table 6.7 shows the parameter correlation matrix , which indicates that:
1) almost all the values are showing low correlation values (thus they are independent);
2) only the two parameters Kh_01 and Kh_03 (horizontal K of the material 1 and 3) are strongly correlated, showing the high value of 0.99;
3) only few of them are showing slightly high correlation values in the range of 0.92-0.95 (Kh_01 and Kh_06, Kh_02 and Kh_06, Kh_03 and Kh_06).
So that, in this study the parameters are generally considered independent, ensuring in this way a strong basis for the calibration procedure.

	kh_01	kv_01	kh_02	kv_02	kh_03	kv_03	kh_04	kv_04	kh_05	kv_05	kh_06	kv_06	kh_07	kv_07	kh_08	kv_08	kh_09	kv_09	kh_10	kv_10	kh_11	kv_11	kh_A	kv_A
kh_01	1.00	0.30	0.92	-0.06	**0.99**	-0.27	0.50	0.07	0.08	0.29	0.93	-0.11	0.85	-0.37	0.27	0.14	-0.10	0.04	0.03	-0.35	0.39	-0.18	-0.25	0.72
kv_01	0.30	1.00	0.41	0.35	0.38	0.31	0.20	-0.12	-0.15	0.31	0.36	-0.24	0.46	-0.35	0.14	0.24	-0.02	0.16	-0.08	-0.27	0.19	-0.08	0.07	-0.10
kh_02	0.92	0.41	1.00	-0.03	0.95	-0.26	0.35	-0.05	0.09	0.36	0.91	-0.17	0.83	-0.41	0.31	0.19	-0.15	-0.01	0.06	-0.34	0.37	-0.18	-0.31	0.63
kv_02	-0.06	0.35	-0.03	1.00	0.01	0.30	-0.49	0.01	0.36	-0.22	0.06	0.05	0.14	-0.26	0.31	0.08	-0.17	-0.14	-0.08	-0.27	0.22	-0.16	-0.05	-0.15
kh_03	**0.99**	0.38	0.95	0.01	1.00	-0.22	0.46	0.04	0.09	0.30	0.94	-0.13	0.88	-0.42	0.30	0.18	-0.12	0.04	0.03	-0.38	0.41	-0.18	-0.29	0.69
kv_03	-0.27	0.31	-0.26	0.30	-0.22	1.00	0.11	-0.02	-0.26	0.04	-0.31	0.00	-0.01	-0.11	-0.01	0.32	0.03	0.27	-0.14	-0.14	-0.04	0.15	0.11	-0.69
kh_04	0.50	0.20	0.35	-0.49	0.46	0.11	1.00	-0.03	-0.68	0.55	0.32	-0.19	0.40	-0.08	-0.19	0.15	0.23	0.42	-0.10	-0.09	0.05	0.12	0.05	0.19
kv_04	0.07	-0.12	-0.05	0.01	0.04	-0.02	-0.03	1.00	-0.08	-0.28	-0.01	-0.04	0.10	-0.03	-0.10	-0.10	0.24	0.24	-0.26	-0.18	0.13	-0.08	0.19	0.08
kh_05	0.08	-0.15	0.09	0.36	0.09	-0.26	-0.68	-0.08	1.00	-0.57	0.18	0.41	0.00	0.07	0.40	-0.06	-0.41	-0.54	0.24	-0.01	0.14	-0.15	-0.32	0.27
kv_05	0.29	0.31	0.36	-0.22	0.30	0.04	0.55	-0.28	-0.57	1.00	0.17	-0.12	0.18	0.07	-0.01	0.21	-0.08	0.08	0.13	0.06	-0.01	-0.11	0.04	0.05
kh_06	0.93	0.36	0.91	0.06	0.94	-0.31	0.32	-0.01	0.18	0.17	1.00	-0.26	0.77	-0.45	0.15	0.11	-0.05	0.05	0.10	-0.21	0.25	-0.10	-0.33	0.71
kv_06	-0.11	-0.24	-0.17	0.05	-0.13	0.00	-0.19	-0.04	0.41	-0.12	-0.26	1.00	-0.17	0.50	0.16	-0.08	-0.12	-0.17	-0.07	-0.06	0.16	0.07	-0.20	0.02
kh_07	0.85	0.46	0.83	0.14	0.88	-0.01	0.40	0.10	0.00	0.18	0.77	-0.17	1.00	-0.65	0.44	0.20	-0.07	0.11	-0.18	-0.68	0.53	-0.22	-0.19	0.46
kv_07	-0.37	-0.35	-0.41	-0.26	-0.42	-0.11	-0.08	-0.03	0.07	0.07	-0.45	0.50	-0.65	1.00	-0.22	-0.12	0.00	-0.09	0.12	0.43	-0.24	0.18	-0.02	-0.15
kh_08	0.27	0.14	0.31	0.31	0.30	-0.01	-0.19	-0.10	0.40	-0.01	0.15	0.16	0.44	-0.22	1.00	0.22	-0.72	-0.65	0.09	-0.57	0.61	-0.55	-0.10	0.16
kv_08	0.14	0.24	0.19	0.08	0.18	0.32	0.15	-0.10	-0.06	0.21	0.11	-0.08	0.20	-0.12	0.22	1.00	-0.53	0.08	0.44	0.08	-0.20	0.04	-0.09	-0.22
kh_09	-0.10	-0.02	-0.15	-0.17	-0.12	0.03	0.23	0.24	-0.41	-0.08	-0.05	-0.12	-0.07	0.00	-0.72	-0.53	1.00	0.76	-0.70	-0.07	-0.01	0.46	0.13	-0.05
kv_09	0.04	0.16	-0.01	-0.14	0.04	0.27	0.42	0.24	-0.54	0.08	0.05	-0.17	0.11	-0.09	-0.65	0.08	0.76	1.00	-0.54	-0.10	-0.08	0.55	0.11	-0.18
kh_10	0.03	-0.08	0.06	-0.08	0.03	-0.14	-0.10	-0.26	0.24	0.13	0.10	-0.07	-0.18	0.12	0.09	0.44	-0.70	-0.54	1.00	0.65	-0.65	-0.13	-0.13	0.06
kv_10	-0.35	-0.27	-0.34	-0.27	-0.38	-0.14	-0.09	-0.18	-0.01	0.06	-0.21	-0.06	-0.68	0.43	-0.57	0.08	-0.07	-0.10	0.65	1.00	-0.85	0.26	0.00	-0.12
kh_11	0.39	0.19	0.37	0.22	0.41	-0.04	0.05	0.13	0.14	-0.01	0.25	0.16	0.53	-0.24	0.61	-0.20	-0.01	-0.08	-0.65	-0.85	1.00	-0.37	-0.02	0.29
kv_11	-0.18	-0.08	-0.18	-0.16	-0.18	0.15	0.12	-0.08	-0.15	-0.11	-0.10	0.07	-0.22	0.18	-0.55	0.04	0.46	0.55	-0.13	0.26	-0.37	1.00	-0.29	-0.21
kh_A	-0.25	0.07	-0.31	-0.05	-0.29	0.11	0.05	0.19	-0.32	0.04	-0.33	-0.20	-0.19	-0.02	-0.10	-0.09	0.13	0.11	-0.13	0.00	-0.02	-0.29	1.00	-0.23
kv_A	0.72	-0.10	0.63	-0.15	0.69	-0.69	0.19	0.08	0.27	0.05	0.71	0.02	0.46	-0.15	0.16	-0.22	-0.05	-0.18	0.06	-0.12	0.29	-0.21	-0.23	1.00

Table 6.7 - Parameter correlation coefficient matrix; in red the highest correlation values (>0.9)

The final output of PEST reports the detailed record of the calibration process, with the optimized parameter values (e.g. K) printed within the 95% confidence limits, together with the parameter covariance and the correlation coefficient matrices. Other important outputs are represented by the parameter sensitivity, which measures composite changes in outputs generated by variations in the value of the parameter, and the observation sensitivity, which measures all adjustable parameters change that followed by changes in the value of real observation. As cited in Chapter 3, paragraph 3.2, parameter sensitivity is useful in order to identify the parameters that could degrade the performance of the optimization process through lack of sensitivity to outputs, while observation sensitivity is useful to identify observations that are more important to the inversion process due to their information content.

In the following, it is briefly reported the sensitivity analysis on the final outputs of the overall calibration process of Calibration Dataset C2 , in terms of parameter sensitivity and observation sensitivity.

6.2.5.1 Parameter sensitivity of Calibration Dataset C2

As above mentioned, during all the iterations, PEST calculates a figure related to the sensitivity of each parameter with respect to all observations. The "composite sensitivity" of parameter i is defined as: $s_i = \left(J^t Q J\right)_{ii}^{1/2} / m$

Where:

- J is the Jacobian matrix (the matrix comprised of m rows (one for each observation), the i elements of each row being the derivatives of one particular "model-generated" observation with respect to each of the i parameters)
- Q is the "cofactor matrix"; in most instances the latter is a diagonal matrix whose elements are comprised of the squared observation weights;
- m is the number of observations with non-zero weights.

Thus the composite sensitivity of the i 'th parameter is the normalised (with respect to the number of observations) magnitude of the column of the Jacobian matrix pertaining to that parameter, with each element of that column multiplied by the weight pertaining to the respective observation. The relative composite sensitivity of a parameter is obtained by multiplying its composite sensitivity by the magnitude of the value of the parameter. It

is thus a measure of the composite changes in model outputs that are incurred by a fractional change in the value of the parameter. Composite parameter sensitivities are useful in identifying those parameters which may be degrading the performance of the parameter estimation process through lack of sensitivity to model outcomes. The use of relative sensitivities in addition to normal sensitivities assists in comparing the effects that different parameters have on the parameter estimation process when these parameters are of different type, and possibly of very different magnitudes.

In Figure 6.11 it is shown the parameter sensitivity file of the calibration procedure; almost all parameters have low sensitivity values, some of them quite moderate sensitivity values (kh_aquif_01, kh_aquif_06, kh_aquif_07) and one of them high sensitivity values (kh_aquif_03). Yet, as generally happens in groundwater flow studies, the most sensitive parameters are those relative to horizontal conductivities (Kh).

The chosen parameter dataset reveals quite good sensitivity values, with only very few parameters that may degrade the performance of the parameter estimation process through lack of sensitivity to model outcomes.

COMPLETION OF OPTIMISATION PROCESS

Composite sensitivities for all observations/prior info ----->

Number of observations with non-zero weight = 43

Parameter name	Group	Current value	Sensitivity	Rel. Sensitivity
kh_aquif-01	k	2.323589E-04	0.243174	0.883655
kv_aquif-01	k	1.000000E-04	6.211509E-04	2.484604E-03
kh_aquif-02	k	1.000000E-04	0.129918	0.519672
kv_aquif-02	k	1.000000E-05	2.041972E-03	1.020986E-02
kh_aquif-03	k	3.146337E-04	1.13431	3.97257
kv_aquif-03	k	1.000000E-04	1.488036E-03	5.952143E-03
kh_aquif-04	k	1.772063E-04	9.001540E-02	0.337695
kv_aquif-04	k	1.906470E-05	8.176022E-05	3.858894E-04
kh_aquif-05	k	1.000000E-03	1.293308E-02	3.879925E-02
kv_aquif-05	k	1.000000E-05	2.743609E-04	1.371805E-03
kh_aquif-06	k	2.755038E-04	0.214278	0.762801
kv_aquif-06	k	7.678402E-05	2.936024E-04	1.208094E-03
kh_aquif-07	k	4.284086E-04	0.188593	0.635209
kv_aquif-07	k	1.000000E-04	2.785648E-04	1.114259E-03
kh_aquif-08	k	2.791802E-04	9.569326E-03	3.401049E-02
kv_aquif-08	k	1.000000E-05	1.143796E-05	5.718981E-05
kh_aquif-09	k	1.000000E-04	6.296759E-03	2.518703E-02
kv_aquif-09	k	1.571747E-05	7.668137E-05	3.683480E-04
kh_aquif-10	k	4.483179E-04	8.485015E-02	0.284113
kv_aquif-10	k	1.000000E-05	1.570510E-03	7.852552E-03
kh_aquif-11	k	1.000000E-04	1.782787E-03	7.131147E-03
kv_aquif-11	k	3.146631E-05	1.338712E-05	6.027089E-05
kh_aquitard	k	5.000000E-07	1.502285E-04	1.051600E-03
kv_aquitard	k	1.000000E-07	2.726386E-02	0.171790

Figure 6.11 - Part of the parameter sensitivity output file of the calibration procedure with PEST

6.2.5.2 Observation sensitivity of Calibration Dataset C2

The composite observation sensitivity of observation is defined as: $o_j = \left\{Q\left(JJ^t\right)\right\}_{jj}^{1/2} / n$

The composite sensitivity of observation j is the magnitude of the j-th row of the Jacobian multiplied by the weight associated with that observation; this magnitude is then divided by the number of adjustable parameters n. It is thus a measure of the sensitivity of that observation to all parameters involved in the parameter estimation process.

Thus while a high value of composite observation sensitivity would, at first sight, indicate that an observation is particularly crucial to the inversion process because of its high information content, this may not necessarily be the case. Another observation made at nearly the same time and/or place as the first observation may carry nearly the same information content. In this case, it may be possible to omit one of these observations from the parameter estimation process with impunity, for the information which it carries is redundant as long as the other observation is included in the process. Thus while a high value of composite observation sensitivity does indeed mean that the observation to which it pertains is possibly sensitive to many parameters, it does not indicate that the observation is particularly indispensable to the parameter estimation process, for this can only be decided in the context of the presence or absence of other observations with similar sensitivities.

In Figure 6.12 it is shown the observation sensitivity file of the calibration procedure. Almost all observations have similar sensitivity values; observation 16 (h016), which lies in proximity of the coastal line, has got very low sensitivity value; observation 43 (h043), which lies in proximity of the north-eastern boundary (see Figure 6.6) and represents the highest observed value, has got the highest sensitivity value.

The observation dataset seems to reveal quite good sensitivity values, with only one observation (h016) that can be considered not particularly indispensable to the parameter estimation process, and only one observation (h043) which can be considered the most sensitive to the chosen parameter dataset. Additional measures in the surroundings of point h043 could be very useful to the inversion procession and thus to the final goal to obtain a better calibrated model.

Observation	Group	Measured	Modelled	Sensitivity
h001	obsgroup	5.200000	5.410419	0.4137387
h002	obsgroup	5.450000	5.769840	0.4315952
h003	obsgroup	6.420000	6.105446	0.4359666
h004	obsgroup	2.640000	2.508869	0.1516375
h005	obsgroup	5.820000	5.971500	0.4205780
h006	obsgroup	7.270000	7.235748	0.5046880
h007	obsgroup	4.520000	4.028400	0.2849690
h008	obsgroup	4.740000	5.256840	0.3588172
h009	obsgroup	4.150000	4.928801	0.3343828
h010	obsgroup	4.650000	4.483519	0.3106021
h011	obsgroup	8.480000	8.186340	0.5745318
h012	obsgroup	2.200000	3.087390	0.1648225
h013	obsgroup	5.700000	6.323229	0.4262380
h014	obsgroup	4.180000	4.422880	0.2586283
h015	obsgroup	4.600000	4.070580	0.2232920
h016	obsgroup	1.720000	1.023261	4.9652285E-02
h017	obsgroup	4.640000	4.272179	0.2318404
h018	obsgroup	7.690000	7.780000	0.5430719
h019	obsgroup	6.150000	6.306469	0.3735685
h020	obsgroup	5.590000	4.478458	0.2469033
h021	obsgroup	4.000000	4.044518	0.2266305
h022	obsgroup	2.330000	2.325171	0.1062155
h023	obsgroup	7.780000	8.209461	0.5412524
h024	obsgroup	4.390000	4.621838	0.2791972
h025	obsgroup	6.420000	6.692589	0.4090831
h026	obsgroup	7.470000	6.602619	0.4088256
h027	obsgroup	5.700000	5.827009	0.3747574
h028	obsgroup	5.290000	4.762030	0.2796839
h029	obsgroup	5.390000	6.673069	0.4252912
h030	obsgroup	5.240000	6.108561	0.4031319
h031	obsgroup	5.930000	5.451683	0.3444520
h032	obsgroup	5.660000	6.152760	0.4188942
h033	obsgroup	5.790000	5.936802	0.3934825
h034	obsgroup	6.200000	7.244831	0.4965572
h035	obsgroup	6.180000	5.704002	0.3678531
h036	obsgroup	9.520000	9.092777	0.6355510
h037	obsgroup	7.200000	7.308128	0.5366366
h038	obsgroup	6.840000	7.951653	0.5867191
h039	obsgroup	7.980000	8.270290	0.6258109
h040	obsgroup	8.660000	8.689247	0.6645355
h041	obsgroup	8.530000	8.447559	0.6501840
h042	obsgroup	9.820000	10.04812	0.7737047
h043	obsgroup	11.42000	11.85528	0.9469053

Figure 6.12 - Part of the observation sensitivity output file of the calibration procedure with PEST

6.3 Validation – period 1935-2010

The Gaza Strip model is validated performing a transient-state simulation for the period 1935-2010, starting from results coming from the 'C2' calibration procedure, setting as initial conditions the calibrated K-values and the initial water level of the steady state flow model for year 1935. The initial concentration in the aquifer is assumed, in the first runs, to be 0 kg/m^3 for the entire domain, and then it is update within field measured Chlorides concentrations. Recharging values due to rainfall and LI are set up within the same mean values of the calibration procedure. For the northern part of the aquifer (North governorate), and only for the period 1980-2000, it is considered an additional recharge of about 5,000-10,000 m^3/day due to the discharge of partially treated wastewater in the

sandy dunes area around Beit Lahia Wastewater Treatment Plant (WWTP, described in Chapter 4). All the parameters that pertain to hydraulic values are setup as illustrated in Table 6.1. As internal stress, they are introduced the estimated pumping rates as described in Chapter 4, paragraph 4.6, taking into consideration the deducted amount (adjusted on the evidence of validation results) in the range between 20 and 30% for each pumping well to represent the return flow which comes from irrigation, sewage infiltration and leakages from water networks. This is done to avoid the setup of recharge zones in the model and to decrease the uncertainty coming from assigning the location of return flow which is not well known. In the southern part of the model (Rafah governorate) another uncertainty has been highlighted about the pumping rates, due to the Israeli settlements during the last part of the studied period, so that the amount of pumping rates has been considerably increased in this area.

6.3.1 Results - validation period 1935-2000

In order to evaluate the numerical model performance on the flow problem throughout all the considered period, there are compared simulated groundwater table values within respective average 1970, 1990 and 2000 groundwater table levels; location of control wells changed during the considered period, but some location (19) have remained the same for each chosen year, so that they are separately analyzed and considered to synthetically represent the groundwater evolution throughout the overall domain. For the solute problem, there are compared simulated salt concentration for 2000 year with respective measured average chlorides (Cl^-) concentrations on control wells within 2.5 km from the coastline.

The results of validation for groundwater table levels are presented in Table 6.8 in terms of statistics of residuals.

For year 1970, the calculated residual mean error and absolute mean error are about 0.09 and 0.58 m, respectively, with a standard deviation for the model domain of 0.70 m; for year 1990, the calculated residual mean error and absolute mean error are about −0.10 and 0.66 m, respectively, with a standard deviation for the model domain of 0.79 m; for year 2000, the calculated residual mean error and absolute mean error are about 0.51 and 0.82 m, respectively, with a standard deviation for the model domain of 0.88 m.

Statistics of residuals	Unit	Symbol	1970	1990	2000
Variance of Absolutes	m	σ_a	0.16	0.19	0.35
Standard deviation of Absolutes	m	σ^2_a	0.40	0.44	0.60
Minimum of Absolutes	m	min_a	0.02	0.04	0.03
Maximum of Absolute	m	Max_a	1.67	1.60	2.75
Mean of Absolutes	m	$mean_a$	0.58	0.66	0.82
Variance	m	σ	0.50	0.62	0.78
Standard deviation	m	σ^2	0.70	0.79	0.88
Minimum	m	min	-1.24	-1.55	-1.73
Maximum	m	Max	1.67	1.60	2.75
Mean	m	mean	0.09	-0.10	0.51
Correlation coefficient	/	R	0.89	0.71	0.82
Square correlation coefficient	/	R^2	0.79	0.51	0.68
No. observation	-	-	38	68	86

Table 6.8 – Statistics of residuals for the 1970, 1990 and 2000 validation datasets

In Figure 6.13, Figure 6.14 and Figure 6.15 are compared real and simulated water levels for 1970, 1990 and 2000 within the location of control wells.

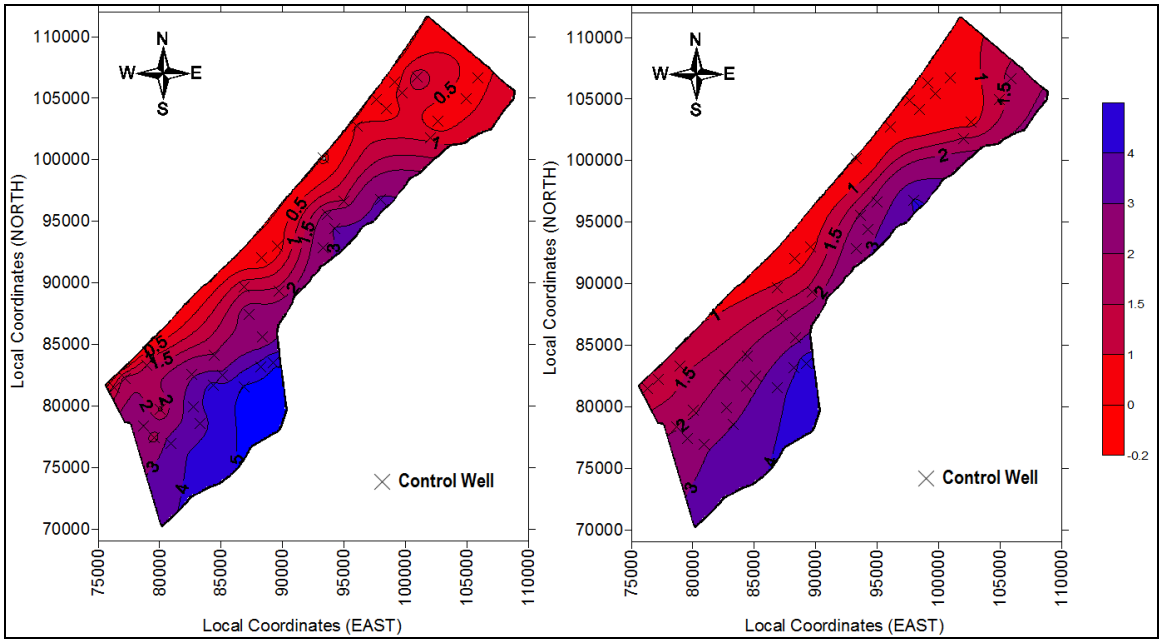

Figure 6.13 - Real (left part) and simulated (right part) water table levels for year 1970

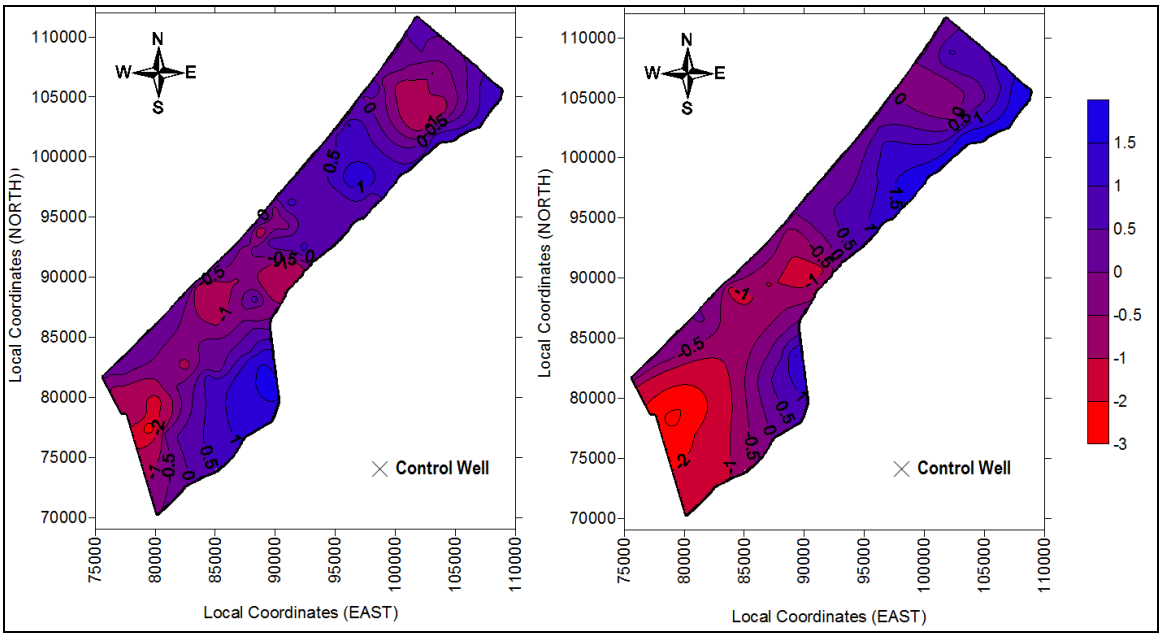

Figure 6.14 - Real (left part) and simulated (right part) water table levels for year 1990

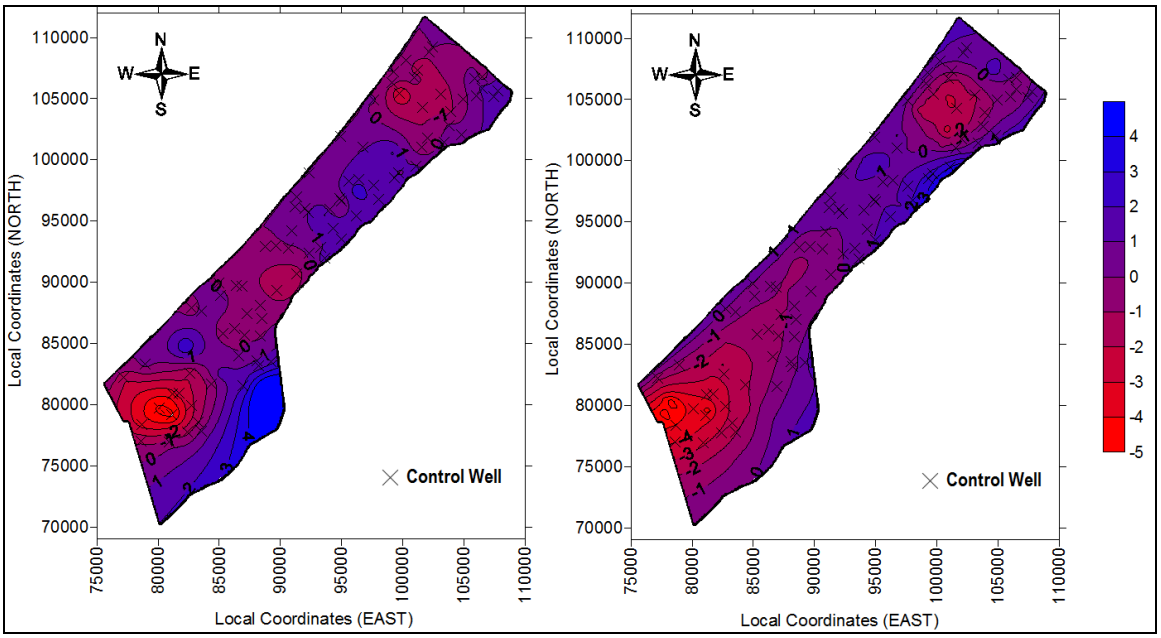

Figure 6.15 - Real (left part) and simulated (right part) water table levels for year 2000

In Table 6.9 are provided results about residuals for the fixed 19 control wells (Figure 6.16) for the same validation datasets; in Table 6.10 is illustrated a comparison between those 19 simulated and real groundwater levels.

Statistics	Unit	Symbol	1970	1990	2000
Variance of Absolutes	m	σ_a	0.20	0.27	0.39
Standard deviation of Absolutes	m	σ^2_a	0.44	0.52	0.63
Minimum of Absolutes	m	min_a	0.03	0.07	0.24
Maximum of Absolute	m	Max_a	1.67	1.60	2.64
Mean of Absolutes	m	$mean_a$	0.74	0.77	0.94
Variance	m	σ	0.74	0.90	0.80
Standard deviation	m	σ^2	0.86	0.95	0.89
Minimum	m	min	-1.24	-1.53	-1.11
Maximum	m	Max	1.67	1.60	2.64
Mean	m	mean	0.19	0.04	0.71
Correlation coefficient	/	R	0.87	0.56	0.82
Square correlation coefficient	/	R^2	0.75	0.32	0.67
No. observation	-	-	19	19	19

Table 6.9 - Statistics of residuals for the 1970, 1990 and 2000 validation datasets (19 observation wells)

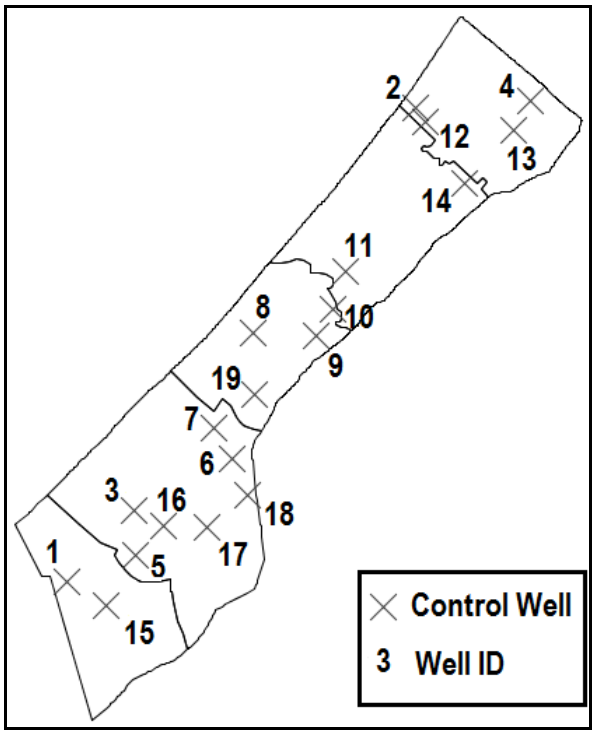

Figure 6.16 – Location of 19 control wells for years 1970, 1990 and 2000.

WELL ID	Real values (h) – in m a.m.s.l.				Simulated values (h) – in m a.m.s.l.			
	1970	1990	2000	Difference 2000-1970	1970	1990	2000	Difference 2000-1970
1	3.05	-1.35	-3.40	-6.45	1.93	-2.94	-4.87	-6.81
2	0.19	-0.82	-0.66	-0.85	0.51	-0.39	-1.57	-2.08
3	2.81	-1.19	-1.86	-4.67	1.97	-1.12	-2.79	-4.76
4	0.43	-0.05	0.65	0.22	1.67	0.94	-0.01	-1.67
5	3.68	-0.22	-2.21	-5.89	2.51	-1.44	-3.10	-5.62
6	1.99	0.11	-0.13	-2.12	2.64	-0.03	-0.50	-3.14
7	2.41	-0.52	-0.41	-2.82	1.83	-0.73	-1.09	-2.91
8	0.25	0.19	-0.11	-0.36	0.87	-0.72	-0.72	-1.58
9	2.59	0.36	0.88	-1.71	2.52	0.44	0.32	-2.20
10	3.07	0.17	1.20	-1.87	2.67	0.84	0.62	-2.05
11	1.52	0.21	0.23	-1.29	2.25	0.76	0.47	-1.78
12	0.74	-0.90	-3.01	-3.75	0.22	-0.38	-2.17	-2.39
13	0.34	-0.67	-0.20	-0.54	1.33	0.46	-0.88	-2.21
14	0.88	-0.69	-0.90	-1.78	1.54	0.83	-1.14	-2.68
15	3.69	-0.20	-0.40	-4.08	2.87	-1.80	-3.04	-5.91
16	4.31	0.68	-0.65	-4.96	2.64	-0.68	-2.10	-4.74
17	5.10	1.17	1.73	-3.37	3.70	0.47	-0.49	-4.20
18	4.88	1.32	1.66	-3.21	4.63	1.59	0.81	-3.82
19	1.63	-1.73	-1.73	-3.37	1.66	-1.04	-0.62	-2.28
mean	2.29	-0.22	-0.49	-2.78	2.10	-0.26	-1.20	-3.31

Table 6.10 - Measured and simulated groundwater heads h in 19 control wells (1970 -1990-2000)

In the above described 19 control wells, the mean difference between averaged real heads from 1970 to 2000 is -2.78 m, while the real mean difference between averaged simulated heads from 1970 to 2000 is -3.31m; so that, it can be inferred that the model is simulating around 0.5 m more of water lowering. Although there are still several uncertainties on illegal wells location and operational rates, and about real pumping rates on the southern area of the domain (Rafah area), the results of transient calibration for the flow problem are considered acceptable for this study purpose. Overall groundwater levels for 1970, 1990 and 2000 simulations are reported in Appendix A.

For the solute problem, there are compared simulated salt concentrations for 2000 year within respective measured average Chlorides (Cl^-) concentrations on control wells within 2.5 km from the coastline. In Figure 6.17 is shown the 0.1 isoline representation of simulated and real normalized chlorides concentrations for 2000.

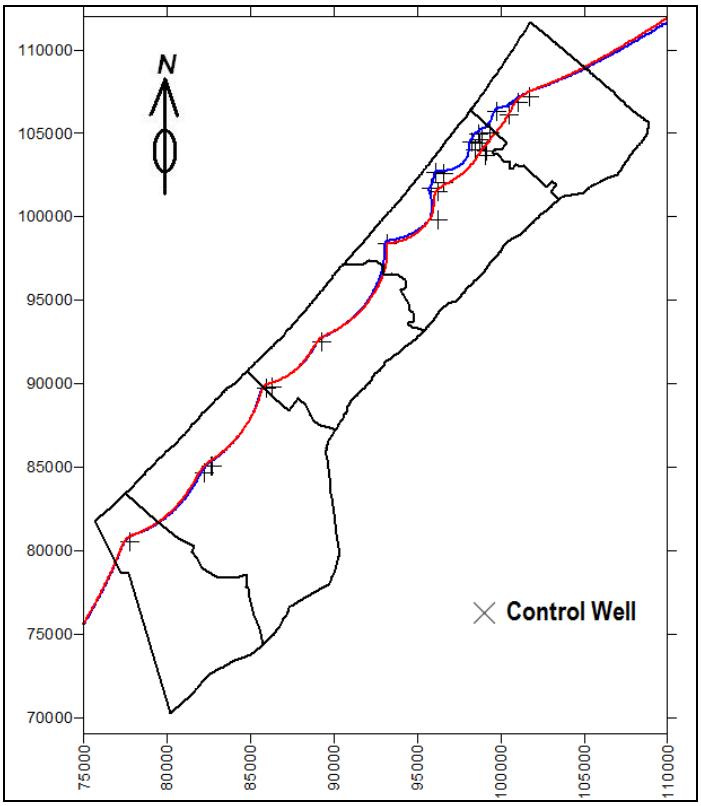

Figure 6.17 – Year 2000: real (blue) and simulated (red) 0.1 normalized Chlorides concentration

6.3.2 Results - validation period 2001-2010

The Gaza Strip model is additionally validated performing a transient-state simulation for the period 2001-2010. Initial conditions are imposed, both for the flow and for the solute problem, as derived from the validation results of the period 1935-2000.

The vertical net recharge rate is calculated as a percentage of the net recharging rainfall (paragraph 6.3.1), which is calculated considering the recorded daily rainfall data from gauging station and evaluating, within the Penman-Monteith method (Appendix B), evapotranspiration according to daily and monthly meteorological data for the period 2001-2010. Internal stresses are inserted as actual municipal and agricultural wells' pumping rates recorded for the same period. Yet, some freshwater recharging areas are located overall the domain (mainly in the northern area), according to WWTP locations and other actual artificial recharging points

In order to evaluate the numerical model performance on the flow problem throughout all the considered period, there are compared simulated groundwater table values within

respective average 2010 groundwater table levels. The results of validation for groundwater table levels are presented in Table 6.11 in terms of statistics of residuals.

Statistics of residuals	Unit	Symbol	2010
Variance of Absolutes	m	σ_a	0.49
Standard deviation of Absolutes	m	σ^2_a	0.70
Minimum of Absolutes	m	min_a	0.01
Maximum of Absolute	m	Max_a	4.07
Mean of Absolutes	m	$mean_a$	0.94
Variance	m	σ	1.39
Standard deviation	m	σ^2	1.18
Minimum	m	min	-3.16
Maximum	m	Max	4.07
Mean	m	mean	-0.04
Correlation coefficient	/	R	0.94
Square correlation coefficient	/	R^2	0.89
No. observation	-	-	67

Table 6.11 - Statistics of residuals for the 2010 validation dataset

For year 2010, the calculated residual mean error and absolute mean error are about -0.04 and 0.94 m, respectively, with a standard deviation for the model domain of 1.18 m. The relative groundwater levels are reported in Appendix A. In Figure 6.18 are compared real and simulated water levels for 2010.

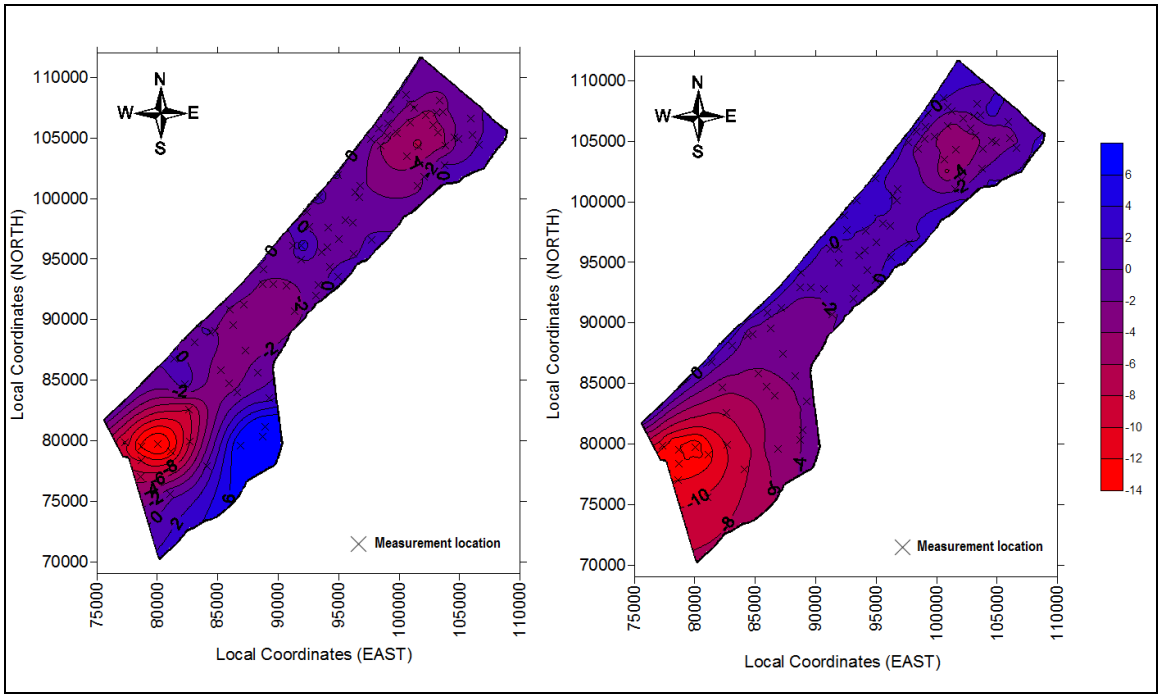

Figure 6.18 - Real (left) and simulated (right) water table - year 2010

As for the previous validation period, there are still several uncertainties on illegal wells location and operational rates, and about real pumping rates on the southern area of the domain (Rafah area). The model is not properly reproducing the real water table levels in the southern uphill part of the study area, but the main scope of this study is to analyse SWI which occurs in the coastal part of the aquifer, where the model is properly reproducing groundwater flow; so that, the results of transient calibration for the flow problem are considered acceptable for this study purpose.

As for the first validation period, location of control wells changed during the considered period, but some locations (14) have remained the same for all every chosen control year from 1970 to 2010. So that, the model performance on the flow problem is finally evaluated in 14 control wells (Table 6.12, with reference to Table 6.10) over all the considered period to synthetically represent the groundwater evolution throughout the domain.

WELL ID	Real values (h) – in m a.m.s.l.					Simulated values (h) - in m a.m.s.l.				
	1970	1990	2000	2010	Difference 2010-1970	1970	1990	2000	2010	Difference 2010-1970
1	3.05	-1.35	-3.40	-10.10	-13.15	1.93	-2.94	-4.87	-13.17	-15.10
2	0.19	-0.82	-0.66	-1.43	-1.62	0.51	-0.39	-1.57	-2.71	-3.22
3	2.81	-1.19	-1.86	-8.00	-10.81	1.97	-1.12	-2.79	-7.76	-9.73
4	0.43	-0.05	0.65	-0.44	-0.86	1.67	0.94	-0.01	-1.53	-3.20
5	3.68	-0.22	-2.21	-7.91	-11.59	2.51	-1.44	-3.10	-9.74	-12.25
6	1.99	0.11	-0.13	-1.11	-3.11	2.64	-0.03	-0.50	-3.41	-6.05
7	2.41	-0.52	-0.41	-2.66	-5.07	1.83	-0.73	-1.09	-3.34	-5.16
8	0.25	0.19	-0.11	-2.52	-2.78	0.87	-0.72	-0.72	-1.53	-2.40
9	2.59	0.36	0.88	-1.29	-3.88	2.52	0.44	0.32	-0.97	-3.49
10	3.07	0.17	1.20	-0.73	-3.80	2.67	0.84	0.62	-0.44	-3.11
11	1.52	0.21	0.23	-1.19	-2.71	2.25	0.76	0.47	-0.39	-2.64
12	0.74	-0.90	-3.01	-4.32	-5.06	0.22	-0.38	-2.17	-3.88	-4.10
13	0.34	-0.67	-0.20	-1.65	-1.99	1.33	0.46	-0.88	-2.70	-4.03
14	0.88	-0.69	-0.90	-1.91	-2.79	1.54	0.83	-1.14	-3.09	-4.63
mean	1.71	-0.38	-0.71	-3.23	-4.94	1.75	-0.25	-1.24	-3.90	-5.65

Table 6.12 - Measured and simulated groundwater heads (h) in m a.m.s.l. for years 1970, 1990, 2000 and 2010 for 14 control wells.

In the above described 14 control wells, the mean difference between averaged real heads from 1970 to 2010 is -4.94 m, while the real mean difference between averaged simulated heads from 1970 to 2000 is –5.65 m; so that, it can be inferred that the model is simulating around 0.7 m more of water lowering in the period 1970-2010.

For the solute problem, there are compared simulated salt concentrations for 2010 year within respective measured average Chlorides (Cl^-) concentrations on control wells within 2.5 km from the coastline. In Figure 6.19 is shown the 0.1 isoline representation of simulated and real chlorides concentrations.

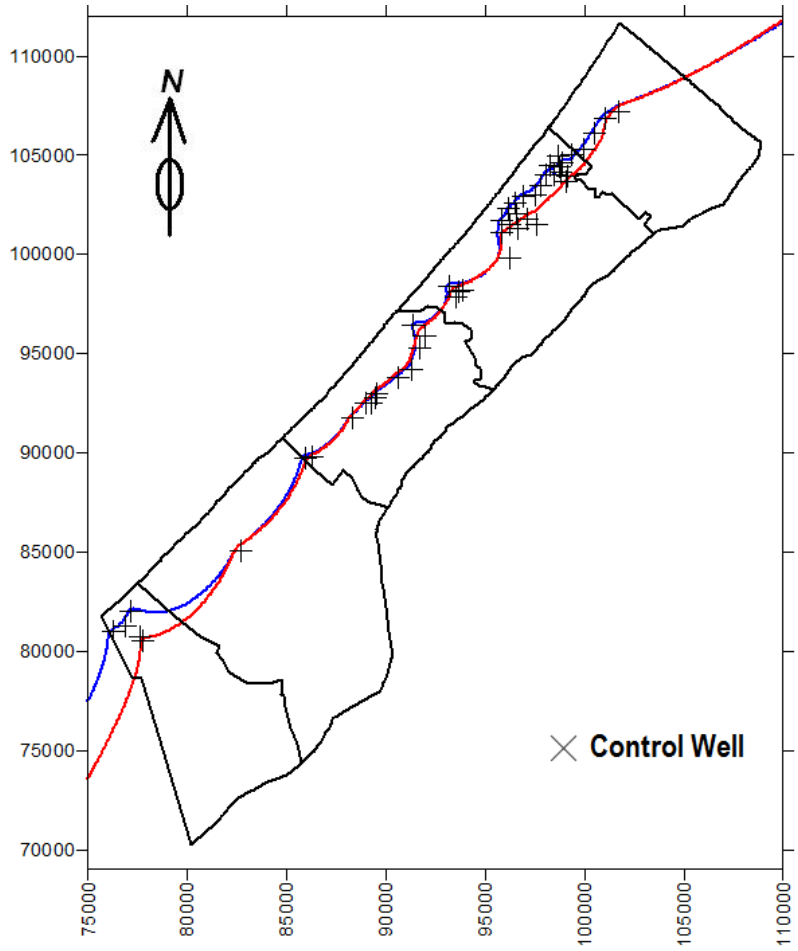

Figure 6.19 – Year 2010: real (blue) and simulated (red) 0.1 normalized Chlorides concentration

6.3.3 Discussion on validation results for the transport problem

In order to evaluate the numerical model performance on the transport problem, it is proposed a deeper analysis of results of certain control wells aiming at synthetically represent the salt concentration evolution in the overall domain in the period 2000-2010 for 17 control points (solute problem, Table 6.13, with reference to Figure 6.20).

In Figure 6.21 are represented the locations of 3 vertical cross sections along the Gaza Strip aquifer in the northern (Figure 6.22), central (Figure 6.23) and southern area (Figure 6.24), adopted to show the simulated salt water intrusion in terms of normalized concentration of Cl^- both for year 2000 and 2010.

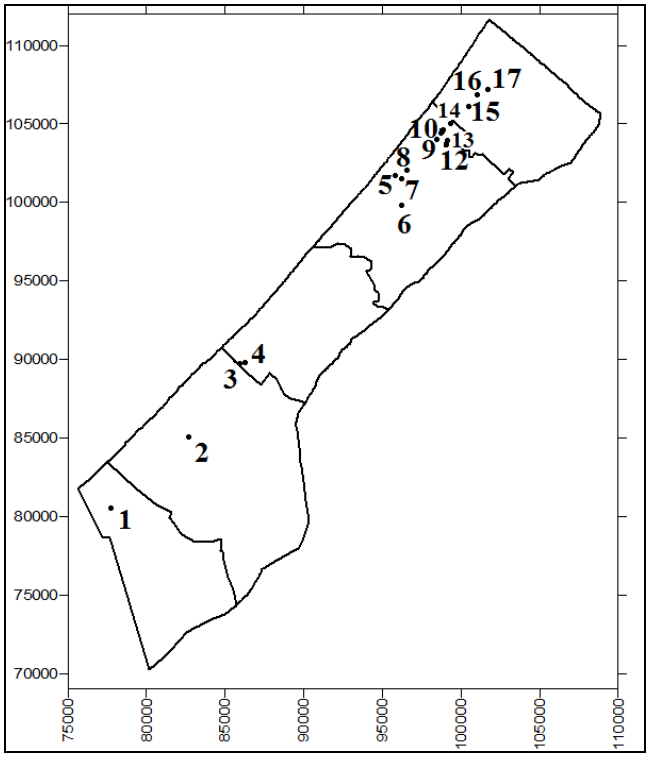

Figure 6.20 – Chlorides concentration 17 control point (2000 and 2010)

Point ID	C real 2000	C real 2010	Difference Real C 2010 - 2000	Difference in Mg/l	Difference in %	C sim 2000	C sim 2010	Difference Simulated C 2010 - 2000	Difference in Mg/l	Difference in %
1	0.00533	0.00482	-0.00051	-12.8	-0.1	0.000068	0.087888	0.087820	2195	1283.2
2	0.01918	0.0268	0.00762	190.5	0.4	0.002203	0.011329	0.009126	228	4.1
3	0.00383	0.04552	0.04169	1042.3	10.9	0.012012	0.137430	0.125418	3135	10.4
4	0.00442	0.04148	0.03706	926.5	8.4	0.005811	0.056257	0.050445	1261	8.7
5	0.00640	0.01854	0.01214	303.5	1.9	0.201036	0.333555	0.132518	3313	0.7
6	0.01285	0.02064	0.00779	194.8	0.6	0.000004	0.000007	0.000003	0	0.7
7	0.00516	0.01562	0.01046	261.5	2.0	0.054079	0.120681	0.066601	1665	1.2
8	0.01610	0.01994	0.00384	96.0	0.2	0.147948	0.251401	0.103453	2586	0.7
9	0.01698	0.03328	0.01630	407.5	1.0	0.187008	0.396436	0.209428	5236	1.1
10	0.00991	0.04814	0.03823	955.8	3.9	0.191701	0.428804	0.237102	5928	1.2
11	0.01068	0.02484	0.01416	354.0	1.3	0.196864	0.428943	0.232079	5802	1.2
12	0.01932	0.02048	0.00116	29.0	0.1	0.018844	0.080373	0.061529	1538	3.3
13	0.01977	0.03722	0.01745	436.3	0.9	0.035011	0.118292	0.083282	2082	2.4
14	0.01386	0.187	0.17314	4328.5	12.5	0.177511	0.401237	0.223726	5593	1.3
15	0.00308	0.0365	0.03342	835.5	10.9	0.074056	0.238815	0.164759	4119	2.2
16	0.00238	0.00268	0.00030	7.5	0.1	0.019977	0.108923	0.088946	2224	4.5
17	0.00154	0.00258	0.00104	26.0	0.7	0.000000	0.007498	0.007498	187	--

Table 6.13 - Chlorides concentration in 17 control point – simulated and real values (2000 and 2010)

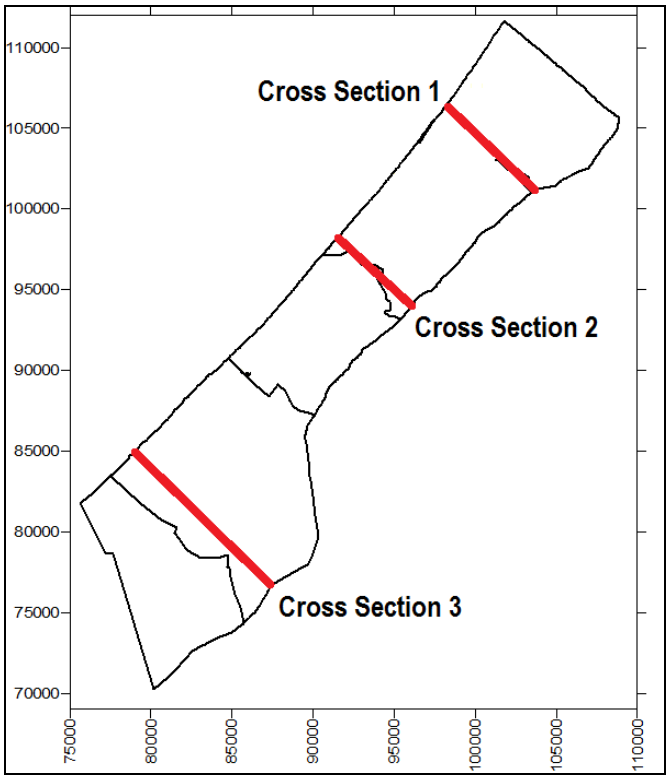

Figure 6.21 –Vertical Cross Sections adopted for SWI

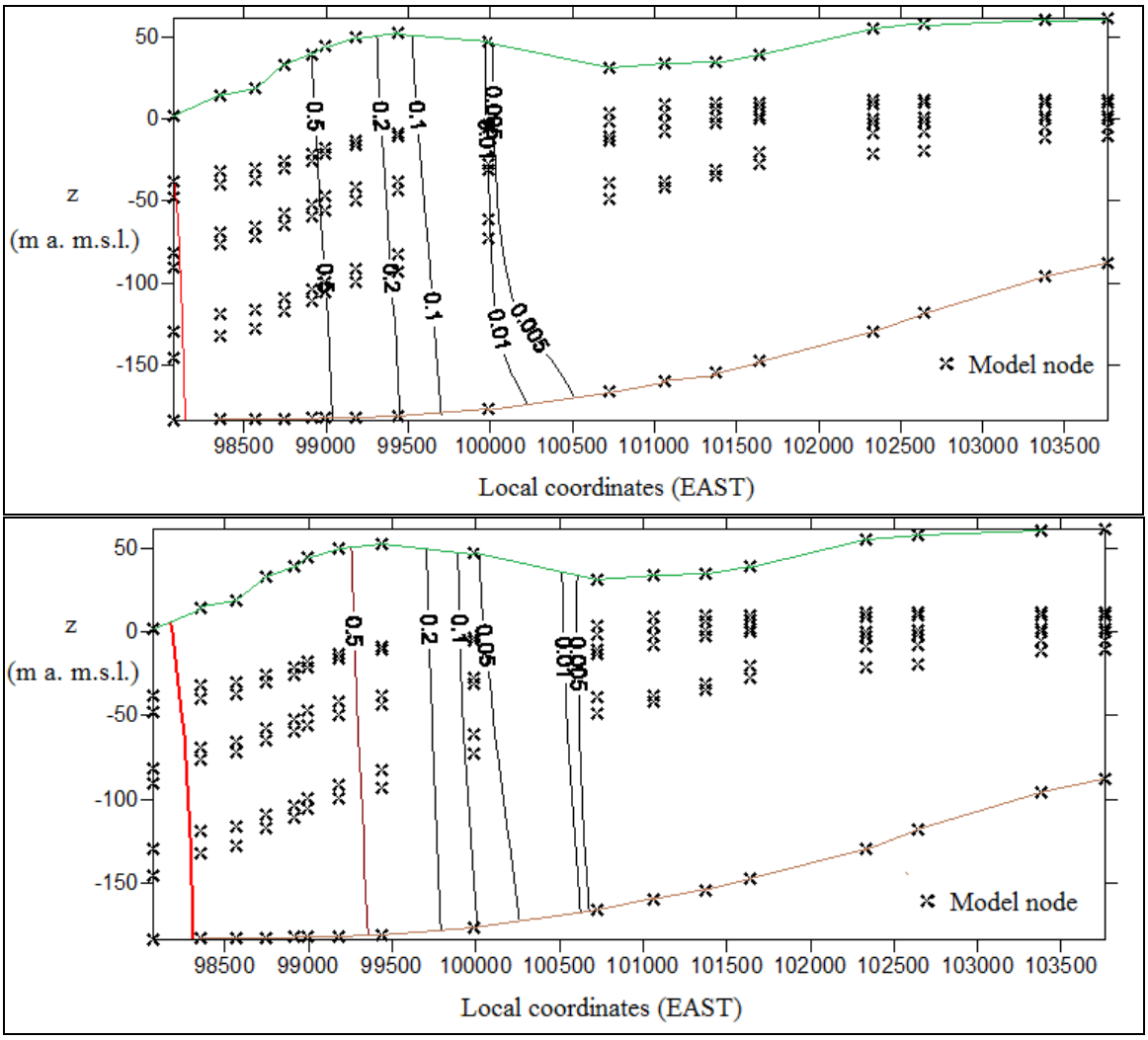

Figure 6.22 - Cross section 1: year 2000 (top) and 2010 (bottom) with the indication of model nodes (cross symbol); in red the 1 isoline of normalized concentration equal to 1, in green the land surface and in brown the bottom surface

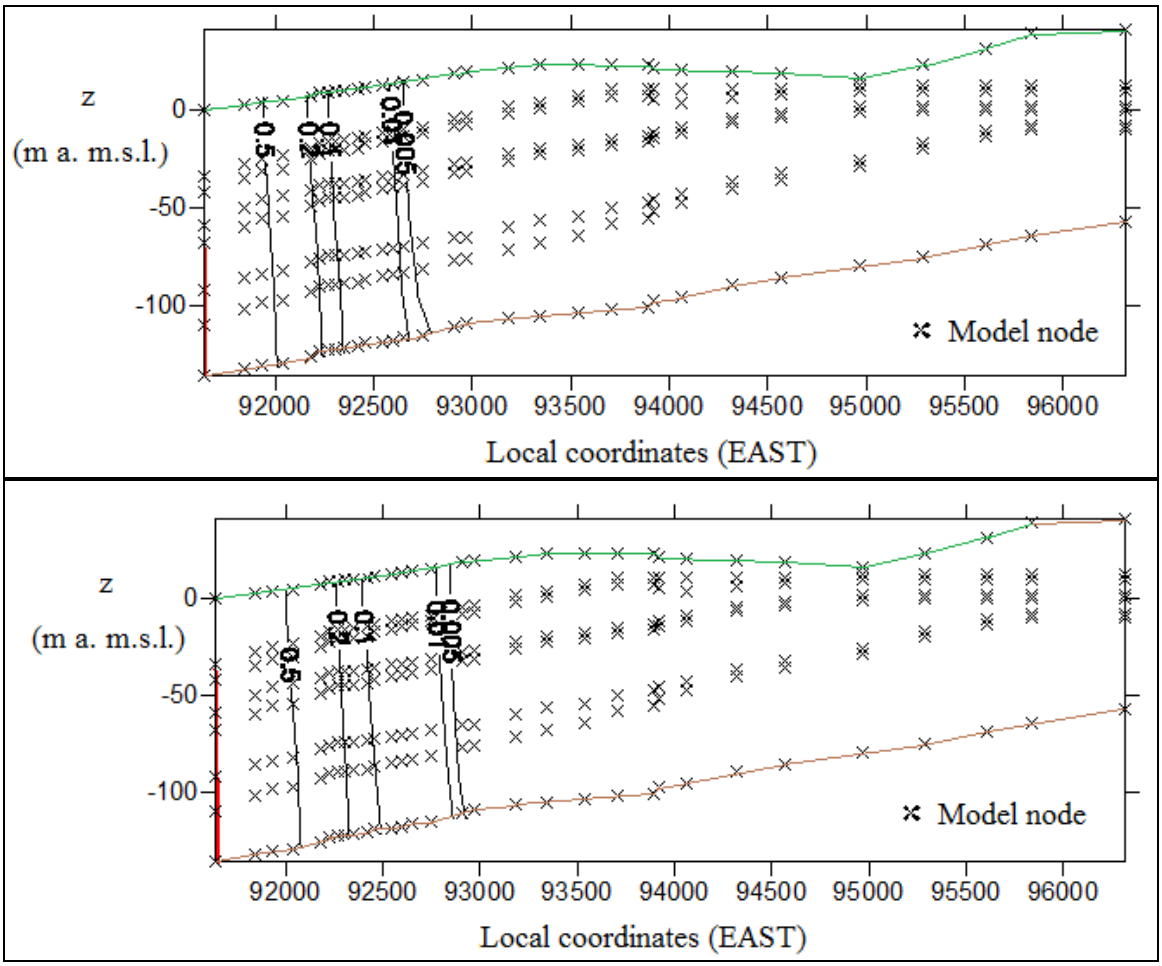

Figure 6.23 - Cross section 2: year 2000 (top) and 2010 (bottom) with the indication of model nodes (cross symbol); in red the 1 isoline of normalized concentration equal to 1, in green the land surface and in brown the bottom surface

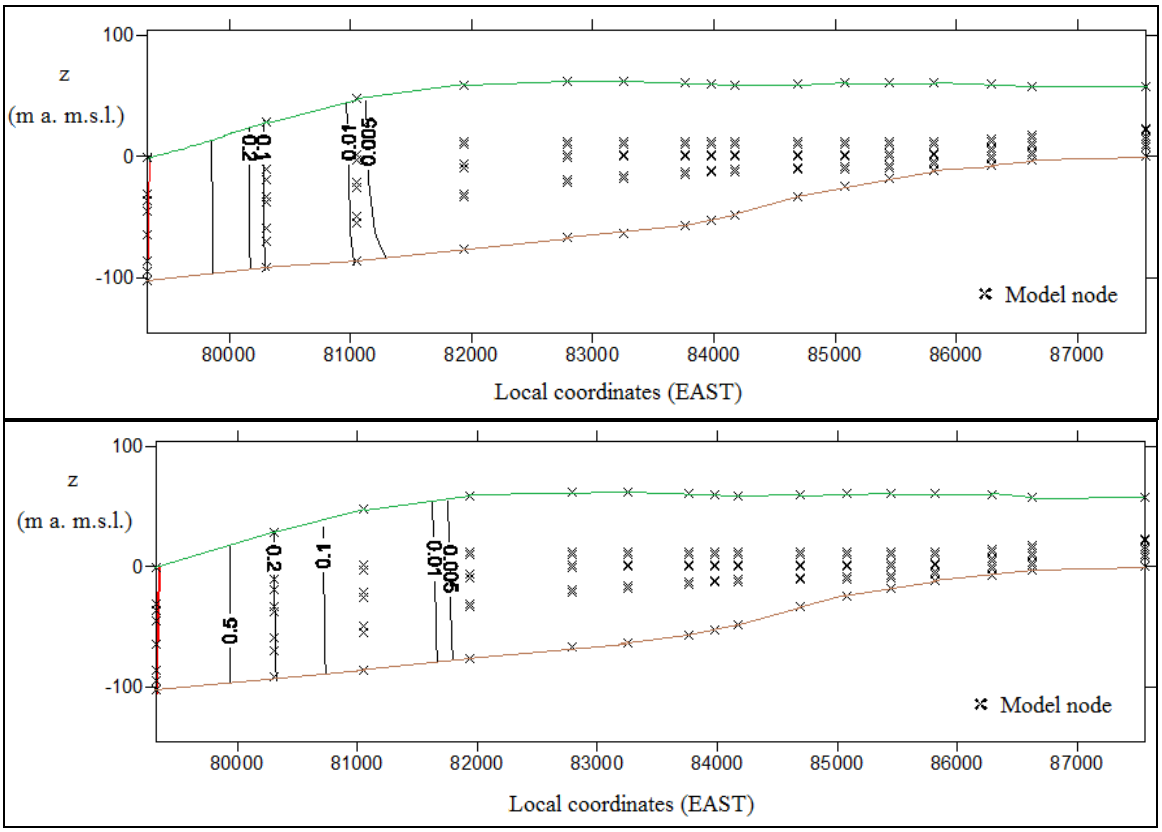

Figure 6.24 - Cross section 3 - year 2000 (top) and 2010 (bottom) with the indication of model nodes (cross symbol); in red the 1 isoline of normalized concentration equal to 1, in green the land surface and in brown the bottom surface

The results show a general encroachment of salt water intrusion, which is stronger in the northern zone. The strong pumpings both in the northern part and in the southern part seem to have significantly changed natural patterns in saltwater intrusion, which seem to go forward the aquifer somehow in a parallel way with respect to the seaside boundary.

While from a qualitative point of view the simulated values seem to represent the actual salt water intrusion, from a quantitative point of view the model seem to properly simulate salt water intrusion only for a part of the study area. This problem seems to depend on available water quality analysis, which are only available in terms of Chlorides concentration and they should not properly represent actual saltwater intrusion. Yet, it is probably that field campaign measurements should have be done within mixing waters coming from different depths throughout the wells, making it difficult to correlate them within the simulated concentrations in the right aquifer layer.

6.4 Future scenarios

The validated hydrogeological model of the Gaza aquifer is used to simulate the response of the hydrological basin to actual and future scenarios of climate change. The system is studied in the periods 2011-2040 and 2041-2070, on the basis of 2010 simulation results both for water levels and for salt concentrations.

In order to avoid overlapping of different impact on the aquifer system, the setup of future climate scenarios is based on the same soil map and the consideration on land use map proposed for the overall validation period. Therefore the water demand is estimated to increase (see Chapter 4, last paragraph, which reports projected values up to year 2035), in this study there have been considered two different scenarios, both starting with pumping amount depicted at the end of 2010:

1) the worst scenario, which considers, at the end of 2040, the estimated increasing of pumping for municipal wells up to around 200 Mm^3/y and a general decrease of pumpings for agricultural wells up to around 60 Mm^3/y, summing up about 260 Mm^3/y of water abstraction;
2) the best scenario, which considers, at the end of 2040, the proposed aquifer management scenario as reported in Chapter 4, last paragraph, considering the illustrated decreasing of pumping for municipal wells up to around 50 Mm^3/y and the same general decrease of pumpings for agricultural wells as illustrated for the worst scenario, summing up about 110 Mm^3/y of water abstraction.

As not any projection about future conditions on the Gaza area has been made available over year 2040, the values of pumpings for the period 2041-2070 are considered constant and equal to those setup at the end of 2040.

Future climate variables impacts are further analysed in the following paragraphs, starting form data and considerations made for the 4 RCMs as described in Chapter 5.

6.4.1 Modeling impacts of climate change on groundwater

As described in Chapter 1 and Chapter 5, precipitation (P) and evaporation (ET) rates will affect directly the recharging amount of coastal aquifers, by determining NetP (that is equal to P-ET); for sure, also the lateral inflow (LI) imposed at the eastern part of the

aquifer will be affected by different uphill recharging patterns, but this boundary condition is not assessed in this study and will be further analysed in other studies.

The variable P can be evaluated from outputs of climate models, while ET should be assessed within a standard method (Penman-Monteith simplified method, Appendix B) starting from other modeled variables, namely temperatures (T), wind (W), relative humidity (RH) and solar radiation (Rs).

The above mentioned variables (P, T, W, RH, Rs) are finally available on daily rates for both considered periods (first (p1): 2011-2040 and second (p2): 2041-2070), for the 4 RCMs models described in Chapter 5; considering that every variable is further analysed in the same Chapter, highlighting the comparisons between past and future climatic conditions, in this part of the study is only described the setup of recharging patterns for the aquifer.

Hence, the adopted P values are those assessed within the methodology described in Chapter 5 (bias correction within the QQplot method); the adopted T values (average, minimum and maximum daily values) are those assessed within the methodology described in Chapter 5 (bias correction within CRU observed data); the adopted W, RH and Rs values are the corresponding values modeled by the adopted RCMs. ET_0 is evaluated as mean daily rate within Penman-Monteith method (Appendix B), according to daily values of T, W, RH and Rs; ET values are set equal to ET_0 for rainy days, and equal to 0 for dry days.

The vertical net recharging patterns are then evaluated separately from the first period and the second period, following the methodology applied for the validation procedure. The net recharging rainfall is evaluated by subtracting daily ET values from P; then, the net recharging rates are calculated as a percentage (according to soil characteristics adopted in the calibration and validation procedures) of the net rain.

Yet, in order to focus more on vertical recharging impacts on the aquifer system, the model is additionally fed, for both considered periods, with the same recharging patterns depicted for the period 1981-2010 climatic conditions; this scenario is further indicated as CC-0. As the study is focusing on climate change impacts, the net vertical recharging rates are analysed and finally setup in the model as yearly mean values along 30 years, according to 'regional climate definition' proposed in Chapter 5; however, within this

proposed setup of the model, it seems not to be possible to properly represent the effects of extreme events on recharging patterns.

As cited in Chapter 5, paragraph 5.4.3, the expected effects of changes in climate dynamics on the aquifer water balance are strongly correlated to the NetP rates; in Table 6.14 are reported the yearly mean values of groundwater vertical recharging values (in terms of Mm^3/y for overall the model domain) for the periods 2011-2040 and 2041-2070 for the 4 climate models considered in this study, relatively to the overall modeled area, compared within the past reference period 1981-2010.

Period / Climate Model	1981-2010 (p0)	2011-2040 (p1)	2041-2070 (p2)	Difference (p1)-(p0)	% Difference (p1)-(p0)	Difference (p2)-(p0)	%Difference (p2)-(p0)
ECH_RCA (CC1)	33.71	37.92	34.52	4.21	+12.5	+0.80	+2.4
ECH_REM (CC2)	33.71	37.14	31.82	3.43	+10.2	-1.89	-5.6
ECH_RMO (CC3)	33.71	39.11	30.41	5.40	+16.0	-3.30	-9.8
HCH_RCA (CC4)	33.71	31.80	33.31	-1.91	-5.7	-0.40	-1.2

Table 6.14 - Mean yearly values of groundwater vertical recharging amount (in terms of Mm^3/y for overall the model domain) due to NetP, for the periods 2011-2040 and 2041-2070 and the historical reference period 1981-2010, for the 4 considered models, used as input for the future simulations.

For the first future period considered (p1), 3 models are showing an increasing trend (with reference to historical scenario p0) in groundwater vertical recharging values of more than 10%, but the HCH_RCA is denoting a decreasing of about -6%; for the second period (p2) 3 models are showing a general decreasing in NetP but the ECH_REM is showing an increasing of about +2%. These values are assuming quite the same magnitudes (in terms of percents) of the ones reported in Table 5.13, which illustrated variations in NetP values.

6.4.2 Modeling Sea Level rise on groundwater

As SLR will affect boundary conditions on the seaside, this phenomenon is also considered in modeling future scenarios. For the Gaza Strip there is no available data for the actual and past sea level rise; all simulations are performed using a past and present day sea level of zero meters. Yet, for the Gaza Strip there is not available data for the projected sea level rise, so that this value is assessed from projections on the Mediterranean area.

According to the greenhouse gas emissions scenario, sea levels at the Mediterranean Sea are forecasted to rise at least 18 to 38 cm and as much as 26 to 59 cm by 2100 (Mason et

al. 2009). For the Mediterranean region, it has been predicted (IPCC, 2007) a possible sea level rise which ranges from 90 to 880 mm by the year 2100, with a central value of 480 mm according to IPCC, 2007.

During the simulations, a medium sea level rise of 39 cm in 100 years is considered as appropriate (IPCC, 2007), within a constant rate of 3.9 mm/y.

The value of sea level rise is setup in the model by updating the imposed Dirichlet boundary conditions (as illustrated in paragraph 6.1.3) at the western boundary, along the coast, where the aquifer is in contact with the seawater body; the constant head (h) along the vertical boundary of the sea side is varied summing up the projected sea level at the end of the studied period, considering always a constant concentration for seawater at the reference salt concentration (in terms of chlorides) of 25 grams/l.

In order to better evaluate the impact of SLR on the studied aquifer, the model is run with and without considering this phenomenon.

6.4.3 Setting Scenarios on the Gaza Aquifer: results

The schematic configuration of all simulations (and their acronyms) run to identify possible future evolution of the aquifer system, is briefly illustrated in Table 6.15 and Table 6.16. For each period, 20 complete simulations covering 30 years time interval are run; considering that each run spent an average CPU time of 6 minutes on a dual CPU quad core 2.8 GHz system, around 4 hours of CPU time are needed to perform all runs.

	Period	2011-2040 (1)			
	SLR	no		yes	
	Pumping Scenario	best	worst	best	worst
Climate Scenario	CC-0	p1b_CC0	p1w_CC0	p1b_SLR_CC0	p1w_SLR_CC0
	ECH_RCA	p1b_CC1	p1w_CC1	p1b_SLR_CC1	p1w_SLR_CC1
	ECH_REM	p1b_CC2	p1w_CC2	p1b_SLR_CC2	p1w_SLR_CC2
	ECH_RMO	p1b_CC3	p1w_CC3	p1b_SLR_CC3	p1w_SLR_CC3
	HCH_RCA	p1b_CC4	p1w_CC4	p1b_SLR_CC4	p1w_SLR_CC4

Table 6.15 - Matrix combinations of climate scenarios involved in the study, and their acronyms (period 2011-2040)

	Period	2041-2070 (2)			
	SLR	no		yes	
	Pumping Scenario	best	worst	best	worst
Climate Scenario	CC-0	p2b_CC0	p2w_CC0	p2b_SLR_CC0	p2w_SLR_CC0
	ECH_RCA	p2b_CC1	p2w_CC1	p2b_SLR_CC1	p2w_SLR_CC1
	ECH_REM	p2b_CC2	p2w_CC2	p2b_SLR_CC2	p2w_SLR_CC2
	ECH_RMO	p2b_CC3	p2w_CC3	p2b_SLR_CC3	p2w_SLR_CC3
	HCH_RCA	p2b_CC4	p2w_CC4	p2b_SLR_CC4	p2w_SLR_CC4

Table 6.16 - Matrix combinations of climate scenarios involved in the study, and their acronyms (period 2011-2040)

As the simulation model can give projections on groundwater levels and normalized salt concentration (in terms of chlorides concentrations) in groundwater, climate changes impacts and SLR on the aquifer are assessed on the basis of analysis of these two variables. Further analyses on changing in recharging patterns are illustrated in Chapter 5 and in the above paragraph 6.6.1 and are briefly considered in the followings.

In figure from Figure 6.25 to Figure 6.32 are represented results at the end of the two simulation periods (i.e. at the end of year 2040 and 2070) for the CC-0 model and the ECH-RMO model, with and without SLR, within increasing of pumping (worst scenario) and the decreasing of pumping (best scenario), in term both of groundwater levels (in m a.m.s.l. in 2010) and salt concentrations (these latter only for the isolines 1, 0.1 and 0.01 of normalized Chlorides concentrations).

From Table 6.17 to Table 6.20 are provided and compared results on groundwater levels for each considered climate model, in terms of mean values for 14 control wells (Figure 6.16, paragraph 6.4.1), for the year 2040 and 2070; these values are also compared with 2010 mean value of the same 14 wells, which corresponds to the value of -3.232 m a.m.s.l. Complete models' results (for each of the representative 14 wells) are reported in Appendix A.

From Table 6.21 to Table 6.24 there are compared simulated salt concentration for overall considered models in 2040 and 2070 in 17 representing wells within 2.5 km from the coastline, within respective measured average Chlorides (Cl^-) concentrations on 2010 control wells, which corresponds to the value of 0.189 normalized concentration of chlorides. Complete models' results (for each of the representative 17 wells) are reported in Appendix A.

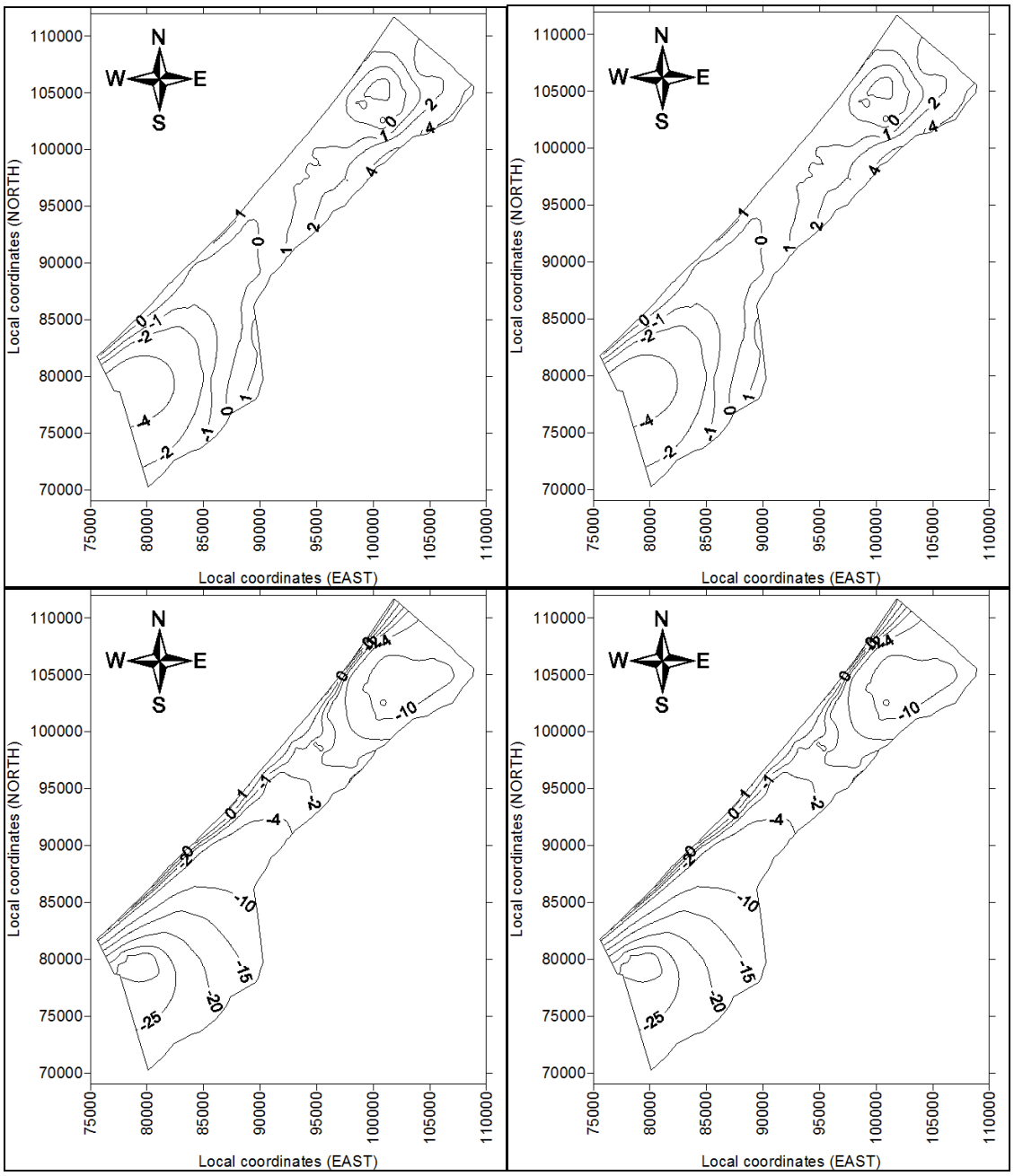

Figure 6.25 – Contour representation of simulated groundwater levels (in m a.m.s.l. in 2010) in 2040 for the only CC-0 climate model: best pumping scenario with SLR (top left); best pumping scenario without SLR (top right); worst pumping scenario with SLR (bottom left); worst pumping scenario without SLR (bottom right).

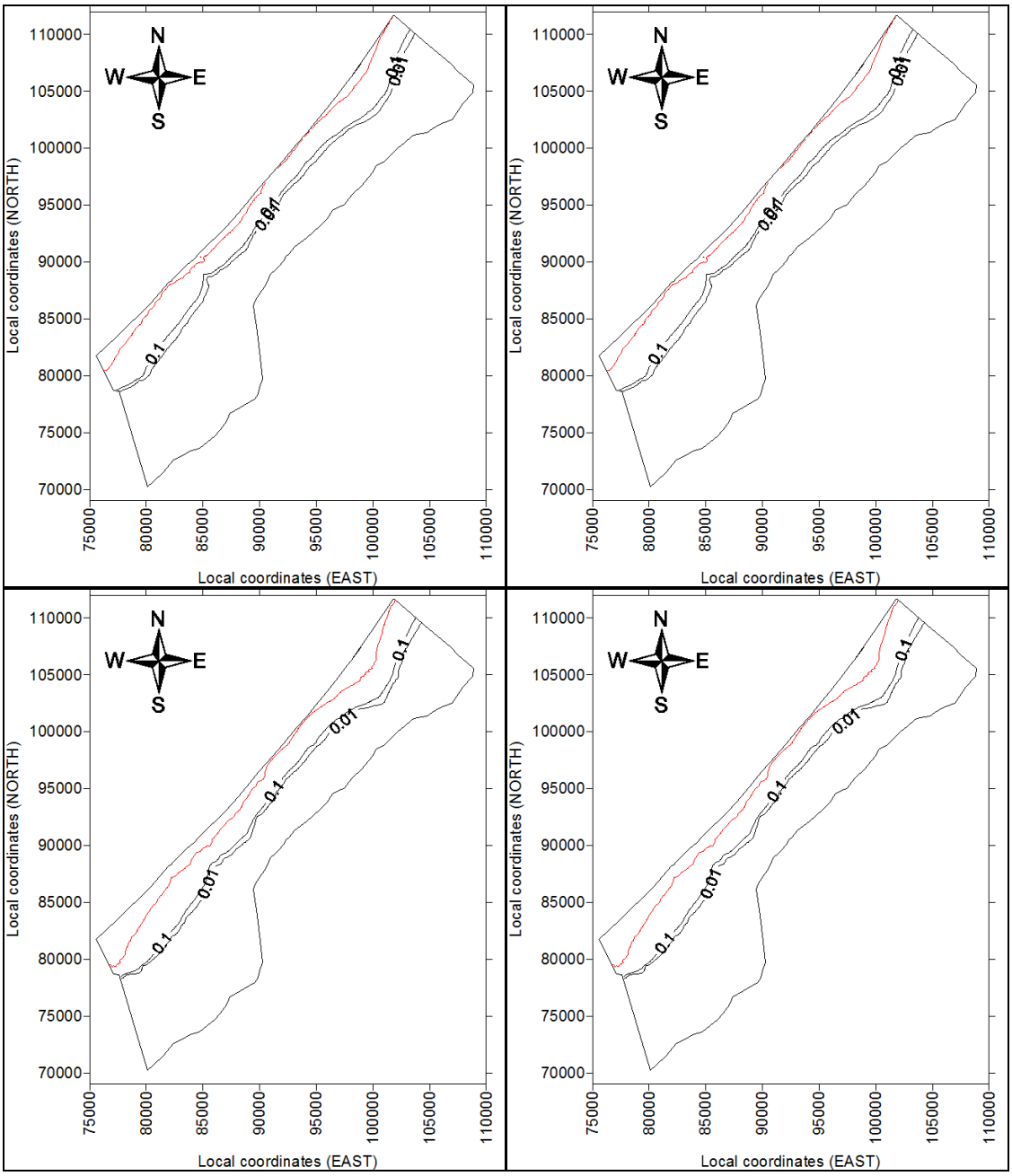

Figure 6.26 – Contour representation of simulated normalized concentration in 2040, for the only CC-0 climate model: best pumping scenario with SLR (top left); best pumping scenario without SLR (top right); worst pumping scenario with SLR (bottom left); worst pumping scenario without SLR (bottom right). In red the isoline of normalized salt concentration equal to 1.

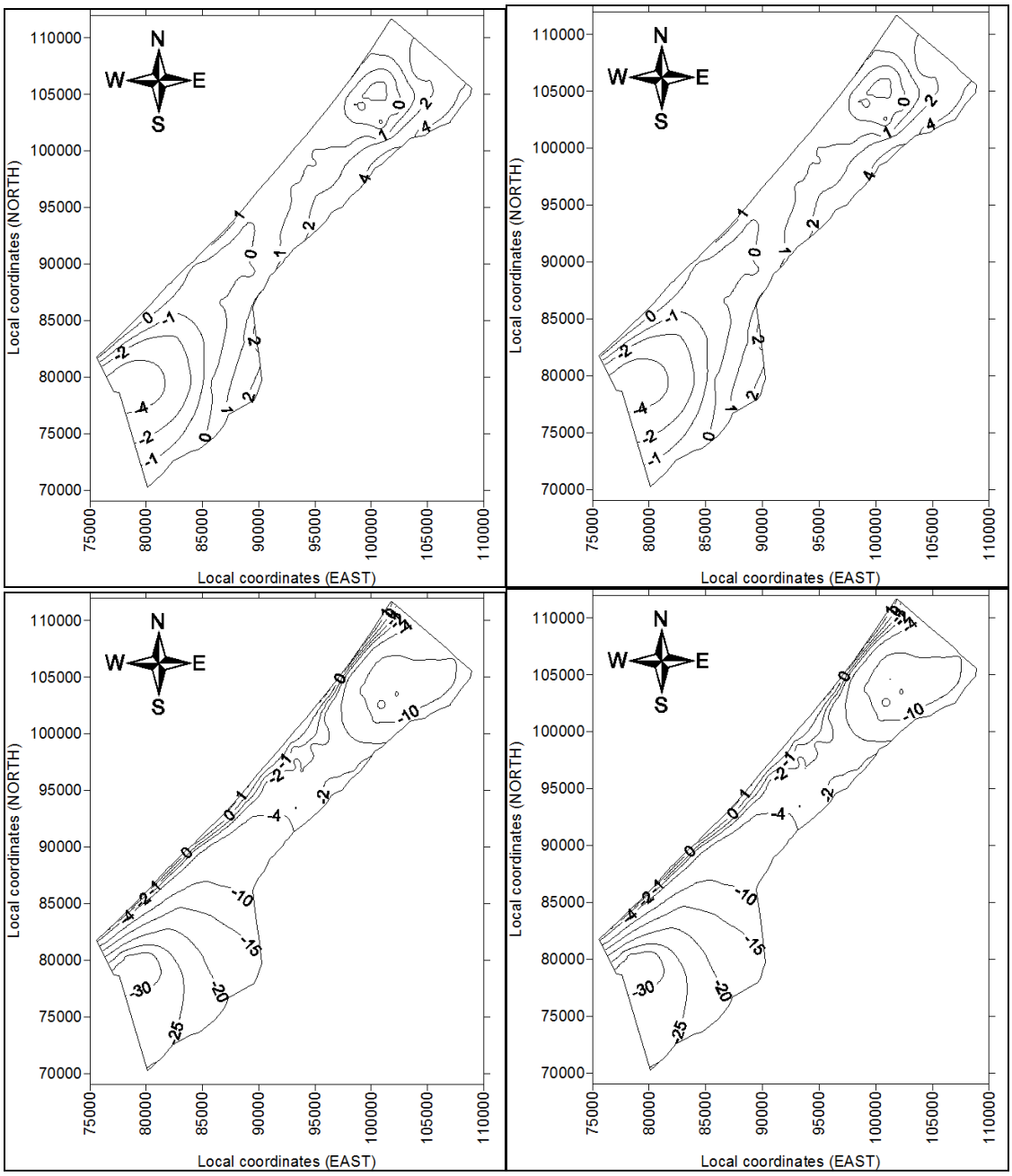

Figure 6.27 - Contour representation of simulated groundwater levels (in m a.m.s.l. in 2010) in 2070 for the only CC-0 climate model: best pumping scenario with SLR (top left); best pumping scenario without SLR (top right); worst pumping scenario with SLR (bottom left); worst pumping scenario without SLR (bottom right).

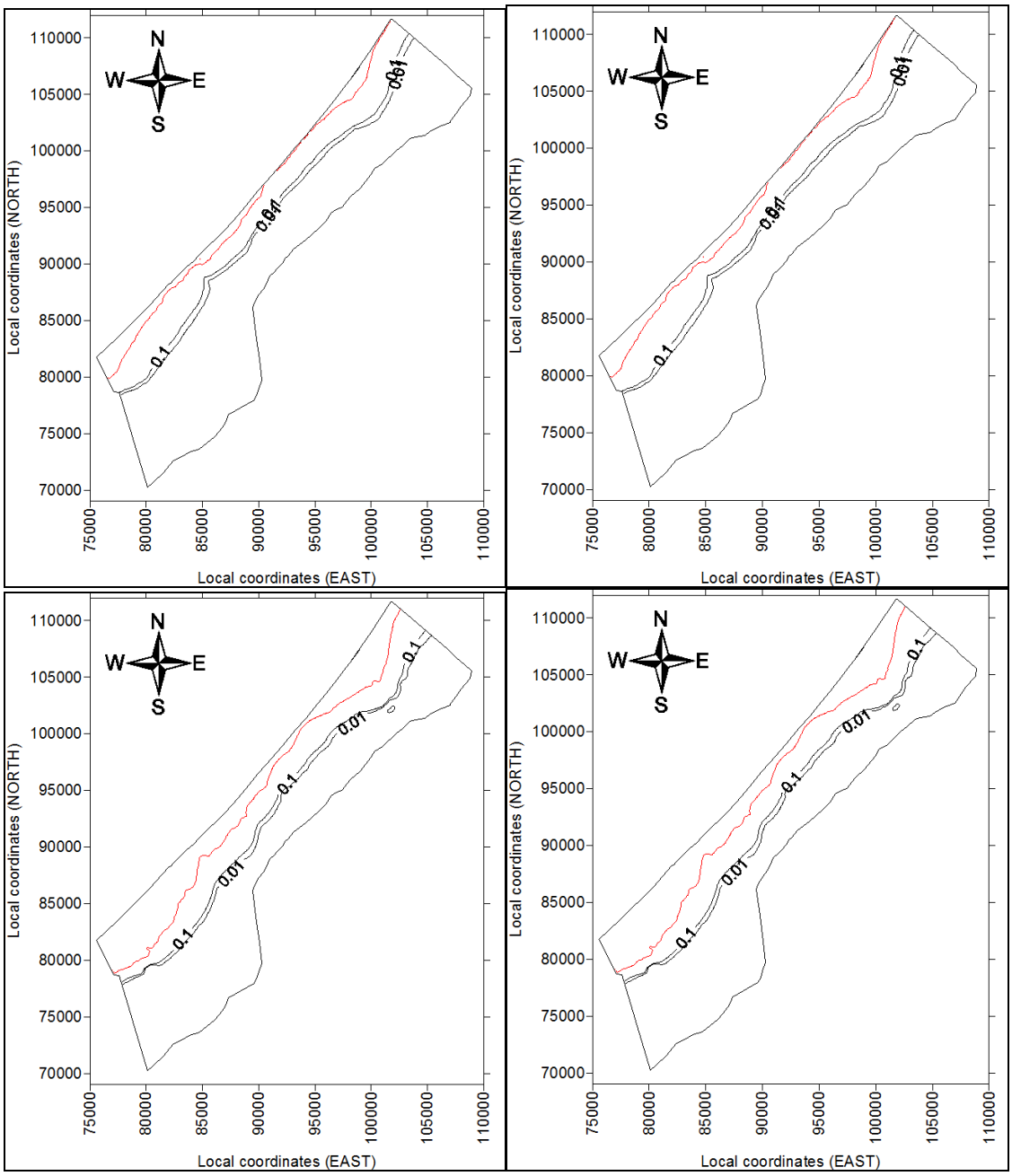

Figure 6.28 - Contour representation of simulated normalized concentration in 2070, for the only CC-0 climate model: best pumping scenario and SLR (top left); best pumping scenario without SLR (top right); worst pumping scenario with SLR (bottom left); worst pumping scenario without SLR (bottom right). In red the isoline of normalized salt concentration equal to 1.

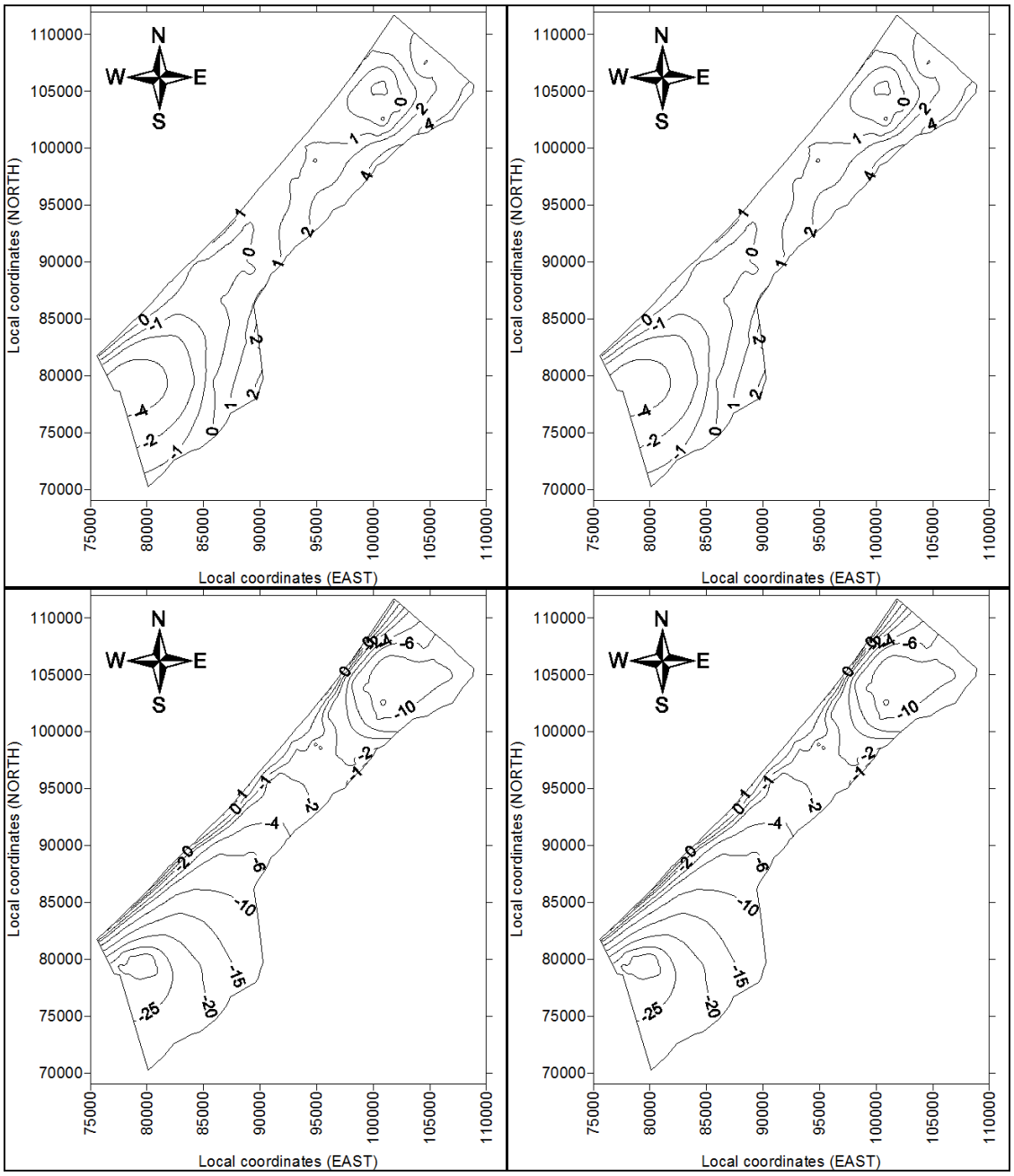

Figure 6.29 - Contour representation of simulated groundwater levels in 2040 (in m a.m.s.l. in 2010) for the only ECH_RMO climate model: best pumping scenario with SLR (top left); best pumping scenario without SLR (top right); worst pumping scenario with SLR (bottom left); worst pumping scenario without SLR (bottom right).

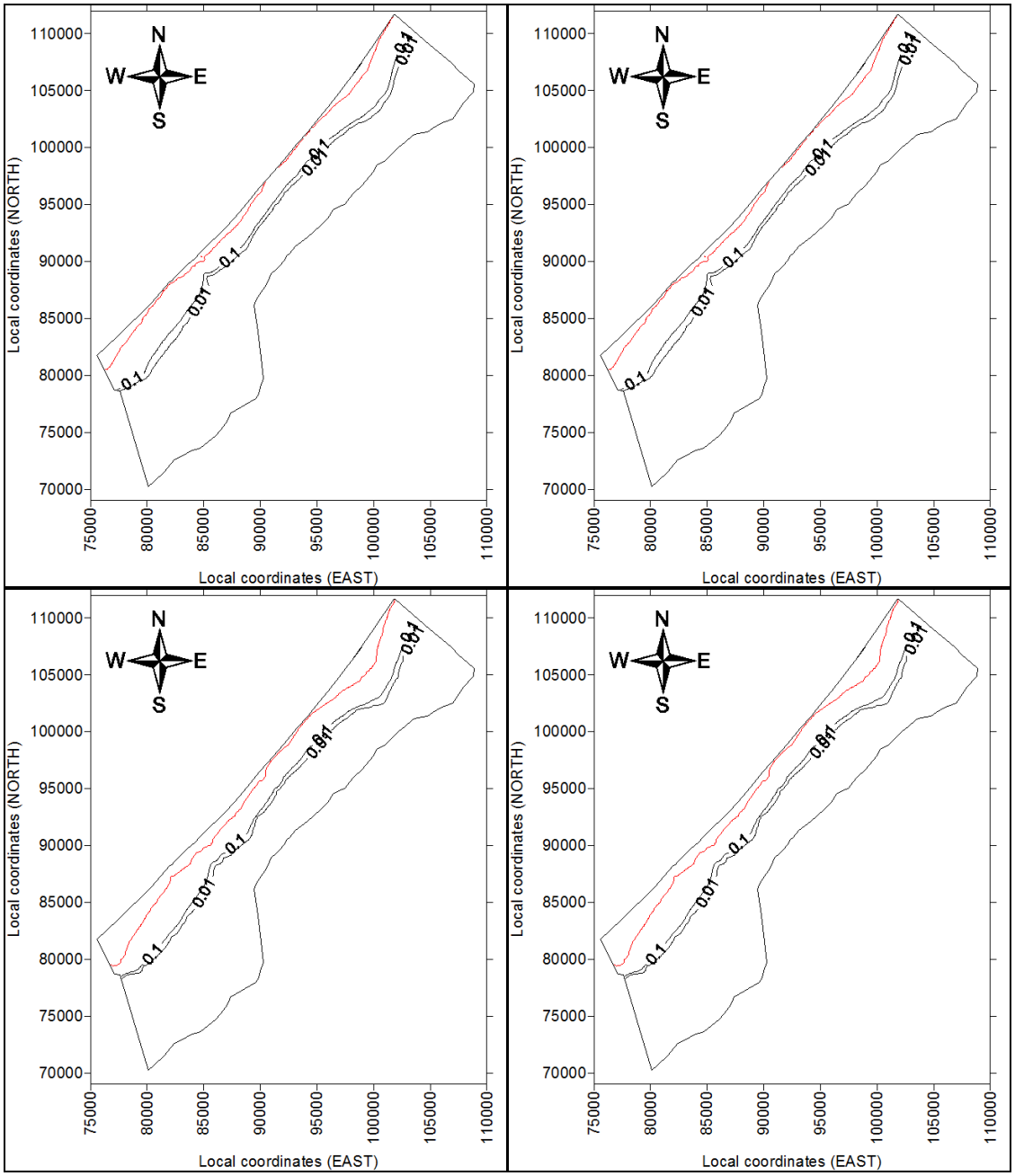

Figure 6.30 – Contour representation of simulated normalized concentration in 2040, for the only ECH_RMO climate model: best pumping scenario with SLR (top left); best pumping scenario without SLR (top right); worst pumping scenario with SLR (bottom left); worst pumping scenario without SLR (bottom right). In red the isoline of normalized salt concentration equal to 1.

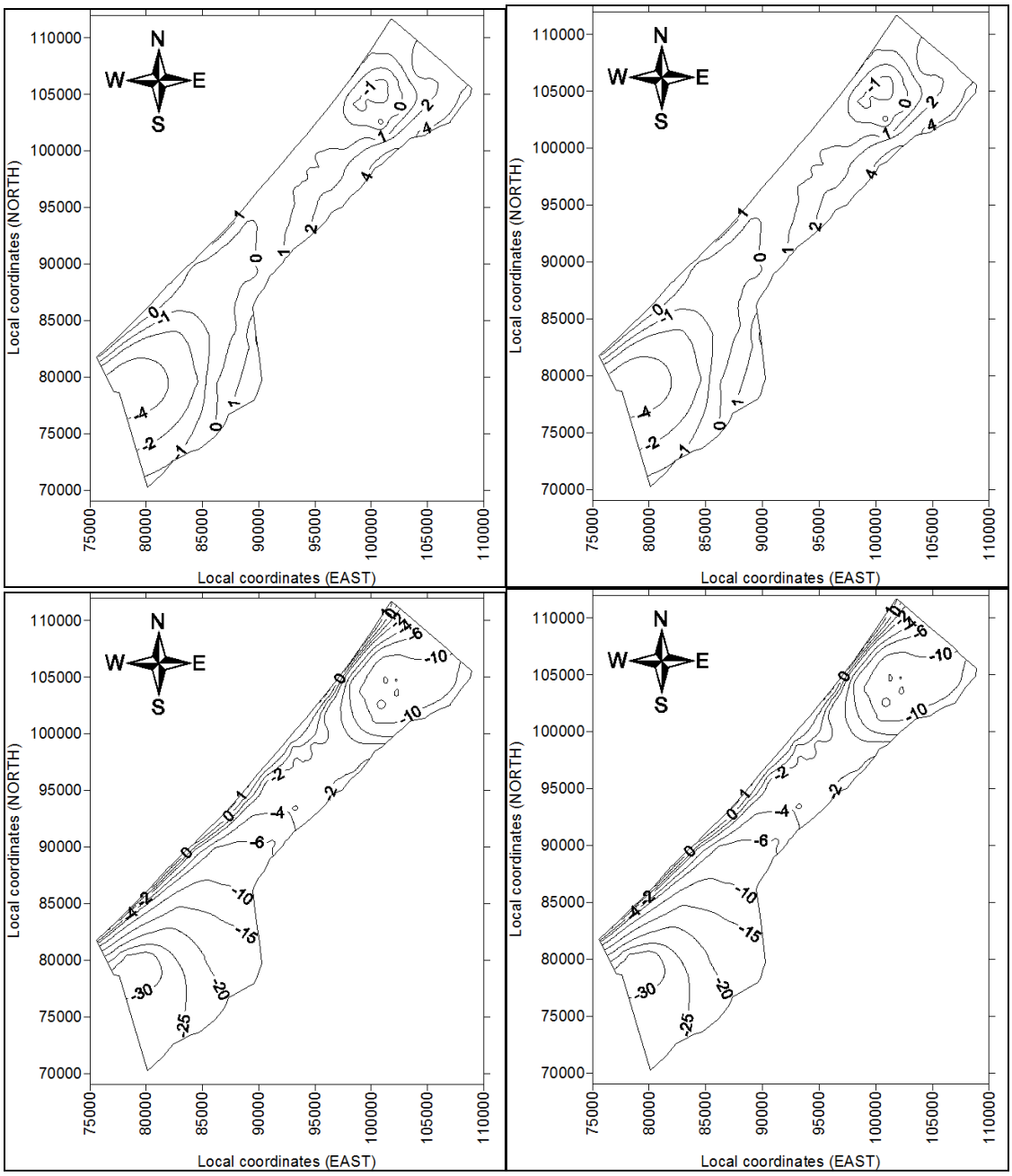

Figure 6.31 - Contour representation of simulated groundwater levels (in m a.m.s.l. in 2010) in 2070 for the only ECH_RMO climate model: best pumping scenario with SLR (top left); best pumping scenario without SLR (top right); worst pumping scenario with SLR (bottom left); worst pumping scenario without SLR (bottom right).

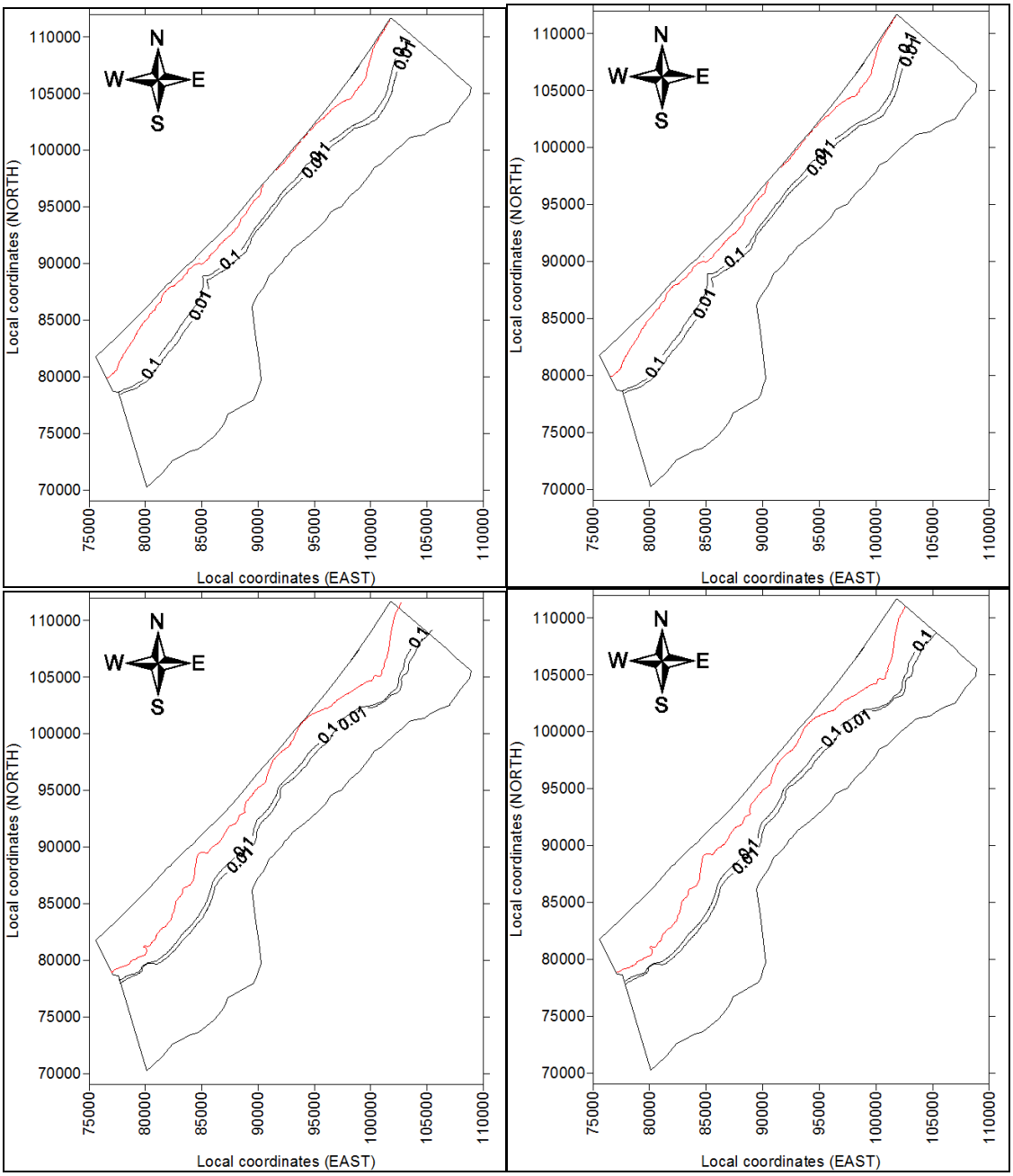

Figure 6.32 - Contour representation of simulated normalized concentration in 2070, for the only ECH_RMO climate model: best pumping scenario with SLR (top left); best pumping scenario without SLR (top right); worst pumping scenario with SLR (bottom left); worst pumping scenario without SLR (bottom right). In red the isoline of normalized salt concentration equal to 1.

Pumping and SLR setup \ Climate model		CC0	CC1	CC2	CC3	CC4
B	No SLR	-0.35	-0.09	-0.15	-0.03	-0.49
W	No SLR	-10.43	-10.17	-10.23	-10.11	-10.56
B	SLR	-0.35	-0.09	-0.15	-0.03	-0.49
W	SLR	-10.88	-10.17	-10.23	-10.11	-10.56

Table 6.17 – Mean averaged groundwater levels (h, in m a.m.s.l. in 2010) in 14 representing wells at the end of the simulation period 2011-2040

Pumping and SLR setup \ Climate model		CC0	CC1	CC2	CC3	CC4
B	No SLR	2.88	3.14	3.08	3.20	2.74
W	No SLR	-7.20	-6.94	-7.00	-6.88	-7.33
B	SLR	2.88	3.14	3.08	3.20	2.74
W	SLR	-7.65	-6.93	-7.00	-6.87	-7.33

Table 6.18 – Comparison (in term of difference, in m) between mean averaged groundwater levels in 14 representing wells at the end of the simulation period 2011-2040 and at the end of year 2010

Pumping and SLR setup \ Climate model		CC0	CC1	CC2	CC3	CC4
B	No SLR	-0.04	0.04	-0.13	-0.22	-0.09
W	No SLR	-11.03	-10.95	-11.12	-11.21	-11.07
B	SLR	-0.04	0.05	-0.13	-0.21	-0.08
W	SLR	-11.03	-10.95	-11.12	-11.21	-11.07

Table 6.19 - Mean averaged groundwater levels (h, in m a.m.s.l. in 2010) in 14 representing wells at the end of the simulation period 2041-2070

Pumping and SLR setup \ Climate model		CC0	CC1	CC2	CC3	CC4
B	No SLR	3.19	3.27	3.10	3.01	3.15
W	No SLR	-7.80	-7.72	-7.89	-7.98	-7.84
B	SLR	3.19	3.28	3.11	3.02	3.15
W	SLR	-7.80	-7.72	-7.89	-7.98	-7.84

Table 6.20 - Comparison (in term of difference, in m) between mean averaged groundwater levels in 14 representing wells at the end of the simulation period 2041-2070 and at the end of year 2010

Pumping and SLR setup \ Climate model		CC0	CC1	CC2	CC3	CC4
B	No SLR	0.413	0.400	0.402	0.396	0.418
W	No SLR	0.842	0.836	0.837	0.834	0.844
B	SLR	0.413	0.400	0.402	0.367	0.418
W	SLR	0.842	0.837	0.837	0.821	0.844

Table 6.21 - Mean averaged normalized salts concentrations in 17 representing wells at the end of the simulation period 2011-2040

Pumping and SLR setup \ Climate model		CC0		CC1		CC2		CC3		CC4	
B	No SLR	0.225	+119.0	0.212	+112.1	0.213	+112.9	0.207	+109.7	0.229	+121.6
W	No SLR	0.653	+346.3	0.648	+343.3	0.649	+343.7	0.646	+342.2	0.655	+347.4
B	SLR	0.225	+119.0	0.212	+112.1	0.213	+112.9	0.179	+94.6	0.229	+121.6
W	SLR	0.653	+346.3	0.648	+343.3	0.649	+343.7	0.632	+335.0	0.655	+347.4

Table 6.22 - Comparison (in terms of absolute and percentual difference) between mean averaged normalized salts concentrations in 17 representing wells at the end of the simulation period 2011-2040 and at the end of year 2010

Pumping and SLR setup \ Climate model		CC0	CC1	CC2	CC3	CC4
B	No SLR	0.512	0.501	0.509	0.509	0.516
W	No SLR	0.938	0.938	0.938	0.938	0.938
B	SLR	0.512	0.482	0.484	0.463	0.487
W	SLR	0.938	0.936	0.936	0.935	0.936

Table 6.23 - Mean averaged normalized salts concentrations in 17 representing wells at the end of the simulation period 2041-2070

Pumping and SLR setup \ Climate model		CC0		CC1		CC2		CC3		CC4	
B	No SLR	0.323	+171.3	0.313	+165.7	0.321	+170.0	0.320	+169.5	0.327	+173.3
W	No SLR	0.749	+397.2	0.749	+396.9	0.749	+397.1	0.749	+397.1	0.750	+397.3
B	SLR	0.323	+171.3	0.293	+155.5	0.295	+156.5	0.275	+145.6	0.298	+158.1
W	SLR	0.750	+397.2	0.747	+396.1	0.747	+396.1	0.746	+395.2	0.748	+396.2

Table 6.24 - Comparison (in terms of absolute and percentual difference) between mean averaged normalized salts concentrations in 17 representing wells at the end of the simulation period 2041-2070 and at the end of year 2010

These results, valid for only the control wells (14 for water levels; 17 for normalized salt concentrations, within 2.5 km from the coastline), can be summarized as follows:

1) Setting different vertical recharging values, coming for the calculation based on different climate modeled variables, lead to different mean water levels; considering the CC-0 scenarios as reference, this range can be assessed for corresponding scenarios between -0.14 and +0.77 meters for the first period (p1), and between -0.18 and +0.08 meters for the second period (p2);
2) Setting different vertical recharging values, coming for the calculation based on different climate modeled variables, lead to different mean normalized salt concentration; considering the CC-0 scenarios as reference, this range can be assessed for corresponding scenarios between -0.046 (-1150 mg/l of Cl^-) and

+0.005 (120 mg/l of Cl^-) for the first period (p1), and in the general range of -0.049 (-1200 mg/l of Cl^-) and +0.004 (93 mg/l of Cl^-) for the second period (p2);

3) The increasing or decreasing in water levels, and higher and lower values of groundwater heads, correspond in general to the NetP trends as reported in Chapter 5, Table 5.13 and in paragraph 6.6.1, Table 6.14;
4) Different pumping scenarios lead to extreme different mean water tables, resulting in the range of 10-11 meters for both considered periods, and extreme different normalized salt concentrations, that in the worst pumping scenarios are around the double than the corresponding best pumping scenarios; yet, also the SWI affected area (intended as the area in which the groundwater salts concentration are equal to 25,000 mg/l of Chlorides, i.e. normalized concentration equal to 1) is around the double in case of the worst pumping scenario is chosen instead of the best one;
5) Different SLR scenarios lead to slightly different water table levels between corresponding scenarios (i.e. around the same magnitude of SLR) and, for salt concentrations, very slightly differences.

In few words, it can be depicted that different climate scenarios variables, in this case, lead to differences in the groundwater system that can be hardly be appreciated if compared with pumping effects; it is evident, in fact, that pumping scenarios have extremely high impacts on the Gaza coastal aquifer system. Thus, it is clear that, for the GCA, the only way to prevent and control SWI consists in assessing and properly adapting a groundwater management strategy.

6.5 Mitigation and adaptation strategies

Although some mitigation options are being evaluated for the GCA, in this study is only proposed a single strategy, which consists in assessing a new management scheme of groundwater by the means of a simulation/optimization procedure, aiming at minimizing the projected pumping rates, while constraining concentrations (by controlling total extracted salts in pumping wells); the adopted procedure is illustrated in Chapter 3.

In this study, it is simply considered that groundwater with high salts concentration need to be desalinized for human consumption, and higher values of total extracted salts means

higher costs for the desalinization process; the actual costs of this process are not further considered in this study, as the purpose of this work is not focus on the economic aspects of desalinization plans.

Hence, the corrective measures are only focused in varying pumping rates at municipal wells in the area, by keeping the total amount of pumped water equal to around 110 Mm^3/y at the end of 2040 (best pumping scenario, as described in paragraph 6.6), as results of future simulations are showing that, for the GCA, it appears to be crucial a substantial reduction in pumping rates.

In order to simplify the possible application of the management option, in this study it is only proposed the direct control of municipal wells abstraction, considering the total amount of pumping equal to the best pumping scenario (paragraph 6.6), i.e. around 50 Mm^3/y.

Although not highlighted in Chapter 4, paragraph 4.7, the overall projected pumping scenario includes itself possible other options to prevent/mitigate SWI, e.g. inland artificial recharge, which can be considered as a part of the proposed management scheme, integrating it projected reductions of pumping rates as indirect effects.

6.5.1 Setting Simulation/Optimization Model

The Gaza Strip Simulation/Optimization model is setup starting from 2010 simulated conditions both for groundwater heads and salt concentration fields. The management scheme is optimized for the period 2011-2040, and results at the end of 2040 are compared within the not-optimized situation previously assessed, with reference to the best pumping scenario. The only-simulation model (S-0) to which compare S/O results are those coming from the ECH-RMO climate variables fed model.

The Simulation/optimization model is setup as described in Chapter 3, some proposed parameters of which are adapted to this Gaza Strip aquifer case study; in particular, they have been optimized only municipal wells' pumping rates (as clustered for the simulation model, accounting 139 locations), the total amount of which, as above cited, has been setup to be the same of the best pumping scenario (paragraph 6.6), i.e. around 50 Mm^3/y. Minimum allowed values for pumping are setup equal to zero for each well, while maximum allowed value is based on the current mean operational rate of each well.

The relative weights in equation (3.4), Chapter 3, are determined by means of a parametric trade-off calculation, as described in the above mentioned Chapter; starting from some partial results, the w_2 values range is 1-100; yet, the Simulation/Optimization model accounts for 1,000 runs (i.e. 5 possible solutions multiplied for 200 generations) of CODESA-3D simulation model. Final GA parameters are summarized in Table 6.25. After model setup and initialization, the transient management scenario (with the different 7 values of salinity weight w_2) is simulated for a 30-years time interval. A single S/O run spent an average CPU time of 72 hours on a dual CPU quad core 2.8 GHz system.

Number of wells	Pumping weight w_1	Salinity weight w_2	Individual length	Population size	Max generations number	Crossover probability	Mutation probability
139	10	1-100	2085	5	200	0.5	0.02

Table 6.25 – GA parameters for the Gaza Strip site

In this case, the optimal value of salinity weighting parameter w_2 is 75, as shown in Figure 6.33, ensuring in this way maximum total pumping (which corresponds to high percentages of the possible total pumping amount) while a total salt mass extracted (which depends on values of salt concentrations) within the reasonable limits of the feasibility region. The best fitness values tends at reaching a slightly increasing trend in the last part of the S/O process, as shown in Figure 6.34, stating that it is not changed by further increasing the number of generations.

Table 6.26 shows the comparison between the optimal pumping strategy (SO-0) with the non-optimized condition (T-0) for the wells of the study area. The analysis is conducted in terms of design and state variables, namely: total discharge (Q, m^3/y), averaged hydraulic head (h, m), total salt normalized concentration (c, /) and total salt mass extracted (S, kg/year of chlorides) at the 139 clustered wells.

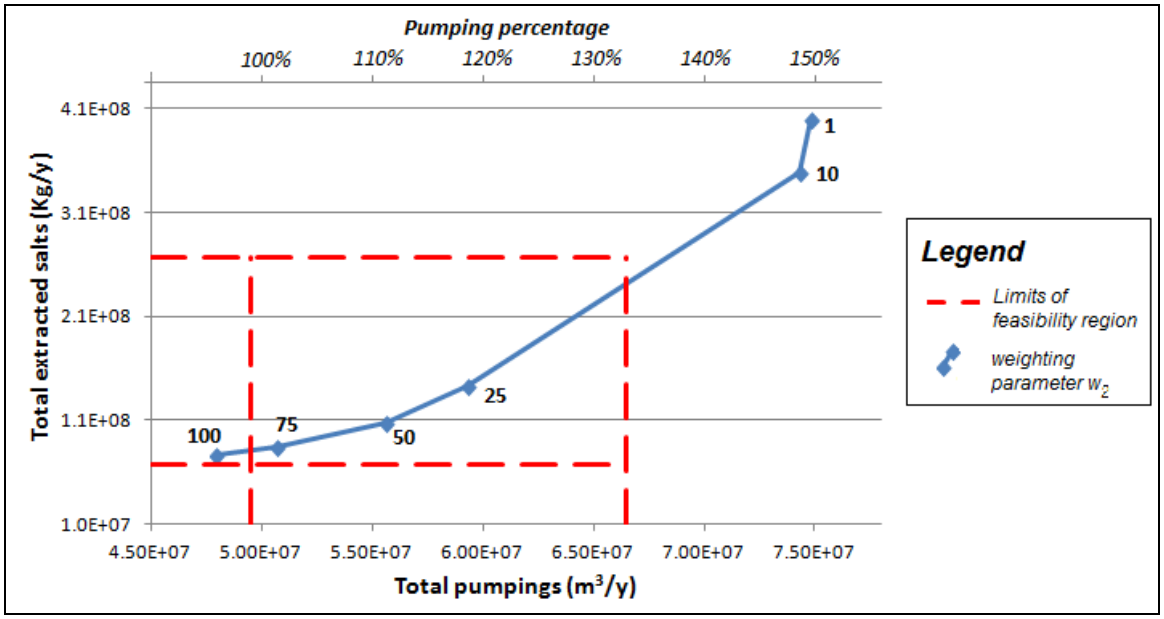

Figure 6.33 – Trade-off curve with indication of limits of feasibility region (red dot lines); total extracted salts are in terms of chlorides.

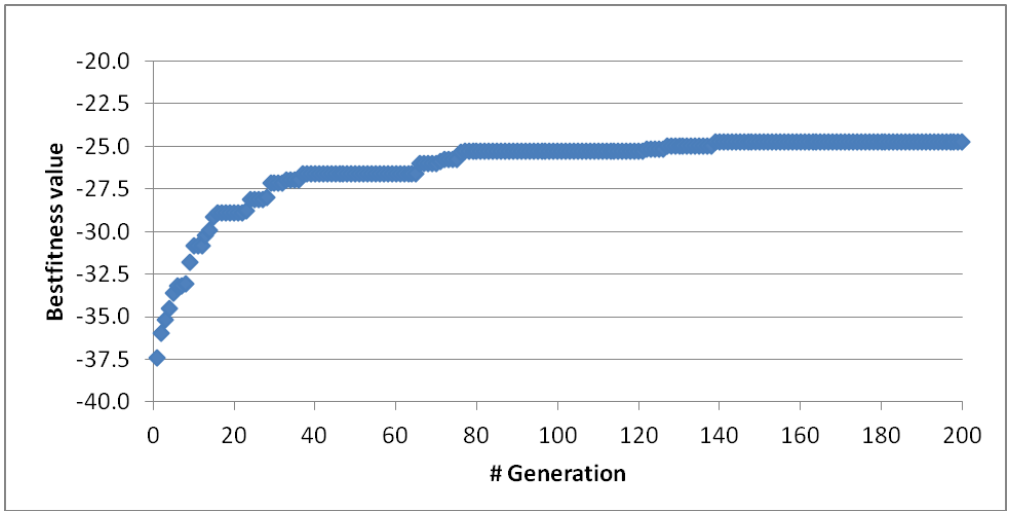

Figure 6.34 – Best fitness function value during the S/O process

T-0	SO-0	T-0	SO-0	T-0	SO-0	T-0	SO-0
Q	Q	h	h	c	c	S	S
m^3/y	m^3/y	m	m	/	/	kg/y	kg/y
49,992,045	50,619,140	-0.68	-0.41	30.45	22.97	266,008,731	84,580,101

Table 6.26 – Comparison of non-optimized (T-0) and optimized (SO-0) pumping strategies: discharge (Q), head (h), normalized concentration (c) and extracted salt mass (S) at the 139 clustered wells.

The optimum pumping strategy ensures a decrease of about -68% in the total extracted salt mass and a recovery of +0.28 m in the hydraulic heads, while allowing to withdrawal

the +1.3% of projected abstraction rates, thus keeping quite equal the total pumping rate with reference to the best pumping scenario, and the total area affected by SWI (intended as the area in which the groundwater salts concentration are equal to 25,000 mg/l of chlorides, i.e. normalized concentration equal to 1) shows a reduction of about -11% (Table 6.27). Spatial distribution of heads and salt concentrations for the two scenarios are also shown in Figure 6.35 and Figure 6.36. A graphical representation of pumping magnitudes for the 139 clustered municipal wells, both for the T-0 and SO-0 situation is illustrated in Figure 6.37.

	T-0	SO-0	Δ	%
Total abstraction (m^3/y)	49,992,045	50,619,140	+627,095	+1.3
Average head (m)	-0.68	-0.41	+0.28	
Total salt mass (kg/y)	266,008,731	84,580,101	-181,428,630	-68.2
Total area affected by SWI (m^2)	17,149,000	15,195,900	1,953,100	-11.3

Table 6.27 – Overall performance of non-optimized (T-0) and optimized (SO-0) pumping strategies and relative benefits

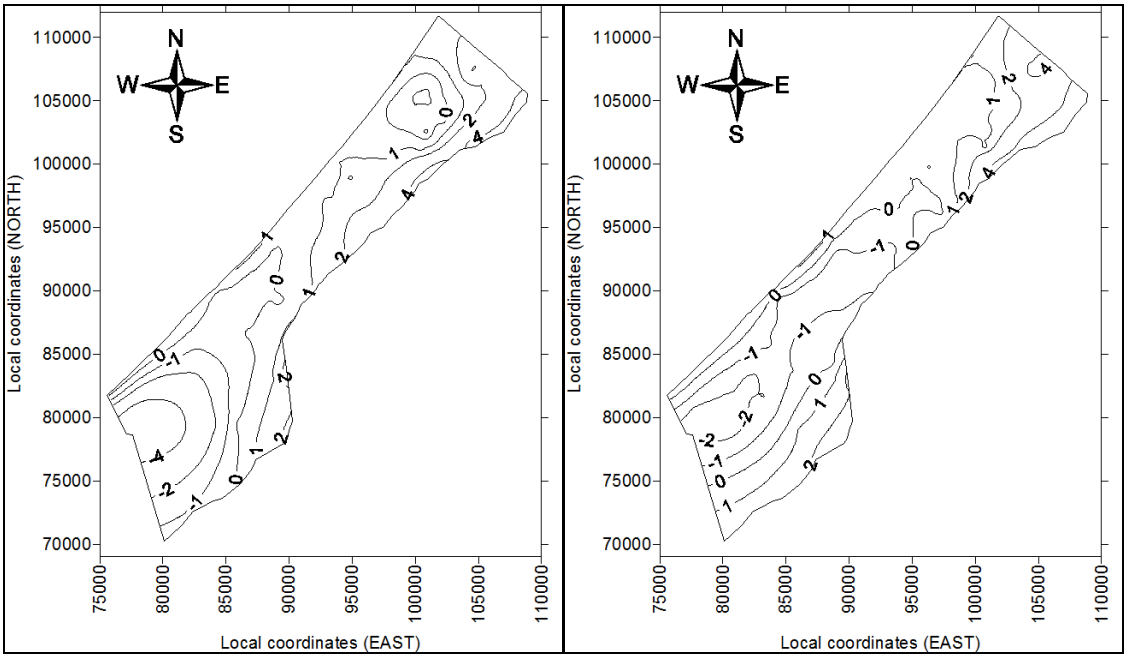

Figure 6.35 - Spatial distribution of groundwater heads (h, in m a.m.s.l.) for the T-0 (left) and SO-0 (right) situation at the end of 2040.

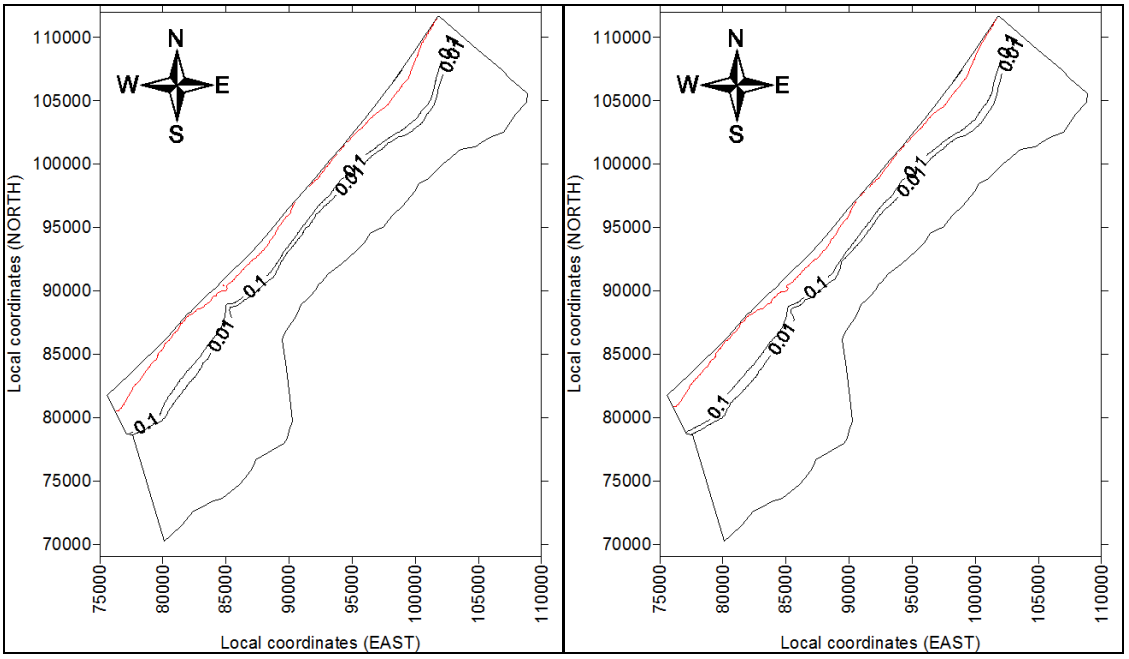

Figure 6.36 - Spatial distribution of normalized salt concentration for the T-0 (left) and SO-0 (right) situation at the end of 2040.

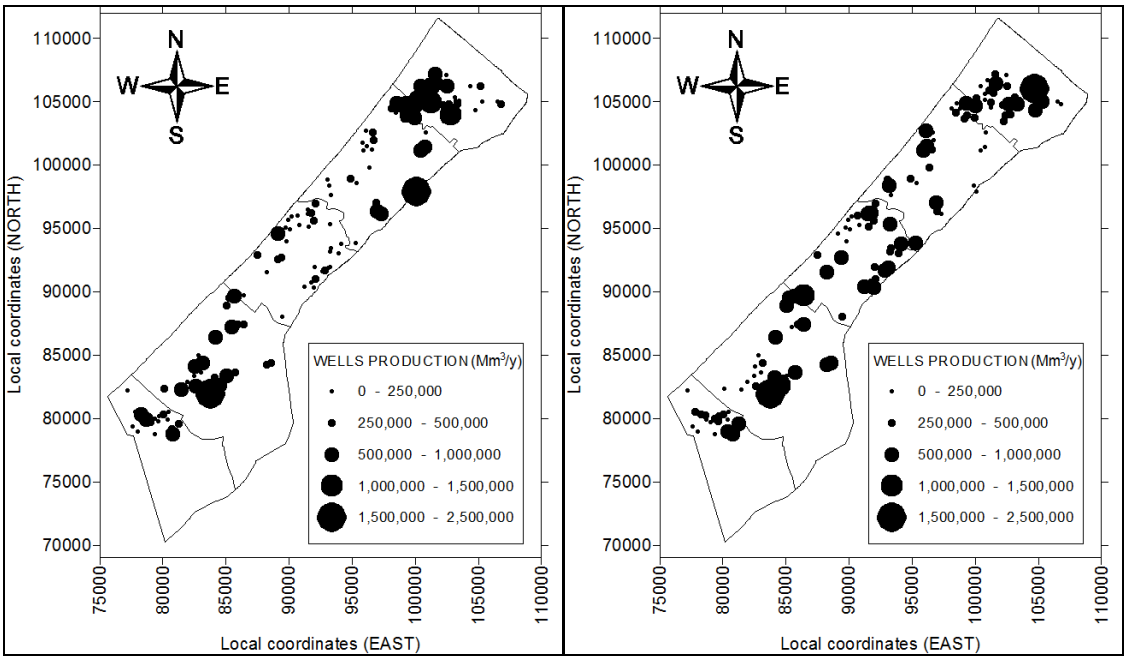

Figure 6.37 - Representation of pumping magnitudes for the 139 clustered municipal wells, both for the T-0 (left) and SO-0 (right) situation at the end of 2040.

As it is shown in the above figures, it is evident how the Simulation/Optimization method is able to identify an optimal solution for the management of the aquifer: while keeping total pumpings quite constant (with reference to the not-optimized situation), SWI

process is slightly blocked, extracted salt water is significantly slower that the previous pumping configuration, and also groundwater levels have significantly increased.

6.6 Summary and conclusions

The 3D hydrogeological model of Gaza Strip coastal aquifer is developed and then implemented using the CODESA-3D code (Gambolati et al,. 1999, Lecca, 2000) allowing to simulate coupled problems of variably saturated flow and contaminant transport in groundwater, in the presence of a fluid phase of variable density.

The hydrogeological model of the Gaza Strip is calibrated in steady-state conditions with 1935 water levels, considering average climate conditions and natural conditions ('no-pumping' scenario), by coupling simulation (CODESA-3D) and optimization (PEST) modules; then, the same calibrated model has been used as basis for the validation procedure, which has been performed for 1935-2000 and 2001-2010 periods. Although there are still some uncertainties in the southern part of the area, where the model seems to reveal some incongruence in the uphill part simulated groundwater table, the overall model is considered to properly represent the Gaza Strip aquifer system.

The simulated fields of water tables and groundwater salt concentration in 2010 are used as basis to simulate the response of the hydrological basin to future scenarios of climate change in the periods 2011-2040 and 2041-2070. In the study are considered a combination of 20 scenarios for each period, resulting from 4 GCM-RCM models and one more 'artificial' RCM (CC-0) within the same trend depicted for the historical period (1981-2010), and a combination of different pumping management and SLR setup.

The analysis of outputs coming from all the simulations shows that the increasing or decreasing in water levels, and higher and lower values of groundwater heads, corresponding in general to the NetP trends as reported in Chapter 5, Table 5.13; however, different climate scenarios variables, in this case, lead to differences in the groundwater system that can be hardly be appreciated if compared with pumping effects; it is evident, in fact, that pumping scenarios have extremely high impacts on the Gaza aquifer system.

Although some mitigation options are being evaluated for the GCA, in this study is only proposed a single strategy, which consists in assessing a new management scheme of

groundwater by the means of a simulation/optimization procedure aiming at maximizing the projected pumping rates, while constraining salt concentrations; the adopted procedure is illustrated in Chapter 3. Results coming from the application of this methodology to the Gaza Strip aquifer show that SWI process is slightly blocked, extracted salted water is significantly lowered, and groundwater levels have significantly increased; so that, the Simulation/Optimization method is able to identify a possible optimal solution for the management of the Gaza coastal aquifer.

Chapter 7 - Risk assessment analysis in the study area

The methodology of SWI risk proposed in Chapter 2 is applied to the Gaza Strip coastal hydrogeological basin (Palestine), the 3D hydrogeological model of which has been developed and then implemented using the CODESA-3D code (Gambolati et al,. 1999; Lecca, 2000) allowing to simulate coupled problems of variably saturated flow and contaminant transport in groundwater, in the presence of a fluid phase of variable density. The final goal is to verify, under climate induced changes, the appropriateness of proposed risk mitigation measures formulated to cope with marine ingression in the study area; a set of management scenarios are assessed using simulation/optimization methods (Qahman et al., 2009, Alnahhal et al., 2010), by coupling a genetic algorithm (GA, Carroll, 1996) with the simulation model, in order to identify optimal schemes to prevent/mitigate saltwater intrusion, taking into account conflicting objectives (e.g. maximizing pumping rates from the aquifer wells while limiting the salinity of the water withdrawn from them).

7.1 Current situation Risk analysis

To set up the current situation risk analysis, they are considered all the available data described in Chapter 4, results from simulation until 2010 and projection until 2040; for the future simulation, they are used only results coming from simulations fed with ECH_RMO modeled variables, as described in Chapter 5 and 6.

7.1.1 Vulnerability assessment and mapping

In this study the GALDIT method illustrated in Chapter 2 is used to assess vulnerability to SWI of the Gaza Strip aquifer. The evaluation of the six factors is proposed as follows.

The Gaza Aquifer is an unconfined aquifer; so that, the corresponding value of Rating is assessed as 7.5 (Figure 7.1).

The Gaza Aquifer is characterized by high values of conductivities (Chapter 4 and 6); so that, the value of hydraulic conductivity is considered over 40 m/d for the entire domain (Figure 7.2).

The overall Gaza Aquifer groundwater level is depicted from 2010 water levels, as illustrated in Figure 7.3.

The "Distance from the shore" factor is simply obtained by the offset of the coastal line, as illustrated in Figure 7.4.

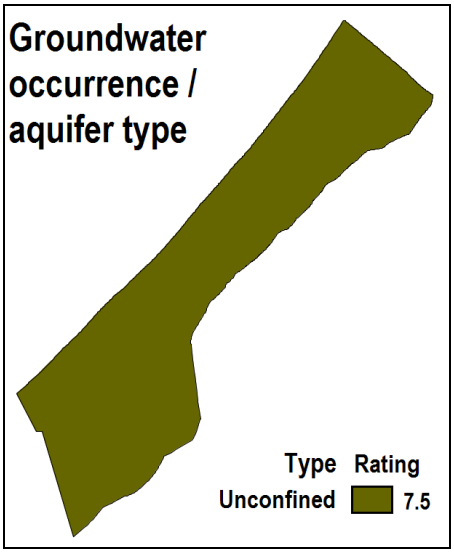

Figure 7.1 – Vulnerability to SWI (GALDIT method): Groundwater occurrence/aquifer type for the Gaza Strip aquifer

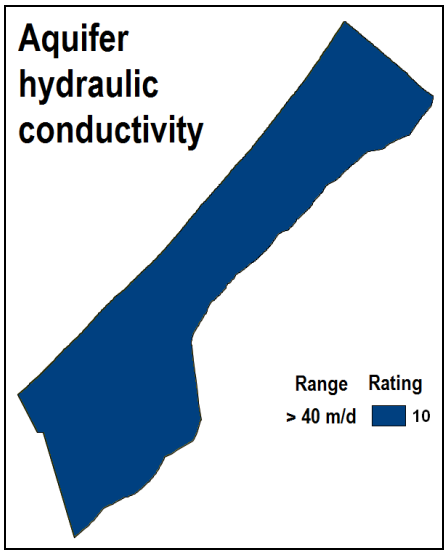

Figure 7.2 - Vulnerability to SWI (GALDIT method): Aquifer hydraulic conductivity for the Gaza Strip aquifer

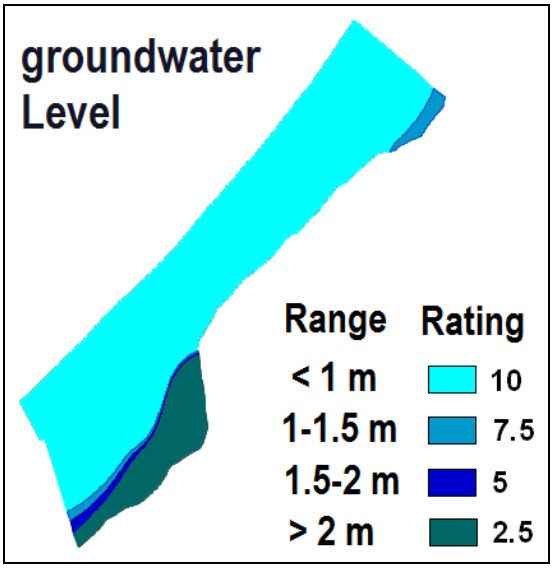

Figure 7.3 – Vulnerability to SWI (GALDIT method): Groundwater Level for the Gaza Strip aquifer

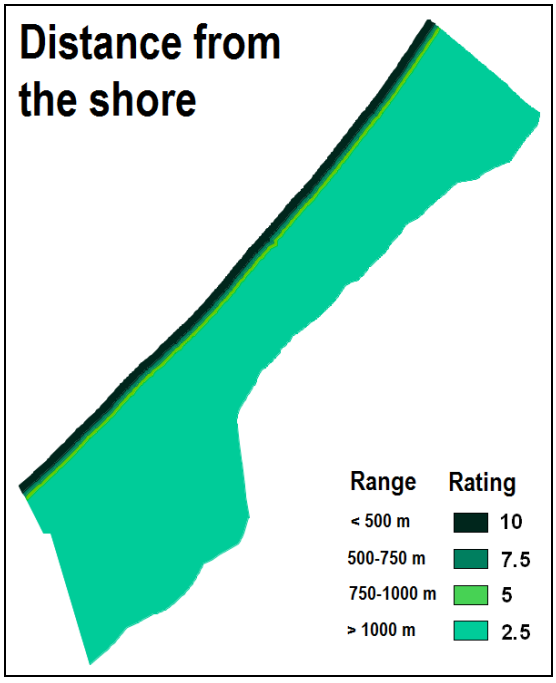

Figure 7.4 - Vulnerability to SWI (GALDIT method): Distance from the shore for the Gaza Strip aquifer

The GALDIT method considers range of $Cl/(HCO_3+CO_3)$ in e.p.m (equivalent per million) in groundwater in order to assess impact of existing SWI. Unfortunately, for this study site are not available those groundwater analysis. So that, ranges of SWI are adapted to available chlorides concentration within 2,5 km from the coastline, as reported in Table 7.1.

New Indicator (I)	Weight (w_5)	Indicator Variables		Importance Rating
		Class	Range of Chlorides in groundwater (mg/l)	
Impact status of existing seawater intrusion	1	Very High	> 5,000	10
		High	2,500 – 5,000	7.5
		Medium	250 – 2,500	5
		Low	< 250	2.5

Table 7.1 - New Ratings adopted for the GALDIT parameter I

The SWI Impact factor is then assessed for 2010 conditions, as illustrated in Figure 7.5.

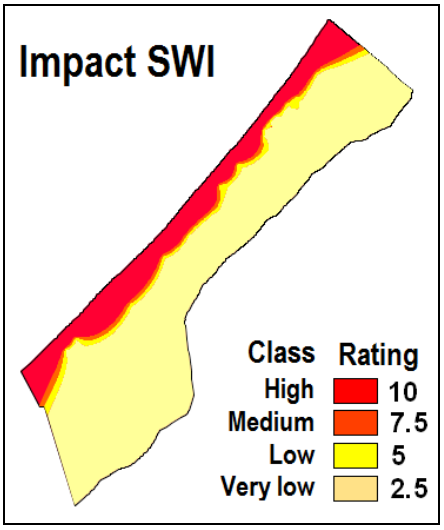

Figure 7.5 - Vulnerability to SWI (GALDIT method): Impact of SWI for the Gaza Strip aquifer

The mean thickness of the Gaza Aquifer is about 150 meters; so that this factor is set in the range > 10 m (Figure 7.6).

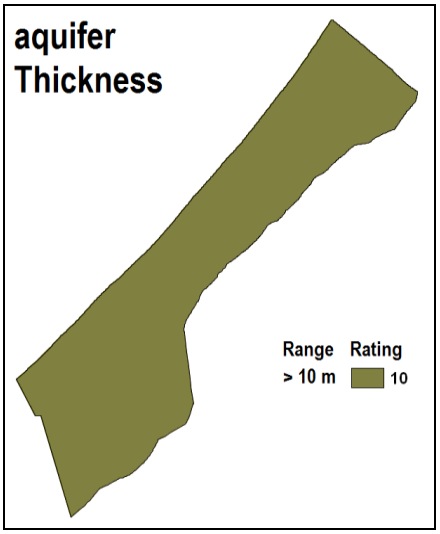

Figure 7.6 - Vulnerability to SWI (GALDIT method): Aquifer Thickness for the Gaza Strip aquifer

The overall GALDIT index is calculated as report in Chapter 2; the vulnerability map, adopting the classed map also illustrated in Chapter 2, is illustrated in Figure 7.7.

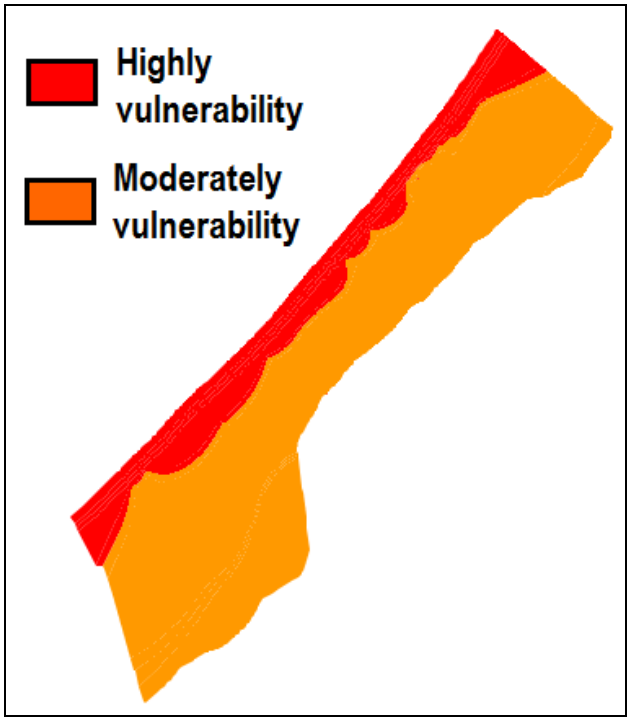

Figure 7.7 - Vulnerability map of the Gaza aquifer (GALDIT method)

It is interesting to note that the Gaza aquifer vulnerability, calculated with the GALDIT method, is classed from moderately to highly.

7.1.2 Hazard mapping

The hazard mapping is depicted from results of simulations of future scenarios, as described in Chapter 6, for the years 2015, 2020, 2030 and 2040; isolines of normalized concentrations of chlorides at levels 0.1 are evaluated and the Hazard map is calculated as shown in Figure 7.8.

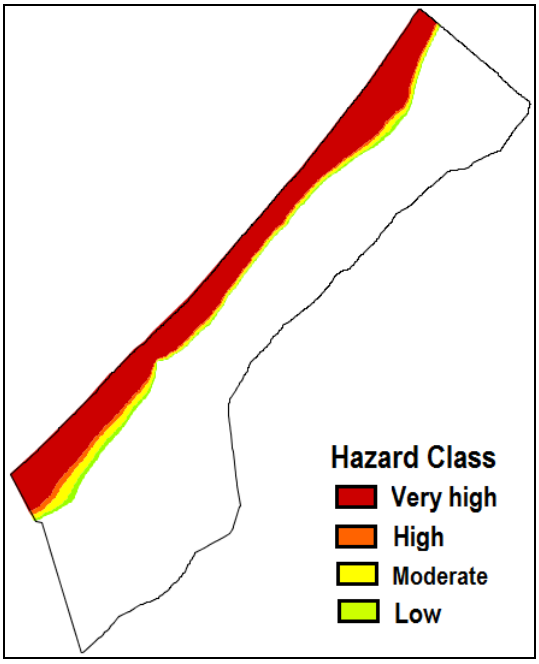

Figure 7.8 – Hazard map of the Gaza Strip site

7.1.3 Elements mapping

The overall wells operating in the area are illustrated in Figure 7.9; the radius of each circular influence area is calculated as function of mean yearly rate of each well. It is assumed that Drinking wells are classed at High level of risk, while agricultural wells are classed at Moderate level of risk.

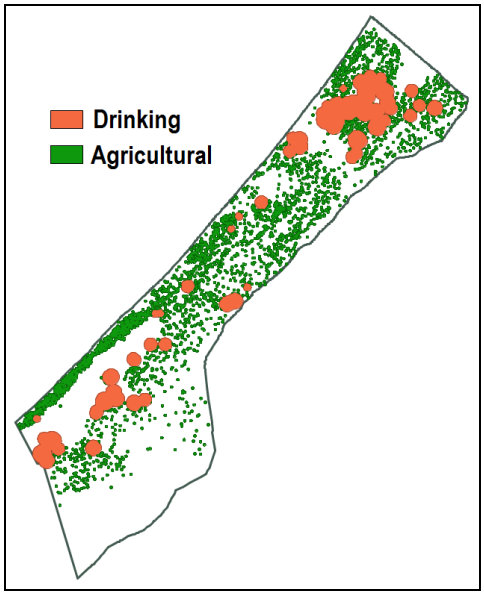

Figure 7.9 – Elements (operational wells in the Gaza Strip)

7.1.4 Risk mapping

In a first step, the hazard and vulnerability indices are aggregates in a "Risk intensity map", as illustrated in Figure 7.10, and in the second step "Risk intensity map" is aggregates within Elements map in a "Total Risk map" (Figure 7.11).

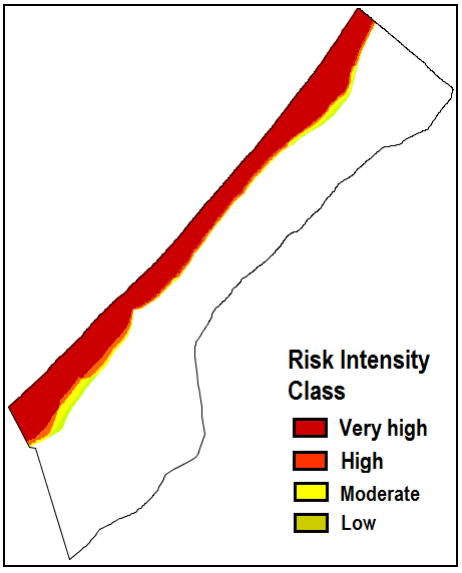

Figure 7.10 – Risk intensity map

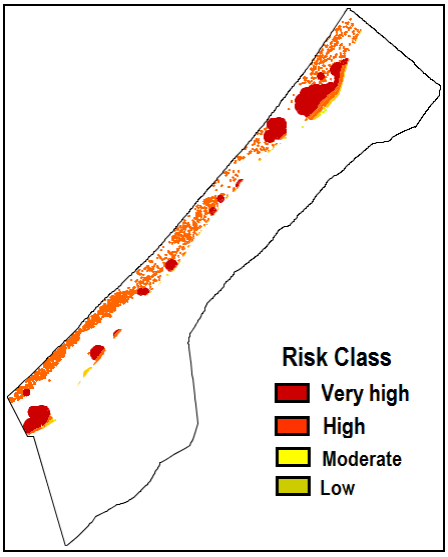

Figure 7.11 – SWI Risk map

As depicted for the map, in the site the Low risk class and the Moderate risk class areas are very small (Table 7.2). The very high risk class areas correspond to the northern and southern areas where there are the major cones of depressions, due to overpumpings and yet, in the northern area SWI is stronger than in other areas.

SWI Risk Class	Area (m^2)	Area (% of total)
Very High	14,916,395	35.4
High	26,685,265	60.9
Medium	1,444,764	3.3
Low	200,863	0.5
total	43,247,287	100

Table 7.2 – Areas (in m^2 and percents) of SWI risk classes for the Gaza Strip aquifer

7.2 SWI risk with mitigation strategies

The mitigation options applied for the Gaza Strip site are assessed within the Simulation/optimization method, as described in Chapter 6.

In this study the GALDIT method illustrated in Chapter 2 is used to assess vulnerability to SWI of the Gaza Strip aquifer; the vulnerability map is the same calculated in the above paragraphs. Hazard and Elements maps area assessed in the following.

7.2.1 Hazard mapping

The hazard mapping is depicted from results of optimized simulations of future scenarios, as described in Chapter 6, for the years 2015, 2020, 2030 and 2040. The isolines of normalized concentrations of chlorides at levels 0.1 are evaluated and the Hazard map is calculated as shown in the following Figure 7.12. 2040.

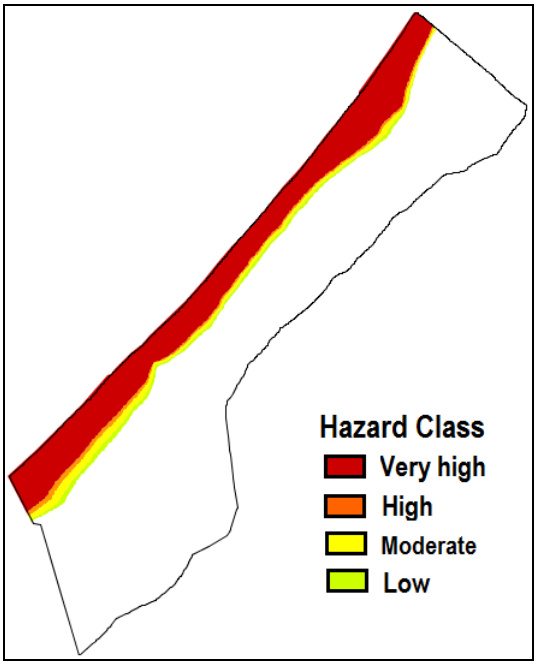

Figure 7.12 – Hazard map within mitigation options

The Hazard map is now showing a general decrease in all classes areas, due to the mitigation management option adopted in Chapter 6, paragraph 6.7, which in general provides a reduction of SWI phenomenon at the end of 2040.

7.2.2 Elements mapping

The overall wells operating in the area, as depicted from the Simulation/Optimization model, are illustrated in the following Figure 7.13; the radius of each circular influence area is assessed as function of mean yearly rate of each well. It is assumed that Drinking wells are classed at High level of risk, while agricultural wells are classed at Moderate level of risk.

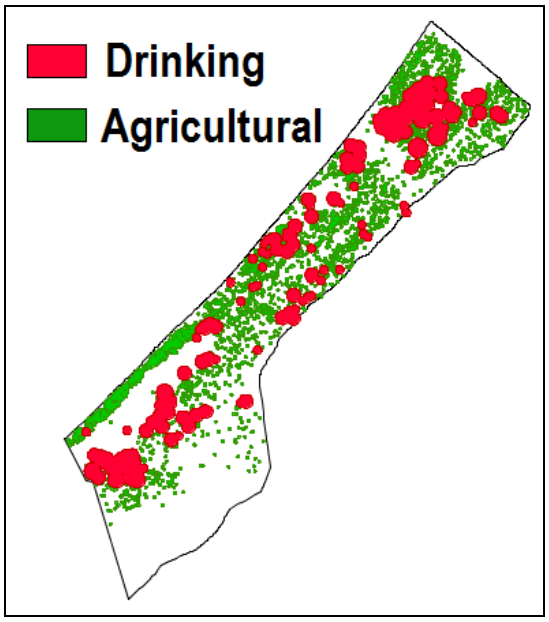

Figure 7.13 – Elements map within mitigation options

7.2.3 Risk mapping

In a first step, the hazard and vulnerability indices are aggregates in a "Risk intensity map", as illustrated in Figure 7.14, and in the second step "Risk intensity map" is aggregated within Elements map in a "Total Risk map" (Figure 7.15).

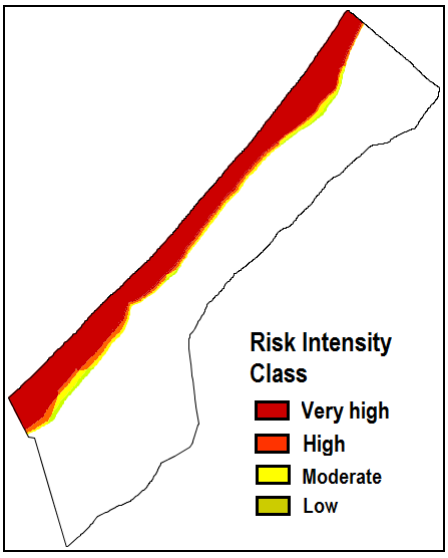

Figure 7.14 – Risk intensity map within mitigation options

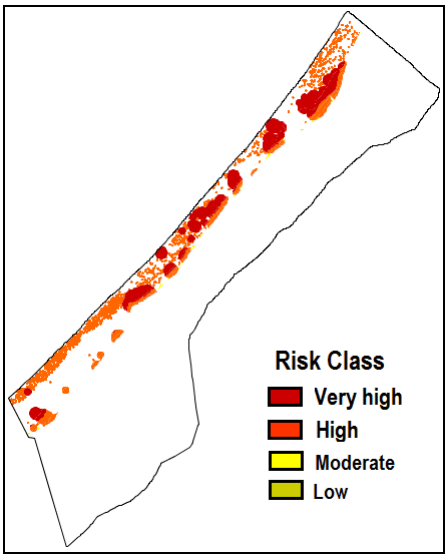

Figure 7.15 – Risk map within mitigation options

It is interesting to note that High and Very High risk areas are now smaller than before in the southern and northern areas, and quite bigger in the middle areas, due to the different location of wells in the optimal management scheme (Chapter 6, paragraph 6.7); in Table 7.3 are reported the different SWI risk classes areas, compared with the previous SWI classes areas in Table 7.4.

SWI Risk Class	Area (m^2)	Area (% of total)
Very High	17,185,110	39.2
High	27,500,530	62.7
Medium	416,949	1.0
Low	126,324	0.3
total	45,228,913	100

Table 7.3 – Areas (in m^2 and percents) of SWI risk classes for the Gaza Strip aquifer with mitigation options

SWI Risk Class	Area (m^2) (1)	Area (m^2) with mitigation options (2)	Difference (m^2)	Difference (%)
Very High	15,516,395	17,185,110	1,668,715	10.8
High	26,685,265	27,500,530	815,265	3.1
Medium	1,444,764	416,949	-1,027,815	-71.1
Low	200,863	126,324	-74,539	-37.1
total	43,847,287	45,228,913	1,381,626	3.2

Table 7.4 – Comparison of SWI risk classes areas (in m^2 and percents) for the Gaza Strip aquifer with and without mitigation options

The total SWI Risk it is slightly increased in the mitigation option configuration (+3%), but it is quite clear that this result is due to the effect of mitigation options on the aquifer system, which considers higher pumping levels in the middle area of the Gaza aquifer, where Very High and High risk classes areas have considerably increased. As results, Very High and High risk classes areas are shown an increase of about +10 and +3% respectively, with reference to the not mitigated situation. However, it must be highlight that the Medium and Low risk classes areas, which are mainly affected by long-term groundwater management options, are considerably decreased (around -70 and -37% respectively) with reference to the not mitigated situation.

It is quite clear that this results, due to the effect of mitigation options on the aquifer system, will have an important impact on the risk assessment mainly on the medium-long term period (i.e. between years 2030 and 2040).

7.3 Summary and conclusions

The application of SWI risk methodology to the Gaza Strip site is an important step on verifying the appropriateness of the method itself; each step of the procedure is then

analysed in the following, focusing at first on results coming from 'actual situation SWI risk'.

Starting from Elements mapping, this step seem to clearly highlight the targets of SWI, and the relative importance of each of them, due to the purposes of pumping waters and on pumping quantities; the Elements mapping procedure reaches the goal to give a simple representation of it.

The Hazard assessment seems to clearly highlight how the SWI could affect groundwater; the Hazard map gives itself a simple representation of possible SWI encroachment in short-medium term periods. The procedure is crucially dependent of 3D-modeling of the studied aquifer, and of the modeling of possible climate changes impacts on groundwater; so that, the entire methodology strongly depend on the modeling procedures.

The Vulnerability assessment highlight the actual propension of the aquifer to be affected by SWI; the used factors in the GALDIT indexing are simple to obtain for each aquifer system. From the other hand, some approximations (i.e. water Levels, chlorides concentration,) can lead to over or underestimate the process.

Comparing those maps within SWI risk mapping with mitigation strategies, it is analysed how the Hazard assessment and Elements mapping affect the final results. Both for Hazard map and Elements map, at a large scale (at the small scale it is more evident), are not clearly evident strong differences; however, the relative changes results in lowering class levels areas of SWI risk mainly in the northern and southern areas, and the most important impacts are shown in several areas of the study site in the medium-long term periods (i.e. between the period 2030-2040).

The risk area maps resulting from this methodology can be adopted as a tool for the design of groundwater management schemes, as they are condensing relevant information from complex dynamic processes obtained from numerical simulations and visualize the results in simple and static maps. This can make it possible to decision makers, who are not familiar with groundwater dynamics, to access to such synthetic simple information.

Chapter 8 - Conclusions

This chapter is a summary of the main contributions provided by this thesis. The main outcome responds to the key objective of this work, that is to elaborate a process-based framework for a SWI risk assessment and to apply it to the real case study of the Gaza Strip aquifer. In few word, the work focuses on developing of a risk assessment methodology of seawater intrusion in coastal aquifers, of the application the methodology to a real case-study and of assessing impact of mitigation strategies (for aquifer restoration) on Salt Water Intrusion (SWI) Risk.

8.1 Summary

Sea water intrusion (or salt water intrusion, SWI) is the encroachment of saline water into fresh ground water regions in coastal aquifer settings. SWI is a global issue, considering that a substantial proportion of the earth's population lives along coastlines, where groundwater is considered the main source of water supply, and that mixing a small quantity (2–3%) of saltwater with groundwater makes it unfit for different uses.

Coastal aquifers in the Mediterranean are often affected by seawater intrusion, which has sometimes become a major threat to coastal area freshwater resources, mainly due to lack of appropriate groundwater resources management. Current projections of future potential climatic scenarios (IPCC, 2007) further complicate the overview, because the worst considered possibilities provide critical predictions about the decline of the average amount of available water, together with a progressive reduction of natural groundwater recharge; yet, the sea-level rise (SLR) could alter the position of coastline, making it possible consistent increasing of Salt Water Intrusion (SWI).

A proper analysis and risk assessment of areas subject to seawater intrusion, and the evaluation of hydrological response of the coastal basins to climate variability, appear to be essential for the design of water management measures that are necessary to mitigate environmental and socio-economic impacts.

The approach of the proposed Saltwater Risk Analysis methodology is based on the assumption that risk can be defined as the probability of harmful consequences or expected losses (e.g. disruption of economic activity or environmental damage), in a certain area and in a certain period of time, resulting from interactions between natural or human-induced hazards and vulnerable conditions. The proposed methodology for the assessment of SWI risk is based on the origin-pathway-target model, in which the 3 elements are described as follows:

1) The origin of seawater intrusion is the seaside boundary of the aquifer, which is a linear source of salinity;
2) The pathway is the horizontal and vertical groundwater flow in the aquifer
3) The target is the water which is extracted from wells;

The final value of SWI risk is evaluated by applying the overlay principle to three thematic maps coming from the 3 elements above described, namely Hazard map (H), Vulnerability map (V) and Elements map (E).

The Vulnerability (V) to SWI is calculated using the GALDIT method, using six parameters that control the potential saltwater intrusion in groundwater. The Hazard (H) to SWI is calculated by the means of a 3D hydrogeological model, allowing to simulate coupled problems of variably saturated flow and contaminant transport in groundwater, in the presence of a fluid phase of variable density, and to assess possible future scenarios of how groundwater system can evolve considering also possible effects of climate induced changes. The possible consequences of a contamination are evaluated on the wells (elements, E) by considering their use (agriculture, industrial, drinkable purposes) and their operational pumping values. The scope of the methodology is to map out zones that are prone to further SWI, so that the spatial overlay principle is applied by the means of risk matrixes, to the hazard map (H), the vulnerability map (V) and elements map (E); evaluation of the SWI Risk provides an indication of a community's probability to consume saltwater contaminated groundwater.

A computational integration of existing tool including all the essential steps to develop and test management measures to restore groundwater quality in coastal aquifers, is presented. The proposed and used framework consists in:

- 3D modeling (coupled density-dependent groundwater flow and miscible salt transport in coastal aquifer) using CODESA-3D (Gambolati et al., 1999; Lecca 2000);
- automatic calibration of the hydrogeological model using PEST (Doherty, 2002);
- simulation/optimization model, to assess management and mitigation strategies for SWI, using a genetic algorithm (Carrol, 1996).

Simulation is based on a density-dependent advective-dispersive solute transport 3D-model, which allows to properly describe SWI problem in coastal aquifers. The calibration procedure is based on the coupling of the physical model with a nonlinear parameter estimation technique, allowing to identify a optimal parameters against field observed values by means of minimization of an objective function. In order to find out a set of plausible management solutions, what is usually done is to run a large set of simulations (each based on a previously calibrated hydrological model) with different management options as input. Genetic algorithm (**GA**) is used as the optimization technique in the proposed Simulation/Optimization model, which allows to identify optimal management schemes under user-prescribed conditions, namely management goals and constraints. The integration of tools consists in a in-house model (CODESA-3D) and two open-source codes: PEST (available at http://www.pesthomepage.org/) and GA (available at http://cuaerospace.com/carroll/ga.html).

The Gaza Strip is a semi-arid region located in the Mediterranean basin; it covers a long and narrow rectangular coastal area of about 365 km^2 between Egypt and Israel.

The Gaza coastal aquifer is the main source of water for agriculture, domestic, and industrial purposes in Gaza Strip. An estimated 1.5 million people live in Gaza by the end of 2010, with a density of about 4,500 people/km^2, making it one of the most overcrowded areas in the world. Due to the continuous population growth, the total water demand in the Gaza Strip is strongly increasing. Nowadays, the need of water is not satisfied by the available resources, and this is causing a huge deficit between water demand and supply (Qahman and Larabi, 2006).

Also, making the aquifer overexploited, the problem of SWI is so exacerbated that corrective measures are needed to restore groundwater quality and properly manage the

aquifer. During the last decades several studies have been carried out to analyze Salt Water Intrusion in the Gaza Strip (Yakirevich et al., 1998; Melloul and Collin, 2000; Moe et al., 2001; Qahman and Larabi, 2006), but the aquifer quality situation is so critical (Shomar et al., 2010) that this problem is still a long way from being solved.

In the future, the Earth system will be affected by the consequences of increasing temperatures, changing patterns of precipitation, and sea level rise; current projections of future potential climatic scenarios (IPCC, 2007) for the Mediterranean area provide critical predictions about the decline of the average amount of water availability (in terms of both inflows than outflows).

Different scenarios have been generated by the International Panel on Climate Change (IPCC); however, only the data for the most probable and accepted scenario, the A1B, are proposed in this study. This research has been undertaken as part of the CLIMB project, funded by the European Commission within the 7th Framework Programme, so that future climate scenarios have been processed and made available by atmosphere experts who collaborate in carrying out the "Climate Models Auditing and Downscaling" Work Package of same project. During the project, a simple but precise and rigorous auditing assessment of mean states, monthly fluctuations, and extremes, of precipitation and temperature has been obtained by comparing the outputs of 14 Regional Climate Models (RCMs) part of the ENSEMBLES project, with a gridded data set of observations (E-OBS). Using this data set for verification in the 1951-2010 period, it has been possible to rank the models' performance, for the chosen parameters. Further analysis on predictions of climate change have been done about the Gaza Strip, for the 4 models ECH_RMO, ECH_REM, ECH_RCA and HCH_RCA, comparing also historical measured daily rainfall rates within modeled daily rainfall rates. Precipitation (P) and evaporation (ET) patterns are supposed to impact on the future hydrological cycle of the Gaza site, as they represent the two factors determining net rainfall recharge. In particular, it is supposed that different patterns in P and ET will affect in different way the aquifer system, as these two values are used as the basis of the setup of recharging patterns for the coastal aquifer, aiming in this way to represent the future evolution of the overall system. It has been proposed a deeper analysis on the Gaza strip area, for only the ECH_RMO modeled

variables, which are bias corrected within CRU data (for P and T variables) and, for P variables, within historical data by the means of the QQplot methodology. Deeper analysis on available climate data highlights that modeled precipitation values (P) are strongly different from historical measured data; this may be due to the different spatial resolutions, and also to series of chained conceptual issues that pertains to RCM gridded points, which actually represents a 'averaged daily value' for the representative squared area of about 22-25 km of side. The trend of bias corrected (with historical data collected in the Gaza Strip) and not bias corrected variables have been further compared, highlighting quite the same trends for both the two future periods considered. The main outcomes from the analysis on future projected variables coming from 4 different GCM-RCM models applied on the Gaza Strip area are summarized in the following, with reference to 1981-2010 historical period:

1) Precipitation rates will have an increase in the next 30 years, and then a decrease in the following 30 years;
2) Extremes precipitations events (daily precipitation >10 mm/d) will have an increase in the next 30 years, and then a decrease in the following 30 years;
3) Very extreme precipitation events (daily precipitation >20 mm/d) will have an increase in the next 30 years and then a decrease in the following 30 years;
4) Temperatures will rise with an increase up to 2°C in the overall 60 next years;
5) ET patterns will slightly increase in the next 30 years and then decrease in the following 30 years;
6) The net recharging precipitation (NetP, set equal to P-ET) will increase in the next 30 years and then decrease in the following 30 years.
7) NetP values will have a direct impact on groundwater recharge, and however it must be considered that, due to the increase of extreme events and very extreme events of precipitation, the patterns should be much less than these, as runoff component for sure will be hampered. Further analysis should be done on this issue.

The expected effects of changes in climate dynamics on the aquifer water balance can be roughly assessed, at least for the vertical inflow fluxes (groundwater vertical recharging

amounts), strongly correlated to the NetP rates. Thus, groundwater recharging amounts due to Net; a briefly discussion about this issue is proposed in Chapter 6.

The 3D hydrogeological model of Gaza Strip coastal aquifer is developed and then implemented using the CODESA-3D code (Gambolati et al,. 1999, Lecca, 2000) allowing to simulate coupled problems of variably saturated flow and contaminant transport in groundwater, in the presence of a fluid phase of variable density.

The hydrogeological model of the Gaza Strip is calibrated in steady-state conditions with 1935 water levels, considering average climate conditions and natural conditions ('no-pumping' scenario), by coupling simulation (CODESA-3D) and optimization (PEST) modules; then, the same calibrated model has been used as basis for the validation procedure, which has been performed for 1935-2000 and 2001-2010 periods. Although there are still some uncertainties in the southern part of the area, where the model seems to reveal some incongruence in the uphill part simulated groundwater table, the overall model is considered to properly represent the Gaza Strip aquifer system.

The expected effects of changes in climate dynamics on the aquifer water balance are assessed in terms of yearly mean values of groundwater vertical recharging values (in terms of Mm^3/y for overall the model domain) for the periods 2011-2040 and 2041-2070 for the 4 climate models considered in this study, relatively to the overall modeled area, compared within the past reference period 1981-2010. The simulated fields of water tables and groundwater salt concentration in 2010 are eventually used to assess the response of the hydrological basin to future scenarios of climate change in the periods 2011-2040 and 2041-2070. In the study are considered a combination of 20 scenarios for each period, resulting from 4 GCM-RCM models and one more 'artificial' RCM' within the same trend depicted for the historical period (1981-2010), and a combination of different pumping and SLR setup.

The analysis of outputs coming from all the simulations shows that the increasing or decreasing in water levels, and higher and lower values of groundwater heads, correspond in general to the NetP trends as reported in Chapter 5; however, different climate scenarios variables, in this case, lead to differences in the groundwater system that can be

hardly be appreciated if compared with pumping effects; it is evident, in fact, that pumping scenarios have extremely high impacts on the Gaza aquifer system.

Although some mitigation options are being evaluated for the GCA, in this study is only proposed a single strategy, which consists in assessing a new management scheme of groundwater by the means of a simulation/optimization procedure aiming at minimizing the projected pumping rates, while constraining concentrations; the adopted procedure is illustrated in Chapter 3. Results coming from the application of this methodology to the Gaza Strip aquifer show that, although SWI process is slightly blocked, extracted salted water is lowered, and groundwater levels have significantly increased; so that, the Simulation/Optimization method is able to identify a possible optimal solution for the management of the aquifer.

The methodology of SWI risk proposed in Chapter 2 is applied to the Gaza Strip coastal hydrogeological basin (Palestine), the 3D hydrogeological model of which has been developed and then implemented using the CODESA-3D code (Gambolati et al,. 1999; Lecca, 2000) allowing to simulate coupled problems of variably saturated flow and contaminant transport in groundwater, in the presence of a fluid phase of variable density. The final goal is to verify, under climate induced changes, the appropriateness of proposed risk mitigation measures formulated to cope with marine ingression in the study area; a set of management scenarios are assessed using simulation/optimization methods (Qahman et al., 2009, Alnahhal et al., 2010), by coupling a genetic algorithm (GA, Carroll 1999) with the simulation model, in order to identify optimal schemes to prevent/mitigate saltwater intrusion, taking into account conflicting objectives (e.g. maximizing pumping rates from the aquifer wells while limiting the salinity of the water withdrawn from them).

The application of SWI risk methodology to the Gaza Strip site is an important step on verifying the appropriateness of the method itself; each step of the procedure is then analysed in the following, focusing at first on results coming from ‘actual situation SWI risk’. The risk area maps resulting from this methodology can be adopted as a tool for the design of groundwater management schemes, as they are condensing relevant information from complex dynamic processes obtained from numerical simulations and visualize the

results in simple and static maps. This can make it possible to decision makers, who are not familiar with groundwater dynamics, to access to such synthetic simple information.

8.2 Outcomes from this study

The work proposed the integration of existing tools for Water Resources Management of coastal aquifers that includes: a complex SWI simulation model (CODESA-3D), risk mapping with GALDIT vulnerability assessment, PEST parameter estimation, and a genetic algorithm for exploring mitigation/remediation strategies.

The proposed methodology of the SWI Risk provides an indication of a community's probability to consume saltwater contaminated groundwater, under climate change conditions; this methodology represents a first step in SWI Risk assessment, which should be integrated by other studies.

Nevertheless, the application of SWI risk methodology to the Gaza Strip site is an important step on verifying the appropriateness of the method itself; each step of the procedure is then analysed in the following, focusing at first on results coming from 'actual situation SWI risk'. Starting from Elements mapping, this step seem to clearly highlight the targets of SWI, and the relative importance of each of them; the Elements mapping procedure reaches the goal to give a simple representation of it. The Hazard assessment seems to clearly highlight how the SWI could affect groundwater; the Hazard map gives itself a simple representation of possible SWI encroachment in short-medium term periods. The procedure is crucially dependent of 3D-modeling of the studied aquifer, and of the modeling of possible climate changes impacts on groundwater; so that, the entire methodology strongly depend on the modeling procedures. The Vulnerability assessment highlight the actual propension of the aquifer to be affected by SWI; the used factors in the GALDIT indexing are simple to obtain for each aquifer system. From the other hand, some approximations (i.e. water Levels, chlorides concentration,) can lead to over or underestimate the process.

Comparing those maps within SWI risk mapping with mitigation strategies, it is analysed how the Hazard assessment and Elements mapping affect the final results. While for the Hazard map, at a large scale (at the small scale it is more evident), are not clearly evident strong differences, the last Elements map is changed from the first one. These changes

results in lowering class levels areas of SWI risk mainly in the northern and southern areas, and the most important impacts are shown in several areas of the study site in the medium-long term periods (i.e. between the period 2030-2040).

Results, with reference to the case study, show that: 1) SWI risk assessment can be addressed by means of groundwater simulation models, calibrated against field measures, as a tool to evaluate future contamination in response to projected climate scenarios and exploitation plans, and that 2) mitigation measures can be ranked, according to some predefined criteria, and expected benefits can be quantified.

8.2.1 Specific recommendations for the Gaza Strip aquifer

Stated that SWI represent an important problem for the Gaza Strip area, results from this study can lead to some further observations.

1) As significant uncertainties still remain on some processes involved the southern area (Rafah), they should be promoted appropriate studies on this area;
2) In order to better reproduce the aquifer system behaviour, it should be adequately quantified recharge and return flow volumes (that in this study have been in part estimated) and water quality data;
3) The problem of low groundwater quality is forecasted to go on; if none appropriate suite of management policies and plans will be adopted, the aquifer depletion and deterioration ought go further for decades;
4) It should be promoted an integration of different water management strategies, which the first one should be lowering pumping rates in the area; these strategies should involve not only hydrogeological but also socioeconomic considerations, as the water demand has been detected to be the main human-induced stress on the aquifer system.

8.3 Open issues and challenges

Based on results coming from this work, it is possible to highlight some issues that are still a challenge to overcome.

1) Coupling climate change conditions and models to forecast SWI. This issue still represents a challenge due to several problems affecting the ‘coupling’ part. First,

GCM and RCM usually have spatial resolutions that differ from real-case study scale resolution in a very strong way; it means that modeled climate variables have to be somehow downscaled in the study site scale, and this procedure is not yet standardized. Secondary, modeled climate variables usually differs from measured values (which also could be affected by human errors) and they should be properly bias corrected, in order –at least- to quite reproduce the past climate; at the moment, there are several methods adopted to try to overcome this problem, but the solution seem not to be unique. As third point, it represent always a challenge to adequately reproduce climate modeled recharging values into a SWI model, as it ought be necessary to reproduce mean climatic values in long term period and also to reproduce extreme events in the short period, while groundwater flow and transport is a very long term and non-linear process.

2) Clear definition of impacts of climate change on groundwater, being the effects of this phenomenon difficult to separate from several human induced changes on environments (groundwater overexploitation, change in land use, …). It is especially true where human impacts on groundwater are extremely high and it is not possible to 'isolate' such effects on aquifers systems. So that, it should be always considered both the climate and the human induced impact; in particular, more attention should be addressed on groundwater withdrawal changes in response to climate change condition;
3) Calibrating complex models with scarcity of data (e.g. lateral inflow, hydrogeological setting, unsaturated soil properties, pumping rates…) and uncertainties on some boundary conditions. This issue represents a challenge whenever and wherever the input dataset is not complete for all the needed inputs; in particular, it should be point out that the estimation (when data missing) of pumping rates is crucial for the right definition of human impacts on aquifers. From a strictly technical point, the way to overcome this problem should consist in calibration and/or optimization procedure, aiming at estimate missing data against all measured data. On the other hand, another possible solution should be based on the possible or most likely local simplified conceptualization of the

aquifer system, and also on expertise of local professionals, who can strong increase the quality of the model.

4) Definition of mitigation strategies under climate change (setting optimal pumpings scheme). The challenge is generally to clearly identify what results should be reached with the management strategy (high water levels and low SWI within high pumping rates, or minimum groundwater levels in such areas, …), what kind of management scheme can be actually adopted, and how to implement it in the optimization procedure.
5) Limitation of index methods for vulnerability assessment (e.g. Water Level in GALDIT). For sure, some approximations can lead to over or underestimate the process; however, as such methods are simple to apply for all aquifer systems, they can be considered as a good approximation of SWI vulnerability.
6) Limitation of SWI risk assessment. Although the proposed risk mapping procedure is theoretically useful, it is based on the underlying assumption of properly-weighted superposition of different single maps with different meanings; the synthesis of the results are static images, which clearly represents a limitation of the provided information. SWI is a dynamic density-driven flow and transport non-linear process, and the results obtained by numerical modeling are strongly dependent on the modeling approach and assumptions, on field data quality and on the model calibration. It should be taken into account that results may be biased by the chosen modeling approach, representing it a severe restriction in some cases. The procedure is crucially dependent of 3D-modeling of the studied aquifer, and of the modeling of possible climate changes impacts on groundwater; so that, the entire methodology strongly depend on the modeling procedures. Although the proposed hazard mapping procedure is based on SWI dynamic non-linear process, the results obtained by numerical modeling are strongly dependent on the modeling assumptions and on field data quality. Furthermore, the syntheses of the results are static images, which clearly represent a limitation of the provided information. However, the risk area maps resulting from this methodology can be adopted as a tool for the design of groundwater management schemes, as they are condensing relevant information from complex dynamic

processes obtained from numerical simulations and visualize the results in simple and static maps. This can make it possible to decision makers, who are not familiar with groundwater dynamics, to access to such synthetic simple information.

Appendix A – Outputs from simulations

In this Appendix are reported all outputs from simulations, as cited in the Chapters of this work. Some graphs and figures are here repeated to facilitate the analysis of outputs.

A.1 Calibration dataset C2

The calibration dataset C2 is the basis for the validation of the model. In Figure A.1 is illustrated for the year 1935 the graphical comparison between measured and simulated (calibrated) heads; their location are illustrated in Figure A.2 and reported in Table A.1.

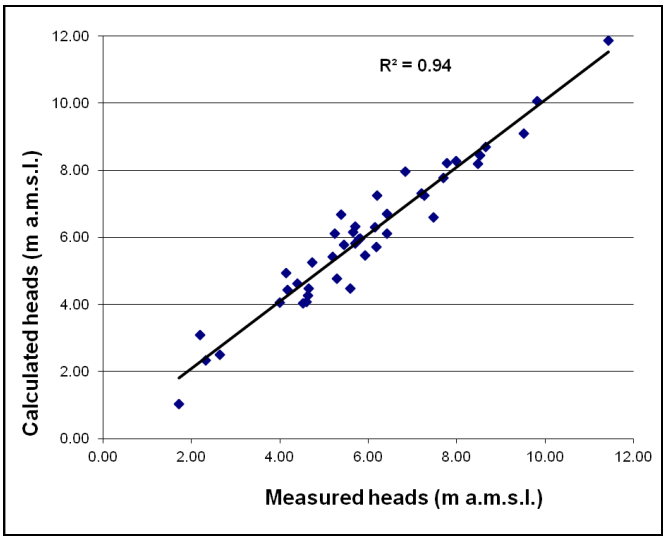

Figure A.1 – Comparison between measured and simulated heads for 1935

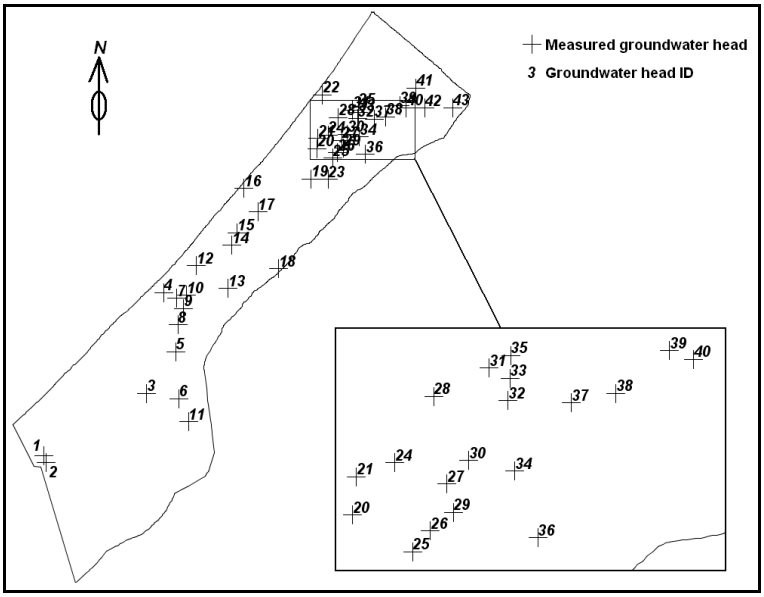

Figure A.2 - Measured and simulated well points ID

Well_ID (1935)	X	Y	Real h (m a.m.s.l)	Simulated h (m a.m.s.l)	Residual (m)
1	77883.70	79469.31	5.20	5.41	-0.21
2	78033.62	78954.26	5.45	5.77	-0.32
3	85368.09	83977.02	6.42	6.11	0.32
4	86611.56	91293.50	2.64	2.51	0.13
5	87471.81	86994.23	5.82	5.97	-0.15
6	87702.27	83601.90	7.27	7.24	0.03
7	87552.02	90881.54	4.52	4.03	0.49
8	87634.49	88956.74	4.74	5.26	-0.52
9	88065.84	90125.07	4.15	4.93	-0.78
10	88275.23	91081.42	4.65	4.48	0.17
11	88413.86	81930.02	8.48	8.19	0.29
12	88997.32	93232.20	2.20	3.09	-0.89
13	91302.20	91586.03	5.70	6.32	-0.62
14	91559.81	94726.42	4.18	4.42	-0.24
15	91949.80	95615.73	4.60	4.07	0.53
16	92449.88	98825.70	1.72	1.02	0.70
17	93457.90	97146.20	4.64	4.27	0.37
18	94975.76	93000.41	7.69	7.78	-0.09
19	97325.63	99530.95	6.15	6.31	-0.16
20	97768.39	101727.77	5.59	4.48	1.11
21	97844.01	102453.70	4.00	4.05	-0.05
22	98170.57	105615.36	2.33	2.33	0.01
23	98581.45	99483.97	7.78	8.21	-0.43
24	98576.85	102719.98	4.39	4.62	-0.23
25	98911.40	101028.27	6.42	6.69	-0.27
26	99252.84	101425.38	7.47	6.60	0.87
27	99565.27	102315.49	5.70	5.83	-0.13
28	99313.17	103976.20	5.29	4.76	0.53
29	99686.56	101774.97	5.39	6.67	-1.28
30	99980.56	102762.32	5.24	6.11	-0.87
31	100369.68	104511.53	5.93	5.45	0.48
32	100726.63	103897.57	5.66	6.15	-0.49
33	100764.20	104316.92	5.79	5.94	-0.15
34	100858.86	102557.86	6.20	7.25	-1.05
35	100777.35	104749.09	6.18	5.70	0.48
36	101293.48	101294.38	9.52	9.09	0.43
37	101936.60	103849.23	7.20	7.31	-0.11
38	102780.69	104029.88	6.84	7.95	-1.11
39	103798.06	104839.49	7.98	8.27	-0.29
40	104260.57	104677.44	8.66	8.69	-0.03
41	104967.89	106101.48	8.53	8.45	0.08
42	105599.75	104665.52	9.82	10.05	-0.23
43	107621.45	104696.78	11.42	11.86	-0.44

Table A.1 - Measured and simulated heads (h), in terms of m a.s.m.l., for year 1935

A.2 Validation – period 1935-2010

For the validation they have been analyzed the outputs of 4 years, which are reported and compared within measured field values in Table A.2, Table A.3, Table A.4 and Table A.5.

Well_ID (1970)	X	Y	Real h (m a.m.s.l)	Simulated h (m a.m.s.l)	Residual (m)
1	76320.24	81452.64	1.21	1.23	-0.02
2	77173.71	82195.70	1.77	1.17	0.60
3	93323.18	100132.62	-0.24	0.00	-0.24
4	78969.83	83288.13	1.54	1.40	0.13
5	78680.00	78390.00	3.05	1.93	1.11
6	79535.65	77429.62	1.61	2.34	-0.73
7	80070.00	79700.00	1.38	1.89	-0.52
8	99113.93	106278.34	0.19	0.51	-0.32
9	97640.00	104910.00	0.24	0.52	-0.28
10	80940.00	76960.00	3.69	2.87	0.81
11	82610.00	82590.00	2.81	1.97	0.84
12	105890.00	106620.00	0.43	1.67	-1.24
13	82720.00	79910.00	3.68	2.51	1.17
14	83298.06	78583.55	3.58	2.99	0.59
15	84370.00	81660.00	4.31	2.64	1.67
16	84440.26	84108.89	2.05	2.08	-0.03
17	85128.58	82468.53	3.18	2.70	0.48
18	86900.00	81550.00	5.10	3.70	1.39
19	89260.00	83500.00	4.88	4.63	0.24
20	88200.00	83200.00	4.35	3.74	0.61
21	88340.00	85640.00	1.99	2.64	-0.65
22	86841.53	89687.49	1.35	1.08	0.27
23	87280.00	87440.00	2.41	1.83	0.59
24	89690.00	89350.00	1.63	1.66	-0.03
25	88297.38	92014.17	0.04	0.71	-0.67
26	89610.00	92970.00	0.25	0.87	-0.61
27	93310.00	92860.00	2.59	2.52	0.07
28	94280.00	94370.00	3.07	2.67	0.40
29	97995.17	96778.24	3.17	4.07	-0.90
30	93620.00	95540.00	2.23	2.06	0.17
31	95000.00	96630.00	1.52	2.25	-0.73
32	96110.90	102708.42	0.72	0.61	0.12
33	100969.37	106688.94	1.36	0.59	0.77
34	99733.65	105434.14	0.74	0.22	0.52
35	98477.71	104140.95	0.17	0.07	0.10
36	104930.00	104930.00	0.34	1.33	-0.99
37	102618.74	103128.48	0.09	0.80	-0.71
38	102030.00	101780.00	0.88	1.54	-0.66

Table A.2 - Measured and simulated heads (h), in terms of m a.m.s.l., for 1970

Well_ID (1990)	X	Y	Real h (m a.m.s.l)	Simulated h (m a.m.s.l)	Residual (m)
1	76320.24	81452.64	-0.90	-0.73	-0.17
2	77173.71	82195.70	-0.28	-0.56	0.28
3	81501.39	86521.08	-0.29	0.08	-0.37
4	83818.43	89076.94	-2.01	-1.15	-0.86
5	89912.07	95679.82	-0.72	0.15	-0.87
6	93323.18	100132.62	0.13	0.00	0.13
7	78969.83	83288.13	-0.27	-0.41	0.15
8	103383.01	101465.33	0.96	2.12	-1.16
9	87365.89	92128.64	-0.83	-0.40	-0.43
10	100282.65	108133.93	-0.19	0.17	-0.36
11	107738.43	105615.98	0.77	1.83	-1.06
12	91190.00	96150.00	0.68	0.45	0.23
13	78680.00	78390.00	-1.35	-2.94	1.59
14	79535.65	77429.62	-3.70	-2.74	-0.96
15	80070.00	79700.00	-2.47	-2.78	0.31
16	99113.93	106278.34	-0.82	-0.39	-0.43
17	98330.00	105800.00	0.46	-0.09	0.55
18	97640.00	104910.00	-0.02	0.02	-0.04
19	80940.00	76960.00	-0.20	-1.80	1.60
20	81170.00	80840.00	-0.51	-1.85	1.34
21	82610.00	82590.00	-1.19	-1.12	-0.07
22	105890.00	106620.00	-0.05	0.94	-0.99
23	81110.00	79150.00	-1.33	-2.37	1.03
24	82720.00	79910.00	-0.22	-1.44	1.22
25	82433.57	77728.60	-0.06	-1.33	1.28
26	84370.00	81660.00	0.68	-0.68	1.35
27	106500.00	105840.00	0.30	1.03	-0.73
28	84440.26	84108.89	-0.13	-0.71	0.58
29	88686.12	93811.03	-1.65	-0.77	-0.88
30	85128.58	82468.53	-0.39	-0.43	0.04
31	86900.00	81550.00	1.17	0.47	0.70
32	89260.00	83500.00	1.32	1.59	-0.27
33	88200.00	83200.00	1.35	0.67	0.68
34	88060.42	83544.95	0.60	0.49	0.11
35	88340.00	85640.00	0.11	-0.03	0.14
36	103760.00	102770.00	-0.06	1.11	-1.17
37	88482.45	87028.82	-1.02	-0.35	-0.67
38	85280.00	85820.00	-0.97	-0.73	-0.23
39	86841.53	89687.49	-1.04	-0.98	-0.06
40	87280.00	87440.00	-0.52	-0.73	0.21
41	88320.00	88120.00	0.29	-0.67	0.95
42	89690.00	89350.00	-1.73	-1.04	-0.69

43	88297.38	92014.17	-0.34	-0.85	0.52
44	91340.00	90670.00	-1.96	-1.10	-0.86
45	88730.00	92930.00	-0.64	-0.92	0.28
46	89610.00	92970.00	0.19	-0.72	0.91
47	90946.43	94186.04	-0.67	0.04	-0.71
48	90660.00	92790.00	0.36	-0.49	0.85
49	92324.77	92344.02	0.62	-0.02	0.64
50	93310.00	92860.00	0.36	0.44	-0.08
51	94280.00	94370.00	0.17	0.84	-0.67
52	97995.17	96778.24	0.38	1.64	-1.26
53	95000.00	96630.00	0.21	0.76	-0.55
54	97637.86	97899.93	1.26	1.52	-0.26
55	96190.00	97990.00	1.22	1.00	0.22
56	96419.12	98395.14	1.26	1.17	0.08
57	94910.00	101910.00	0.49	0.13	0.35
58	96110.90	102708.42	1.07	0.45	0.62
59	102176.22	108801.30	0.02	1.07	-1.05
60	101227.38	107329.87	-0.64	0.30	-0.94
61	100969.37	106688.94	-0.61	-0.19	-0.42
62	100920.00	106290.00	-1.19	-0.50	-0.69
63	99733.65	105434.14	-0.90	-0.38	-0.52
64	103100.00	107070.00	-1.01	0.54	-1.55
65	96770.00	101060.00	0.67	1.10	-0.44
66	103126.43	105397.48	-0.86	-0.05	-0.81
67	104930.00	104930.00	-0.67	0.46	-1.12
68	102030.00	101780.00	-0.69	0.83	-1.53

Table A.3 - Measured and simulated heads (h), in terms of m a.m.s.l., for 1990

Well_ID (2000)	X	Y	Real h (m a.m.s.l)	Simulated h (m a.m.s.l)	Residual (m)
1	77173.71	82195.70	-1.88	-2.04	0.16
2	82745.71	87886.31	-0.63	-0.38	-0.25
3	99213.48	107172.63	0.00	-0.79	0.79
4	78969.83	83288.13	0.34	-1.45	1.79
5	102445.26	109237.86	0.04	0.69	-0.65
6	104766.66	102033.63	0.38	0.64	-0.26
7	103383.01	101465.33	0.40	0.30	0.10
8	101080.56	99494.96	1.08	2.81	-1.73
9	83518.19	87652.79	0.22	-0.69	0.91
10	84962.34	89949.13	-0.40	-0.55	0.15
11	100282.65	108133.93	-0.24	-0.49	0.25
12	107738.43	105615.98	1.92	0.18	1.74
13	91345.75	96963.22	0.58	0.28	0.30
14	92377.00	98909.00	0.23	0.13	0.10

15	91190.00	96150.00	0.37	0.17	0.20
16	107410.00	105170.00	1.78	0.15	1.63
17	106508.92	106769.51	-0.45	-0.11	-0.34
18	78610.00	77040.00	-1.21	-3.96	2.75
19	78680.00	78390.00	-3.40	-4.87	1.47
20	80070.00	79700.00	-5.25	-4.59	-0.66
21	99113.93	106278.34	-0.66	-1.57	0.91
22	97640.00	104910.00	0.10	-0.80	0.90
23	80940.00	76960.00	-0.45	-3.04	2.59
24	81170.00	80840.00	-3.44	-3.66	0.22
25	81692.10	80903.85	-2.57	-3.45	0.88
26	82610.00	82590.00	-1.86	-2.79	0.93
27	105890.00	106620.00	0.65	-0.01	0.66
28	81110.00	79150.00	-5.25	-4.44	-0.81
29	82720.00	79910.00	-2.21	-3.10	0.89
30	82433.57	77728.60	-1.21	-2.66	1.45
31	83540.00	77840.00	0.18	-1.99	2.17
32	83298.06	78583.55	-1.12	-2.50	1.38
33	84370.00	81660.00	-0.65	-2.10	1.45
34	92029.43	96011.82	0.49	0.24	0.25
35	106500.00	105840.00	1.33	-0.39	1.72
36	85073.95	88937.00	-0.82	-0.70	-0.11
37	86900.00	81550.00	1.73	-0.49	2.22
38	89260.00	83500.00	1.66	0.81	0.85
39	88200.00	83200.00	1.30	-0.21	1.51
40	88060.42	83544.95	1.11	-0.40	1.51
41	86610.00	84010.00	0.09	-1.10	1.19
42	88340.00	85640.00	-0.13	-0.50	0.37
43	99302.50	98499.01	1.37	2.48	-1.11
44	99676.57	98945.67	0.88	2.44	-1.56
45	103760.00	102770.00	0.14	-0.70	0.84
46	88482.45	87028.82	-0.20	-0.67	0.47
47	85280.00	85820.00	-0.43	-1.53	1.10
48	87080.00	85660.00	-0.13	-1.05	0.92
49	86250.00	86210.00	-0.43	-1.32	0.89
50	86406.81	89756.95	-0.54	-0.89	0.35
51	86841.53	89687.49	-0.67	-0.95	0.28
52	87280.00	87440.00	-0.41	-1.09	0.68
53	88320.00	88120.00	-0.08	-0.81	0.73
54	89690.00	89350.00	-1.73	-0.62	-1.11
55	91340.00	90670.00	-1.44	-0.60	-0.84
56	93660.00	91960.00	1.56	0.57	0.99
57	88730.00	92930.00	-0.30	-0.89	0.59

58	89610.00	92970.00	-0.11	-0.72	0.61
59	92278.99	95657.10	1.06	0.20	0.86
60	90946.43	94186.04	0.22	-0.09	0.31
61	90660.00	92790.00	-0.07	-0.51	0.44
62	92324.77	92344.02	0.13	-0.03	0.16
63	93310.00	92860.00	0.88	0.32	0.56
64	94970.00	93540.00	1.71	0.98	0.73
65	94280.00	94370.00	1.20	0.62	0.58
66	96220.00	95430.00	1.41	1.11	0.30
67	97995.17	96778.24	1.84	2.02	-0.18
68	94060.00	95960.00	0.45	0.39	0.06
69	95000.00	96630.00	0.23	0.47	-0.24
70	94822.76	96834.94	0.66	0.36	0.30
71	97637.86	97899.93	1.33	1.36	-0.03
72	96419.12	98395.14	1.63	0.76	0.87
73	95580.00	98230.00	1.45	0.66	0.79
74	94910.00	101910.00	0.60	0.03	0.57
75	102176.22	108801.30	-0.71	0.47	-1.18
76	101227.38	107329.87	-1.81	-0.87	-0.94
77	100969.37	106688.94	-0.31	-1.81	1.50
78	99733.65	105434.14	-3.01	-2.17	-0.84
79	96770.00	101060.00	0.89	0.37	0.52
80	101590.00	104300.00	-1.19	-2.78	1.59
81	106030.00	105240.00	0.39	-0.64	1.03
82	103126.43	105397.48	-1.57	-1.95	0.38
83	104930.00	104930.00	-0.21	-0.88	0.67
84	103935.67	103952.04	-1.12	-1.29	0.17
85	102030.00	101780.00	-0.90	-1.14	0.24
86	101520.00	101060.00	-0.86	-0.29	-0.57

Table A.4 - Measured and simulated heads (h), in terms of m a.m.s.l., for 2000

Well_ID (2010)	X	Y	Real h (m a.m.s.l)	Simulated h (m a.m.s.l)	Residual (m)
1	76320.24	81452.64	77350.00	79850.00	-9.69
2	77173.71	82195.70	81501.39	86521.08	0.31
3	81501.39	86521.08	99213.48	107172.63	-0.40
4	83818.43	89076.94	100550.00	108580.00	-0.57
5	89912.07	95679.82	78690.00	79540.00	-14.27
6	93323.18	100132.62	92377.00	98909.00	-0.07
7	78969.83	83288.13	93410.77	100107.92	0.52
8	103383.01	101465.33	91190.00	96150.00	-1.12
9	87365.89	92128.64	92590.00	97660.00	-0.43
10	100282.65	108133.93	78610.00	77040.00	-7.15
11	107738.43	105615.98	78680.00	78390.00	-10.10

12	91190.00	96150.00	80070.00	79700.00	-16.69
13	78680.00	78390.00	99113.93	106278.34	-1.43
14	79535.65	77429.62	98330.00	105800.00	-1.50
15	80070.00	79700.00	97640.00	104910.00	-0.84
16	99113.93	106278.34	82610.00	82590.00	-8.00
17	98330.00	105800.00	105890.00	106620.00	-0.44
18	97640.00	104910.00	81110.00	79150.00	-13.20
19	80940.00	76960.00	82720.00	79910.00	-7.91
20	81170.00	80840.00	85073.95	88937.00	-2.12
21	82610.00	82590.00	85990.00	90850.00	-2.30
22	105890.00	106620.00	87322.57	91221.96	-2.86
23	81110.00	79150.00	88780.00	94160.00	-0.50
24	82720.00	79910.00	88340.00	85640.00	-1.11
25	82433.57	77728.60	85970.00	84740.00	-3.02
26	84370.00	81660.00	103760.00	102770.00	0.14
27	106500.00	105840.00	85280.00	85820.00	-3.12
28	84440.26	84108.89	86406.81	89756.95	-3.58
29	88686.12	93811.03	87280.00	87440.00	-2.66
30	85128.58	82468.53	91340.00	90670.00	-2.76
31	86900.00	81550.00	88730.00	92930.00	-2.49
32	89260.00	83500.00	93109.90	91929.57	-0.79
33	88200.00	83200.00	89610.00	92970.00	-2.52
34	88060.42	83544.95	91920.00	94940.00	-0.09
35	88340.00	85640.00	90660.00	92790.00	-2.33
36	103760.00	102770.00	93310.00	92860.00	-1.29
37	88482.45	87028.82	94280.00	94370.00	-0.73
38	85280.00	85820.00	96220.00	95430.00	-0.28
39	86841.53	89687.49	97740.00	96580.00	0.38
40	87280.00	87440.00	93620.00	95540.00	-0.95
41	88320.00	88120.00	94060.00	95960.00	-1.05
42	89690.00	89350.00	95000.00	96630.00	-1.19
43	88297.38	92014.17	96190.00	97990.00	-0.73
44	91340.00	90670.00	94150.00	97590.00	-1.58
45	88730.00	92930.00	95580.00	98230.00	-1.11
46	89610.00	92970.00	94910.00	101910.00	0.20
47	90946.43	94186.04	103330.00	108100.00	-2.73
48	90660.00	92790.00	100870.00	107860.00	-2.39
49	92324.77	92344.02	101227.38	107329.87	-1.83
50	93310.00	92860.00	103590.00	107120.00	-2.27
51	94280.00	94370.00	100920.00	106290.00	-4.69
52	97995.17	96778.24	99733.65	105434.14	-4.32
53	95000.00	96630.00	98980.00	105210.00	-3.36
54	97637.86	97899.93	98490.00	104400.00	-4.07

55	96190.00	97990.00	96770.00	101060.00	-1.71
56	96419.12	98395.14	102770.00	106050.00	-4.57
57	94910.00	101910.00	100650.00	103490.00	-5.23
58	96110.90	102708.42	101590.00	104300.00	-6.15
59	102176.22	108801.30	96340.00	100540.00	-1.33
60	101227.38	107329.87	106030.00	105240.00	-0.82
61	100969.37	106688.94	103126.43	105397.48	-5.23
62	100920.00	106290.00	104930.00	104930.00	-1.65
63	99733.65	105434.14	104580.00	105090.00	-1.82
64	103100.00	107070.00	103790.00	104380.00	-4.01
65	96770.00	101060.00	102030.00	101780.00	-1.91
66	103126.43	105397.48	101520.00	101060.00	-2.51
67	104930.00	104930.00	96680.00	100110.00	-1.25

Table A.5 - Measured and simulated heads (h), in terms of m a.m.s.l., for year 2010

A.3 Future Scenarios

Outputs of simulated water tables in 14 representative wells for the 40 different future scenarios (reported with acronyms in Table 6.15 and Table 6.16) at the end of the period 2011-2040 and 2041-2070 are reported in the following Table A.8 and Table A.9; in Table A.10 and Table A.11 are reported simulated normalized salt concentrations for 17 representative wells for the same 40 scenarios.

	Period	2011-2040 (1)			
	SLR	no		yes	
	Pumping Scenario	best	worst	best	worst
Climate Scenario	CC-0	p1b_CC0	p1w_CC0	p1b_SLR_CC0	p1w_SLR_CC0
	ECH_RCA (CC1)	p1b_CC1	p1w_CC1	p1b_SLR_CC1	p1w_SLR_CC1
	ECH_REM (CC2)	p1b_CC2	p1w_CC2	p1b_SLR_CC2	p1w_SLR_CC2
	ECH_RMO (CC3)	p1b_CC3	p1w_CC3	p1b_SLR_CC3	p1w_SLR_CC3
	HCH_RCA (CC4)	p1b_CC4	p1w_CC4	p1b_SLR_CC4	p1w_SLR_CC4

Table A.6 - Matrix combinations of climate scenarios involved in the study, and their acronyms (period 2011-2040)

	Period	2041-2070 (2)			
	SLR	no		yes	
	Pumping Scenario	best	worst	best	worst
Climate Scenario	CC-0	p2b_CC0	p2w_CC0	p2b_SLR_CC0	p2w_SLR_CC0
	ECH_RCA (CC1)	p2b_CC1	p2w_CC1	p2b_SLR_CC1	p2w_SLR_CC1
	ECH_REM (CC2)	p2b_CC2	p2w_CC2	p2b_SLR_CC2	p2w_SLR_CC2
	ECH_RMO (CC3)	p2b_CC3	p2w_CC3	p2b_SLR_CC3	p2w_SLR_CC3
	HCH_RCA (CC4)	p2b_CC4	p2w_CC4	p2b_SLR_CC4	p2w_SLR_CC4

Table A.7 - Matrix combinations of climate scenarios involved in the study, and their acronyms (period 2011-2040)

Model Acronym / WELL ID	p1b_CC0	p1w_CC0	p1b_S_CC0	p1w_S_CC0	p1b_CC1	p1w_CC1	p1b_S_CC1	p1w_S_CC1	p1b_CC2	p1w_CC2	p1b_S_CC2	p1w_S_CC2	p1b_CC3	p1w_CC3	p1b_S_CC3	p1w_S_CC3	p1b_CC4	p1w_CC4	p1b_S_CC4	p1w_S_CC4
1	-5.865	-30.453	-5.862	-31.622	-5.298	-29.888	-5.295	-29.885	-5.503	-30.092	-5.500	-30.090	-5.237	-29.828	-5.235	-29.825	-6.248	-30.835	-6.245	-30.832
2	-0.054	-3.921	-0.051	-3.999	0.006	-3.864	0.009	-3.861	0.010	-3.861	0.012	-3.858	0.037	-3.835	0.040	-3.832	-0.058	-3.925	-0.055	-3.922
3	-2.922	-18.901	-2.920	-19.774	-2.448	-18.429	-2.445	-18.426	-2.625	-18.605	-2.622	-18.602	-2.395	-18.376	-2.393	-18.374	-3.242	-19.220	-3.240	-19.217
4	2.180	-9.305	2.183	-9.702	2.379	-9.108	2.381	-9.105	2.388	-9.099	2.390	-9.097	2.488	-9.000	2.491	-8.997	2.156	-9.329	2.159	-9.326
5	-3.700	-23.553	-3.698	-24.644	-3.128	-22.985	-3.126	-22.982	-3.339	-23.194	-3.336	-23.191	-3.066	-22.923	-3.063	-22.920	-4.087	-23.936	-4.084	-23.934
6	-0.004	-9.527	-0.002	-10.154	0.399	-9.126	0.402	-9.124	0.254	-9.270	0.257	-9.267	0.451	-9.074	0.454	-9.072	-0.268	-9.789	-0.266	-9.786
7	-0.381	-8.098	-0.378	-8.581	-0.042	-7.762	-0.039	-7.760	-0.162	-7.881	-0.159	-7.878	0.004	-7.716	0.007	-7.714	-0.599	-8.315	-0.596	-8.312
8	-0.106	-3.249	-0.104	-3.418	0.046	-3.097	0.049	-3.095	0.013	-3.130	0.016	-3.127	0.083	-3.061	0.086	-3.058	-0.190	-3.332	-0.187	-3.329
9	1.313	-3.386	1.316	-3.571	1.497	-3.204	1.500	-3.201	1.481	-3.220	1.483	-3.217	1.557	-3.144	1.560	-3.142	1.225	-3.474	1.228	-3.471
10	1.687	-2.263	1.690	-2.419	1.841	-2.110	1.844	-2.108	1.841	-2.111	1.844	-2.108	1.901	-2.051	1.904	-2.048	1.623	-2.327	1.626	-2.324
11	1.398	-1.915	1.401	-2.045	1.515	-1.799	1.518	-1.796	1.520	-1.794	1.523	-1.791	1.566	-1.749	1.568	-1.746	1.354	-1.958	1.357	-1.955
12	-1.080	-9.136	-1.077	-9.313	-0.977	-9.039	-0.975	-9.036	-0.971	-9.032	-0.968	-9.029	-0.923	-8.987	-0.920	-8.984	-1.087	-9.143	-1.085	-9.140
13	1.460	-11.200	1.463	-11.607	1.646	-11.016	1.648	-11.013	1.655	-11.007	1.657	-11.004	1.747	-10.915	1.750	-10.912	1.438	-11.222	1.441	-11.219
14	1.112	-11.085	1.115	-11.448	1.260	-10.938	1.263	-10.935	1.272	-10.927	1.274	-10.924	1.343	-10.856	1.346	-10.853	1.095	-11.101	1.098	-11.099
mean	-0.354	-10.428	-0.352	-10.878	-0.093	-10.169	-0.090	-10.166	-0.155	-10.230	-0.152	-10.227	-0.032	-10.108	-0.029	-10.105	-0.492	-10.565	-0.489	-10.562

Table A.8 - Outputs of simulated water tables (in terms of m a.m.s.l. in 2010) for the 14 representative control wells for the 20 different future scenarios at the end of the period 2011-2040

Model Acronym / WELL ID	p2b_CC0	p2w_CC0	p2b_S_CC0	p2w_S_CC0	p2b_CC1	p2w_CC1	p2b_S_CC1	p2w_S_CC1	p2b_CC2	p2w_CC2	p2b_S_CC2	p2w_S_CC2	p2b_CC3	p2w_CC3	p2b_S_CC3	p2w_S_CC3	p2b_CC4	p2w_CC4	p2b_S_CC4	p2w_S_CC4
1	-5.068	-31.797	-5.063	-31.792	-4.753	-31.491	-4.748	-31.486	-5.152	-31.885	-5.147	-31.880	-5.372	-32.108	-5.367	-32.102	-5.233	-31.957	-5.228	-31.951
2	-0.031	-4.031	-0.025	-4.025	-0.047	-4.048	-0.041	-4.043	-0.073	-4.073	-0.067	-4.067	-0.088	-4.088	-0.082	-4.082	-0.019	-4.018	-0.013	-4.013
3	-2.380	-20.072	-2.374	-20.067	-2.115	-19.819	-2.109	-19.814	-2.461	-20.158	-2.455	-20.152	-2.637	-20.337	-2.632	-20.331	-2.520	-20.205	-2.514	-20.199
4	2.480	-9.842	2.485	-9.836	2.417	-9.905	2.423	-9.900	2.329	-9.993	2.335	-9.987	2.273	-10.049	2.279	-10.043	2.527	-9.795	2.533	-9.789
5	-2.944	-24.818	-2.938	-24.812	-2.629	-24.512	-2.623	-24.507	-3.038	-24.915	-3.032	-24.910	-3.256	-25.136	-3.251	-25.130	-3.109	-24.977	-3.103	-24.972
6	0.459	-10.306	0.464	-10.300	0.669	-10.101	0.675	-10.096	0.368	-10.399	0.373	-10.393	0.222	-10.545	0.227	-10.540	0.349	-10.412	0.354	-10.407
7	-0.025	-8.748	-0.019	-8.743	0.149	-8.576	0.155	-8.571	-0.108	-8.832	-0.102	-8.826	-0.227	-8.952	-0.222	-8.946	-0.115	-8.838	-0.110	-8.832
8	-0.022	-3.686	-0.016	-3.680	0.037	-3.635	0.043	-3.629	-0.076	-3.741	-0.070	-3.736	-0.119	-3.785	-0.113	-3.779	-0.056	-3.715	-0.051	-3.709
9	1.474	-3.697	1.480	-3.691	1.502	-3.673	1.508	-3.667	1.386	-3.786	1.392	-3.781	1.331	-3.841	1.337	-3.836	1.449	-3.720	1.455	-3.714
10	1.830	-2.544	1.835	-2.539	1.834	-2.543	1.840	-2.537	1.746	-2.629	1.751	-2.624	1.702	-2.673	1.708	-2.667	1.817	-2.556	1.822	-2.550
11	1.514	-2.175	1.519	-2.169	1.510	-2.181	1.515	-2.176	1.446	-2.244	1.451	-2.238	1.414	-2.276	1.419	-2.270	1.508	-2.180	1.514	-2.174
12	-1.056	-9.411	-1.050	-9.405	-1.082	-9.441	-1.076	-9.435	-1.126	-9.483	-1.121	-9.477	-1.151	-9.508	-1.145	-9.503	-1.035	-9.390	-1.029	-9.384
13	1.770	-11.745	1.776	-11.739	1.712	-11.804	1.718	-11.798	1.629	-11.886	1.635	-11.880	1.578	-11.938	1.583	-11.932	1.814	-11.701	1.820	-11.696
14	1.396	-11.591	1.402	-11.585	1.350	-11.638	1.355	-11.632	1.282	-11.705	1.287	-11.699	1.241	-11.745	1.247	-11.740	1.427	-11.560	1.433	-11.554
mean	-0.043	-11.033	-0.038	-11.027	0.040	-10.955	0.045	-10.949	-0.132	-11.124	-0.126	-11.118	-0.221	-11.213	-0.215	-11.207	-0.085	-11.073	-0.080	-11.067

Table A.9 - Outputs of simulated water tables (in terms of m a.m.s.l. in 2010) for the 14 representative control wells for the 20 different future scenarios at the end of the period 2041-2070

Model Acronym / WELL ID	p1b_CC0	p1w_CC0	p1b_S_CC0	p1w_S_CC0	p1b_CC1	p1w_CC1	p1b_S_CC1	p1w_S_CC1	p1b_CC2	p1w_CC2	p1b_S_CC2	p1w_S_CC2	p1b_CC3	p1w_CC3	p1b_S_CC3	p1w_S_CC3	p1b_CC4	p1w_CC4	p1b_S_CC4	p1w_S_CC4
1	0.7644	0.9999	0.7644	0.9999	0.7397	0.9999	0.7398	0.9999	0.7489	0.9999	0.7489	0.9999	0.7370	0.9999	0.6870	0.9998	0.7802	0.9999	0.7802	0.8455
2	0.1285	0.8347	0.1285	0.8347	0.1138	0.8177	0.1138	0.8177	0.1191	0.8242	0.1191	0.8242	0.1121	0.8156	0.0877	0.7808	0.1390	0.8455	0.1390	0.9236
3	0.3567	0.9177	0.3568	0.9177	0.3200	0.9076	0.3200	0.9076	0.3326	0.9112	0.3326	0.9112	0.3149	0.9061	0.2499	0.8840	0.3807	0.9236	0.3807	0.8286
4	0.2031	0.8164	0.2032	0.8164	0.1746	0.7962	0.1746	0.7962	0.1842	0.8032	0.1842	0.8032	0.1707	0.7931	0.1232	0.7510	0.2224	0.8286	0.2224	0.9131
5	0.5205	0.9124	0.5205	0.9124	0.5106	0.9076	0.5106	0.9076	0.5090	0.9068	0.5090	0.9068	0.5047	0.9046	0.4785	0.8900	0.5219	0.9131	0.5220	0.0076
6	0.0000	0.0075	0.0000	0.0075	0.0000	0.0069	0.0000	0.0069	0.0000	0.0068	0.0000	0.0068	0.0000	0.0066	0.0000	0.0054	0.0000	0.0076	0.0000	0.6552
7	0.2946	0.6538	0.2946	0.6539	0.2877	0.6453	0.2877	0.6453	0.2867	0.6440	0.2867	0.6440	0.2837	0.6402	0.2660	0.6167	0.2957	0.6552	0.2957	0.8685
8	0.4431	0.8678	0.4431	0.8678	0.4346	0.8625	0.4346	0.8625	0.4333	0.8616	0.4333	0.8616	0.4295	0.8591	0.4071	0.8433	0.4442	0.8685	0.4442	0.9866
9	0.6441	0.9865	0.6441	0.9865	0.6339	0.9856	0.6339	0.9856	0.6327	0.9855	0.6327	0.9855	0.6279	0.9851	0.6010	0.9824	0.6451	0.9866	0.6451	0.9963
10	0.7135	0.9963	0.7135	0.9963	0.7026	0.9961	0.7027	0.9961	0.7016	0.9960	0.7016	0.9960	0.6964	0.9959	0.6679	0.9953	0.7144	0.9963	0.7144	0.9982
11	0.7161	0.9981	0.7161	0.9981	0.7048	0.9980	0.7048	0.9980	0.7038	0.9980	0.7038	0.9980	0.6984	0.9980	0.6688	0.9976	0.7170	0.9982	0.7171	0.7854
12	0.2814	0.7847	0.2814	0.7847	0.2741	0.7784	0.2741	0.7784	0.2733	0.7776	0.2733	0.7776	0.2699	0.7746	0.2514	0.7572	0.2822	0.7854	0.2822	0.9002
13	0.3531	0.8998	0.3531	0.8998	0.3445	0.8958	0.3445	0.8958	0.3436	0.8953	0.3436	0.8953	0.3396	0.8934	0.3178	0.8821	0.3540	0.9002	0.3540	0.9984
14	0.6922	0.9984	0.6922	0.9984	0.6808	0.9983	0.6808	0.9983	0.6798	0.9983	0.6799	0.9983	0.6744	0.9983	0.6449	0.9979	0.6932	0.9984	0.6932	0.9929
15	0.5239	0.9928	0.5239	0.9928	0.5111	0.9923	0.5111	0.9923	0.5106	0.9923	0.5106	0.9923	0.5045	0.9921	0.4733	0.9906	0.5252	0.9929	0.5252	0.9595
16	0.3214	0.9592	0.3214	0.9592	0.3087	0.9562	0.3087	0.9562	0.3083	0.9561	0.3083	0.9561	0.3022	0.9546	0.2723	0.9460	0.3227	0.9595	0.3227	0.6913
17	0.0687	0.6898	0.0687	0.6898	0.0627	0.6761	0.0627	0.6761	0.0625	0.6757	0.0625	0.6757	0.0596	0.6689	0.0469	0.6339	0.0694	0.6912	0.0694	0.8344
mean	0.4133	0.8421	0.4133	0.8421	0.4003	0.8365	0.4003	0.8365	0.4018	0.8372	0.4018	0.8372	0.3956	0.8345	0.3673	0.8208	0.4181	0.8442	0.4181	0.8344

Table A.10 - Outputs of simulated normalized salt concentrations in 17 representative wells for the 20 different future scenarios at the end of the period 2011-2040

Model Acronym / WELL ID	p2b_CC0	p2w_CC0	p2b_S_CC0	p2w_S_CC0	p2b_CC1	p2w_CC1	p2b_S_CC1	p2w_S_CC1	p2b_CC2	p2w_CC2	p2b_S_CC2	p2w_S_CC2	p2b_CC3	p2w_CC3	p2b_S_CC3	p2w_S_CC3	p2b_CC4	p2w_CC4	p2b_S_CC4	p2w_S_CC4
1	0.9591	1.0000	0.9591	1.0000	0.9477	1.0000	0.9301	1.0000	0.9551	1.0000	0.9341	1.0000	0.9536	1.0000	0.9210	1.0000	0.9650	1.0000	0.9442	1.0000
2	0.2566	0.9979	0.2566	0.9979	0.2245	0.9977	0.1903	0.9973	0.2461	0.9977	0.1994	0.9974	0.2421	0.9977	0.1746	0.9969	0.2775	0.9980	0.2185	0.9975
3	0.4233	0.9959	0.4234	0.9959	0.3809	0.9950	0.3420	0.9939	0.4176	0.9957	0.3658	0.9944	0.4198	0.9956	0.3131	0.9931	0.4486	0.9963	0.3853	0.9949
4	0.2634	0.9895	0.2635	0.9895	0.2279	0.9870	0.1964	0.9842	0.2582	0.9892	0.2151	0.9859	0.2599	0.9893	0.1738	0.9816	0.2852	0.9908	0.2310	0.9872
5	0.5933	0.9934	0.5933	0.9934	0.5887	0.9931	0.5714	0.9921	0.5920	0.9932	0.5694	0.9920	0.5910	0.9933	0.5503	0.9909	0.5933	0.9934	0.5686	0.9921
6	0.0011	0.1084	0.0011	0.1084	0.0010	0.1057	0.0007	0.0984	0.0010	0.1069	0.0007	0.0974	0.0010	0.1063	0.0005	0.0917	0.0011	0.1089	0.0007	0.0985
7	0.3849	0.9077	0.3849	0.9077	0.3803	0.9059	0.3651	0.8995	0.3826	0.9074	0.3629	0.8988	0.3814	0.9071	0.3492	0.8909	0.3851	0.9078	0.3636	0.8986
8	0.5346	0.9892	0.5346	0.9893	0.5299	0.9890	0.5133	0.9878	0.5328	0.9892	0.5110	0.9877	0.5316	0.9891	0.4942	0.9862	0.5343	0.9892	0.5107	0.9876
9	0.7420	0.9997	0.7420	0.9997	0.7381	0.9998	0.7218	0.9998	0.7412	0.9998	0.7199	0.9997	0.7402	0.9999	0.7013	0.9997	0.7411	0.9998	0.7183	0.9997
10	0.8250	0.9999	0.8250	0.9999	0.8214	0.9999	0.8063	1.0000	0.8247	0.9999	0.8050	1.0000	0.8240	0.9999	0.7860	1.0000	0.8238	0.9999	0.8028	1.0000
11	0.8305	1.0000	0.8305	1.0000	0.8269	1.0000	0.8117	1.0001	0.8304	1.0000	0.8106	1.0001	0.8298	1.0000	0.7908	1.0001	0.8292	1.0000	0.8080	1.0001
12	0.4056	0.9850	0.4056	0.9850	0.4013	0.9846	0.3860	0.9831	0.4037	0.9849	0.3837	0.9829	0.4026	0.9848	0.3688	0.9808	0.4051	0.9849	0.3833	0.9828
13	0.4905	0.9966	0.4904	0.9966	0.4857	0.9967	0.4690	0.9962	0.4887	0.9965	0.4667	0.9960	0.4875	0.9965	0.4497	0.9956	0.4896	0.9965	0.4660	0.9960
14	0.8139	1.0000	0.8140	1.0000	0.8097	1.0000	0.7934	1.0000	0.8133	1.0000	0.7919	1.0000	0.8124	1.0000	0.7720	1.0000	0.8126	1.0000	0.7897	1.0000
15	0.6492	1.0001	0.6492	1.0001	0.6425	1.0000	0.6201	1.0000	0.6474	1.0000	0.6181	1.0000	0.6457	1.0000	0.5943	1.0001	0.6474	1.0001	0.6163	1.0000
16	0.4135	0.9998	0.4135	0.9998	0.4061	0.9998	0.3823	0.9997	0.4113	0.9998	0.3801	0.9997	0.4093	0.9998	0.3562	0.9997	0.4117	0.9998	0.3785	0.9997
17	0.1161	0.9862	0.1161	0.9862	0.1113	0.9854	0.0968	0.9827	0.1144	0.9859	0.0953	0.9823	0.1129	0.9856	0.0824	0.9794	0.1151	0.9861	0.0948	0.9823
mean	0.5119	0.9382	0.5119	0.9382	0.5014	0.9376	0.4821	0.9362	0.5095	0.9380	0.4841	0.9361	0.5085	0.9379	0.4634	0.9345	0.5156	0.9383	0.4871	0.9363

Table A.11 - Outputs of simulated normalized salt concentrations in 17 representative wells for the 20 different future scenarios at the end of the period 2041-2070

Appendix B – FAO Penman-Monteith equation as standard method to evaluate ET, and its application to the Gaza Strip

Evapotranspiration data are frequently needed at short notice for project planning or irrigation scheduling design. Over the last 50 years, a large of number of empirical methods have been developed worldwide to estimate evapotranspiration from different climatic variables; relationships are often subject to rigorous local calibrations and proved to have limited global validity.

The FAO Irrigation and Drainage Paper No. 24 'Crop water requirements' (Aller and Pruitt, 1991), and then the FAO Irrigation and Drainage Paper No. 56 'Crop evapotranspiration - Guidelines for computing crop water' (Aller et al., 1998), illustrate developed guidelines on evapotranspiration, presenting four methods to calculate the reference crop evapotranspiration (ET_o): the Blaney-Criddle, radiation, modified Penman-Monteith and pan evaporation methods. The modified Penman-Monteith method is considered to offer the best results for calculating reference evapotranspiration (ET_o) with minimum possible error in relation to a living grass reference crop.

This method is applied for the Gaza Strip area; due to availability of data, it is illustrated its application for the year 2005.

B.1 The Penman-Monteith equation

In 1948, Penman combined the energy balance with the mass transfer method and derived an equation to compute the evaporation from an open water surface from standard climatological records of sunshine, temperature, humidity and wind speed. This so-called combination method was further developed by many researchers and extended to cropped surfaces by introducing resistance factors. The original Penman-Monteith equation is:

$$\lambda ET = \frac{\Delta(R_n - G) + \rho_a c_p \dfrac{(e_s - \mathrm{e_a})}{r_\mathrm{a}}}{\Delta + \gamma\left(1 + \dfrac{r_s}{r_\mathrm{a}}\right)} \qquad \text{(B.1)}$$

where R_n is the net radiation; G is the soil heat flux, (e_s - e_a) represents the vapour pressure deficit of the air, ρ_a is the mean air density at constant pressure, c_p is the specific heat of the air, Δ represents the slope of the saturation vapour pressure temperature

relationship, γ is the psychrometric constant, and r_s and r_a are the (bulk) surface and aerodynamic resistances.

The aerodynamic resistance (r_a) is given by:

$$r_a = \frac{\ln\left[\frac{z_m - d}{z_{om}}\right] \ln\left[\frac{z_h - d}{z_{oh}}\right]}{k^2 u_z} \qquad \text{(B.2)}$$

Where:

r_a aerodynamic resistance [s m^{-1}],

z_m height of wind measurements [m],

z_h height of humidity measurements [m],

d zero plane displacement height [m],

z_{om} roughness length governing momentum transfer [m],

z_{oh} roughness length governing transfer of heat and vapour [m],

k von Karman's constant, 0.41 [-],

u_z wind speed at height z [m s^{-1}].

An acceptable approximation to a much more complex relation of the surface resistance of dense full cover vegetation is:

$$r_s = \frac{r_l}{LAI_{active}} \qquad \text{(B.3)}$$

Where:

r_s (bulk) surface resistance [s m^{-1}],

r_l bulk stomatal resistance of the well-illuminated leaf [s m^{-1}],

LAI_{active} active (sunlit) Leaf Area Index [m^2 (leaf area) m^{-2} (soil surface)].

From the original Penman-Monteith equation (Equation B.1) and the equations of the aerodynamic (Equation B.2) and surface resistance (Equation B.3), the FAO Penman-Monteith method to estimate ET_o can be derived as:

$$ET_o = \frac{0.408\Delta(R_n - G) + \gamma \frac{900}{T + 273} u_2 (e_s - e_a)}{\Delta + \gamma(1 + 0.34u_2)} \qquad \text{(B.4)}$$

Where:

ET_o reference evapotranspiration [mm day^{-1}];

R_n net radiation at the crop surface [MJ m^{-2} day^{-1}];

G soil heat flux density [MJ m^{-2} day^{-1}];

γ psychrometric constant [kPa $°C^{-1}$];

T mean daily air temperature at 2 m height [°C];

U_2 wind speed at 2 m height [m s^{-1}];

e_s saturation vapour pressure [kPa];

e_a actual vapour pressure [kPa];

$e_s - e_a$ saturation vapour pressure deficit [kPa];

Δ slope vapour pressure curve [kPa $°C^{-1}$].

The FAO Penman-Monteith equation requires air temperature, solar radiation, air humidity and wind speed data for daily, weekly, ten-day or monthly calculations. The computation of all data required for the calculation of the reference evapotranspiration is given in the following.

B.1.1 Net radiation at the crop surface (R_n)

The net radiation, R_n, is the difference between incoming and outgoing radiation of both short and long wavelengths, i.e. the incoming net shortwave (R_{ns}) and the net outgoing longwave (R_{nl}) radiation. The net radiation at the crop surface (R_n) is given by the equation:

$$R_n = R_{ns} - R_{nl} \qquad \text{(B.5)}$$

where (R_{ns}) is the net solar or shortwave radiation [MJ m^{-2} day^{-1}] and R_{nl} is the net outgoing longwave radiation [MJ m^{-2} day^{-1}].

B.1.1.1 The net solar or shortwave radiation (R_{ns})

A considerable amount of solar radiation reaching the earth's surface is reflected. The fraction, α, of the solar radiation reflected by the surface is known as the albedo. The albedo may be as large as 0.95 for freshly fallen snow and as small as 0.05 for a wet bare soil. A green vegetation cover has an albedo of about 0.20-0.25. For the green grass reference crop, α is assumed to have a value of 0.23.

The net solar radiation, R_{ns}, is the fraction of the solar radiation R_s that is not reflected from the surface, and it is given by:

$$R_{ns} = (1 - \alpha)R_s = 0.77R_s \qquad \text{(B.6)}$$

Where:

α albedo or canopy reflection coefficient, which is 0.23 for the hypothetical grass reference crop [dimensionless];

R_s the incoming solar radiation [MJ m^{-2} day^{-1}],

If the solar radiation, R_s, is not measured, it can be calculated with the Angstrom formula which relates solar radiation to extraterrestrial radiation and relative sunshine duration:

$$R_s = \left(a_s + b_b \frac{n}{N}\right)R_a \qquad \text{(B.7)}$$

where

n actual duration of sunshine [hour];

N maximum possible duration of sunshine or daylight hours [hour], depends on the position of the sun and is hence a function of latitude and date;

n/N relative sunshine duration [-];

R_a extraterrestrial radiation [MJ m^{-2} day^{-1}], which is a function of latitude, date and time of day;

a_s+b_s fraction of extraterrestrial radiation reaching the earth on clear days (n = N); the values a_s=0.25 and b_s=0.50 are recommended if no actual solar radiation data are available and no calibration has been carried out.

B.1.1.2 The net ongoing longwave radiation (R_{nl})

The solar radiation absorbed by the earth is converted to heat energy. By several processes, including emission of radiation, the earth loses this energy. The earth, which is at a much lower temperature than the sun, emits radiative energy with wavelengths longer than those from the sun. Therefore, the terrestrial radiation is referred to as longwave radiation. The difference between outgoing and incoming longwave radiation is called the net longwave radiation, R_{nl}. As the outgoing longwave radiation is almost always greater than the incoming longwave radiation, R_{nl} represents an energy loss.

The net outgoing longwave radiation (R_{nl}), is based on the Stefan-Boltzmann law and it is given by:

$$R_{nl} = \sigma\left[\frac{T^4_{max,K} + T^4_{min,K}}{2}\right](0.34 - 0.14\sqrt{e_a})\left(1.35\frac{R_s}{R_{so}} - 0.35\right) \qquad \text{(B.8)}$$

Where:

σ: Stefan-Boltzmann constant [4.903×10^{-9} MJ K^{-4} m^{-2} day^{-1}];

$T_{max,K}$: maximum absolute temperature during the 24-hour period [K = °C + 273.16];

$T_{min\,K}$: minimum absolute temperature during the 24-hour period [K = °C + 273.16];

e_a : actual vapour pressure [kPa];

R_s/R_{so} : relative shortwave radiation (limited to ≤ 1.0);

R_s :measured or calculated solar radiation [MJ m^{-2} day^{-1}];

R_{so} :calculated clear-sky radiation [MJ m^{-2} day^{-1}].

The clear-sky radiation (R_{so}) is given by:

$$R_{so} = (0.75 + 2\cdot10^{-5}z)R_a \qquad \text{(B.9)}$$

where

z station elevation above sea level [m];

R_a extraterrestrial radiation [MJ m^{-2} day^{-1}].

B.1.2 Soil heat flux density

Complex models are available to describe soil heat flux. Because soil heat flux is small compared to R_n, particularly when the surface is covered by vegetation and calculation time steps are 24 hours or longer, a simple calculation procedure is presented here for long time steps, based on the idea that the soil temperature follows air temperature:

$$G = c_s\frac{T_i - T_{i-1}}{\Delta t}\Delta z \qquad \text{(B.10)}$$

where

G soil heat flux [MJ m^{-2} day^{-1}];

c_s soil heat capacity [MJ m^{-3} $°C^{-1}$];

T_i air temperature at time i [°C];

T_{i-1} air temperature at time i-1 [°C];

Δt length of time interval [day];

Δz effective soil depth [m].

As the soil temperature lags air temperature, the average temperature for a period should be considered when assessing me daily soil heat flux, i.e., Δ t should exceed one day. The depth of penetration of the temperature wave is determined by the length of the time interval. The effective soil depth, Δz, is only 0.10-0.20 m for a time interval of one or a few days but might be 2 m or more for monthly periods.

When assuming a constant soil heat capacity (c_s) of 2.1 MJ m^{-3} $°C^{-1}$ and an appropriate soil depth, it is possible to derive G for monthly periods:

$$G_{month,i} = 0.07\left(T_{month,i+1} - T_{month,i-1}\right) \qquad \text{(B.11)}$$

or, if $T_{month,i+1}$ is unknown:

$$G_{month,i} = 0.14\left(T_{month,i} - T_{month,i-1}\right) \qquad \text{(B.12)}$$

where

$T_{month,i}$ mean air temperature of month i [°C];

$T_{month,i-1}$ mean air temperature of previous month [°C];

$T_{month,i+1}$ mean air temperature of next month [°C].

B.1.3 Psychrometric constant

The psychrometric constant, γ, is given by:

$$\gamma = \frac{c_p P}{\varepsilon \lambda} = 0.655 \cdot 10^{-3} P \qquad \text{(B.13)}$$

where

γ psychrometric constant [kPa $°C^{-1}$],

P atmospheric pressure [kPa];

λ latent heat of vaporization, 2.45 [MJ kg^{-1}] taken in the simplification of the FAO Penman-Monteith equation, being the latent heat for an air temperature of about 20°C;

c_p specific heat at constant pressure, 1.013×10^{-3} [MJ kg^{-1} $°C^{-1}$] taken for average atmospheric conditions;

ε ratio molecular weight of water vapour/dry air = 0.622.

The atmospheric pressure, P, is the pressure exerted by the weight of the earth's atmosphere. A simplification of the ideal gas law, assuming 20°C for a standard atmosphere, can be employed to calculate P:

$$P = 101.3 \cdot \left(\frac{293 - 0.0065z}{293} \right)^{5.26} \qquad \text{(B.14)}$$

where

z elevation above sea level [m].

B.1.4 Temperature

The daily maximum air temperature (T_{max}) and daily minimum air temperature (T_{min}) are, respectively, the maximum and minimum air temperature observed during the 24-hour period, beginning at midnight. The mean daily air temperature (T_{mean}) is only employed in the FAO Penman-Monteith equation to calculate the slope of the saturation vapour pressure curves (γ) and the impact of mean air density (P_a) as the effect of temperature variations on the value of the climatic parameter is small in these cases. For standardization, T_{mean} for 24-hour periods is defined as the mean of the daily maximum (T_{max}) and minimum temperatures (T_{min}) rather than as the average of hourly temperature measurements:

$$T_{mean} = \frac{T_{max} - T_{min}}{2} \qquad \text{(B.15)}$$

In some calculation procedures, temperature is required in Kelvin degrees (°K), which can be obtained by adding 273.16 to the temperature expressed in degrees Celsius (°C).

B.1.5 Wind speed

Wind speeds measured at different heights above the soil surface are different. Surface friction tends to slow down wind passing over it. Wind speed is slowest at the surface and increases with height; for the calculation of evapotranspiration, wind speed measured at 2 m above the surface is required. To adjust wind speed data obtained from instruments placed at elevations other than the standard height of 2m, a logarithmic wind speed profile may be used for measurements above a short grassed surface:

$$u_2 = u_z \frac{4.87}{\ln(67.8z - 5.42)} \qquad \text{(B.16)}$$

where

u_2 wind speed at 2 m above ground surface [m s^{-1}];

u_z measured wind speed at z m above ground surface [m s^{-1}];

z height of measurement above ground surface [m].

B.1.6 Vapour pressure and slope of saturation vapour

As saturation vapour pressure is related to air temperature, it can be calculated from the air temperature. The relationship is expressed by:

$$e^0(T) = 0.6108 \exp\left[\frac{17.27T}{T + 237.3}\right] \qquad \text{(B.17)}$$

where

$e^0(T)$ saturation vapour pressure at the air temperature T [kPa];

T air temperature [°C].

Due to the non-linearity of the above equation, the mean saturation vapour pressure (e_s) for a day, week, decade or month should be computed as the mean between the saturation vapour pressure at the mean daily maximum and minimum air temperatures for that period:

$$e_s = \frac{e^0(T_{max}) + e^0(T_{min})}{2} \qquad \text{(B.18)}$$

It is not possible to directly measure the actual vapour pressure (e_a). The vapour pressure is commonly derived from relative humidity or dewpoint temperature. Depending on the availability of the humidity data, different equations should be used; in terms of RH_{max} and RH_{min}, it is given by:

$$e_a = \frac{e^0(T_{min})\frac{RH_{max}}{100} + e^0(T_{max})\frac{RH_{min}}{100}}{2} \qquad \text{(B.19)}$$

where

e_a actual vapour pressure [kPa];

$e^0(T_{min})$ saturation vapour pressure at daily minimum temperature [kPa];

$e^0(T_{max})$ saturation vapour pressure at daily maximum temperature [kPa];

RH_{max} maximum relative humidity [%];

RH_{min} minimum relative humidity [%].

In the absence of RH_{max} and RH_{min}, another equation can be used to estimate e_a:

$$e_a = \frac{RH_{mean}}{100}\left[\frac{e^0(T_{max})+e^0(T_{min})}{2}\right] \qquad \text{(B.20)}$$

where RH_{mean} is the mean relative humidity, defined as the average between RH_{max} and RH_{min}.

For the calculation of evapotranspiration, the slope of the relationship between saturation vapour pressure and temperature, Δ, is required. The slope of the curve (saturation vapour pressure as a function of temperature) at a given temperature is given by:

$$\Delta = \frac{4098 \cdot \left[0.6108\exp\left(\frac{17.27T}{T+237.3}\right)\right]}{(T+273.2)^2} \qquad \text{(B.21)}$$

where

Δ slope of saturation vapour pressure curve at air temperature T [kPa °C^{-1}];

T air temperature [°C].

In the FAO Penman-Monteith equation, where Δ occurs in the numerator and denominator, the slope of the vapour pressure curve is calculated using mean air temperature.

B.2 Calculation of ET_o for the Gaza Strip – year 2005

Reference evapotranspiration rates for the Gaza Strip are assessed within Penman-Monteith method as described in the above paragraph. In order to illustrate a mean yearly ET_0 pattern, and depending on data availability (Appendix C), it is chosen to illustrate the representative year 2005. The monthly values of all of the above parameters for Gaza Strip are shown in Table B.1.

Parameter \ Month	JAN 2005	FEB 2005	MAR 2005	APR 2005	MAY 2005	JUN 2005	JUL 2005	AUG 2005	SEP 2005	OCT 2005	NOV 2005	DEC 2005
Δ	0.11	0.11	0.12	0.14	0.15	0.18	0.20	0.21	0.20	0.17	0.13	0.12
R_n	4.18	6.29	9.23	11.37	15.07	15.43	16.75	15.19	12.29	9.20	5.12	3.60
R_{ns}	8.16	10.61	13.98	15.46	19.49	19.07	20.64	18.78	16.52	13.64	9.10	6.63
R_{nl}	3.98	4.32	4.75	4.09	4.41	3.64	3.90	3.59	4.23	4.44	3.99	3.03
R_s	10.60	13.78	18.16	20.08	25.31	24.77	26.81	24.39	21.46	17.71	11.82	8.61
R_{so}	15.38	18.99	23.30	27.50	30.02	30.99	30.50	28.48	24.84	20.34	16.25	14.37
R_s/R_{so}	0.69	0.73	0.78	0.73	0.84	0.80	0.88	0.86	0.86	0.87	0.73	0.60
n	5.45	6.45	7.90	7.59	10.37	9.79	11.35	10.33	9.72	9.08	6.16	3.99
N	10.20	10.95	11.80	12.75	13.55	14.00	13.85	13.15	12.20	11.25	10.40	10.00
R_a	20.50	25.30	31.05	36.65	40.00	41.30	40.65	37.95	33.10	27.10	21.65	19.15
$T_{max-abs}$	28.67	27.53	33.81	33.08	27.34	30.07	31.01	30.98	30.68	27.97	28.43	25.96
$T_{min-abs}$	8.32	7.76	10.45	11.43	14.01	19.68	22.11	23.22	21.07	15.91	12.44	9.62
T_{max}	18.66	17.62	19.88	22.58	23.51	26.16	28.70	29.40	28.83	25.64	22.11	19.59
T_{min}	11.14	11.34	13.28	15.72	18.13	21.72	23.78	25.11	23.24	19.96	15.17	13.60
T_{avg}	14.90	14.48	16.58	19.15	20.82	23.94	26.24	27.26	26.03	22.80	18.64	16.60
e_a	1.12	1.08	1.31	1.46	1.79	2.27	2.52	2.66	2.21	1.96	1.43	1.19
$e^0(T_{max})$	2.15	2.02	2.32	2.74	2.90	3.39	3.94	4.10	3.97	3.29	2.66	2.28
$e^0(T_{min})$	1.33	1.34	1.53	1.79	2.08	2.60	2.94	3.19	2.85	2.33	1.72	1.56
$e^0(T)$	1.69	1.65	1.89	2.22	2.46	2.97	3.41	3.62	3.37	2.78	2.15	1.89
e_s	1.74	1.68	1.92	2.26	2.49	3.00	3.44	3.64	3.41	2.81	2.19	1.92
RH_{mean}	64.16	64.36	68.15	64.45	71.90	75.81	73.39	73.08	64.77	69.56	65.41	62.01
G	-0.03	0.12	0.33	0.30	0.33	0.38	0.23	-0.01	-0.31	-0.52	-0.43	-0.29
γ	0.07	0.07	0.07	0.07	0.07	0.07	0.07	0.07	0.07	0.07	0.07	0.07
P	101.06	101.06	101.06	101.06	101.06	101.06	101.06	101.06	101.06	101.06	101.06	101.06
u (km/h)	10.84	10.86	10.16	8.70	9.81	9.57	8.90	9.48	9.70	10.94	8.90	8.56
u_2	2.03	2.03	1.90	1.63	1.83	1.79	1.67	1.77	1.81	2.05	1.66	1.60
ET_0 (mm/day)	2.03	2.38	2.94	3.69	4.51	4.75	5.43	5.21	4.76	3.63	2.36	1.94
ET_0 (mm/month)	61.00	71.39	88.35	110.73	135.23	142.38	162.89	156.30	142.74	108.95	70.88	58.16

Table B.1 - Calculation of reference evapotranspiration (ET_0) from meteorological data

The annual ET_0 is equal to 1309 mm/y. The monthly values of ET_0 are compared to the relative monthly rainfall rates measured in the Rainfall Stations in the area, in Table B.2 and Figure B.1.

		Month/yy	01/05	02/05	03/05	04/05	05/05	06/05	07/05	08/05	09/05	10/05	11/05	12/05
		ET_0	61	71.39	88.35	110.73	135.23	142.38	162.89	156.3	142.74	108.95	70.88	58.16
Measured precipitation	**North**	**Beit Hanon**	88.0	50.0	29.5	0.0	0.0	0.0	0.0	0.0	0.0	23.5	73.0	72.6
		Beit Lahia	90.0	57.0	30.0	0.0	0.0	0.0	0.0	0.0	0.0	21.0	52.5	68.1
		Jabalia	79.5	56.0	30.0	0.0	0.0	0.0	0.0	0.0	0.0	23.5	39.8	76.5
	Gaza	**Shati**	64.0	46.5	31.0	0.0	0.0	0.0	0.0	0.0	0.0	16.5	42.4	62.5
		Gaza City	48.6	47.3	39.9	0.0	0.0	0.0	0.0	0.0	0.0	7.3	60.2	57.9
		Tuffah	54.5	50.1	41.8	0.4	0.0	0.0	0.0	0.0	0.0	5.6	80.6	61.0
		Gaza South	67.4	60.9	28.2	0.0	0.0	0.0	0.0	0.0	0.0	5.7	63.4	61.8
	Middle	**Nussirat**	93.5	78.5	37.0	0.0	0.0	0.0	0.0	0.0	0.0	5.0	69.0	82.0
		Dair Balah	87.0	62.5	38.5	0.0	0.0	0.0	0.0	0.0	0.0	2.0	52.5	75.0
	Khan Younis	**Khan Younis**	54.5	55.5	55.0	3.5	0.0	0.0	0.0	0.0	0.0	0.0	59.0	62.5
		Khuzaa	62.0	49.0	39.0	2.0	0.0	0.0	0.0	0.0	0.0	0.0	44.5	43.5
	Rafah	**Rafah**	44.0	67.2	33.0	2.0	0.0	0.0	0.0	0.0	0.0	0.0	33.0	34.0

Table B.2 – Comparison between measured Rainfall and ET_0 – in mm

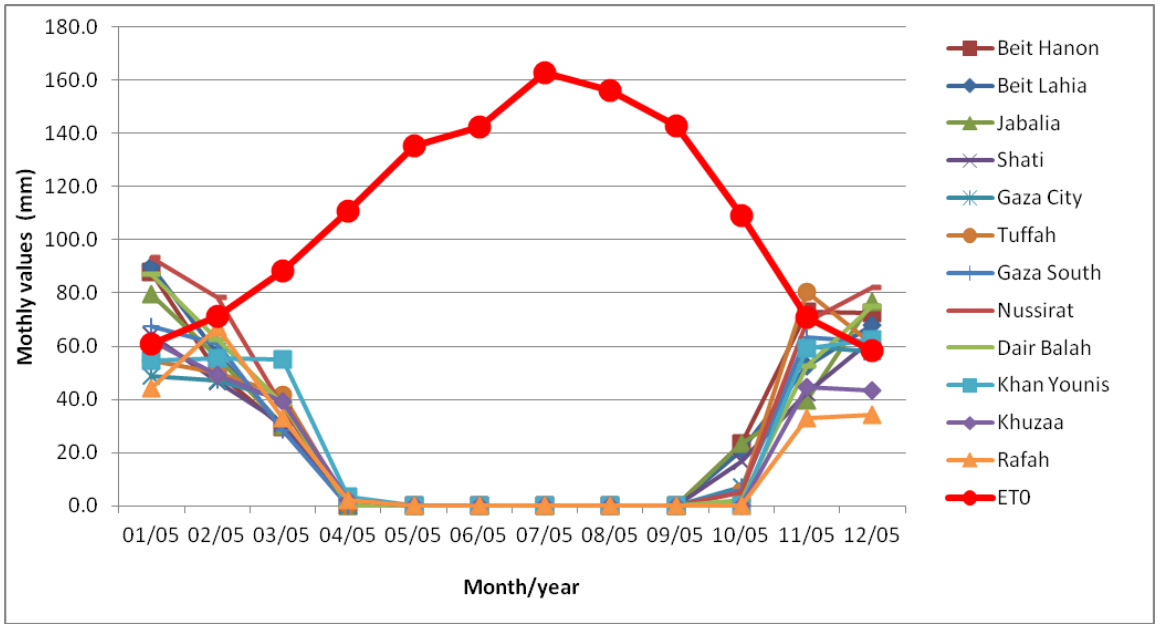

Figure B.1 - Graphical comparison between monthly measured rainfall and ET_0

It is evident how the ET_0 is much more high in dry-season months (May-September) than in wet-season months (October-April). ET values are finally assessed day by day, considered equal to ET_0 during rainy days and equal to 0 in dry days.

Appendix C – Data used in the study

A large amount of data have been provided by the Islamic University of Gaza (IUG) on geology and geomorphology, hydrology, hydrogeology, estimates of natural recharge and available water resources as a result of groundwater exploitation, historical data of hydraulic heads and salt concentrations.

In this Appendix, it is briefly illustrated the only dataset used for this study on the Gaza Strip coastal area.

C.1 Geological and soil type data

The provided geological dataset is made by:

- Images of cross sections, relative to several field campaigns until 2011;
- Spreadsheets of bottoms and tops of each geological stratum, as interpreted from available cross sections data, gridded with a resolution of about 50-100 m;
- Shape files of 1996 soil map, with indication of soil types and features (e.g. texture).

C.2 Hydrogeological data

The used hydrogeological dataset is made by:

- Shape files of 23 punctual hydraulic conductivity values;
- Spreadsheets and publications within indication of several hydraulic parameters of the aquifer (e.g. transmissivity, storativity, …);
- Water levels in terms of mean yearly values for the year 1935, for the period 1970-1998 and for the period 1999-2010;
- Water quality data in terms of mean yearly values of Chlorides (in mg/l) for the year 1935 and for the period 1970-2010;
- Estimations of well pumpings from 1935 to 1998, on the basis of several studies made by IUG on this issue;
- Punctual well productions in terms of mean yearly pumping values for agricultural wells (period 1998-2010), for municipal wells (period 1998- 2010,

with some missing years data), and for some illegal wells; wells depths for most of punctual location.

C.3 Meteorological data

The used meteorological dataset is made by:

- Estimated evaporation (period 1991-2006) for the only Gaza Station;
- Rainfall daily readings from 1973 to 2011 for 12 Rainfall Station throughout the Gaza Strip area, with missing data for 4 Rainfall Stations, and several statistics on monthly, yearly, seasonally averages;
- Relative humidity from 1995 to 2006 and 2009, in terms of monthly maximum, minimum, and average values for the only Gaza Station;
- Solar radiation for the only Gaza Station, in terms of daily values for the period 2002-2006 and in terms of monthly averages for year 2009;
- Sunshine for the only Gaza Station, in terms of hours per day for the period 1990-2006, and in terms of mean monthly hours per day for year 2009;
- Temperatures for the only Gaza Station, in terms of daily minimum and maximum for the period 1999-2006, in terms of monthly averages of minimum, maximum, average and absolute minimum and absolute maximum for the period 1995-2006 and for 2009;
- Wind for the only Gaza Station, in terms of monthly mean values for the period 1999-2005.

Bibliography

Abarca Cameo E. (2006) Seawater intrusion in complex geological environments. *Ph.D. Thesis, Technical University of Catalonia (UPC), Barcellona, Spain.*

Abarca E., Carrera J., Sanchez-Vila X., Dentz M. (2007) Anisotropic dispersive Henry problem. *Adv Water Res* 30 (2007) 913–926.

Abd-Elhamid H. F. and Javadi A. A. (2010). A Simulation-Optimization Model to Study the Control of Seawater Intrusion in Coastal Aquifers Using ADR Methodology. *Proceeding of 21st SWIM, June 21-26, 2010, Azores, Portogal.*

Adams B., Foster S.S.D. (1992) Land-surface zoning for groundwater protection. *J. Inst. Water Environ Managmt*, 6, 312-320.

Allen R.G., Pereira L.S., Raes D. and Smith M. (1998) Crop evapotranspiration-guidelines for computing crop water requirements. FAO Irrigation and Drainage Paper No. 56, FAO, Rome, Italy. http//www.fao.org/docrep/X0490E/x0490e00.htm.

Allen R.G., Pruitt W.O. (1991) FAO-24 reference evapotranspiration factors. J. Irrigation Drainage Eng., 5: 758-773.

Aller L., Bennet T., Lehr J.H., Petty, R.J. (1987) DRASTIC: A standardised system for evaluating groundwater pollution potential using hydrologic settings. *US EPA Report, 600/2-87/035,* Robert S. Kerr Environmental Research Laboratory, Ada, OK.

Alnahhal S. (2009) Recharge Assessment and Modeling Issues to the north of Wadi Gaza coastal Aquifer. *Thesis.* Islamic University of Gaza, Palestine.

Alnahhal S., Afifi S., Qahman K., Dentoni M., Lecca G. (2010). A Simulation/Optimization Approach to Manage Groundwater Resources in the Gaza Aquifer (Palestine). *In: Proceedings of the XVIII Conference on Computational Methods in Water Resources (CMWR 2010)*. Barcelona, June 21-24, 2010, Barcelona, J. Carrera (Ed).

Anandhi A. A., Frei D. C., Pierson E. M., Schneiderman M. S., Zion D., Lounsbury, Matonse A. H. (2011) Examination of change factor methodologies for climate change impact assessment, *Water Resour Res*, 47, W03501, doi:10.1029/2010WR009104.

Andreo B., Goldscheider N., Vadillo I., Vías J. M., Neukum C., Sinreich M., Jiménez P., Brechenmacher J., Carrasco F., Hötzl H., Perles M. J., Zwahlen F. (2006) Karst groundwater protection: First application of a Pan-European Approach to vulnerability, hazard and risk mapping in the Sierra de Líbar (Southern Spain). *Sci Total Environ* 357 pp.54– 73. doi:10.1016/j.scitotenv.2005.05.019.

Antonellini M., Mollema P., Giambastiani B., Bishop K., Caruso L., Minchio A., Pellegrini L., Sabia M., Ulazzi E., Gabbianelli G. (2008) Salt water intrusion in the coastal aquifer of the southern Po Plain, Italy. *Hydrogeol J* 16, pp.1541–1556, DOI 10.1007/s10040-008-0319-9.

Arnell N. W. (1999) "Climate change and global water resources", *Glob Environ Change*, Vol. 9, Supplement 1, pp. S31-S49, DOI: 10.1016/S0959-3780(99)00017-5

Arnold G., Allen P.M., Bernhardt G. (1993). A comprehensive surface-groundwater flow model. *J Hydrol*, 142 (1993), pp. 47–69.

Assaf S.A. (2001) Existing and the future planned desalination facilities in the Gaza Strip of Palestine and their socio-economic and environmental impact. *Desalination*, Volume 138, Issues 1–3, 20 September 2001, Pages 17-28, ISSN 0011-9164, 10.1016/S0011-9164(01)00240-5.

Ataie-Ashtiani B., Ketabchi H. (2011) Elitist continuous ant colony optimization algorithm for optimal management of coastal aquifers. *Water Resour Manage* 2011; 25:165–90.

Ataie-Ashtiani B., Volker R.E., Lockington D.A. (1999) Tidal effects on sea water intrusion in unconfined aquifers. *J Hydrol* 1999; 216:17–31.

Ataie-Ashtiani B., Volker R.E., Lockington D.A. (2001) Tidal effects on groundwater dynamics in unconfined aquifers. *Hydrol Process* 2001;15:655–69.

Austin, J., Zhang, L., Jones, R. N., Durack, P., Dawes, W., Hairsine, P. (2009), Climate change impact on water and salt balances: an assessment of the impact of climate change on catchment salt and water balances in the Murray-Darling Basin, Australia. *Climatic Change*, Vol. 100, pp. 607–631, DOI 10.1007/s10584-009-9714-z.

Badon-Ghyben W. (1888) Nota in verband met de voorgenomen putboring nabij Amsterdam" (Notes on the probable results of well drilling near Amsterdam). Tijdcschrift van het Koninklijk Instituut van Ingenieurs, Tha Hague, 1888/9, 8-22, 1888.

Ball D., Campbell E. (2006) Saline intrusion: a screening tool for the assessment of risk to coastal aquifers in Scotland. *British Geological Survey Internal Report*, CR/06/025N. 19pp.

Barlow P. (2005) Use of Simulation-Optimization Modeling to Assess Regional Ground-Water Systems. *U.S. Department of the Interior-U.S. Geological Survey*, Fact Sheet 2005–3095, August 2005.

Bhattacharjya R.K., Datta B. (2005) Optimal Management of Coastal Aquifers Using Linked Simulation Optimization Approach. *Water Resour Manage*, Vol. 19, Number 3, 295-320, DOI: 10.1007/s11269-005-3180-9.

Bear, J. 1979. Hydraulics of Groundwater. McGraw-Hill, New York, 569 pp.

Bear J., Cheng A.H.-D., Sorek S., Ouazar D., Herrera I., ed. (1999). Seawater Intrusion in Coastal Aquifers—Concepts, Methods, and Practices. Dordrecht, The Netherlands. Kluwer Academic Publishers.

Bloomfield J.P., Gaus I., Wade S.D. (2003) A method for investigating the potential impacts of climate change scenarios on annual minimum groundwater levels. *Water Environ J* 17:86–91.

Bobba A. G. (2002) Numerical modelling of salt-water intrusion due to human activities and sea-level change in the Godavari Delta, India", *Hydrol Sci J*, 47: 4, pp. S67 — S80 DOI: 10.1080/02626660209493023.

Brouyére S., Carabin G., Dassargues A. (2004) Climate change impacts on groundwater resources: modelled deficits in a chalky aquifer, Geer basin, Belgium. *Hydrogeol J* Vol. 12, no. 2, pp.123–134, DOI: 10.1007/s10040-003-0293-1.

Calvache M.L., Pulido-Bosch A. (1997) Effects of geology and human activity on the dynamics of salt-water intrusion in three coastal aquifers in southern Spain. *Environ Geol* 1997;30:215–23.

Candela L., von Igel W., Elorza F. J., Aronica G. (2009) Impact assessment of combined climate and management scenarios on groundwater resources and associated wetland (Majorca, Spain). *J Hydrol*, Vol. 376, Issues 3-4, pp.510-527, DOI: 10.1016/j.jhydrol.2009.07.057.

Carrera J., Alcolea A., Medina A., Hidalgo J., Slooten L.J. (2005) Inverse problem in hydrogeology, *Hydrogeol J* (2005) 13:206–222, DOI 10.1007/s10040-004-0404-7.

Carrera J., Hidalgo J. J., Slooten L. J., Vázquez-Suñé E. (2010) Computational and conceptual issues in the calibration of seawater intrusion models. *Hydrogeol J* (2010) 18: 131–145, DOI 10.1007/s10040-009-0524-1.

Carroll D. L. (1996) Genetic Algorithms and Optimizing Chemical Oxygen-Iodine Lasers. *Developments in Theoretical and Applied Mechanics*, Vol. XVIII, eds. H.B. Wilson, R.C. Batra, C.W. Bert, A.M.J. Davis, R.A. Schapery, D.S. Stewart, and F.F. Swinson, School of Engineering, The University of Alabama, 1996, pp.411-424.

Cau P., Lecca G., Muscas L., Barrocu G., Uras G. (2002) Seawater Intrusion in the Plain of Oristano - Sardinia, Italy. *17th Salt Water Intrusion Meeting*, Delft, The Netherlands, 6-10 May 2002.

Chachadi A. G., Lobo-Ferreira J.P. (2001) Sea water intrusion vulnerability mapping of aquifers using the GALDIT method. *In: COASTIN A Coastal Policy Research Newsletter*, Number 4, March 2001. New Delhi, TERI, pp. 7-9.

Chachadi A.G., Lobo-Ferreira J.P. (2007) Assessing aquifer vulnerability to seawater intrusion using GALDIT method: Part 2 - GALDIT Indicators Description. *Water in Celtic Countries: Quantity, Quality and Climate Variability* 310: 172–180.

Cheng A. H. –D., Halhal D., Naji A., Ouazar, D. (2000) Pumping optimization in saltwater intruded coastal aquifers, *Water Resour Res*, 36(8), 2155-2165.

Civita M., De Regibus C. (1995) Sperimentazione di alcune metodologie per la valutazione della vulnerabilità degli acquiferi. *Atti 2° Conv. Naz., "Protezione e Gestione delle Acque Sotterranee: Metodologie, Tecnologie e Obiett Nonantola* (Modena) Italy, 1995, Vol. 3, pp 63-72.

Coastal Municipalities Water Utility (CMWU) Annual Report on Water Status in the Gaza Strip 2010, March 2011.

Cooper, H.H. Jr., Kohout, F.A., Henry, H.R. and Glover, R.E., Sea Water in Coastal Aquifers, U.S. Geol. Survey Water-Supply Paper 1613-C, 1964.

Crosbie R.S., McCallum J. L., Walker G. R., Chiew F. H. S. (2010) Modelling climate-change impacts on groundwater recharge in the Murray-Darling Basin, Australia", *Hydrogeol J* Vol. 18, No. 7, pp.1639-1656, DOI: 10.1007/s10040-010-0625-x.

Custodio E. (1987) Methods to control and combat saltwater intrusion. *In: Custodio E, Bruggeman GA, editors. Studies and reports in hydrology: groundwater problems in coastal areas.* Paris, France: UNESCO; 1987. p. 396–433.

Custodio, E. (2010), "Coastal aquifers of Europe: An overview", *Hydrogeol J*, 18(1), pp.269–280, doi:10.1007/s10040-009-0496-1.

Daly D., Misstear B. D. (2002) The groundwater protection scheme in Ireland: a risk-based tool for effective land-use planning. *Proceedings of Conference 'Protecting Groundwater', Birmingham*. Environment Agency (England and Wales), 134-144.

Das A., Datta B. (1999) Development of multiobjective management models for coastal aquifers, *J Water Resour Plann Manage*, 125, 76- 87.

Das A., Datta B. (2001) Application of Optimisation Techniques in Groundwater Quantity and Quality Management, S. Adhan, Vol. 26, Part 4, pp. 293-316.

Dhar A., Datta B. (2009) Saltwater intrusion management of coastal aquifers. I: Linked simulation–optimization. *J Hydrol Eng* 2009;14:1263–72.
Diersch H.-J.G., Kolditz O. (2002) Variable-density flow and transport in porous media: approaches and challenges, *Adv Water Resour*, 25 (2002) 899–944.

Doerflinger N., Zwahlen F. (1998) Practical Guide: Groundwater Vulnerability Mapping in Karstic Regions (EPIK). 56 p., Swiss Agency for Environment, Forests and Landscape (SAEFL), Bern.

Doherty J. (2002), *PEST Model-Independent parameter estimation*, Watermark Numerical Computing, 2002.

Döll P. (2009) Vulnerability to the impact of climate change on renewable groundwater resources: a global-scale assessment. *Environmental Research Letters*, Vol. 4, No. 3, doi: 10.1088/1748-9326/4/3/035006.

Döll P., Flörke M. (2005) Global-scale estimation of diffuse groundwater recharge. *Frankfurt Hydrology Paper 03, Institute of Physical Geography*, Frankfurt University, Germany.

Dragoni W., Sukhija B. S. (2008) Climate change and groundwater: a short review. *Geological Society, London, Special Publications* 2008; Vol. 288; pp. 1-12, DOI:10.1144/SP288.1.

Duan Q., Sorooshian S. , Gupta V.K. (1992) Effective and efficient global optimization for conceptual rainfall-runoff models. *Water Resour Res*, 28 (4) (1992), pp. 1015–1031.

Eliasson A., Rinaldi F.M., Linde N. (2003) Multicriteria decision aid in supporting decisions related to groundwater protection. *Environ Manag* 2003;32(5):589– 601.

European Commission (2000), Directive 2000/60/EC of the European Parliament and of the Council establishing a framework for the Community action in the field of water policy (EU – Water Framework Directive).

Fetter C.W. (2001) Applied Hydrogeology (4th edition). Prentice Hall, 598 pp.

Freeze R.A., Cherry J.A. (1979) Groundwater. Prentice-Hall, Inc. Englewood Cliffs, NJ. 604 p.

Foster S.S.D. (1987) Fundamental Concepts in Aquifer Vulnerability, Pollution Risk and Protection Strategy. Vulnerability of soil and groundwater to pollutants ed. Proceedings and information committee for hydrological research, TNO, p.69-86.

Gambolati G., Putti M., Paniconi C. (1999) Three dimensional model of coupled density dependent flow and miscible salt transport in groundwater. in: *Seawater intrusion in coastal aquifers: Concepts, Methods, and Practices*, Kluwer Academic Publisher, Dordrecht, The Netherlands, pp. 315-362.

Gerth J., Forstner U. (2004) Long-term forecast: key to groundwater protection. *Environ Sci Pollut Res Int* 2004;11(1):49– 56.

Ghabayen S.M.S., McKee M., Kemblowski M. (2006) Ionic and isotopic ratios for identification of salinity sources and missing data in the Gaza aquifer. *J Hydrol* vol. 318 issue 1-4 March 1, 2006. p. 360-373.

Giambastiani B.M.S., Antonellini M., Oude Essink G.H.P., Stuurman R.J. (2007) Saltwater intrusion in the unconfined coastal aquifer of Ravenna (Italy): A numerical model. *J of Hydrol*, Vol. 340, Issues 1-2, 30 June 2007, pp. 91-104, ISSN 0022-1694, DOI: 10.1016/j.jhydrol.2007.04.001.

Gogu R.C., Dassargues A. (2000) Current trends and future challenges in groundwater vulnerability assessment using overlay and index methods. *Environ Geol*, Vol. 39, No. 6, pp.549–559, DOI: 10.1007/s00254005046.

Goldberg D. E. (1989) Genetic Algorithms in Search Optimization and Machine Learning. Addison Wesley. p. 41. ISBN 0201157675.

Gorelick S. M. (1983) A review of distributed parameter groundwater management modeling methods. *Water Resour Res*, 19(2), 305–319, doi:10.1029/WR019i002p00305.

Gornitz V. (1991) Global coastal hazards from future sea level rise. *Palaeogeography, Palaeoclimatology, Palaeoecology (Global Planet. Change Sect.),* Vol. 89, Issue 4, pp. 379-398, doi:10.1016/0031-0182(91)90173-O.

Haylock M.R., Hofstra N., Klein Tank A.M.G., Klok E.J., Jones P.D., New M. (2008) A European daily high-resolution gridded data set of surface temperature and precipitation for 1950–2006. *J Geophys Res*, 113, D20119, doi:10.1029/2008JD010201.

Henry H.R. (1964) Effects on dispersion on salt encroachment in coastal aquifers. *U.S. Geol. Survey Water-Supply Paper* 1613-C, C71-C84, 1964.

Herzberg A. (1901) "Die Wasserversorgung einiger Nordseebder (The water supply of parts of the North Sea coast in Germany)" Z.Gasbeleucht. Wasserversorg., 44, 815-819 and 45, 842-844, 1901.

Hill M.C. (1998) Methods and Guidelines for Effective Model Calibration. *U.S. Geological Survey Water-Resources Investigations Report 98-4005*.

Holman I.P. (2006) Climate change impacts on groundwater recharge: uncertainty, shortcomings and the way forward? *Hydrogeol J*, Vol. 14, No. 5, pp.637–647, DOI: 10.1007/s10040-005-0467-0.

Holman, I., Allen, D.M., Cuthbert, M.O. and Goderniaux, P. (2011) Towards best practice for assessing the impacts of climate change on groundwater. Hydrogeology Journal 20(1): 1-4. DOI 10.1007/s10040-011-0805-3.

Huyakorn P.S., Thomson S.D., Thompson B.M. (1984) Techniques for making finite elements competitive in modeling flow in variably saturated porous media. *Water Resour Res* 20(8), 1099-1115, 1984.

Illangasekare T., Tyler S.W., Clement T.P., Villholth K.G., Perera A.P.G.R.L., Obeysekera J., et al. (2006) Impacts of the 2004 tsunami on groundwater resources in Sri Lanka. *Water Resour Res* 2006;42:W05201.

IPCC, 2007, Climate Change 2007, the Fourth IPCC Assessment Report.

Javandel I., Tsang, C.-F. (1986) Capture-Zone Type Curves: A Tool for Aquifer Cleanup. *Ground Water*, 24: 616–625. doi: 10.1111/j.1745-6584.1986.tb03710.x.

Jyrkama M.I., Sykes J.F. (2007) The impact of climate change on spatially varying groundwater recharge in the Grand River Watershed (Ontario). *J Hydrol* 338:237–250.

Kerrou J., Lecca G., Murgia F., Renard P. (2007) Grid-enabled Simulation of the Impact of Exploitation Uncertainty on the Seawater Intrusion of the Korba Aquifer (Tunisia). *Proceedings of IST-Africa Conference, Maputo* (Mozambico), May 2007.

Kerrou J., Renard P. A numerical analysis of dimensionality and heterogeneity effects on advective dispersive seawater intrusion processes. *Hydrogeol J* 2010;18:55–72.

Kourakos G., Mantoglou A., (2011) Simulation and multi-objective management of coastal aquifers in semi-arid regions. *Water Resour Manage* 2011;25: 1063–74.

Kundzewicz Z. W. (2008) Climate change impacts on the hydrological cycle. *Ecohydrology and Hydrobiology*, Vol. 8, No. 2 – 4, pp. 195-203, DOI:10.2478/v10104-009-0015-y.

Kundzewicz Z. W., Mata L. J., Arnell N., Döll P., Kabat P., Jiménez B., Miller K., Oki T., Şen Z., Shiklomanov, I.(2007) Freshwater resources and their management. *Climate Change 2007: Impacts, Adaptation and Vulnerability.* Contribution of Working Group II to the Fourth Assessment Report of the Intergovernmental Panel on Climate Change (ed. by M. L. Parry, O. F. Canziani, J. P. Palutikof, P. J. van der Linden & C. E. Hanson), 173–210. Cambridge University Press, UK.

Kundzewicz Z. W., Mata L. J., Arnell N., Döll P., Jiménez B., Miller K., Oki T., Şen Z., Shiklomanov I. (2008) The implications of projected climate change for freshwater resources and their management. *Hydrol Sci J*, Vol.53, Issue.1, pp. 3-10, doi: 10.1623/hysj.53.1.3.

Lecca G. (2000) Implementation and testing of the CODESA-3D model for density dependent flow and transport problems in porous media. *Center for Advanced studies, Research and development (CRS4)*, Sardinia, Italy.

Lecca G. (2004) Modeling issues: the CODESA-3D code. *In: Benavente J et al (ed) Monitoring, modeling and management of coastal aquifers.* Water Research Institute, University of Granada, Spain (ISBN 84-699-7903-5).

Lecca G., Berjamy B., Paniconi C., El Hebil A. (2001) Numerical modeling of seawater intrusion in the Sahel region of the Atlantic coast of Morocco. *CyberProceedings of the First International Conference on Saltwater Intrusion and Coastal Aquifers—Monitoring, Modeling, and Management*. Essaouira, Morocco, April 23–25, 2001.

Lecca G., Cau P. (2006) Automatic calibration of a 3D groundwater model applied to the Muravera-Flumendosa coastal aquifer (SE Sardinia, Italy). *In: Binning PJ, Engesgaard PK, Dahle HK, Pinder GF, Gray WG (eds) Proceedings of the XVI international conference on computational methods in water resources.* Copenhagen, Denmark, June, 2006.

Levenberg K. (1944) A Method for the Solution of Certain Problems in Least Squares. *Quart Appl Math* 2, 164-168, 1944.

Loáiciga H. A., Valdes J. B., Vogel R., Garvey J., Schwarz H. (1996) Global warming and the hydrologic cycle. *J Hydrol*, Vol. 174, Issues 1-2, January 1996, pp. 83-127, doi: 10.1016/0022-1694(95)02753-X.

Loáiciga H. A, Pingel T. J., Garcia, E. S. (2009) *Assessment of Seawater Intrusion Potential From Sea-level Rise in Coastal Aquifers of California*. UC Berkeley: University of California Water Resources Center.

Lobo-Ferreira J.P., Chachadi A.G., Diamantino C., Henriques M.J. (2007) Assessing aquifer vulnerability to seawater intrusion using the GALDIT method: part 1 – application to the Portuguese Monte Gordo aquifer. In Proceedings of Water in Celtic Countries: Quantity, Quality and Climate Variability, IAHS Publication 310, ed. J.P. Lobo Ferreira and J.M.P. Viera, 161–171. Wallingford: International Association of Hydrological Sciences.

Mantoglou A. (2003) Pumping management of coastal aquifers using analytical models of saltwater intrusion. *Water Resour Res* 2003; 39:1335. http:// dx.doi.org/10.1029/2002WR00189.

Mantoglou A., Papantoniou M. (2008) Optimal design of pumping networks in coastal aquifers using sharp interface models, *J Hydrol*, Volume 361, Issues 1–2, 30 October 2008, Pages 52-63, ISSN 0022-1694, 10.1016/j.jhydrol.2008.07.022.

Marquardt D. (1963). An Algorithm for Least-Squares Estimation of Nonlinear Parameters. *SIAM J ApplMath* 11: pp. 431–441. doi:10.1137/0111030.

Mason M., Mimi Z. and Zeitoun M.(2009) Climate Change Adaptation Strategy for the Occupied Palestinian Territory, Final report to the UNDP/PAPP initiative: Climate Change Adaptation Strategy and Programme for Action for Palestinian Authority. (Program initiated by Environmental Quality Authority (EQA) and financed by UNDP/PAPP)

Maurer E. P., H. G. Hidalgo (2008) Utility of daily vs. monthly largescale climate data: An intercomparison of two statistical downscaling methods, *Hydrol Earth Syst Sci*, 12(2), 551–563.

McDonald M.G., Harbaugh A.W. (1988) A modular three-dimensional finite-difference ground-water flow model. *US Geological Survey Techniques of Water Resources Investigations Report* Book 6, Chapter A1, p. 528.

Melloul A., Collin, M. (2000) Sustainable groundwater management of the stressed Coastal aquifer in the Gaza region. *Hydrolo Sci-Journal-des Sciences Hydrologiques*, 45(1) February 2000.

Milnes E. (2005), Modelling Groundwater Salinisation in Irrigated Coastal Areas: from Solute Recycling Concepts to Quantitative Risk Assessment. *PhD Thesis*, University of Neuchâtel (Switzerland).

Milnes E. (2011) Process-based groundwater salinisation risk assessment methodology: Application to the Akrotiri aquifer (Southern Cyprus), *J Hydrol*, Volume 399, Issues 1–2, 8 March 2011, Pages 29-47, ISSN 0022-1694, 10.1016/j.jhydrol.2010.12.032.

Mimi Z.A., Assi A. (2009) Intrinsic vulnerability, hazard and risk mapping for karst aquifers: A case study. *J Hydrol* 364, pp.298–310, doi:10.1016/j.jhydrol.2008.11.008

Moe H., Hossain R., Fitzgerald R., Banna M., Mushtaha A., Yaqubi A. (2001), Application of a 3-dimensional coupled flow and transport model in the Gaza Strip. *In: First International Conference on Saltwater Intrusion and Coastal Aquifers - Monitoring, Modeling, and Management*, April 23-25, 2001, Essaouira, Morocco.

Morris B.L., Foster S.S.D. (2001). Cryptosporidium. Contamination Hazard Assessment and Risk Management for British Groundwater Sources. *Water Sci Techn*, 41, 7, 67-77.

Mpelasoka F.S., Chiew F.H.S. (2009) Influence of Rainfall Scenario Construction Methods on Runoff Projections. *J Hydrometeor*, 10, 1168–1183. doi: 10.1175/2009JHM1045.1.

Ndambuki J. M., Otieno F.A.O., Stroet C.B.M., Veling E.J.M. (2000) Groundwater management under uncertainty: a multi-objective approach. *Water SA*, 26(1), 35-42.
Nicklow J., Reed P., Savic D., Dessalegne T., Harrell L., Chan-Hilton A., et al. (2010) State of the art for genetic algorithm and beyond in water resources planning and management. *J Water Resour Plan Manage* 2010;136:412–32.

Nicholls R.J., Lowe J. A. (2004) Benefits of mitigation of climate change for coastal areas. *Glob Environ Chang*, Vol. 14, Iss. 3, pp. 229–244, doi:10.1016/j.gloenvcha.2004.04.005.

Nielsen P. (1990) Tidal dynamics of the water table in beaches. *Water Resour Res* 1990;26:2127–34.

Nisi M.F., Gabellini M. , Silenzi S. (2000) La valutazione del rischio da ingressione marina nelle aree di piana costiera" in: *Mare e cambiamenti globali*, pp. 199-206, ICRAM.

Nobre R.C.M., Rotunno Filho O.C., Mansur W.J., Nobre M.M.M., Cosenza C.A.N. (2007) Groundwater vulnerability and risk mapping using GIS, modeling and a fuzzy logic tool. *J Contam Hydrol*, No. 94, pp. 277–292, doi:10.1016/j.jconhyd.2007.07.008.

Nyenje P.M., Batelaan O. (2009) Estimating the effects of climate change on groundwater recharge and baseflow in the upper Ssezibwa catchment, Uganda. *Hydrol Sci J* 54(4):713–726.

Oude Essink G.H.P. (2001) Improving fresh groundwater supply-problems and solutions", *Ocean Coast Manage*, Vol. 44, 2001, Pages 429-449, ISSN 0964-5691, DOI: 10.1016/S0964-5691(01)00057-6.

Oude Essink G.H.P., van Baaren E. S., de Louw P. G. B. (2010) Effects of climate change on coastal groundwater systems: A modeling study in the Netherlands. *Water Resour Res*, Vol. 46, W00F04, doi:10.1029/2009WR008719.

Ozyurt G. (2007) Vulnerability of coastal areas to sea level rise: a case of study on Göksu Delta. *Thesis submitted to the Graduate School of Natural and Applied Sciences of Middle-East Technical University*. January 2007.

Palestinian Water Authority -PWA (2007) Agricultural And Municipal Water Demand in Gaza Governorates for 2006, PWA, Gaza, Palestine. August 2007.

Paniconi C., Khlaifi I. Lecca G. , Giacomelli A., Tarhouni, J. (2001) Modeling and Analysis of Seawater Intrusion in the Coastal Aquifer of Eastern Cap-Bon, Tunisia. *Springer, Earth and Environmental Science*, Vol. 43, No. 1.

Park C.H., Aral M. M. (2002) Multi-objective optimization of pumping rates and well placement in coastal aquifers", *J Hydrol*, Vol. 290, No. 1-2, 2004, pp. 80-99.

Pinder G.F., Cooper H.H.Jr. (1970) A numerical technique of calculating the transient position of the saltwater front. *Water Resour Res*, 3,875-881, 1970.

Poeter E.P., Hill M.C. (1997) Inverse models: A necessary next step in groundwater modeling. *Ground Water* 35(2):250–260.

Pulido-Bosch A., Tahiri A., Vallejos A. (1999). Hydrogeochemical characteristics of processes in the Temara aquifer in northwestern Morocco. *Water Air Soil Pollution* 114 (3–4), 323–337.

Putti M., Paniconi C. (1995) Picard and Newton linearization for the coupled model of saltwater intrusion in aquifers. *Adv Water Resour* 18(3), 159-170, 1995.

Qahman K. (2004), *Aspects of Hydrogeology, Modeling, and Management of Seawater Intrusion for Gaza Aquifer – Palestine*, PhD Thesis, Mohamed V-Agdal University.

Qahman K., Larabi A. (2006) Evaluation and numerical modeling of seawater intrusion in the Gaza aquifer (Palestine). *Hydrogeol J*, No. 14, pp. 713–728 DOI 10.1007/s10040-005-003-2.

Qahman K., Larabi A., Ouazar D., Naji A., Cheng A. H.-D. (2005) Optimal and sustainable extraction of groundwater in coastal aquifers. *Stochastic Environ Res Risk Assess J*, Vol. 19, No . 2, pp. 99–110, 2005.

Qahman K., Larabi A., Ouzar D., Naji A., Cheng H.D. (2009) Optimal Extraction of Groundwater in Gaza Coastal Aquifer. *J Water Resour Protect*, Vol. 4, pp. 249-259. DOI: 10.4236/jwarp.2009.14030.

Ranjan P., Kazama S., Sawamoto M**.** (2006) Effects of climate change and land use changes on groundwater resources in coastal aquifers. *Glob Environ Chang*, Vol. 16, Issue 4, pp.388-399, doi:10.1016/j.gloenvcha.2006.03.006.

Refsgaard J.C., Van der Sluijs J. P., Lajer Højberg A., Vanrolleghem P. A. (2007) Uncertainty in the environmental modelling process - A framework and guidance. *Environ Model Soft*, no.22, pp.1543-1556, doi:10.1016/j.envsoft.2007.02.004

Reilly T.E., Goodman A.S. (1987) Analysis of saltwater upconing beneath a pumping well. *J Hydrol* 1987;89:169–204.

Rozell D. J., Wong, T. (2010) Effects of climate change on groundwater resources at Shelter Island, New York State, USA. *Hydrogeol J*, Vol. 18, No. 7, 1657-1665; DOI: 10.1007/s10040-010-0615-z.

Royal Society Study Group 1992. Risk: Analysis, Perception and Management. The Royal Society, London.

Saeed M.M., Bruen M., Asghar M.N. (2002) A review of modeling approaches to simulate saline-upconing under skimming wells. *Nord Hydrol* 2002;33:165–88.

Sanford W. E., Konikow, L. F. (1985) A two-constituent solute-transport model for ground water having variable density. *USGS Water-Resources Investigations Report*. 85-4279, 88 p.

Scibek J., Allen D.M. (2006) Modeled impacts of predicted climate change on recharge and groundwater levels. *Water Resour Res* 42:W11405.

Scibek J., Allen D.M., Cannon A., et al. (2007) Groundwater–surface water interaction under scenarios of climate change using a high resolution transient groundwater model. *J Hydrol* 333:165–181.

Segol G., Pinder G. F. (1976) Transient simulation of saltwater intrusion in southeastern Florida. *Water Resour Res*, 12(1), 65–70, doi:10.1029/WR012i001p00065.

Shamir U., Bear J., Gamliel A. (1984) Optimal annual operation of a coastal aquifer. *Water Resour Res* 20(4), 435–444.

Sherif M.M., Singh, V.P. (1999) Effects of climate change on seawater intrusion in coastal aquifers", *Hydrol Processes*, 13, 1277–1287.

Shomar B., Abu Fakher S., Yahya A. 82010) Assessment of Groundwater Quality in the Gaza Strip, Palestine Using GIS Mapping. *J Water Res Protection*, 2010, 2, 93-104 doi:10.4236/jwarp.2010.22011.

Song Z., Li L., Nielsen P., Lockington D. (2006) Quantification of tidal watertable overheight in a coastal unconfined aquifer. *J Eng Math* 2006;56:437–44.

Stoll S., Hendricks Franssen H. J., Butts M., Kinzelbach W. (2011) Analysis of the impact of climate change on groundwater related hydrological fluxes: A multi-model approach including different downscaling methods. *Hydrol Earth Syst Sci*, 15(1), 21–38.

Sulis M., Paniconi C., Rivard C., Harvey R., Chaumont D. (2011). Assessment of climate change impacts at the catchment scale with a detailed hydrological model of surface-subsurface interactions and comparison with a land surface model. *Water Resour Res*, 47, W01513, doi:10.1029/2010WR009167.

Sulis M., Paniconi C., Marrocu M., Huard D., Chaumont D. (2012) Hydrologic response to multimodel climate output using a physically based model of groundwater/surface water interactions. *Water Resour Res*, 48, W12510, doi:10.1029/2012WR012304.

Sumner N.R. , Fleming P.M., Bates B.C. (1997) Calibration of a modified SFB model for twenty-five Australian catchments using simulated annealing, *J Hydrol*, Volume 197, Issues 1–4, 1 October 1997, Pages 166-188, ISSN 0022-1694; doi:10.1016/S0022-1694(96)03277-5.

Themeßl M. J., Gobiet A., Leuprecht A. (2011) Empirical-statistical downscaling and error correction of daily precipitation from regional climate models. *Int J Climatol*, 31(10), 1530–1544.

Thieler E.R., Hammar-Klose, E.S.,(1999) National Assessment of Coastal Vulnerability to Future Sea-Level Rise: Preliminary Results for the U.S. Atlantic Coast. *U.S. Geological Survey,* Open-File Report 99-593.

Todd D.K. (19599 Ground Water Hydrology. Willey, London, pp: 185.

Toews M.W., Allen, D.M. (2009a) Evaluating different GCMs for predicting spatial recharge in an irrigated arid region. *J Hydrol* 374:265–281.

Toews M.W., Allen, D.M., (2009b) Simulated response of groundwater to predicted recharge in a semi-arid region using a scenario of modelled climate change. *Environ Res Lett* 4:035003.

Violette S., Boulicot G., Gorelick S.M. (2009)Tsunami-induced groundwater salinization in southeastern India. *CR Geosci* 2009;341:339–46.

Voss C.I. (1984) A finite-element simulation model for saturated-unsaturated, fluid-density-dependent ground-water flow with energy transport or chemically-reactive single-species solute transport: U.S. Geological Survey Water-Resources Investigations Report 84-4369, 409 p.

Voss C.I., Souza, W.R. (1987) Variable density flow and solute transport simulation of regional aquifers containing a narrow freshwater-saltwater transition zone *Water Resour Res*, 23(10), 1851-1866, 1987.

Watson T. A., Werner A. D., Simmons C. T. (2010) Transience of seawater intrusion in response to sea level rise. Water Resour Res, 46, W12533, doi:10.1029/2010WR009564.

Webb M.D., Howard K.W. (2011) Modeling the transient response of saline intrusion to rising sea-levels. Ground Water. 2011 Jul-Aug;49(4):560-9. doi: 10.1111/j.1745-6584.2010.00758.x. Epub 2010 Sep 22.

Weinthal E., Vengosh A., Marei A., Gutierrez A., Kloppmann W. (2005) The Water Crisis in the Gaza Strip: Prospects for Resolution. *Ground Water*, 43: 653–660. doi: 10.1111/j.1745-6584.2005.00064.x.

Werner A.D., Gallagher M.R. (2006) Characterisation of sea-water intrusion in the Pioneer Valley, Australia using hydrochemistry and three-dimensional numerical modeling. *Hydrogeol J* 14:1452–1469; DOI: 10.1007/s10040-006-0059-7

Werner A.D., Simmons C.T. (2009) Impact of Sea-Level Rise on Sea Water Intrusion in Coastal Aquifers. *Ground Water*, Vol. 47, Issue 2, pp.197–204, doi: 10.1111/j.1745-6584.2008.00535.x.

Werner A. D., Ward J.D., Morgan L.K., Simmons C.T., Robinson N.I., Teubner M.D. (2011) Vulnerability Indicators of Sea Water Intrusion. *Ground Water*. doi: 10.1111/j.1745-6584.2011.00817.x

Werner A.D., et al. (2012) Seawater intrusion processes, investigation and management: Recent advances and future challenges. *Adv Water Resour* (2012), http://dx.doi.org/10.1016/j.advwatres.2012.03.004.

Willis R., Finney B.A. (1988) Planning model for optimal control of saltwater intrusion. *J Water Resour Plan Manage*, 114(2), 163–178.

Wood A.W., Leung L.R., Sridhar V., Lettenmaier D. P. (2004) Hydrologic implications of dynamical and statistical approaches to downscaling climate model outputs. *Clim Change*, 62(1–3), 189–216.

Wriedt G., Bouraoui F. (2009) Large Scale Screening of Seawater Intrusion Risk in Europe - Methodological Development and Pilot Application Along the Spanish Mediterranean Coast, *JRC Scientific and Technical Reports.* DOI: 10.2788/19371.

Yakirevich A., Melloul A., Sorek S., Shaath S., Borisov V. (1998) Simulation of seawater intrusion into the Khan Yunis area of the Gaza Strip coastal aquifer *Hydrogeol J* 6: pp 549-559.

Yang Y.S., Kalin R.M., Zhang Y., Lin X., Zou L. (2001) Multi-objective optimization for sustainable groundwater resource management in a semiarid catchment. *Hydrol Sci J*, Vol. 46, Issue 1 February 2001, pp 55 – 72.

Zhou X., Chen M., Liang C. (2003) Optimal schemes of groundwater exploitation for prevention of seawater intrusion in the Leizhou Peninsula in southern China. *Environm geol*, 43: 978-985.

Zwahlen, F. (ed) (2004) Vulnerability and risk mapping for the protection of carbonate (karst) aquifers, final report (COST Action 620). European Commission, Directorate-General XII Science, Research and Development. Brussels, pp. 297.